Design of Polymer Coated Magnetic Nanoparticles for the Selective Isolation of Bacteria from Mixed Populations

Joshua Edward Petch, MSc, BSc.

Thesis submitted to the University of Nottingham for the degree of Doctor of Philosophy

November 2019

Declaration

Unless otherwise acknowledged, the work presented in this thesis is my own. No part has been submitted for another degree at the University of Nottingham or any other institute of learning.

Joshua Petch, November 2019.

Contents

i. Abstract

The ability to selectively sequester bacteria from a mixed population is a desirable aim across a range of fields. Already some technologies exist to attempt to meet these aims however, these are generally limited to the confinement of small populations in defined locations and may be unable to differentiate between morphologically similar but phenotypically distinct cells. Furthermore, the use of immunomagnetic nanomaterials is likely to be prohibitively expensive for many scaled-up applications.

Magnetic glyconanoparticles (MGNPs) as a platform for specific bacterial capture by lectin-mediated attachment appear promising but have yet to be utilised for the extraction of bacteria from mixed populations. The work described in this thesis attempted to address this shortcoming.

An inducible mutant of the Type 1 fimbriae, a mannose-specific lectin, was produced in a wildtype *E. coli* background via a homologous recombination strategy. Binding to glycopolymers was only observed in the presence of the inducer and was specific for mannosylated but not galactosylated glycopolymers.

Well-defined glycopolymers of mannose and galactose acrylamides of varying chain length were synthesised by RAFT polymerisation with a dopamine terminal chain transfer agent and polymerisation kinetics was investigated. Binding studies revealed a complex relationship between lectin avidity and glycopolymer chain length. The dopamine functionality of these glycomaterials allowed for facile functionalisation of

superparamagnetic iron oxide nanoparticles with glycopolymers and lectin affinity was retained upon particle decoration.

Delivery of these glycopolymer-decorated nanoparticles to co-cultures of fluorescently labelled bacteria facilitated efficient depletion of Type 1 fimbriated target cells from wildtype or afimbriate *E. coli*. Extraction efficiency of fimbriated *E. coli* was improved when the counterpart strain did not harbour the genetic apparatus for expression of the Type 1 fimbriae. However, release of the captured cells from the nanoparticles by addition of a monovalent competitive ligand could not be adequately demonstrated under the tested conditions.

Overall this work suggests that MGNPs may prove a versatile tool for the extraction of bacteria from mixed populations based on the sugar-binding preferences of different bacteria or control over the genetic apparatus encoding bacterial surface associated lectins. However, additional investigation is required to fully investigate the limitations of this system.

ii. Acknowledgements

First and foremost, I would like to extend my sincerest gratitude to my supervisors Beppe Mantovani, Miguel Camara and Stephan Heeb for their constant support and guidance throughout this project. To Beppe, thanks for taking a chance on a novice chemist. Very few other supervisors would be so ready to take the time to support me in the early days of synthesis or keen to get stuck in. To Stephan, your molecular biology expertise has been invaluable and I have always enjoying our discussions on cloning strategies. Miguel, your constant enthusiasm and positive outlook has helped motivate me through some of the deepest troughs of the PhD rollercoaster. I have been incredibly fortunate to begin my career with such a great team, and it has moulded me into the scientist I am today.

Of course science is no individual feat, while the number of contributors to this project are too numerous to name some special thanks must be extended. To Rosa Catania, thanks for taking me under your wing when I was still a wayward molecular microbiologist and the help with glycomonomers synthesis. To Francesca Mastrotto, whose kind donation of fluorescent glycopolymers made the CLSM studies possible. To Robert Markus, whose help in designing and supporting microscopy experiments has been invaluable. To Denise Maclean, for her expertise and assistance with TEM imaging. To Gokhan Yilmaz, for his glycopolymer expertise and assistance in SPR experiments. To Gokhan Takan for the kind donation of protected galactose monomer. To Eduards Krumins, for running TGA samples. To Erik Hanko, for the kind donation of the constitutive promoter

library (and being an excellent office buddy). To David Onion and Nicola Croxall, for their flow cytometry support. Finally, to Pratik Gurnani, thanks for being my personal RAFT guru and helping me rediscover my passion for science when I was too deep in the synthesis hole to see the light.

PhDs are no minor undertaking and I can imagine would be incredibly tedious without some good company along the way. Thanks to my constant friends and colleagues in C75; Paolo, Edu, Ioanna, Natalia, Manu, Matt, Sam, Kiril, Daniella & Fran, thanks for bringing some good humour to the otherwise dull days of cloning and PCR and being an excellent sounding board for my occasionally quite wacky ideas. May cowboy science live on!

To my friends in B15; Pratik, Lorenzo, Catherine, Ruggero, Rosa, Shelly, Akosua, Alessandra, Lucy, Thais and the Gokhans, no matter how many of us were crammed in the fumehoods we still managed to maintain a convivial spirit! I am sorry (read, not sorry) to have bored so many chemists with molecular biology, but feel this has perhaps been fair pay back for my baptism of fire in a chemistry lab.

Also, to my office friends in C51, past and present, thanks for all the laughter, support and, occasionally, a good vent. Christmas will never be the same without our office parties, roast ham and feuerzangenbowle. I have made some lifelong friends through this adventure and will forever be grateful for it.

I would also like to extend my appreciation to my parents, who are always ready and willing to support me in any way they can. Thank you. I hope this

achievement will provide you with exemplary parental bragging rights for years to come.

To Dan and Ingrid, thank you for welcoming me into your family and being every bit as supportive as my own parents.

Finally, to Alex, who has kept me going these past four years. You have seen me at my best and my worst throughout this experience and it can't have been easy. You always believe in me, even when I don't believe in myself. I couldn't have done this without you.

iii. List of Abbreviations

Abbreviation	Description
::	Fusion mutant
@	Conjugated
^{13}C NMR	Carbon 13 NMR
^{1}H NMR	Proton NMR
AEMA	2-aminoethyl methacrylate
AIBN	Azobisisobutyronitrile
Amp	Ampicillin
ARGET ATRP	Activators regenerated electron transfer atom transfer radical polymerization
Atc	Anhydrotetracycline
ATRP	Atom transfer radical polymerisation
BOP	Benzotriazol-1-yloxytris(dimethylamino)phosphonium hexafluorophosphate
bp	Base pair
$CDCl_3$	Deuterated chloroform
CLSM	Confocal laser scanning microscopy
Cm	Chloramphenicol
Con A	Concanavalin A
Conv	Monomer Conversion
CTA	Chain transfer agent
CuAAC	Copper azide-alkyne cycloaddition
Cup	*N*-nitrosophenylhydroxylamine
Đ	Dispersity
D2O	Deuterated water
D6-DMSO	Deuterated DMSO
DAPI	4′,6-diamidino-2-phenylindole
DCC	Dicyclohexylcarbodiimide
DCM	Dichloromethane
DC-SIGN	Dendritic Cell-Specific Intercellular adhesion molecule-3-Grabbing Non-Integrin
dH2O	Distilled water
DIPEA	*N,N*-Diisopropylethylamine
DMAm	Dihydroxyphenylalanine methacrylamide
DMAP	4-Dimethylaminopyridine
DMAPAm	*N*-[3-(dimethylamino)propyl]methacrylamide
DMF	Dimethylformamide
DMSO	Dimethylsulfoxide
DNA	Deoxyribonucleic acid
dNTP	Deoxynucleotide
Dopa-PABTC	Dopamine functionalised propanoic acid butyl trithiocarbonate
DP	Degree of Polymerisation
EDC	1-Ethyl-3-(3-dimethylaminopropyl)carbodiimide

eGFP	Enhanced green fluorescent protein
ESI-TOF MS	Electrospray ionisation time-og-flight mass spectrometry
Et_2O	Diethyl ether
ETEC	Enterotoxigenic *E. coli*
EtOAc	Ethyl Acetate
FITC	Fluorescein isothiocyanate
FRP	Free radical polymerisation
FTIR	Fourier transform infrared spectroscopy
Fuc	Fucose
Gal	Galactose
GalAA	Galactose acrylamide
GalNAc	*N*-Acetyl galactosamine
GlcNAc	*N*-Acetyl glucosamine
HBTU	Hexafluorophosphate benzotriazole tetramethyl uronium
HEAA	Hydroxyethyl acrylamide
IO	Iron Oxide
Kan	Kanamycin
kb	Kilobase
kDa	kilodalton
LB	Lysogeny Broth
LCST	Lower critical solution temperature
M9F	Fructose supplemented M9 minimal media
Man	Mannose
ManA	Mannose acrylate
ManAA	Mannose acrylamide
MBL	Mannose binding lectin
MEDSA	[2-(Methacryloyloxy)ethyl]dimethyl-(3-sulfopropyl)ammonium hydroxide
MeOH	Methanol
MGNPs	Magnetic glyconanoparticles
MNPs	Magnetic nanoparticles
$M_{n,\,NMR}$	Number average molar mass determined by ^1H NMR
$M_{n,\,SEC}$	Number average molar mass determined by SEC
$M_{n,th}$	Theoretical number average molar mass
mol/mol	Mole to mole ratio
mRuby	Monomeric Ruby 2 fluorescent protein
$M_{w,\,SEC}$	Weight average molar mass determined by SEC
MWCO	Molecular weight cut off
NAM	*N*-acryloyl morpholine
NeuAc	*N*-Acetyl neuraminic acid
NHS	*N*-hydroxysuccinimide
NHS-PABTC	NHS functionalised propanoic acid butyl trithiocarbonate
NIPAM	*N*-isopropylacrylamide
NMP	Nitroxide mediated polymerisation
OD600	Optical Density at 600 nm

PABTC	Propanoic acid butyl trithiocarbonate
PBS	Phosphate buffered saline
PCR	Polymerase chain reaction
PEG	poly(ethylene glycol)
PetEt	Petroleum Ether
PFA	Paraformaldehyde
PyBOP	(Benzotriazol-1-yloxy)tripyrrolidinophosphonium hexafluorophosphate
^{R}	Resistance
RAFT	Reversible addition-fragmentation chain transfer
RBS	Ribosome binding site
RDRP	Reversible deactivation radical polymerisation
RI	Refractive index
RPM	Revolutions per minute
^{S}	Sensitivity
SEC	Size exclusion chromatography
SET-LRP	Single-electron transfer living radical polymerisation
SPION	Superparamagnetic Iron Oxide Nanoparticles
TBAF	tetra-*N*-butylammonium fluoride
TEA	Triethylamine
TEM	Transmission electron microscopy
TGA	Thermogravimetric analysis
TLC	Thin layer chromatography
TMAEMA	2-(methacryloyloxy)-*N,N,N*-trimethylethanaminium chloride
TMAOH	Tetramethylammonium hydroxide
TOC	Total Organic Content
UPEC	Uropathogenic *E. coli*
v/v	Volume to volume ratio
VA-044	2,2'-Azobis[2-(2-imidazolin-2-yl)propane]dihydrochloride
w/v	Weight to volume ratio
Δ	Deletion Mutant

1. General Introduction

1.1. The Industrial Biotechnology Revolution

Since its advent, the field of industrial biotechnology have been decisively transformative technologies with the propensity to revolutionise the way we manufacture chemicals, materials and pharmaceuticals (Singh, 2011). Genomic engineering of microorganisms has already resulted in the ability to biosynthesise chiral intermediates (Tseng *et al.*, 2010), which are key components in the chemical industry; synthesis of key feedstock compounds such as butanone and ethylene glycol (Pereira *et al.*, 2016; Srirangan *et al.*, 2016); and biosynthesis of fatty acid methyl esters (FAME) by *Escherichia coli* thus negating reliance on transesterification of plant oils with methanol for biofuel production (Sherkhanov *et al.*, 2016). Such contemporary advances synchronise well with concurrent global desires to reduce the burden of climate change and decrease reliance on non-renewable enterprise by investing in renewable technologies.

In the pharmaceuticals industry, industrial biotechnology has allowed for the development of new and more effective therapies. Indeed, approximately 30% of all therapeutic proteins licensed for use are synthesized in *E. coli* as a heterologous host (Baeshen *et al.*, 2015). Well documented examples of this include the production of humanised insulin in recombinant *E. coli* (Williams *et al.*, 1982); the production of recombinant murine monoclonal antibodies for the treatment of rheumatoid arthritis and various cancers (Souriau & Hudson, 2003); and the production of semi-synthetic artemisinin, the most potent currently

known antimalarial, by the generation of novel biosynthetic pathways (Paddon & Keasling, 2014; Paddon, 2013; White, 1997).

However, while the industrial fermentation of metabolically engineered microorganisms is becoming more commonplace, it is still not viable for a variety of biosynthetic applications. Furthermore, studies are beginning to emerge which challenge the old paradigm of complete biosynthetic pathway reconstitution in a single strain. These works have demonstrated that engineering microbial consortia to express complex pathways in distinct modules may be more efficient and robust allowing for the production of desirable biochemicals including bioethanol, polyketides, aromatic compounds and plastics precursors (He *et al.*, 2011; Jiang *et al.*, 2019; Li *et al.*, 2019a; Liu *et al.*, 2017; Park *et al.*, 2012; Ross *et al.*, 2014; Wang *et al.*, 2016a; Xin & He, 2013; Zhang *et al.*, 2015a; Zhang *et al.*, 2015b; Zhou *et al.*, 2019). In their seminal work Zhang & co-workers were able to produce *cis,cis*-muconic acid, a key precursor in the production adipic acid, which is used to make nylon and polyurethane, and terephthalic acid, a monomer of polyethylene terephthalate using a co-culture approach. A maximal production of 0.35 g/g of carbon source was achieved – a significantly higher yield than other biosynthetic production methods (Zhang *et al.*, 2015a). Moreover, engineering metabolic modules across synthetic microbial consortia as opposed to a single chassis can reduce metabolic load upon the host organism(s) as well as limiting the crosstalk between native and non-native pathways or signalling mechanisms

(Gerchman & Weiss, 2004; Jia *et al.*, 2016; McCarty & Ledesma-Amaro, 2019; Roell *et al.*, 2019; Shong *et al.*, 2012).

However, the increased complexicity of microbial cultures in bioindustrial applications resulting from increasing utilisation of synthetic consortia will likely require specialised tools for organism differentiation, capture and processing. Selectively removing bacteria from a biosynthetic reaction culture at suitable time points could improve the yield and efficiency of such reactions by the removal of an organism expressing no longer useful enzymes which may lead to non-desirable reactions (Bernstein *et al.*, 2017; Zhang *et al.*, 2018). Furthermore, this could allow for the selective removal of organisms in which the desired product has been internalised, as in inclusion bodies (Peternel *et al.*, 2008), thus allowing for harvest of this product while mediating the shift from batch based bioreactors to continuous bioreactors. Some of the existing cellular confinement strategies, along with their merits and limitations, are discussed below. These strategies, however, do not appear to be feasible for large scale selective sequestration of bacteria from large populations concurrent with those in industrial bioreactors.

1.2. Existing Bacterial Confinement Technologies

1.2.1. Microfluidics

Microfluidic devices are frequently used in microbiology to isolate small bacterial populations and can be utilised to monitor their response to specific microenvironments and cell to cell signalling (Shields *et al.*, 2015; Wessel *et al.*, 2013). Typically these microfluidic devices are made from poly(dimethylsiloxane) (PDMS) and the employment of soft-lithography/wet etching techniques are able to pattern these devices with specific topographic structures producing channels and mazes for physical isolation of cells (Fig 1.1) (Li *et al.*, 2005; McDonald *et al.*, 2000; Park *et al.*, 2003).

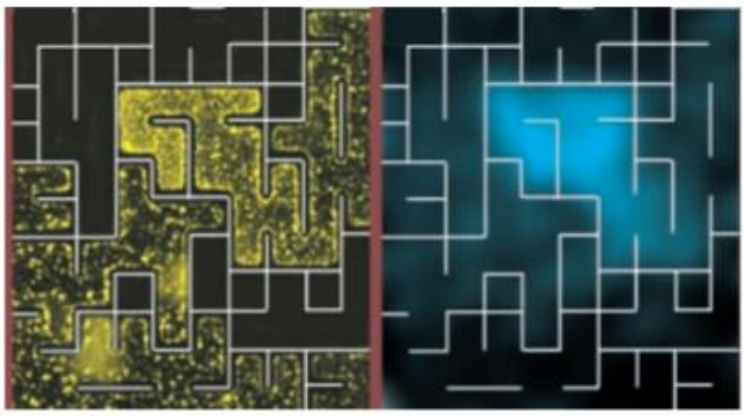

Figure 1.1. *Vibrio harveyi* accumulation in a microfabricated maze. *V. harveyi* accumulation after 8 hours occurs due to self-attractive behaviour and causes increased population density. The dark-field image (left) displays autoaggregation of cells at dead ends and cul-de-sacs of the maze. Autoaggregation results in the quorum sensing-dependent production of luminescence as detected by a photon-counting (right image). Adapted from Park et al, 2003.

Thus far these technologies have been employed to isolate small populations of *E. coli* to produce travelling waves of cell density to replicate precursor conditions of quorum sensing in this organism (Park *et al.*, 2003). Another group has successfully used this technology to isolate singular *S. aureus* and *P. aeruginosa* cells and demonstrate that a singule bacterium, isolated from a low density culture, was able to stimulate quorum sensing-like events (Boedicker *et al.*, 2009). Microfluidics has also been employed for 'stochastic confinement' of bacteria where individual bacteria have been confined in nanolitre scale droplets (Boedicker *et al.*, 2008). This method of confinement helped increase colony cell density and allowed molecule accumulation around the cells enabling high throughput analysis of antibiotic sensitivity of a variety of cells (Boedicker *et al.*, 2008).

Microfluidics have also been coupled with immunomagnetic particles to separate two distinct eukaryotic cells types in one of the most promising developments in this field to date (Osman *et al.*, 2013). In this work Jurkat and HEK 293 cells were isolated from a mixed population by labelling them under microfluidic flow with specific antibodies coupled to magnetic nanoparticles and extracting the labelled cells with micro-magnets (Osman *et al.*, 2013). This technology is currently unsuitable for large-scale industrial application due to the high cost associated with immunomagnetic particles but this pioneering study demonstrated the viability of this approach, paving the way for future innovation. Simultaneous microfluidic sorting of multiple bacterial targets has also been performed by Kim & Soh using a novel integrated dieletrophoretic-

magnetic activated cell sorter with concurrent expression of T7 tag peptides or streptavidin binding peptides on the surface of target cells (Kim & Soh, 2009).

Despite the apparent explosion in the invention of successful lab-on-a-chip microfluidic cell separation devices relatively few have been translated to successful commercialisation, with no wide clinical distribution of any device. An exhaustive review by Shields *et al* partly attributes this to a saturated patent environment, with over 2750 microfluidic device patents as of 2017 in the USA alone, limited post-invention investment and generally poor user interfaces of microfluidic devices (Shields *et al.*, 2017).

1.2.2. Hydrogels

Hydrogels are networks of cross-linked hydrophilic polymer chains. Hydrogels have commonly been used in tandem with microfluidic devices to confine small bacterial populations and offer the core advantage that they are able to create environments which have specific and defined mass transfer properties (Wessel *et al.*, 2013). Hydrogels can be used to immobilise cells in media but have also been used to study intercellular interactions by allowing the diffusion of small hydrophilic molecules through them (Degiorgi *et al.*, 2002; Jasinska *et al.*, 2018; Wessel *et al.*, 2013). In this way, the impact of intracellular signalling systems, particularly quorum sensing have been extensively studied (Carnes, 2010; Flickinger *et al.*, 2011).

Furthermore, hydrogels can be supplemented with optical trapping methods to confine small populations of bacteria into microchambers within the hydrogel matrix (Harper *et al.*, 2012; Perroud *et al.*, 2009). A particularly powerful technique, multiphoton lithography, is capable of producing microcompartments within a hydrogel matrix with which have picolitre scale pores within their walls. Due to their strikingly familiar structure, these have been dubbed 'bacterial lobster traps' and they have the ability to isolate a single cell to small populations (Fig. 1.2) (Connell *et al.*, 2010; Harper *et al.*, 2012; Nielson *et al.*, 2009).

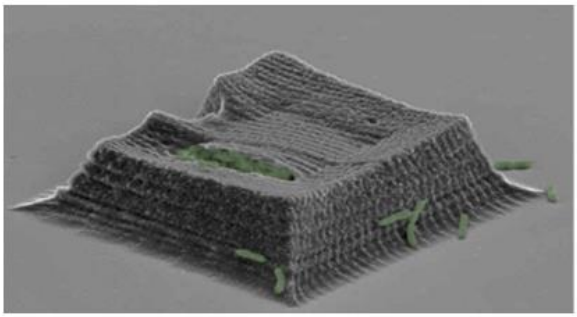

Figure 1.2. Scanning electron micrograph of bacterial lobster pot entrapping *Pseudomonas aeruginosa* cells. *P. aeruginosa* shown in false colour (green) Adapted from Connell *et al*, 2010.

In their landmark study Connell *et al*, where able to isolate single *Pseudomonas aeruginosa* cells in such permeable microcavities and demonstrate that quorum sensing in these bacteria is not just modulated by cell density but also media flow and total population size (Connell *et al.*, 2010). Additionally this study showed that as few as 150 confined cells were able to demonstrate an antibiotic resistant phenotype consistent with that demonstrated in biofilm growth (Connell *et al.*, 2010). Soft lithography structure design within hydrogels has also been exploited in tandem with

microfluidics to interrogate chemotactic decision making with clonal bacterial populations. A study by Salek and co-workers demonstrated the construction of branching mazes structures within a hydrogel which, coupled with microfluidics, was seeded with a chemoattractant gradient (Salek *et al.*, 2019). Better chemotaxers became increasing concentrated at sequential junctions.

With both of these techniques there are some key limitations. Firstly, most of these approaches are limited to the confinement of small populations of bacterial cells in defined locations and low volumes; for microfluidic channels this is typically less than 10 μL (Wessel *et al.*, 2013). Furthermore, physical separation lacks the ability to differentiate between cell populations that are morphologically identical yet phenotypically different. A population of cells in a biosynthetic pathway is likely to consist of the same chassis, but be engineered to have divergent metabolisms. Confinement techniques which are based on temporal and spatial separation are unlikely to be able to distinguish these distinct subpopulations present in one mixed population.

1.2.3. Flow cytometry

A typical strategy used to investigate individual cells in larger populations involves the use of flow cytometry. Indeed the use of flow cytometry has already been identified as having the potential to monitor population heterogeneity within industrial bioreactors (Brognaux *et al.*, 2013). Microbial populations are capable of displaying phenotypic heterogeneity in industrial bioreactors due to the fluctuating conditions they are exposed to as they move through the reaction vessel. Heterogeneity can impact cellular metabolism and, consequently, yields and quality of desired products (Lara *et al.*, 2006). Brognaux *et al* describe a novel strategy using a simplified, automated flow cytometry procedure which was able to monitor multiple conditions within a bioreactor as indicators of microbial stress in real time (Brognaux *et al.*, 2013). This automated approach could provide the basis for high-throughput analysis of cells within a fermentation vessel using flow cytometry.

Fluorescence assisted cell sorting (FACS) is already a well-established modification of flow cytometry for the selective sorting of different cells via fluorescence labelling, differential marker expression as detected by labelled antibodies and specific optical properties of differing cells, particularly in immunology (Cossarizza *et al.*, 2017; Jan *et al.*, 2011). Detection of pathogenic bacteria and single cell sorting of bacteria using multicolour flow cytometry with fluorescent probes has already been achieved (Kennedy & Wilkinson, 2017; Nebe-von-Caron *et al.*, 2000).

However, thus far it appears that such flow cytometry based strategies have only been successfully employed at the laboratory benchtop (Brognaux *et al.*, 2013; DeLisa *et al.*, 1999; Leelavatcharamas *et al.*, 1997). Without practical large scale data, success when scaled up to industrial bioreactors cannot be assumed. Additionally, adaption of flow cytometers to industrial scale bioreactors will require novel partner technologies to couple the reactors and cytometers and allow for confinement of cells from the reactor. Some magnetic separation technologies have been adapted to this aim but are highly specialised and, thus, expensive (Golden *et al.*, 2013). Until these technologies can be optimised and become cost-effective it is unlikely they will experience pervasive uptake. Furthermore, cell separation via flow cytometry is normally mediated by fluorescent antibodies as the discriminatory agent; these are prohibitively expensive for large scale application. Alternatively, cells with distinguishably different morphologies can be sorted by the use of differing fluorescent dyes (Ambriz-Avina *et al.*, 2014).

1.2.4. Immunomagnetic separation

The binding properties of antibodies to cell-specific antigens has also been exploited for selective detection, separation and isolation of cells in mixed populations by coupling them to magnetic particles (Bohara & Pawar, 2015; Gallo *et al.*, 2011; Qiu *et al.*, 2009; Singh *et al.*, 2016; Wang *et al.*, 2016b).

Many magnetic particles are available commercially with microscale magnetic beads (>2 μm) available from Dynal, or beads in the nanoscale (<100 nm) available from Miltenyi Biotech (Miltenyi *et al.*, 1990; Neurauter *et al.*, 2007). Furthermore, these particles can often be purchased directly conjugated with primary antibodies against cell-specific targets as part of kits. Alternatively antibodies may be labelled with biotin through traditional EDC/NHS amide coupling and conjugated to streptavidin decorated magnetic particles; streptavidin/biotin interactions are one of the strongest non-covalent interactions known with K_d in the order of 10^{-5} nM (Dundas *et al.*, 2013; Strachan *et al.*, 2004). IgG anti-human CD45 labelled magnetic nanoparticles have previously been used for the selective capture of white blood cells from human whole blood with a capture efficiency of >99% (Gourikutty *et al.*, 2016). Immunomagnetic separation has also been used to capture circulating tumour cells in human peripheral blood samples with cancer specific markers, potentially offering enhanced scope for cancer diagnostics and metastasis detection (Cao *et al.*, 2017; Hoshino *et al.*, 2011).

In terms of bacterial capture, immunomagnetic separation by antibody conjugated nanoparticles has been utilised to isolation pathogenic *E. coli*

0151:H7 from foodstuffs with a minimum capture efficiency of 94% and no observable capture of other common foodborne organisms including *Salmonella, Citrobacter and Listeris spps* (Varshney et al., 2005). Kumar & co-workers were able to generate anti-*P. aeruginosa* antibody functionalised magnetic carbon nanotubes and demonstrate ability of these materials to selectively isolate *P. aeruginosa* from a mixed culture with *S. aureus* with no cross-reactivity, demonstrating the potential of this technology as a rapid, diagnostic bioprobe for use in co-infection analysis (Kumar *et al.*, 2013). Others have designed a continuous flow device for continual detection and isolation of *Salmonella typhirium* using self-assembled magnetic nanoparticle chains conjugated with anti-*S. typhirium* polyclonal antibodies with 80% separation achieved in 45 mins (Cai *et al.*, 2018). A transiently magnetisable pipette tip incorporating a ferromagnetic matrix of nickel meshes has also been developed to allow for the high-throughput sorting of immunomagnetically labelled bacteria from mixed populations spiked into whole blood samples (Fig 1.3) (Oh *et al.*, 2018). 90.5% of targeted *E. coli* could be recovered using this device.

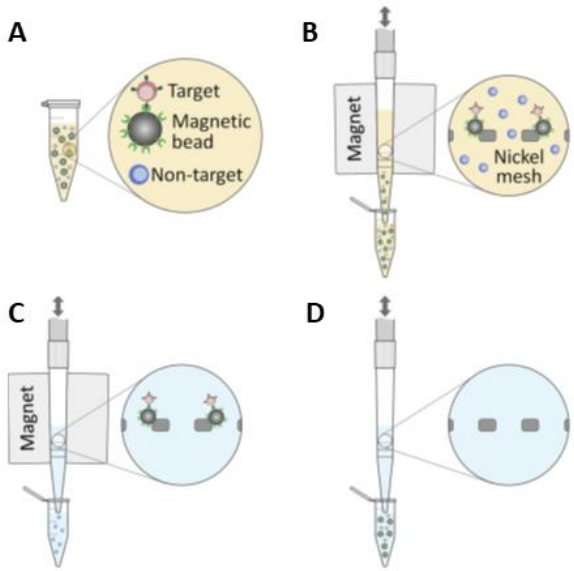

Figure 1.3. Separation of target bacteria using MACS pipette tip and immunomagentic beads. A) A mixed bacterial sample is incubated with magnetic beads conjugated with antibodies against the target cell, leading to specific attachment to target cells. B) The bacterial sample is aspirated into the MACS Tip, immunomagnetically labelled cells are captured by the integrated nickel mesh. C) Non-immunomagnetically labelled cells are removed by washing. D) The MACS Tip is removed from the magnetic field and conjugated target cells are recovered from the nickel mesh by washing. Adapted from Oh et al, 2018.

However, while immunomagnetic systems are becoming increasingly more diverse and commercially available the prohibitively high cost of these systems tends to limit their application to either cell detection or low scale isolation of specific cells in the academic setting. Industrial scale immunoseparation appears to be economically non-viable without significant cost reduction of antibodies and their accompanying magnetic particles.

1.2.5. Aptamer-based bacterial isolation

Aptamers are short DNA or RNA oligonucleotides which fold and bind to a specific target with high affinity and specificity (Ellington & Szostak, 1990; Lakhin *et al.*, 2013; Tuerk & Gold, 1990). While earlier methods for aptamer identification involved the screening of large combinatorial libraries of oligonucleotides, the conventional method for aptamer engineering is known as SELEX (systemic evolution of ligands by exponential enrichment) (Bouchard *et al.*, 2010; Lakhin *et al.*, 2013). Through iterative cycles of selection, increasing competition for binding sites enriches the recovery of high affinity aptamers, with maximal enrichment for the highest affinity aptamers usually seen with 5-20 rounds (Fig 1.4) (Kulbachinskiy, 2007; Stoltenburg *et al.*, 2007).

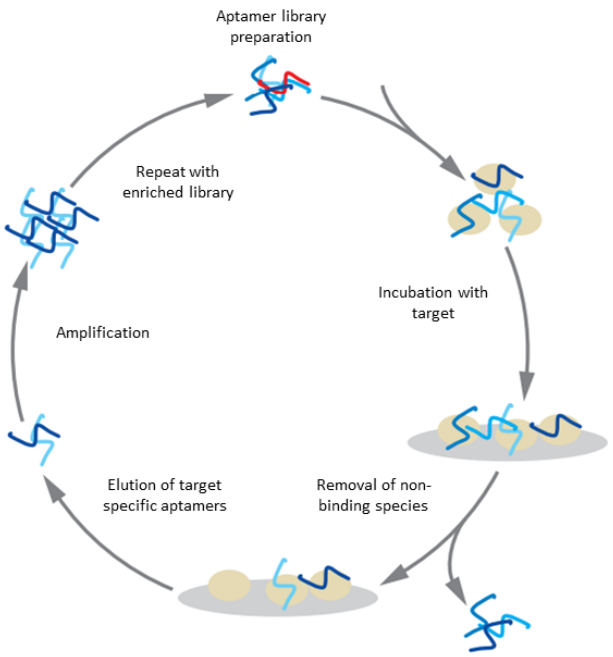

Figure 1.4. SELEX process for specific aptamer discovery. A pool of oligonucleotides is prepared by PCR amplification or RT-PCR, for DNA and RNA aptamers respectively. This library is then incubated with target molecules or whole target cells. Non-binding oligos are separated from bound molecules by washing. Target specific aptamers are then removed from the target and amplified to generate a less diverse library with higher specificity to the target. Iterative rounds of competition and selection leads to the evolution of highly specific aptamers. Adapted from Bouchard *et al*, 2010.

SELEX has allowed for the identification of high affinity aptamers against bacteria including *E. coli*, *Staphylococcus aureus* and *Salmonella enterica spp* (Dwivedi *et al.*, 2013; Hamula *et al.*, 2011; Kim *et al.*, 2013; Marton *et al.*, 2016; Moon *et al.*, 2015).

Due to their specificity, aptamers have been adapted to specific cell isolation techniques. Using a whole cell SELEX approach Dwivedi & co-workers were able to isolate a DNA aptamer with avidity for *Salmonella typhimurium* (K_d = 1.73 ± 0.54 μM) but low cross-reactivity with other organisms suggesting specificity (Dwivedi *et al.*, 2013). Biotinylation of aptamers against *S. typhimurium* allowed for the capture of aptamer-bound

cells by commercially available streptavidin-coated magnetic beads and subsequent detection of *S. typhimurium* down to 10^2-10^3 CFU in 290 μL (Dwivedi *et al.*, 2013). Aptamer-conjugated magnetic nanoparticles have also been used for the selective isolation of acute leukaemia cells from mixed cell and whole blood samples, suggesting the potential of aptamer conjugated magnetic nanoparticles for medical diagnostics and cell separation (Gedi & Kim, 2014). Aptamers in this study were also produced via a SELEX strategy.

Aptamers are particularly advantageous as an alternative to antibodies as their generation is significantly easier and cheaper than antibody production; they are also neither immunogenic nor toxic (Blind & Blank, 2015; Bouchard *et al.*, 2010; Kulbachinskiy, 2007). However some issues with aptamer stability in physiological media has been reported, particularly for RNA aptamers (Adler *et al.*, 2008; Mallikaratchy *et al.*, 2011). Significant effort is currently being expended in chemical modification of aptamers to improve stability (Wang *et al.*, 2011; Ye *et al.*, 2016). Some cross-reactivity for aptamers has also been recorded, which may limit their application in cell-specific isolation techniques (Bruno *et al.*, 2009; Gening *et al.*, 2006).

1.2.6. Lectins and their use in cellular isolation techniques

1.2.6.1. Lectin structure and funtion

Lectins are a heterogeneous group of oligomeric proteins which bind carbohydrates (Lis & Sharon, 1998; Schnaar, 2016). These proteins are typically di- or polyvalent, that is they possess at least two carbohydrate binding domains which allows for cross-linking between macromolecules containing sugar residues or cross-linking between cells by binding to polysaccharides displayed on their cell surface (Sharon & Lis, 2004). This multivalency results in the characteristic abilities of lectins to agglutinate cells and precipitate polysaccharides and glycoproteins (Sharon & Lis, 2004).

Lectins typically recognise a core group of primary monosaccharides: mannose, glucose, galactose, *N*-acetylglucosamine, *N*-acetylgalactose, fucose and *N*-acetylneuraminic acid (Gupta *et al.*, 2009). While many more exist in nature, a common similarity between these key monosaccharides is their frequent inclusion in animal glycoconjugates and their presence in glycoproteins and glycolipids displayed on cell surfaces, including erythrocytes (Anderson *et al.*, 2002; Sharon & Lis, 2004). This inclusion in glycoporteins in glycolipids pertains directly to the function of lectins; their specificity for common glycan elements of cells and their outer membranes allows lectins to function as recognition molecules within a cell, between different cells, and between different organisms (Chrispeels & Raikhel, 1991; Sharon & Lis, 2004). Another interesting observation which relates to the function of lectins is their respective affinities for monosaccharides

and complex polysaccharides. The binding affinity of most lectins for a particular monosaccharide is particularly weak; typically in the millimolar range (Ambrosi *et al.*, 2005; Lis & Sharon, 1998; Wesener *et al.*, 2017). In contrast lectins have a high affinity and exquisite specificity for particular oligosaccharides (Ambrosi *et al.*, 2005; Deniaud *et al.*, 2011; Lis & Sharon, 1998). This enhanced binding ability of multivalent sugar ligands to bind lectins with high avidity – for specific synthetic glycopolymers K_D values in the nanomolar range have been reported – has been widely investigated and it is known as 'cluster glycoside effect' (Becer *et al.*, 2010). This affinity for a particular oligosaccharide, which is likely to exist on the cell surface of a particular cell or group of closely related cells, furthers the specificity of lectins and improves their utility as recognition molecules.

1.2.6.2. Lectins in bacteria: cellular expression and carbohydrate specificity

Lectins in bacteria are surface associated; commonly they form part of sub-microscopic filamentous multi-subunit proteins called fimbriae or pili, derived from the Latin for fringes or hairs respectively (Hospenthal *et al.*, 2017). The carbohydrate specificities of a range of bacterial lectins and the organisms from which they are derived are shown in Table 1.1. Bacterial lectins are present across broad bacterial genera with diverse sugar binding preferences. Gram negative bacteria, such as *E. coli* may express one or more different fimbriae at a particular time and through a range of assembly pathways (Mortezaei *et al*, 2015). Of the identified bacterial lectins the most prevalent, and best characterised, are those derived from enterobacterial strains of *E. coli* (Korea et al., 2011). These lectins are key determinants of pathogenicity and are involved in the recognition and primary attachment to the urinary tract mucosa in uropathogenic *E. coli* (UPEC) and intestinal epithelium attachment in enterotoxigenic *E. coli* (ETEC) (Imberty & Varrot, 2008; Terlizzi *et al.*, 2017; Xia *et al.*, 2015).

Table 1.1. Exemplar bacterial lectins and specific carbohydrate binding preferences.

Lectin Origin	Fimbriae/Lectin	Mono/(Poly)saccharide Specificity	Reference
A. naeslundii, A. viscosus	Type 2 (FimP)	Galactose (Galβ(1-3)GalNAc)	(Stromberg & Karlsson, 1990)
B. ambifaria	BambL	Fucose (GalNAcα(1-3)Gal(2-1)αFuc)	(Audfray *et al.*, 2012)
E. coli	Type 1 (FimH)	Mannose (Manα(1-3)Manα(1-6)ManαOMe)	(Bouckaert *et al.*, 2006)
	P (PapG)	Galactose (Galα(1-4)Galβ)	(Hansson *et al.*, 1995)
	E. coli common pili (EcpA)	Arabinose	(Rossez *et al.*, 2014)
	S (SfaH)	NeuAc NeuAcα(2–3)Galβ	(Parkkinen *et al.*, 1986)
	F1C (FocH)	Galactose (GalNAc(1,4)Galβ)	(Backhed *et al.*, 2002)
	G (GafD)	GlcNAc	(Saarela *et al.*, 1995)
	Long Polar Fimbriae (LpfD)	Fibronectin (specific sugar preference unknown)	(Coppens *et al.*, 2015)
H. influenzae	HMW adhesin (HmwA)	NeuAc (NeuAcα(2-6)Galβ(1-4)GlcNAcβ)	(Atack *et al.*, 2018)
H. pylori	SabA	Sialic acids (NeuAc(α2–3)Galβ4GlcNAc)	(Aspholm *et al.*, 2006)
K. pneumoniae	Type 1 (FimH)	Mannose (Manα(1-3)Manβ(1-4)GlcNAc)	(Stahlhut *et al.*, 2009)
N. gonorrhoea	Type IV (PilC)	Lactosylceramides (Galα(1-4)Glcβ(1-1)Cer)	(Paruchuri *et al.*, 1990)
P. aeruginosa	Type IV (LecA)	Galactose (Galα(1-3)Galβ(1-4)GlcNAc)	(Kirkeby *et al.*, 2006)
	Type IV (LecB)	Fucose (NeuAc(2-3)Galβ(1-3)Fucα(1-4)GlcNAc	(Mitchell et al., 2002)
S. pneumoniae	BgaA	N-Acetyllactosamine (β-Gal-(1-4)GlcNAc)	(Limoli et al., 2011)
S. suis	SadP	Galactose (Galα(1-4)Galβ oligos	(Kouki et al., 2011)
V. cholerea	HlyA	GlcNAc	(Sasmal et al., 1992)

1.2.6.3. Applications: Lectins in healthcare and industry

Since adhesion of bacteria to host cells is required for attachment and colonization, novel high affinity therapies which target and inhibit adhesion machinery may offer a unique solution to tackling the challenge of infectious disease (Beloin et al., 2014; Hevey, 2019; Imberty et al., 2008; Sharon, 2006; Zhang & Ye, 2018). Furthermore the increasing incidence of antibiotic resistant organisms has made the search for novel therapeutic approaches of paramount importance (Ernst & Magnani, 2009). Since therapeutics which can inhibit lectin-mediated cellular adhesion are not bactericidal, these therapies are less likely to induce a selective pressure resulting in the propagation of resistant strains than therapies which rely on antibiotics (Ernst & Magnani, 2009).

Glycomimetic ligands of FimH, the lectin responsible for uropathogenic *E coli* (UPEC) colonisation of the bladder epithelium, have been shown to be potent inhibitors of adhesion during urinary tract infections (Kalas *et al.*, 2018). Glycomimetics such as low molecular weight cinnamides and sulfonamides with high affinities for LecB have also been shown to inhibit biofilm formation of *P. aeruginosa PAO1 in vitro* (Sommer *et al.*, 2018). These compounds were shown to have good bioavailability when delivered both intravenously or perorally in mice, but their biofilm inhibition efficacy has yet to be analysed *in viv*o.

Since glycopolymers (synthetic polymers with pendant carbohydrates) can be designed which display many copies of a bacterial lectin ligand, these

have also been developed as potential anti-attachment therapeutics (Sattin & Bernardi, 2016). *N*-heptyl mannose glycopolymers with nanomolar affinities for FimH have been developed as an antagonist of Type 1 fimbriated *E. coli* which can disrupt adhesion to intestinal epithelial cells (Gouin *et al.*, 2009; Yan *et al.*, 2015b). Galactosylated glycopolymers with a high avidity for *Streptococcus mutans* are potent sequestrants, suggesting the potential translation of these materials to oral biofilm disruption therapies (Magennis *et al.*, 2017). Additionally, galactosylated dendrimers also act as excellent biofilm inhibitors against *S. aureus* and *E. coli* (Agrahari et al., 2019).

Previous research has shown antibodies raised against bacterial lectins and the carbohydrate ligands to which they bind confer some resistance to infection (Abraham *et al.*, 1985; Aronson *et al.*, 1979; Thankavel *et al.*, 1997). The logical progression for therapeutic development is the formulation of vaccines against bacterial lectins. In an initial proof of concept cynomolgus monkeys were inoculated with a vaccine consisting of FimCH adhesin-chaperone complex; susceptibility to infection was decreased by 75% in immunised individuals (Langermann *et al.*, 2000).

The specific binding properties of lectins have also been of significant interest in the industrial and research sectors as a tool with myriad applications. Some of these applications include lectin-mediated cell separation techniques (Campuzano *et al.*, 2012; Porter *et al.*, 1998), isolation and identification of glycoproteins (Wang *et al.*, 2006) and interrogation of cell surface glycans (Laughlin & Bertozzi, 2009). Lectin-

mediated bacterial isolation techniques are discussed in more detail in Section 1.2.6.4.

1.2.6.4. Lectin-mediated bacterial separation techniques

Several attempts have been made previously to utilise lectin-carbohydrate interactions as components in biosensors for the detection of pathogenic bacteria (Saucedo *et al.*, 2018; Shen *et al.*, 2007; Wang & Anzai, 2015; Zheng *et al.*, 2017). Some researchers however have taken this further and attempted to utilise lectins for the selective separation of bacteria.

Work by Porter & co-workers at the end of the 20th century, was one of the earliest to show the potential of lectins as a microbial extraction tool (Porter *et al.*, 1998). Lectin-labelled magnetic beads, with a range of lectins from various sources, were tested for their ability to capture bacteria from either pure and mixed laboratory cultures, or environmental samples. Under the tested conditions, ConA presented the greatest potential for bacterial extraction (Porter *et al.*, 1998).

Similarly, Bicart-See & co-workers utilised a chimeric opsonin, Fc-mannose-binding lectin (Fc-MBL) to coat magnetic beads to isolate *S. aureus* from clinical samples of articular fluid and synovial tissue samples (Bicart-See *et al.*, 2016). Importantly though, while *S. aureus* could be extracted from laboratory cultures very well, Fc-MBL coated magnetic bead mediated extraction of *S. aureus* from clinical samples was initially poor (<5% efficient) without extensive treatment of these samples with hypotonic washes and proteases (Bicart-See *et al.*, 2016). The author's

speculate that this could be due to the presence of immunoglobulins on the target cells, masking the Fc-MBL attachment sites. Importantly this suggests that lectin-based cell separation techniques may be limited by the secretion of recognition molecules by other cells in a heterogeneous population.

Lectin-coated surfaces have also been used for selective bacterial confinement. Hansen & co-workers coated silicon wafers with a poly(glycidyl methacrylate)-*b*-poly(vinyldimethyl azlactone) copolymer as a surface support for wheat germ agglutinin allowing for high avidity capture of *Pseudomonas fluorescens* (Hansen *et al.*, 2013).

Other lectin-mediated techniques have involved the use of innovative engineered systems. In a seminal piece of work Campuzano and co-workers synthesised self-propelled microtubular microengines functionalised with ConA and demonstrate the capacity of this system to selectively isolate *E. coli* from human urine samples inoculated with either *S. cerevisiae* or *S. aureus* (Campuzano *et al.*, 2012). Furthermore, this work demonstrated that these lectin-functionalised microengines could capture, mobilise and release *E. coli* in alternate locations to the capture site (Campuzano *et al.*, 2012).

While promising for the detection and isolation of specific bacteria in diverse sample compositions, and potential theranostics, this system is unlikely to be adopted for large scale bacterial isolation due to the low capacity of the microengines and complexity of construction.

1.3.7. Antibody-free magnetic nanoparticle bacterial capture strategies

Several studies have attempted to exploit electrostatic interactions of negatively charged bacterial cell membranes with magnetic nanoparticles coated with a plethora of cationic materials to capture diverse bacteria from aqueous environments. Typical coating materials used in these strategies have included polyethylenimine (PEI) (Fang *et al.*, 2016; Li *et al.*, 2019b), poly(allylamine hydrochloride) (PAAH) (Xu *et al.*, 2014), arginine and cysteine (Figueredo *et al.*, 2018), lysine (Raee *et al.*, 2018) and ethanolamine (Bohara *et al.*, 2017). Bacteria captured have included *E. coli (Li et al., 2019b)*, *P. putida* (Figueredo *et al.*, 2018), *S. aureus* (Bohara et al., 2017), amongst many others (Gao *et al.*, 2016). Huang & co-workers reported the synthesis of magnetic nanoparticles functionalised with primary amines which allowed for the capture and depletion of 8 bacterial pathogens (Huang *et al.*, 2010). Furthermore, depletion of bacteria from aqueous samples, food matrixes, and a urine could be achieved with 88.5% to 99.1% efficiency (Huang *et al.*, 2010).

Chen & co-workers have also utilised Fe_3O_4 core/silica shell nanospheres with the surfactant cetyltrimethylammonium bromide (CTAB) embedded in the porous silica shell for the capture of Gram-negative (*E. coli*) and Gram-positive (*B. subtilis*) which demonstrated >97% inhibition of bacterial growth after capture and thus potential as a novel antimicrobial agent (Chen *et al.*, 2016a).

Importantly though these methods do not appear to have any ability to target specific bacteria, interaction is purely mediated through non-specific

electrostatic interactions. While such non-specific surface modified magnetic nanomaterials may not be useful for specific bacterial isolation they have been suggested as powerful tools for pathogen decontamination of drinking water (Bohara *et al.*, 2017; Xu *et al.*, 2014).

Alternatively, for more specific bacterial isolation, some strategies have focused on using specific glycomaterials coupled to magnetic nanoparticles to target cell associated lectins. Cell associated lectin targetting contrasts against methods described in Section 1.6 where lectins were used to target the glycocalyx and glycoproteins of bacteria.

In an earlier work El-Boubbou & co-workers were able to functionalise silica-coated magnetic nanoparticles with D-mannose by either amide coupling between a mannose amido-acid and an amine terminal linker, or CuAAC (copper catalysed azide-alkyne click) chemistry between 3-α-azido D-mannopyranoside and an alkyne linker on the nanoparticle surface (El-Boubbou *et al.*, 2007). *E. coli* capture efficiencies of up to 88% were demonstrated for these materials in single strain extraction experiments (El-Boubbou *et al.*, 2007). Pera & co-workers have also reported the synthesis of magnetic Fe_3O_4 nanoparticles conjugated to monovalent and tetravalent galabiose constructs using streptavidin-biotin coupling which could be used for the detection of *Streptococcus suis* after magnetic separation using a standard ATP-dependant luminescence assay (Pera *et al.*, 2010).

Similarly, glucose-decorated magnetic Fe_3O_4/cellulose nanoparticles were prepared by Malakootikhah & co-workers using various either arginine or

lysine amino acid linkers (Malakootikhah *et al.*, 2017). These nanohybrids could be used for the capture of *B. subtilis*, removing >80% of cells from aqueous and complex media in most conditions (Malakootikhah *et al.*, 2017). Chen & co-workers were able to produce nanoparticles functionalised with a glycopolymer of trehalose (a disaccharide of glucose) by coupling pentynoic acid to a lactide/benzyloxylactide copolymer and subsequent CuAAC between the resulting alkyne functionalised poly(lactic acid) and an azide of trehalose (Chen *et al.*, 2016b). These nanoparticles where shown to aggregate *M. smegmatis* but not *E. coli* or *S. epidermis* (Chen et al., 2016b), demonstrating the potential of multivalent glyconanoparticles for selective bacterial isolation. Behra & co-workers prepared mannose functionalised porous PEG microgels, which were then loaded with citrate-coated iron oxide nanoparticles, to facilitate extraction of *E. coli* from solution (Behra *et al.*, 2013).

In a very recent work, Miao & co-workers produced magnetic nanoparticles functionalised with a chitosan-mimicking cationic copolymer of 2-aminoethyl methacrylate (AEMA) and a mannose acrylate (ManA) monomer which could capture and deplete *E. coli* from aqueous media (Fig. 1.5) (Miao *et al.*, 2019).

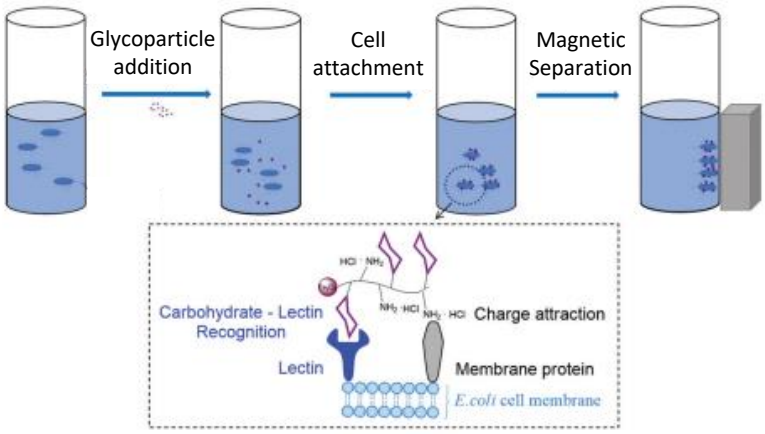

Figure 1.5. Schematic representation of *E. coli* capture and magnetic separation using cationic glyconanoparticles. Attachment of chitosan mimicking Fe_3O_4@poly(ManA)-*r*-(AEMA) is mediated by carbohydrate-lectin recognition and charge attraction between pendant amine groups and *E. coli*. Adapted from Miao *et al*, 2019.

Importantly, none of these materials were tested for the ability to differentiate between, and selectively isolate, different bacteria in mixed populations leaving a fundamental gap in the collective knowledge before these technologies can be translated to selective bacterial isolation. Additionally, most reported methods feature the decoration of magnetic nanoparticles with monovalent ligands of bacterial lectins (El-Boubbou *et al.*, 2007; Malakootikhah *et al.*, 2017; Pera *et al.*, 2010). As polyvalent sugar ligands demonstrate increased avidity for lectins compared to their monovalent counterparts due to the cluster glycoside effect (Gou *et al.*, 2013; Lee & Lee, 2000; Lundquist & Toone, 2002) these may be preferential for magnetic glyconanoparticles mediated bacterial isolation strategies. Currently, while present in the work of Chen *et al* and Miao *et al*, few reports exist documenting the use of magnetic nanoparticles decorated with polyvalent sugar ligands for specific bacterial isolation. However magnetic

nanoparticles coated with polyvalent glycopolymers have been utilised for the separation and isolation ConA from PNA (peanut agglutinin) in a mixed sample (Oz *et al.*, 2019). Extrapolation from these studies in tandem may suggest the utility of polyvalent glycopolymer coated magnetic nanoparticles for specific isolation of bacteria in a mixed sample by specific lectin targeting.

1.3.8. Polymers for bacterial isolation

Similarly to those materials used for the coating of magnetic nanoparticles, a key strategy in the production of polymers which can sequester bacteria has involved the production of polycationic materials (Leire *et al.*, 2016; Louzao *et al.*, 2015; Perez-Soto *et al.*, 2018; Richards *et al.*, 2018; Xue *et al.*, 2011). In a study by Louzao & co-workers both homo- and copolymers of *N*-[3-(dimethylamino)propyl]methacrylamide (DMAPAm) and dihydroxyphenylalanine methacrylamide (DMAm) were prepared by RAFT polymerisation which were able to cluster a range of Gram-positive and Gram-negative bacteria including *Staphylococcus aureus, Vibrio harveyi, E. coli* and *P. aeruginosa* (Louzao et al., 2015). Moreover this study also demonstrated that bacterial clustering by polycationic materials was not simply correlated with material charge. Material hydrophobicity as modulated by changes in pH was also implicated in bacterial interaction, with clustering of *P. aeruginosa* completely inhibited at pH 6 presumably by protonation of the amine residues of the tested cationic materials.

Similarly, a cationic polymer of [(3-methacryloylamino)propyl] trimethylammonium chloride was produced by Foster & co-workers which

could aggregate planktonic *P. aeruginosa*, inhibiting the formation of biofilm without any bactericidal effects (Foster *et al.*, 2019). In contrast, anionic and uncharged polymers could not aggregate planktonic bacteria or reduce biofilm formation. Clustering of bacteria by cationic materials has also been demonstrated with primary amine functionalised dendrimers of gallic acid-triethylene glycol (Leire *et al.*, 2016).

Cationic polymers of *N*-aminopropyl methacrylamide and *N*-[3-(dimethylamino)-propyl] methacrylamide have also been produced by Perez-Soto and co-workers which were able to induce clustering of *Vibrio cholerae* (Perez-Soto *et al.*, 2018). Intriguingly, this cationic polymer induced bacterial aggregation lead to the induction of quorum sensing regulated luminescence due to the rapid increase in the local autoinducer concentration in the vicinity of bacterial aggregates while simultaneously upregulating expression of the biofilm-specific regulator VspR and the structural biofilm protein RbmA thus overriding the usual biofilm dissipation response during autoinduction (Perez-Soto *et al.*, 2018). This cell clustering effect triggered by the electrostatic interaction of cationic polymers with bacterial membranes and induction of quorum sensing regulated phenotypes of clustered bacteria has been reported by several authors (Lui *et al.*, 2013; Perez-Soto *et al.*, 2018; Xue *et al.*, 2011; Zhang *et al.*, 2016a).

Bacterial entrapment by cationic polymers has been developed further by Magennis & co-workers (Magennis *et al.*, 2014). In their seminal work this group was able to exploit the native copper-homeostasis mechanisms of

E. coli to trigger co-polymerisation of 2-(methacryloyloxy)-*N,N,N*-trimethylethanaminium chloride (TMAEMA), a permanent cation, and a zwitterionic sulphobetaine (MEDSA) in a process they dubbed bacteria-mediated atom transfer radical polymerisation (b-ATRP) for *in situ* aggregation of bacteria (Fig. 1.6)(Magennis *et al.*, 2014). This process was further expanded for subsequent bacterial copper reduction mediated CuAAC 'click' ('b-click') with azide functionalised coumarin to allow for concurrent labelling in addition to bacterial capture.

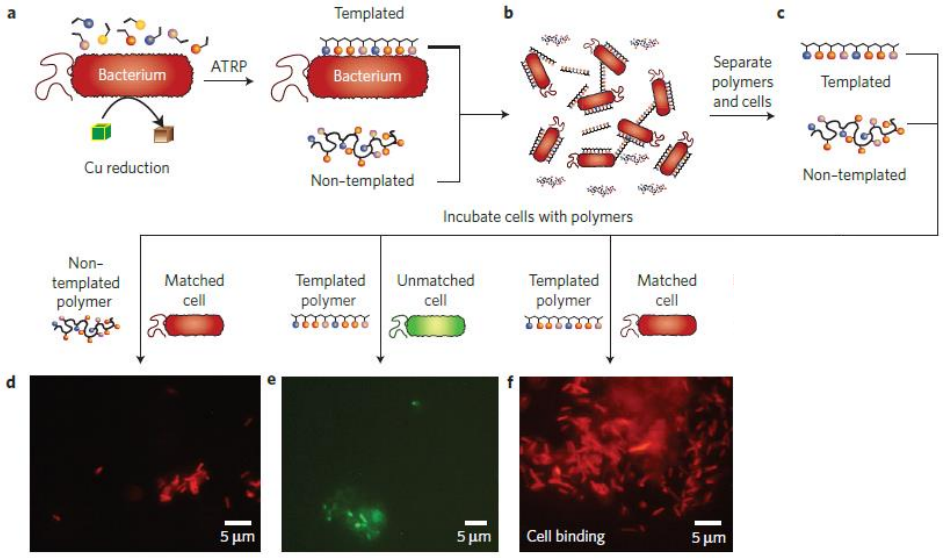

Figure 1.6. Bacteria-instructed ATRP for the synthesis of self-chelating cationic polymers. a) Bacterial redox processes reduce copper for ATRP catalysis in monomer/initiator/ligand solutions. b) This generates a synthetic extracellular polymer matrix around bacterial cells. c) Recovery of polymers from bacteria surfaces gave two fractions; one from the supernatant (non-tenplated polymer), and one obtained from a salt wash of bacterial surfaces (templated polymer). Incubation of the templated polymer with an mCherry-labelled bacterial population of the same strain lead to formation of large clusters as seen by fluorescent microscopy (f), however lesser aggregation was seen for the non-templated polymer (d). Additionally, incubation of the templated polymer with an alternative green labelled cell population did not induce aggregation, suggesting bacteria could instruct the synthesis of polymers with varying affinities for different cell types (e). Adapted from Magennis *et al*, 2014.

However, bacterial isolation mediated by cationic polymers suffers from the same limitation as cationic magnetic nanoparticles – cellular sequestration is generally not organism-specific.

For organism-specific targeting, glycopolymers have been devised which display pendant groups which are ligands of carbohydrate-binding proteins displayed on bacterial surfaces. Many of these systems have been constructed as organism/toxin specific sensors (Ajish *et al.*, 2018; Disney & Seeberger, 2004; Feng *et al.*, 2019; Richards & Gibson, 2014; Saucedo *et al.*, 2018; Wang *et al.*, 2014; Xue *et al.*, 2009), as anti-adhesive therapies (Bernardi *et al.*, 2013; Imberty *et al.*, 2008; Magennis *et al.*, 2017; Yan *et al.*, 2015b) or for targeted antimicrobial therapies (Narayanaswamy *et al.*, 2018; Pranantyo *et al.*, 2017; Ramstrom & Yan, 2015; Richards *et al.*, 2018).

Specific bacterial capture using glycopolymers has also been achieved (Luo *et al.*, 2019; Magennis *et al.*, 2017; Pasparakis *et al.*, 2007; Paul *et al.*, 2019; Pranantyo *et al.*, 2017; Yan *et al.*, 2015a; Yang *et al.*, 2010). Yang & co-workers modified a polypropylene microfiltration membrane with poly(2-lactobionamidoethyl methacrylate) (poly(LAMA)), a material displaying pendant cyclic galactose residues, which could be used for the selective capture of *Enterococcus faecalis* but not *Stenotrophomonas maltophilia* (Yang *et al.*, 2010). Additionally, attachment of *E. faecalis* could be reversed by the addition of free galactose. The authors suggest that patterning of porous membranes with bacteria-specific glycopolymers could be used for capture, and release, of specific bacteria in flow systems for water treatment, analytical or biomedical applications.

Thermo-responsive polymers have also been developed for selective entrapment of bacteria. Carbohydrate functionalised poly(NIPAM) linear polymers (Pasparakis *et al.*, 2007) and microgels (Paul *et al.*, 2019) were designed such that pendant sugar residues could be exposed or hidden via temperature dependant phase transition, allowing for the capture of *E. coli* upon ligand presentation (Fig 1.7). Importantly, both of these studies demonstrated the reversibility of thermo-responsive glycopolymer-cell interactions suggesting that such materials could allow for stimulus coupled capture and release of specific bacteria from solutions.

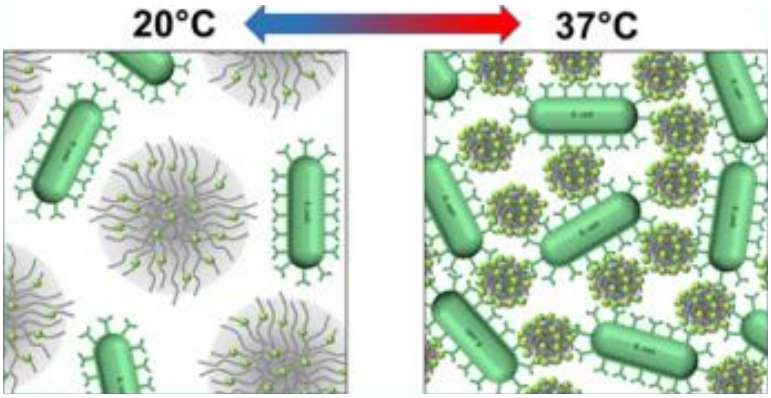

Figure 1.7. Schematic of Type 1 fimbriated *E. coli* capture by thermoresponsive mannose functionalised p(NIPAM) microgels. Below the lower critical solution temperature (LCST) the microgels are fully hydrated and swollen, leading to masking of the FimH specific mannose moieties (left). Above the LCST, the microgels transition to a hydrophobic state and the hydrodynamic radius decreases leading to an increase in carbohydrate density at the microgel surface. This facilitates greater *E. coli* capture by carbohydrate interaction with the surface associated FimH lectin. Adapted from Paul *et al*, 2019.

Bacterially-instructed polymerisation has also been adapted by Luo & co-workers for the *in situ* generation of glycopolymers with high avidity for fimbriated *E. coli* (Luo *et al.*, 2019). In this work the reducing properties of *E. coli* MG1655 were used to facilitate activators regenerated by electron

transfer atom transfer radical polymerization (ARGET ATRP) of a glucose methacrylamide and MEDSA. Intriguingly the authors recovered two distinct polymers from the bacterial ARGET ATRP; one from the supernatant and one from bacterial surface. The bacterial surface polymer exhibited an exquisite ability to cluster *E. coli* MG1655 but not DH5α, an afimbriate strain. Furthermore, the bacterial glycopolymer demonstrated a greater ability to cluster MG1655 than control homo and copolymers of MEDSA and glucose methacrylamide, suggesting this method may be useful for optimal permutation of glycopolymer architecture for bacterial capture (Luo *et al.*, 2019).

While many of these glycopolymer systems appear promising for specific bacterial capture based on their carbohydrate binding preferences, thus far little precedence has been established for glycopolymers to capture specific bacteria from mixed populations.

1.3.9. Affitins

In a recent study, Vukojicic & co-workers utilised a particularly novel strategy for the specific capture of bacteria using affitins (Vukojicic *et al.*, 2019). Affitins are short artificial proteins, typically around 7 kDa, derived from archaeal Sul7d proteins (Kalichuk *et al.*, 2016). Affitins demonstrate high avidity for molecular targets and also demonstrate higher stability and lower production costs than antibodies (Correa *et al.*, 2014).

This group produced gallic acid-triethylene glycol (GATG) dendrimers conjugated with an Affitin (C5) against staphylococcal protein A (SpA) displayed on the *S. aureus* cell surface (Fig 1.8). This 'Affidendron' was shown to selectively agglutinate *S. aureus* but not *S. epidermis*, *E. coli* or a SpA-deficient mutant of *S. aureus* confirming the specificity of the affidendrons for SpA (Vukojicic *et al.*, 2019). Furthermore, multivalent presentation of the C5 Affitin on the dendrimers facilitated an approximately three orders of magnitude in K_d compared to the monovalent affitin (108 nM C5 alone, 0.17 nM for the affidendron) in tandem with a slower dissociation rate multiple suggesting multiple epitope binding on the SPR chip and confirming the chelating properties of the designed nanoparticles (Vukojicic *et al.*, 2019).

Figure 1.8. Schematic of multivalent affidendron for *S. aureus* capture. *S. aureus* specific C5 affitin (green) conjugated to GATG dendrimer (red). FITC (stars) are also included for fluorescence imaging. Adapted from Vukojicic *et al*, 2019.

These materials were also shown to be potent inhibitors of *S. aureus* biofilm formation (Vukojicic *et al.*, 2019). This work suggests that affitin-conjugated materials could be a viable strategy for the selective isolation of bacteria but significantly more investigation is required to move beyond proof of concept. Principally, identification of specific affitins to various bacterial species would be required in addition to the demonstration of an absence of cross-reactivity in mixed populations as opposed to the pure cultures used by Vukojicic *et al*. Conjugation of affitins to magnetic particles may be an interesting avenue of investigation for the isolation of bacteria from mixed populations but thus far no reports using this techniques have appeared in the literature.

1.4. Selective confinement of bacteria using cell-encoded lectins and magnetic glyconanoparticles: A missed opportunity?

As shown in this review, a vast array of differing techniques and strategies have been employed for bacterial isolation. Both selective and non-selective techniques have been employed ranging from physical separation to precisely engineered materials featuring specific binding epitopes.

As lectins are natively expressed by microorganisms as part of cell-surface associated appendages, lectin-targeted materials could be utilised as the basis of novel selective sequestration techniques for bacterial strains routinely used in industrial scale biotechnology platforms. However, very few studies have attempted to utilise selective bacterial isolation techniques to selectively separate target bacteria from mixed populations, representing a significant gap in collective scientific knowledge. Additionally, to date no studies have used bacterial lectin-targeted magnetic nanomaterials to demonstrate selective isolation of bacteria from mixed populations.

Magnetic nanoparticles coated with high avidity, specific ligands of bacterial lectins, such as glycopolymers, may be useful for translating the success of earlier studies to specific extraction bacteria from mixed populations.

However, there is one factor which could seriously impede on the success of such a system: expression of many genes encoding lectins is phase variation dependent, and therefore subject to a high degree of stochasticity

(Schwan, 2011; Sokurenko *et al.*, 1997). Expression of the functional elements of bacterial fimbriae gene clusters under the control of synthetic, inducible promoters, without the phase variance components, would be desirable as this could be a potent strategy for the selective sequestration of particular strains in tandem with complementary magnetic glyconanoparticles.

1.5. Aims and Objectives

The aim of this study is to generate a novel platform technology which allows for the selective sequestration of bacteria from mixed populations using a combined strain engineering and materials science approach. This will be achieved by meeting the following objectives:

- Genetic modification of industrially relevant bacteria for controllable expression of surface-associated lectins
- Chromosomal tagging of bacterial strains with fluorescent protein expression systems to allow for bacterial population monitoring
- Synthesis of glycopolymers by RAFT polymerisation with reactive termini for functionalisation of iron oxide nanoparticles
- Synthesis of magnetic iron oxide nanoparticles and decoration with glycopolymers
- Growing co-cultures of industrially relevant bacteria and using magnetic glycomaterials for the selective isolation of one strain, monitored by flow cytometry.

2. Construction of an Anhydrotetracyline Inducible Fim Mutant and Constitutively Fluorescent Transposon Mutants in *Escherichia coli*

2.1. Introduction

2.1.1. FimH and Type 1 fimbriae in *E. coli*

Perhaps the best characterised fimbrial expression system identified in prokaryotes is the Type 1 fimbriae of *E. coli*. These organelles range in length typically between 1 and 2 microns and are 7 nm thick (Connell *et al.*, 1996). The extracellular portion of the organelle is composed of a right handed helical rod formed from repeating subunits of the FimA protein joined to the distal tip which contains the two adaptor proteins, FimG and FimF, bound to FimH, the mannose specific adhesin which can bind to mannose moieties present in glycoproteins (Krogfelt *et al.*, 1990; Mulvey *et al.*, 2001). FimH binds strongly to mannose residues with K_d values calculated at around 2.3 μM but has particularly high affinities for mannose polymers and aryl mannosides (Bouckaert *et al.*, 2005; Bouckaert *et al.*, 2006). However, expression, assembly and exportation of the fimbriae requires the concurrent expression of several other genes in a well-defined chaperone/outer membrane usher pathway.

FimC is a molecular chaperone which is part of the PapD superfamily of chaperones. Like other members of this family FimC has three primary functions: to guide the folding of the other fimbrial subunits as they pass through the cytoplasmic membrane, combining with subunits in the periplasm to form stable soluble chaperone-subunit complexes, and

protection of subunit active sites whilst in the periplasm (Mulvey *et al.*, 2001).

Once these subunit-chaperone complexes have formed, they are targeted to FimD, the outer membrane usher. This usher protein forms a channel 2-3 nm in diameter, which allows for the passage of fimbrial subunits and facilitates their exportation to the outer membrane (Mulvey *et al.*, 2001).

A further molecular component which is essential for the biosynthesis and assembly has been identified: FimI. While this protein appears to be necessary in type 1 fimbriae expression, as chromosomal mutations in FimI produce a non-fimbriated phenotype, the function of this particular element remains unresolved (Valenski *et al.*, 2003).

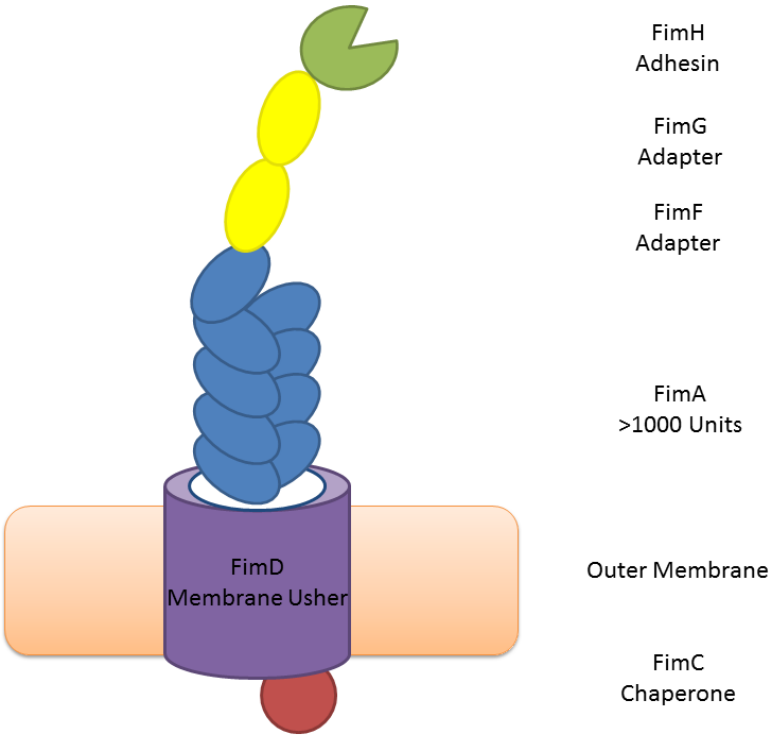

Figure 2.1. Schematic structural organisation of the Type 1 fimbriae in *E. coli*.

2.1.2. Genetic regulation of the *fim* operon in *E. coli*

In *E. coli* and other bacteria, Type 1 fimbriae are encoded by a contiguous chromosomal DNA segment under the control of a single promoter upstream of the primary structural gene *fimA* (Fig 2.2). This *fim* operon is under the control of a sophisticated regulatory circuit. In a given cellular population which possesses the genetic information for the production of adhesive fimbriae, individual cells are able to oscillate between a fimbriated and afimbriated state; this phenomenon, phase variation, occurs in regulatory circuits in other prokaryotes as well (Gally *et al.*, 1993; Holden *et al.*, 2007). Phase variation in the expression of Type 1 fimbriae is associated with the inversion of a 314-bp element, which has been dubbed the *fim* switch (*fimS*) (Schwan, 2011). This invertible switch contains the *fimA* promoter and thus the operon is active in one orientation (Phase-ON) and not (Phase-OFF) in the other. Furthermore the switching of this invertible element is not dependent on RecA; it instead requires recombination by FimB or FimE. The genes encoding these regulatory recombinases are located proximally upstream of the switch. FimB and FimE specifically recognise two 9 bp inverted repeats either side of the *fim* switch (Schwan, 2011). FimB catalyses the inversion of this switch in both directions at equivalent frequencies, whereas FimE catalyses inversion at a higher frequency than FimB and only in favour of the on to off recombination (Blomfield *et al.*, 1997; Gally, 2007; McClain *et al.*, 1991).

Further to this, these recombinases and the phase switch are subject to regulation by a range of global regulators which allow a particular cell to

appropriately respond to its environment by altering its fimbriation state. These global regulators which effect the expression of Type 1 fimbriae include the leucine-responsive regulatory protein Lrp (Blomfield *et al.*, 1993), *leuX*, which transcribes the tRNA specific for the rare leucine codon UUG (Newman *et al.*, 1994), the histone-like nucleoid-structuring protein H-NS (Olsen *et al.*, 1998), the IHF integration host factor proteins (Blomfield *et al.*, 1997), and the stationary phase sigma factor RpoS (Dove *et al.*, 1997). *fimB* and *fimE* both have their own promoters which have been previously characterised (Schwan, 2011). Three potential promoters have been identified for *fimB*: P1 and P2 have been identified in UPEC strains starting transcription respectively 148 and 288 bp upstream of the translational start site (Schwan *et al.*, 1994). A third potential promoter, P3, has also been characterised by this group, a further 650bp upstream of P2, but thus far this has yet to be confirmed by other authors (Schwan, 2011; Schwan *et al.*, 1994). So far only a single promoter has been identified for *fimE* (Olsen & Klemm, 1994).

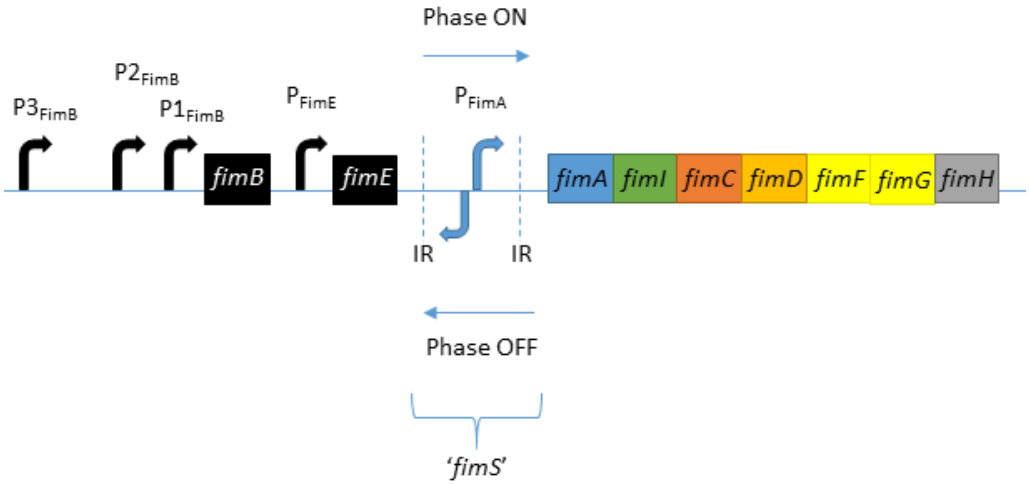

Figure 2.2. Schematic representation of the operonic structure of the *fim* gene cluster. Arrows indicate identified promoters. *fimB* and *fimE* are located upstream of the phase switch, designated *fimS*. The *fimS* switch is composed of the promoter for *fimA* (P_{fimA}) and two inverted repeats (IR). Inversion between these repeat elements is propagated by FimE and FimB, altering the transcription of the *fim* operon by induction of either the phase on or phase off state. The functional genes *fimA, fimI, fimC, fimD, fimF, fimG* and *fimH* are located downstream from the phase switch which carries the *fimA* promoter. Adapted from Schwan, 2011.

2.1.3. RNA polymerase recruitment, transcription factors and inducible promoter systems

The regulation of all bacterial gene expression is initially governed by recruitment of RNA polymerase (RNAP), the multi-domain enzyme complex responsible for the transcription of DNA to messenger RNA (mRNA), (Browning & Busby, 2004). Promoters are sequence elements found upstream of functional genes within bacterial genomes which contain structural elements, essentially the -35 and -10 sites, which are recognised by the σ subunit (sigma factor) of the RNAP. Once bound to DNA, sigma factors recruit the α and β subunits of the RNA polymerase to form the holoenzyme and begin transcription at nucleotide +1. Different promoters may have varying affinity for different sigma factors depending on their -10 and -35 sequences, with those approaching the consensus sequence for the housekeeping sigma factor σ^{70} operating the most efficiently (-35: TTGACA; -10: TATAAT) (Shimada *et al.*, 2014). As such, promoter sequence can be viewed as the primary determinant for RNAP recruitment and differential gene expression levels.

However, few promoters contain all of the structural elements involved in RNA polymerase holoenzyme recruitment or conform to the consensus σ^{70} sequence. Consequently, for the transcription of many genes the presence or absence of additional sigma/anti-sigma factors and additional transcription factors, may be required.

Transcription factors affect the recognition of promoters by the σ factors or the α subunit C-terminal domains by forming DNA-protein and protein-

protein interactions with both promoter DNA and RNAP. These interactions may bring the holoenzyme into close proximity with transcriptional promoters or sterically hinder RNA polymerase from access to promoter sites (Browning & Busby, 2004; Lee *et al.*, 2012). Transcription factors may also affect transcription initiation rates by changing the conformation of template DNA (Browning & Busby, 2004; Lee *et al.*, 2012).

Transcription factors may also be modulated, adding a further level of complexity to the regulation of transcription initiation. For example, the DNA-binding activity of the *lac* repressor LacI is modulated by the presence of a small ligand, lactose, such that repression of transcription of the *lac* operon is relieved by environmental presence of this disaccharide (Becker *et al.*, 2013). Many such ligand-responsive transcription factors have been described. Some response regulators, may only bind to their target DNA site when phosphorylated by their cognate sensor kinase – as in the case of NarL, the nitrite response regulator protein, which is activated by the sensor kinases NarX and NarQ in response to nitrite/nitrate (Darwin & Stewart, 1995). In such ways transcription factors can be coupled to external stimuli, thus allowing bacterial gene expression to be regulated based on environmental cues.

For the synthetic biologist, precise control over recruitment of RNA polymerase to a particular gene of interest, and hence expression of the desired gene, may be achieved by the construction of gene expression cassettes which are controlled by a promoter regulated by a transcriptional repressor modulated by a small ligand. Of these inducible promoters, the

most used are the *tetA* promoter, the arabinose inducible P_{BAD} promoter and the *tac* promoter, a synthetic hybrid promoter formed by fusion of the *trp* and *lac* promoters (Brosius *et al.*, 1985; De Boer *et al.*, 1983; Guzman *et al.*, 1995; Skerra, 1994). Furthermore, significant effort has been invested in the analysis of native and construction of synthetic promoters, constitutive and otherwise, for heterologous gene expression in a range of industrially relevant microorganisms ranging from *E. coli* and *Saccharomyces cerevisiae* to *Pseudomonas spp*., *Cupriavidus spp*.and *Geobacter* spp amongst others (Alagesan *et al.*, 2018; De Mey *et al.*, 2007; Elmore *et al.*, 2017; Johnson *et al.*, 2018; Krushkal *et al.*, 2009; Machens *et al.*, 2017; Sanches-Medeiros *et al.*, 2018; Wang *et al.*, 2019)

The *tetA* promoter is particularly useful for gene expression in *E. coli* due to its tight regulation and high level of heterologous protein production (Skerra, 1994). Furthermore, an analogue of tetracycline, the ligand of the *tet* repressor protein TetR, is available which binds to the ligand binding domain of the repressor with a 35-fold higher affinity than the native ligand and also exhibits little antibiotic activity (100-fold lower than tetracycline) (Degenkolb *et al.*, 1991). Using anhydrotetracycline (ATc) at concentrations of 50 ng/ml and above is sufficient for full induction of gene expression from this promoter with no deleterious effects on growth of *E. coli* (Lutz & Bujard, 1997).

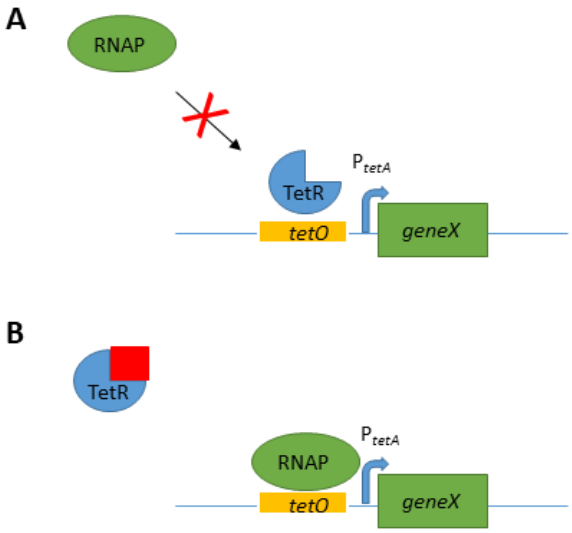

Figure 2.3. Inducible gene expression from the *tetA* promoter. A) In the absence of the autoinducer ATc (red square) the transcription factor TetR binds to the *tet* operator (*tetO*) precluding RNA polymerase (RNAP) from promoter recognition by steric hinderance. B) In the presence of the autoinducer, TetR is unable to bind to *tetO* and transcription from the promoter of *geneX* proceeds unhindered. *tetR* is constitutively transcribed from its native promoter and often supplied at a site distal to the *tetA* promoter.

2.1.4. Precision engineering of prokaryotic genomes

In order to suitably control the expression of native bacterial lectin-bearing organelles, such as the Type 1 fimbriae, it is necessary to precisely alter the genome of bacterial strains bearing these transcriptional units. Some techniques for precision genome editing, in addition to their merits and flaws, are discussed herein.

Allelic exchange is an efficient and versatile method for bacterial genome editing which exploits the ability of native recombinases, principally the RecBCD/RecA pathway, to incorporate plasmid derived homologous DNA onto the bacterial chromosome (Claverys *et al.*, 2009; Hmelo *et al.*, 2015). In most reported techniques an allelic exchange vector is constructed with

a copy of the gene of interest, modified as desired, as well as flanking regions either side of this gene which have homology to regions flanking the gene of interest on the chromosome. Allelic exchange vectors are constructed as suicide vectors, containing origins of replication that are not functional in the strain which they are designed to mutate. For allelic exchange in *Pseudomonas spp*. the ColE1 replicon, which will replicate in *E. coli* but not *Pseudomonas* has routinely been used (Hmelo *et al.*, 2015). For allelic exchange in *E. coli* temperature sensitive origins of replication, such as pSC101, or those requiring an exogenous replicative protein, namely the R6K *ori* with *pir* provided on a defective prophage are utilised (Blomfield *et al.*, 1991; Simon *et al.*, 1983). The rate at which RecA-mediated homologous recombination occurs increases with increasing homologous sequence length; hence a flanking homology arm length of ≥500 bp is often utilised for high efficiency (Morel *et al.*, 1994). These recombination plasmids may then be introduced into the host via electroporation or conjugal transfer. However, since most of the vectors described in the literature contain the origin of transfer, *oriT*, from pRP4, and may be mobilized by conjugation, conjugal transfer is preferred due to higher efficiency of plasmid transfer and recombination rates.

After transfer, the recipient strain is challenged against the antibiotic marker present on the suicide plasmid. Only those cells which have undergone a homologous recombination event, thus integrating the plasmid backbone onto the chromosome, will be resistant and develop as colonies as the vector is unable to replicate in the host.

After integration of the plasmid in the host chromosome a small subset of isolated merodiploids will be allowed to undergo a second homologous recombination event excising the plasmid from the chromosome. Secondary recombination events are typically selected for by the inclusion of a counter-selectable marker. Although many have been utilised the most common counter selectable marker is *sacB* from *Bacillus subtilis*, which confers acute sucrose sensitivity (Pelicic *et al.*, 1996). After a second crossover only those bacterial cells which have excised and lost the plasmid should be able to proliferate on sucrose-supplemented media. Two genotypes may result from successful counter-selection after the second homologous recombination: return to the wild type allele or replacement of the wild type allele by the mutant one in the chromosome (Fig. 2.4.). The resulting clones are then screened by PCR to discriminate unwanted wild type from wanted recombinant clones.

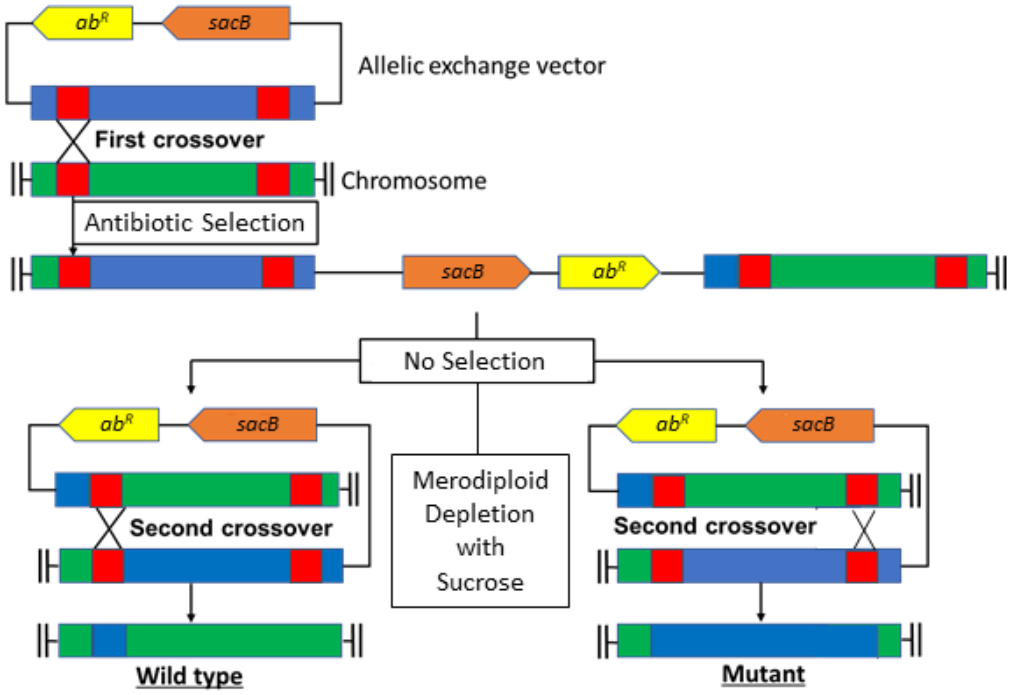

Figure 2.4. Construction of genomic mutations by double-crossover homologous recombination. A suicide vector bearing the desired mutation flanked by regions of homology to the chromosome is delivered to the recipient strain via conjugal transfer. After the first crossover, antibiotic selection is used to screen for merodiploids. Isolated merodiploids are then grown in non-selective media to facilitate the rare second recombination event. Sucrose counter-selection is then utilised to select double crosses from merodiploids by the conditional lethality of *sacB*. The locus at which the second crossover occurs determines whether the wild type allele is restored or if the desired allele is replaced in the bacterial chromosome and may be differentiated by PCR screening. Adapted from Hmelo *et al* (Hmelo *et al.*, 2015). Chromosomal DNA shown in green, plasmid sourced DNA shown in blue, regions of homology between vector and chromosome shown as red squares.

Allelic exchange poses some distinct advantages in terms of prokaryotic genome modification. This technique is able to generate precise, scarless and unmarked mutations at various loci within prokaryotic genomes which may be determined by the operator. These genetic alterations can target most genomic sites and can be performed with single nucleotide precision (Philippe *et al.*, 2004). Other systems have successfully utilised Flp-*FRT* or Cre-*loxP* recombination to remove a selectable marker after allelic exchange vector integration onto the chromosome (Hoang *et al.*, 1998;

Quenee *et al.*, 2005). However, use of non-native recombinases requires additional genomic manipulation to achieve and retains the exogenous Flp/Cre recombinase recognition sites on the chromosome which could generate polar effects on neighbouring genes. Furthermore, expression of a non-native recombinase may lead to aberrance in recombination events. Other prokaryotic gene replacement systems have been devised which use the λ Red recombinase system (Datsenko & Wanner, 2000; Kim *et al.*, 2014). This recombinase is more efficient than native bacterial recombinases yielding mutants with increased frequency and catalysing homologous recombination with homology arms as short as 9 bp (Fujimoto *et al.*, 2009). However construction of cassettes for λ Red recombination requires far more laborious cloning processes to generate mutant alleles. Furthermore, the recipient must express the λ Red recombinase genes *gam, bet* and *oxo* prior to receipt of the donor vector. λ Red recombinase expression requires the delivery of an additional λ Red expressing plasmid prior to mutation and once again risks the possibly of off-site recombination events occurring due to the expression of a non-native recombination complex.

While allelic exchange is a versatile and powerful tool with decades of successful application it does suffer from some distinct limitations. As allelic exchange depends on native recombinase proteins to occur, this procedure cannot be used to modify bacteria which are recombination-deficient (such as *ΔrecA* strains of *E. coli*). Furthermore, recombination occurs at different frequencies between different bacterial strains. Hence multiple cassettes with differing homology arm lengths may have to be

cloned to generate the desired mutation. Furthermore, genes which are essential for growth may not be targeted by this system as their disruption will be lethal.

Transposons represent mobile genetic elements which are able to integrate into chromosomal or extrachromosomal DNA at sites which lack homology by self-encoded recombinases called transposases and change their position within a genome (Bourque *et al.*, 2018). Genomic data from a wide array of biological taxa and ecosystems have demonstrated that that transposase encoding genes are the most abundant and ubiquitous in nature (Aziz *et al.*, 2010). Furthermore, transposable elements or their artefacts have been found in all organisms analysed genomically and may comprise up to 45% of the human genome (Lander *et al.*, 2001; Munoz-Lopez & Garcia-Perez, 2010). While random transposon mutagenesis using non-selective transposons has been pivotal for the determination of gene function and antibacterial target identification these techniques are not applicable to the construction of precise genomic alterations (Melnyk *et al.*, 2014; Meredith *et al.*, 2012).

In bacteria a uniquely refined transposon, Tn7, has evolved two distinct transposition pathways to promote its propagation between bacterial cells or within bacterial genetic material (Fig. 2.5.) (Craig, 1991). A TnsABCE mediated non-selective pathway and a TnsACBD pathway which integrates at a single, highly conserved site in bacterial chromosomes (Peters & Craig, 2001).

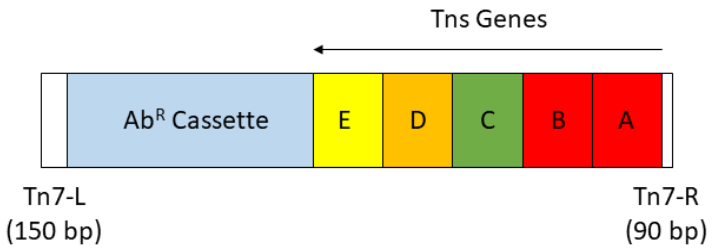

Figure 2.5. Structure of Tn7 transposon. Tn7 has two distinct left and right ends (Tn7-L and R) which facilitates integration which a characteristic orientation. Each Tn7 end contains 22 bp transposase binding sites (3 in Tn7-L and 4 in Tn7-R). The *tnsABCDE* transposition genes are encoded at the right end of the transposon typically contains antibiotic resistance cassettes. Adapted from Peters and Craig (2001).

The transposon encodes five proteins involved in transposition: TnsA, TnsB, TnsC, TnsD and TnE (Peters & Craig, 2001). The heteromeric TnsAB complex forms the key transposase, with TnsA mediating DNA cleavage at the 5' ends of the Tn7 transposon. TnsB mediates DNA cleavage at the 3' ends of the transposon (Sarnovsky *et al.*, 1996). TnsC appears to be an ATP-dependant DNA-binding protein and interacts with TnsAB and hydrolyses ATP to promote the transposition process (Stellwagen & Craig, 2001). TnsD and TnsE are proteins involved in transposition target selection. TnsABCE promotes transposition with relatively little site selection, but with a peculiar preference for conjugal plasmids which can mobilise between cells, presumably facilitating the promiscuous propagation of the transposon between cells and at multiple, random sites (Wolkow *et al.*, 1996).

Conversely, TnsABCD catalysed transposition facilitates insertion into a specific DNA sequence. TnsD is a sequence specific DNA-binding protein which recognises *attTn7*, a transcriptional terminator sequence in the 3'

end of *glmS*, a gene which is highly conserved gene across bacterial species due to its role in glutamate synthesis (Gay *et al.*, 1986). However, the actual transposon insertion point lies downstream of *attTn7* and hence Tn7 insertion via the specific pathway does not disrupt the essential gene *glmS* and does not appear to have any deleterious effect on the host (Choi *et al.*, 2005; Peters & Craig, 2001).

While the native Tn7 is excessively large for genomic engineering, 'mini-Tn7' systems have been devised that separate the transposable element and the TnsABCD machinery onto distinct suicide plasmids. Use of mini-Tn7 systems allows for the transposition of smaller Tn7R/L flanked constructs onto the chromosome using only the site specific TnsABCD pathway, without chromosomal integration of the transposases. Such mini-Tn7 systems have been exploited for the site-specific insertion of genetic constructs into the chromosome for a variety of bacterial species including *E. coli, Salmonella spp*., *Klebsiella spp*., *Cronobacter spp*., *Xanthomonas spp*., *Pseudomonas spp*. and *Yersinia pestis* (Choi *et al.*, 2005; Crepin *et al.*, 2012; Jittawuttipoka *et al.*, 2009). These systems are highly applicable to the tagging of bacterial cells with fluorescent proteins by integrating a single copy of a fluorescent protein transcriptional unit onto the chromosome at a non-deleterious site (Lambertsen *et al.*, 2004). They may also limit some of the issues which arise from the delivery of such cassettes on a multicopy plasmid due to plasmid copy number heterogeneity across a population (Ghozzi *et al.*, 2010; Ng *et al.*, 2010). Mini-Tn7s are also routinely used as a more robust alternative to chromosomal complementation by

reintroducing functional copies of deleted or mutated genes on a recombinant plasmid (Crepin *et al.*, 2012; Jittawuttipoka *et al.*, 2009; LoVullo *et al.*, 2009). A single copy Tn7 chromosomal insertion may be preferable to plasmid complementation due to poor plasmid retention, gene copy number effects, and better comparability to the parental strain in which the gene of interest has not been mutated or deleted. Furthermore, integrating a transposable element onto the chromosome of a target organism which is devoid of any transposon machinery in the absence of a suicide plasmid ensures stable integration of the construct. Crucially however, mini-Tn7 mediated chromosomal insertions are limited to a single copy at one, pre-defined chromosomal locus; other locations may not be targeted.

CRISPR-Cas9 systems have come under particular attention in recent years for genomic editing due to the versatility these systems offer – potentially allowing for precise genome alteration across myriad organisms (Doudna & Charpentier, 2014). These advances have had greater significance in the case of eukaryotic genome editing where the existing tools available have been more limited.

Clustered regularly interspaced short palindromic repeats (CRISPR) were first identified as short palindromic sequences in the *E. coli* genome but bioinformatics quickly identified similar CRISPR loci in a range of bacteria and archaea (Ishino *et al.*, 1987; Mojica *et al.*, 2000). Further investigation of this phenomenon suggested that these palindromic repeat sequences where extrachromosomal in origin, and bacterial susceptibility to phage

infection was correlated with the number of repeat sequences in these loci (Bolotin *et al.*, 2005). In tandem with this discovery it was shown that CRISPR loci were transcribed and that CRISPR associated genes (*cas* genes) encode proteins with putative nuclease domains (Haft *et al.*, 2005; Tang *et al.*, 2002). These findings led to the prevailing hypothesis that CRISPR loci and their associated nucleases may function as a prokaryotic analogue of adaptive immunity where sequences acquired from previous infections could be targeted for cleavage using antisense RNAs, thus providing defence against genetic parasites such as phage. In 2008 short RNAs, termed CRISPR RNAs (crRNAs), where shown to guide theses nucleases to the genetic material of invading viruses, leading to its cleavage (Brouns *et al.*, 2008). Three distinct CRISPR systems have been described so far in the literature with type I and II systems using an assortment of CRISPR-associated proteins for crRNA-guided targeting and cleavage (Nam *et al.*, 2012). In contrast the type II system uses a single protein, Cas9, for crRNA-guided DNA recognition and cleavage improving the utility of this system for genome editing (Jinek *et al.*, 2012). However the type II CRISPR/Cas9 system from *Streptomyces pyogenes* also requires a trans-activating CRISPR RNA (tracrRNA) for maturation of guiding crRNAs (Deltcheva *et al.*, 2011). The dual tracrRNA:crRNA complex has since been replaced by a chimeric single guide RNA (sgRNA) which retains the 20-nucleotide sequence on the 5' end which will bind to the target site by complimentary base pairing and the hairpin-like structure at the 3' end which coordinates Cas9 (Jinek *et al.*, 2012).

CRISPR based genome editing systems exploit the nuclease activity of Cas9 and the targeting ability of synthetic sgRNA to induce double stranded breaks in genomic DNA. These breaks may then be repaired by non-homologous end joining (NHEJ), leading to deletions, or by homology-directed repair (HDR), when an exogenous homologous repair template is supplied, thus producing insertions or replacements (Gratz *et al.*, 2014; Su *et al.*, 2016).

CRISPR/Cas9 has since been utilised to produce precise genomic alterations in bacteria, plants, insects and eukaryotes including human germ cells (Gratz *et al.*, 2014; Jiang *et al.*, 2013a; Mali *et al.*, 2013; Tang *et al.*, 2017; Xing *et al.*, 2014). Furthermore, targeting multiple sequences for genome editing at once by delivery of multiple sgRNAs has been achieved with the CRISPR/Cas9 allowing for multiplex genome editing strategies to be employed with this technique in both prokaryotes and eukaryotes (Cobb *et al.*, 2015; Cong *et al.*, 2013; Xing *et al.*, 2014).

While broad in scope and programmability, CRISPR/Cas9 based genome editing is not without its flaws. Sequences which can be targeted by an sgRNA must be followed by a protospacer adjacent motif (PAM), a 2-6 bp sequence, canonically 5'-NGG-3' for Cas9 (Shah *et al.*, 2013). PAM specificity somewhat limits the availability of sites which may be targeted by CRISPR/cas9, however Kleinstiver and co-workers have attempted to alter the PAM requirements of the Cas9 protein to minimise the impact of this limitation (Kleinstiver *et al.*, 2015). The prokaryotic enzymes responsible for NHEJ (Ku/LigD), which has been extensively used for eukaryotic

genomic deletions via CRISPR/Cas9, are not encoded by many bacterial genomes including *E. coli* (Bowater & Doherty, 2006). Hence CRISPR/Cas9 may not be suitable for the construction of genomic deletion mutants in many bacterial species.

Prokaryote engineering by CRISPR/Cas9 requires the delivery of sgRNA, Cas9 and homologous template, typically as transcriptional units on plasmid vectors. Such multi-component systems may require cumbersome cloning and/or delivery of multiple vectors, with tedious optimisation to achieve efficient genome alteration. Some one-vector systems have been developed but these are likely to be highly specific to the intended host strain (Berlec *et al.*, 2018). Furthermore, genome engineering of bacteria via homologous recombination can already be achieved by allelic exchange, a well-established and far less technically challenging method.

Finally, off target mutagenesis events and mosaicism has been observed in human cells which have been modified by CRISPR/Cas9 systems, suggesting this technique may not offer the specificity required for precise genome editing (Fu *et al.*, 2013; Liang *et al.*, 2015).

2.1.5. Chapter aims

This chapter describes the generation of a novel, inducible mutant of the Type 1 Fimbriae in *E. coli* to provide control over the expression of this sugar-binding organelle by replacement of the native regulon with the *tetR*-P_{tetA} inducible system by allelic exchange, thus facilitating switchable binding of bacterial cells to glyconanoparticles. Furthermore, generation of a battery of autofluorescent mutants of key *E. coli* strains by Tn7-mediated transposon insertion mutagenesis is also desired so that there population dynamics could be feasibly monitored by flow cytometry.

2.2. Materials and Methods

2.2.1. Bacterial strains, media and growth conditions

2.2.1.1. Liquid growth media

Lysogony broth (LB) contained 10 g/L tryptone, 5 g/L yeast extract and 10 g/L NaCl dissolved in reverse osmosis (RO) water. M9 minimal media supplemented with fructose as a carbon source (M9F) contained 0.4% D-fructose, 240.7 mg/L MgSO4, 11.098 mg/L CaCl2 and a selection of salts, previously made up as a 5x stock, with a final concentration of 12.8g/L $Na_2HPO_4.7H_2O$, 3 g/L KH_2PO_4, 0.5 g/L NaCl and 1 g/L NH_4Cl. Media was sterilised by autoclaving at 121 °C and 15 psi prior to use.

2.2.1.2. Solid growth media

Solid growth media was prepared as per liquid media described in Section 2.1.1.1. with the addition of 15 g/L bacteriological agar No. 1 (Oxoid). Solid media was sterilised by autoclaving at 121 °C and 15 psi, then allowed to cool to ~50 °C before the addition of antibiotics and other supplements. Agar plates were prepared by pouring ~20 mL molten agar media into a Petri dish under aseptic conditions and allowed to set at room temperature. Agar plates were dried and stored at 4 °C prior to use.

2.2.1.3. Antibiotics

Antibiotic stock solutions were added to liquid and solid media where appropriate to give the working concentrations: 100 μg/mL Ampicillin (Amp); 25 μg/mL Chloramphenicol (Cm); 25 μg/mL Kanamycin (Km); 15 μg/mL Trimethoprim (Trim) and 20 μg/mL Tetracycline (Tet). Ampicillin and kanamycin were prepared by dissolving the antibiotic powder in distilled water and then filter sterilised with a 0.22 μM PES filter. Chloramphenicol was dissolved in 100% ethanol, Trimethoprim in Dimethyl Sulfoxide (DMSO) and Tetracycline in 50% ethanol. All antibiotic stock solutions were stored at -20 °C.

2.2.1.4. Bacterial strains and storage

The bacterial strains used in this study are documented in Table 2.1. Bacteria were isolated to clonal populations by streaking to obtain single colonies on LB agar plates supplemented with the appropriate antibiotics. Bacterial strains were grown by overnight incubation at 37 °C with aeration (200 rpm) unless otherwise stated. Glycerol stocks of bacterial strains were prepared for long term storage. A 1 mL aliquot of an overnight culture of the strain on interest was mixed with 1 mL of sterile 50% glycerol and transferred to a sterile 2 mL screw cap tube. These stocks were then stored at -80 °C.

Table 2.1. Bacterial strains used in this study.

Strain	Characteristics	Source or Reference
MG1655	Wild type E. coli K-12 F-, λ-, rph	(Blattner et al., 1997)
DH5α	Plasmid propagation strain. fhuA2 lac(del)U169 phoA glnV44 Φ80' lacZ(del)M15 gyrA96 recA1 relA1 endA1 thi-1 hsdR17	Invitrogen
JW4283-3	E. coli K-12 F-, λ-, rph-, Δ(araD-araB)567, ΔlacZ4787(::rrnB-3), Δ(rhaD-rhaB)568, ΔfimH788::kan, hsdR514	(Baba et al., 2006)
S17-1(λpir)	λpir lysogen of S17-1 used for conjugal mating plasmid transfer (Tpr Smr thi pro hsdR hsdM recA RP4::2-Tc::Mu-km::Tn7)	(Simon et al., 1983)
ST18	S17-1(λpir) ΔhemA	(Thoma & Schobert, 2009)
JEP01	Anhydrotetracycline inducible mutant of fim operon in E. coli MG1655 ΔfimBEPfimA::tetR PtetA	This study
JEP01::P11Ruby	Tn7 insertional mutant of JEP01 bearing P11 controlled constitutive mRuby2 expression cassette downstream of glmS	This study
JEP01::P24Ruby	Tn7 insertional mutant of JEP01 bearing P24 controlled constitutive mRuby2 expression cassette downstream of glmS	This study
JEP01::P11Neon	Tn7 insertional mutant of JEP01 bearing P11 controlled constitutive mNeonGreen expression cassette downstream of glmS	This study
JEP01::P24Neon	Tn7 insertional mutant of JEP01 bearing P24 controlled constitutive mNeonGreen expression cassette downstream of glmS	This study
MG1655::P11Ruby	Tn7 insertional mutant of MG1655 bearing P11 controlled constitutive mRuby2 expression cassette downstream of glmS	This study
MG1655::P24Ruby	Tn7 insertional mutant of MG1655 bearing P24 controlled constitutive mRuby2 expression cassette downstream of glmS	This study
MG1655::P11Neon	Tn7 insertional mutant of MG1655 bearing P11 controlled constitutive mNeonGreen expression cassette downstream of glmS	This study
MG1655::P24Neon	Tn7 insertional mutant of MG1655 bearing P24 controlled constitutive mNeonGreen expression cassette downstream of glmS	This study
JW4283::P11Ruby	Tn7 insertional mutant of JW4283-3 bearing P11 controlled constitutive mRuby2 expression cassette downstream of glmS	This study
JW4283::P24Ruby	Tn7 insertional mutant of JW4283-3 bearing P24 controlled constitutive mRuby2 expression cassette downstream of glmS	This study
JW4283::P11Neon	Tn7 insertional mutant of JW4283-3 bearing P11 controlled constitutive mNeonGreen expression cassette downstream of glmS	This study

JW4283::P24Neon	Tn7 insertional mutant of JW4283-3 bearing P24 controlled constitutive mNeonGreen expression cassette downstream of glmS	This study
JEP01::P11eGFP	Tn7 insertional mutant of JEP01 bearing P11 controlled constitutive eGFP expression cassette downstream of glmS	This study
JEP01::P24eGFP	Tn7 insertional mutant of JEP01 bearing P24 controlled constitutive eGFP expression cassette downstream of glmS	This study
MG1655::P11eGFP	Tn7 insertional mutant of MG1655 bearing P11 controlled constitutive eGFP expression cassette downstream of glmS	This study
MG1655::P24eGFP	Tn7 insertional mutant of MG1655 bearing P24 controlled constitutive eGFP expression cassette downstream of glmS	This study
JW4283::P11eGFP	Tn7 insertional mutant of JW4238-3 bearing P11 controlled constitutive eGFP expression cassette downstream of glmS	This study
JW4283::P24eGFP	Tn7 insertional mutant of JW4283-3 bearing P24 controlled constitutive eGFP expression cassette downstream of glmS	This study

2.2.1.5. Plasmids

Purified plasmid DNA was obtained using the 'miniprep' procedure as described in 2.2.3 and stored at -20 °C . For longer term storage plasmid DNA was transformed into electrocompetent DH5α as described below and stored as glycerol stocks at -80 °C. Plasmids used in this study are listed in table 4.2. below. Detailed plasmid maps, drawn in SnapGene, are available in Appendix 1.

Table 2.2. Plasmids used in this study.

Plasmid	Characteristics	Reference
pDM4(Cm)	Suicide vector for construction of deletion mutants by double crossover homologous recombination. sacBR; oriR6K; CmR .	(Milton et al., 1996)
pMKFimAE	Synthetic fim allelic exchange mutation cassette from GeneART synthesis in cloning vector pMK-RQ. KanR.	This study
pDM4FimAE	Suicide vector for construction of anhydrotetracycline inducible mutant of the fim operon in Escherichia coli	This study
pSW002-Pc-mRuby2	Source of mRuby2	(Wilton et al., 2018)
pSW002-Pc-mNeonGreen	Source of mNeonGreen	(Wilton et al., 2018)
pBBR1-P11-eYFP	Source of P11 insulated strong constitutive promoter	(Alagesan et al., 2018)
pBBR1-P24-eYFP	Source of P24 insulated very strong constitutive promoter	(Alagesan et al., 2018)
pBBR1-P11mRuby2	pBBR1-P11-eYFP, eYFP replaced by mRuby2 as EcoRI/BamHI fragment	This study
pBBR1-P24mRuby2	pBBR1-P24-eYFP, eYFP replaced by mRuby2 as EcoRI/BamHI fragment	This study
pBBR1-P11mNeonGreen	pBBR1-P11-eYFP, eYFP replaced by mNeonGreen as EcoRI/BamHI fragment	This study
pBBR1-P24mNeonGreen	pBBR1-P24-eYFP, eYFP replaced by mNeonGreen as EcoRI/BamHI fragment	This study
pBBR1-P11eGFP	pBBR1-P11-eYFP, eYFP replaced by eGFP as EcoRI/BamHI fragment	This study
pBBR1-P24eGFP	pBBR1-P24-eYFP, eYFP replaced by mNeonGreen as EcoRI/BamHI fragment	This study
pGP-Tn7-Cm	Chloramphenicol resistant suicide vector for Tn7 insertional transposon mutagenesis	(Crepin et al., 2012)
pSTNSK	Helper vector for Tn7 insertional transposon mutagenesis. Ori pSC101, tnsABCD, KmR	(Crepin et al., 2012)
pGP-Tn7-Cm-P11mRuby2	pGP-Tn7-Cm with P11mRuby2 cassette inserted as XhoI/NsiI fragment	This study
pGP-Tn7-Cm-P24mRuby2	pGP-Tn7-Cm with P24mRuby2 cassette inserted as XhoI/NsiI fragment	This study
pGP-Tn7-Cm-P11mNeonGreen	pGP-Tn7-Cm with P11mNeonGreen cassette inserted as XhoI/NsiI fragment	This study
pGP-Tn7-Cm-P24mNeonGreen	pGP-Tn7-Cm with P24mNeonGreen cassette inserted as XhoI/NsiI fragment	This study
pGP-Tn7-Cm-P11eGFP	pGP-Tn7-Cm with P11eGFP cassette inserted as XhoI/NsiI fragment	This study
pGP-Tn7-Cm-P24eGFP	pGP-Tn7-Cm with P24eGFP cassette inserted as XhoI/NsiI fragment	This study

2.2.2. Bacterial transformations

2.2.2.1. Preparation of electrocompetent *Escherichia coli*

A 5 mL aliquot of LB was inoculated with the appropriate *E. coli* strain and incubated overnight at 37 °C with aeration (200 rpm). 1 mL of this culture was then used to inoculate 500 mL of fresh LB and incubated at 37 °C to OD_{600} 0.4-0.6. This culture was then divided equally between 6 Corning 250 mL sterile centrifuge bottles and centrifuged at 4 °C for 5 minutes at 3500 x g. The supernatant was discarded and each pellet resuspended in 10 mL of ice cold, sterile glycerol MOPS (3-(N-morpholino)propanesulfonic acid) solution (10%, 1 mM respectively). This suspension was divided between two Falcon 50 mL Conical Centrifuge Tubes and centrifuged at 4 °C for 5 mins at 10,367 rcf. Each pellet was then resuspended in 40 mL ice cold glycerol MOPS solution before centrifugation at 4 °C for 5 mins at 10,367 rcf. Each pellet was then resuspended in 5 mL ice cold glycerol MOPS solution and pooled into a single 50 mL conical centrifuge tube. This solution was centrifuged at 4 °C for 5 mins at 10,367 rcf and the supernatant was removed. The pellet was then suspended in a volume of ice cold glycerol MOPS solution roughly equivalent to the volume of the pellet. The electrocompetent cells were distributed in 50 µL aliquots and snap frozen in liquid nitrogen. These aliquots were stored at -80 °C until required.

2.2.2.2. Electroporation of *Escherichia coli* and transformation with plasmid DNA

For electroporation a 50 µL aliquot of competent cells were thawed on ice. Once thawed, 100 ng of DNA of interest was added to the cells and gently mixed by pipetting. This cell/DNA suspension was then transferred to a 2 mm electroporation cuvette such that the electrodes were equally covered and no air bubbles were present. The electroporation cuvette was transferred to a Bio-Rad Micropulser electroporation apparatus and the sample pulsed with 2.5 kV. Following exposure to a pulse of electric current the cell/DNA solution was transferred to a 1.5mL Eppendorf tube. 950 µL of sterile LB was then added and the culture incubated for 1 hour to facilitate recovery of the cells and expression of antibiotic resistance genes. 200 µL aliquots were spread onto appropriate selective agar plates then incubated overnight at 37 °C.

2.2.3. Recombinant DNA techniques

2.2.3.1. Extraction of genomic DNA without RNA

A culture inoculated with the strain of interest was grown overnight at 37 °C with aeration (200 rpm). A 1.5 mL aliquot of this overnight culture was then centrifuged at 10,000 x g for 2 mins and resuspended in 400 µL TE buffer (Tris-HCl 10 mM, EDTA 1 mM, adjusted to pH 8). After centrifugation 50 µL Sodium Dodecyl Sulphate (SDS), 50 µL Proteinase K and 10 µL RNAse A were added. This mixture was then incubated for >3 hours at 37 °C . Once the cells had been lysed the solution was vortexed intensely for at least 1 min to fragment the genomic DNA. The volume was then increased to 700 µL. 700 µL of phenol:chloroform:Isoamyl alcohol (25:24:1, pH8) was added and the aqueous phase extracted >3 times with phenol:chloroform:isoamyl alcohol until the aqueous phase appeared clear. Nucleic acids were then precipitated by adding 2.5 volumes of ice cold 100% ethanol and mixing well by inversion until DNA was observable. The solution was then centrifuged at 10,000 x g for 10 minutes to pellet the DNA. The pellet was then washed once with 70% ethanol and dried briefly under vacuum prior to resuspension in 100 µL sterile dH_2O.

2.2.3.2. Extraction of plasmid DNA using the GenElute miniprep kit (Sigma Aldritch)

An overnight culture of a strain carrying the plasmid of interest was grown in 5 mL LB broth supplemented with the appropriate antibiotics. Plasmid DNA was then extracted from the culture using the GenElute miniprep kit following the manufacturer's instructions.

2.2.3.3. Agarose gel electrophoresis of DNA

DNA fragments were separated using gel electrophoresis for visualisation or isolation and extraction. Agarose gels were prepared by dissolving molecular biology grade agarose in 1 x Tris-Acetate-EDTA (TAE) buffer, containing 40 mM Tris base, 20 mM acetic acid and 1 mM EDTA, to a concentration of 1% (m/v) and briefly boiling in a microwave. Water loss was monitored by weighing by difference and compensated by the addition of RO water. The agarose was stained with SYBR Safe DNA Gel Stain (Thermo Scientific) at a concentration of 0.01% (v/v). The molten agarose solution was then poured into a gel casting cassette and allowed to set a room temperature. DNA samples for electrophoresis where mixed with Purple Gel Loading Dye (6x) (New England Biolabs) and loaded into the gel. Gels were run in 1 x TAE buffer at 100 V for 30 min to 1 hour. Gels were visualised using the Gel Doc XR+ transilluminator system (BioRad). 100 bp ladder or 1 kb ladder (New England Biolabs/Promega) were included as size standards as appropriate.

2.2.3.4. Extraction of DNA from agarose gels using the Monarch Gel Extraction Kit (New England Biolabs)

Bands of DNA of interest were excised from a 1% agarose gel stained with SybrSafe with a sterile razor blade with UV illumination. DNA was extracted from the gel fragment using the Monarch Gel Extraction kit following the manufacturer's instructions.

2.2.3.5. DNA amplification by polymerase chain reaction (PCR)

The polymerase chain reaction was used to amplify specific DNA fragments for use in molecular cloning techniques. For example, the mutation cassette from plasmid pMKFimAE, for use in the double crossover homologous recombination genomic mutation method, was amplified with primers which were specific for the mutation cassette to demonstrate the presence of the mutation cassette in this construct. A typical PCR 25 µL reaction was set up containing: 0.25 µL Q5 High-Fidelity DNA Polymerase (NEB), 5 µL 5X Q5 Reaction Buffer, 0,5 µL 10 mM dNTPs, 1.25 µL 10 µM Forward Primer, 1.25 µL 10 µM Reverse Primer and 2 µL of template DNA (1ng/µL). The reaction was incubated in a thermocycler which provided the conditions described in table 2.3. below.

Table 2.3. PCR cycling conditions for general DNA amplification.

Temperature (°C)	Time		Purpose
98	30		Initial Denature
98	30 sec	30-35 cycles	Denature
Primer dependant	30 sec		Annealing
72	30 sec/kb		Extension
72	5 min		Final Extension
4	∞		Hold

2.2.3.6. Restriction digestion of DNA

Purified PCR products or miniprep DNA was digested by the addition of 1 µL of appropriate restriction enzyme(s) to 1 µg of DNA with 10x CutSmart buffer (NEB) in a total reaction volume of 20 µL. The reaction was then incubated at 37 °C for 2 hours. Restriction enzymes were purchased from New England Biolabs. In the case where a restriction digest would yield a linearized vector with complimentary sticky ends, the reaction was subsequently treated with 1 µL Calf Intestinal Alkaline Phosphotase (CIP) (NEB) for 1 hour at 37 °C . This allows for the dephosphorylation of the 5' and 3' ends of the restricted vector.

2.2.3.7. DNA ligations

The vector: insert ratio routinely used in this study was 1:3. A ligation reaction constituted a mixture of digested vector DNA and digested insert DNA with 1 µL T4 DNA ligase (NEB), 2 µL T4 DNA ligase buffer (NEB) in a total reaction volume of 20 µL made up with sterile PCR grade H_2O. Ligation reactions were incubated at 16 °C overnight. The required mass of insert DNA required for a ligation reaction was calculated as follows:

$$insert\ mass\ = 3\ \times \frac{insert\ size\ (kb)}{vector\ size\ (kb)} \times vector\ mass$$

2.2.3.8. Assessment of nucleic acid concentration by fluorescence

The concentration and purity of nucleic acid samples was assessed by automated spectrophotometric analysis performed on a NanoDrop 1000

(ThermoScientific) based on UV absorbance at 230, 260 and 280 nm following the manufacturer's instructions.

2.2.3.9. DNA sequencing

Sequencing of PCR fragments cloned into vectors to generate the cassettes for allelic exchange and Tn7 transposon mutagenesis was performed by Source Bioscience using appropriate primers. The provided sequence was the aligned against *in silico* constructs using CLUSTL Omega to determine sequence homology.

2.2.4. Construction of an inducible Type 1 fimbriae mutant in *Escherichia coli* via the double crossover homologous recombination method

2.2.4.1 Cloning of mutation cassettes

The mutation cassettes for making an anhydrotetracyline inducible mutant of the Fim operon and a constitutive 5R-carbapenem resistant *E. coli* mutant were synthesised by Thermo Fischer using the GeneArt Custom Gene Synthesis service. These cassettes were amplified from the pMKFimAE by PCR using primers Fim1_Fw and Fim1_Rv described in Table 2.3., then subcloned into the suicide plasmid pDM4 using conventional restriction cloning techniques with XhoI and XbaI. Design of the FimAE construct is shown in Appendix 7.1.

2.2.4.2. Conjugal transfer of suicide plasmids into recipient strains

Conjugation of suicide plasmids into their recipient strains were performed using the 'puddle mating' technique. Cultures of an *E. coli* donor strain containing the suicide plasmid (S17-1(λpir)/pDM4FimAE) as well as the recipient strain (MG1655) were cultivated at 37˚C overnight in LB media with appropriate selection. 500 µL of each S17 strain was mixed with 100 µL of MG1655 and the cells pelleted via centrifugation at 10,000 x g for 5 minutes. The supernatant was discarded and each pellet resuspended in 1 mL fresh LB medium. The cells were spun and washed a second time before being resuspended in 30 µL fresh LB medium. 30 µL of each conjugation mixture was spotted onto a non-selective LB agar plate and incubated without inversion for 5 hours. After incubation the bacterial growth was scrapped off the LB with a sterile culture loop and resuspended in 200 µL fresh LB medium. The resuspended conjugation mixtures were spread out in 10 µL volumes onto M9F agar plates to select against the S17 donor strain, and incubated at 30 °C until individual colony growth was observed (typically 2 to 3 days).

2.2.4.3. Screening for homologous recombination events

To screen for single crossover events, facilitating the integration of suicide vector DNA onto the chromosome of MG1655, colonies which grew on the M9F plates were restreaked onto M9F with Chloramphenicol 25 µg/µL (M9FCm) plates. Individual colonies which grew on these plates were then grown overnight in liquid M9FCm medium. To enrich the cultures for clones having accomplished double crossover events, in which the suicide plasmid

excised leaving the chromosome back to wild type allele or causing an allelic exchange, the toxic effects of the *sacB* gene on the suicide vector was exploited. Single crossover isolates were grown overnight in no salt LB medium (NSLB) at 30 °C. This culture was diluted 1:100 in fresh NSLB medium supplemented with sucrose 15% and grown overnight at 30 °C, this process was repeated twice. After this the cultures which displayed growth were serially diluted to 10^{-6} and 100 µL of each serial dilution was plated onto a NSLB sucrose 15% agar plate and grown overnight at 30 °C. Sucrose-resistant colonies were picked from these plates and patched onto NSLB agar plate, a NSLB sucrose 15% plate and a NSLB chloramphenicol 25 µg/µL. Growth on NSLB and NSLB sucrose 15% plates but not NSLBCm represented clones having achieved successful double crossovers. Double crossover colonies were then screened for allelic replacement in the chromosome by colony PCR.

2.2.4.4. Confirmation of allelic exchange by colony PCR

The presence of desired recombinant constructs in isolated double crossover colonies was confirmed by colony PCR using the OneTaq 2 x Mastermix (New England Biolabs) and primers flanking the region of insertion (Fim2_Fw Fim2_Rv, Table 3.6) in a total volume of 25 µL. Thermocycling reaction conditions are described in Table 2.3. below.

Table 2.3. PCR Primers used for anhydrotetracyline inducible *fim* operon mutant construction and double crossover detection by PCR. Restriction enzyme sites underlined. Fw, forward; Rv, reverse.

Name	Sequence (5' to 3')	Purpose
Fim1_Fw	cagCTCGAGCTAAACAAGGGGAGCTTTGC	Forward primer for amplification of allelic exchange cassette from pMK-FimAE. XhoI site.
Fim1_Rv	cagACTAGTTGGAACGGAATGGTATTGGT	Reverse primer for amplification of allelic exchange cassette from pMK-FimAE. SpeI site.
Fim2_Fw	TGAAGCCAGACGAACACTTG	Forward primer for genomic region upstream of fimB promoters.
Fim2_Rv	CTGCTGATTTGCCCCATATT	Reverse primer for genomic region downstream of fimA.

Table 2.4. PCR cycling conditions for colony PCR for allelic exchange mutant confirmation.

Temperature (°C)	Time		Purpose
94	5 min		Colony Lysis
94	30 sec	30-35 cycles	Denature
55	1 min		Anneal
68	1 min		Extension
68	5 min		Final extension
4	∞		Hold

2.2.4.5. Confirmation of inducible mutant phenotype by fluorescent glycopolymer binding assay as determined by confocal microscopy

A 5-mL culture of the strains of interest (the *fim* inducible mutant, JEP01; wild type *E coli*, MG1655; and the adhesin deficient mutant, JW4283-3) were grown overnight in LB media at 37 °C with agitation at 200 rpm for aeration. The following morning, 5 mL of fresh LB media was inoculated with 50 μL of the overnight culture and this procedure was repeated for all strains. The fresh cultures were grown at 37 °C with agitation at 200 rpm until the mid-logarithmic growth phase (typically ~0.4-0.6 at OD_{600nm}). After this, anhydrotetracycline was added to the JEP01 culture (final concentration in solution 100 ng/mL) and grown for a further 2-4 hours to induce expression of the Type 1 Fimbriae. 1 mL of each culture was then dispensed into a sterile 1.5 mL microfuge tube (Eppendorf) and pelleted by centrifugation at 5000 rpm for 5 min. The pellet was washed with 200 μL PBS (Phosphate Buffered Saline), and the centrifugation-washing procedure repeated 3 times. 100 μL cells of each strain/condition was aliquoted into a fresh, sterile 1.5 mL microfuge tube (Eppendorf) and stained with 4′,6-diamidino-2-phenylindole (DAPI). 1 μL DAPI (1 μg/mL stock in PBS) was added to each strain incubated for 15-60 min in order to stain the cell nuclei. The cell suspensions were pelleted by centrifugation and was washed with 200 μL PBS, the centrifugation-washing procedure repeated 3 times. 100 μL of each strain/condition was then stained with the lipophilic far red dye FM 4-64FX (1 μL of 1 μg/mL solution in DMSO) in order to stain the cell membrane. The suspensions were incubated for 30

min on turning rack at 4 °C. The cell suspensions were pelleted by centrifugation and was washed with 200ul PBS, the centrifugation-washing procedure repeated 3 times. The cell pellets were then resuspended in 50 µL 1 mM Oregon Green labelled mannosylated/galactosylated polymer solution for one hour at 37 °C. The cell suspensions were pelleted by centrifugation and was washed with 200 µL PBS, the centrifugation-washing procedure repeated 3 times. The cell suspensions were then chilled on ice for 20 min prior to the addition of 100 µL 4% paraformaldehyde (PFA)(Sigma Aldritch) and then incubated for 15 minutes at room temperature to fix the cells. The cell suspensions were pelleted by centrifugation and was washed with 200 µL PBS, the centrifugation-washing procedure repeated 3 times. The pellet was then resuspended in 20 µL FluoroGel Mounting Media (GeneTex) and a 10 µL aliquot of each strain/condition was dispensed onto a high performance coverglass (D = 0.17mm, RI = 1.5255)(Zeiss). The cover glasses containing the stained cells in mounting medium were then mounted onto a Super Premium Microscopy slide (VWR) by inversion. The slides were left to cure overnight and imaged via confocal microscopy the following day. Total green and red fluorescence was quantified in Volocity Multi-Dimensional Imaging Software (Quorum Technologies) and reported as total green/red fluorescence in Prism (GraphPad).

2.2.5. Mini-Tn7 mediated tagging to yield autofluorescent strains

2.2.5.1. Construction of mini-Tn7 delivery vectors containing constitutive expression cassettes for the red and green fluorescent proteins mRuby2 and mNeongreen/eGFP

The constitutive promoters P_{11}, P_{13} and P_{24} were obtained cloned in a pBBR1 replicon vector fused to eYFP (Alagesan *et al*, 2018). eYFP was excised from these plasmids by digestion with EcoRI and BamHI. The fluorescent proteins mRuby, mNeongreen and eGFP were amplified by PCR from pSW002-Pc-mRuby2, pSW002-Pc-mNeongreen and pJH257-2 respectively, with the Primers listed in Table 2.5. These primer sets had a 5' extension on the forward primer to restore the RBS (Ribosome Binding Site) lost from the pBBR1 vector series by EcoRI/BamHI digestion. The PCR products were digested with EcoRI and BamHI and then ligated into the pBBR1-P_{11}-eYFP and pBBR1-P_{24}-eYFP vectors previously digested with EcoRI and BamHI yielding the pBBR1 P_{11}/P_{24} mRuby2/mNeonGreen vector series. Analysis of plasmid borne cassette fluorescence revealed that strong fluorescence was only seen in the case of the two strongest promoters P_{11} and P_{24}. Next the insulated constitutive fluorescent protein expression cassettes were amplified from the pBBR1 intermediate vectors with the P_{xx}F/R primer set, digested with XhoI/NsiI and ligated into pGP-Tn7-Cm digested with XhoI/NsiI yielding the vector series: pGP-Tn7-Cm-P_{11}mRuby; pGP-Tn7-Cm-P_{11}Neon; pGP-Tn7-Cm-P_{24}mRuby and pGP-Tn7-Cm-P_{24}Neon. Since the promoter insulation motif upstream of the promoters and fluorescent protein C-termini were identical for all the constructs, a single

primer set was sufficient for all mRuby/mNeonGreen constructs. After discovery that the mNeon cassettes were non-functional upon insertion onto the chromosome, eGFP was amplified from the vector pJH257-2 for SpeI/NsiI subcloning into the Tn7 suicide vectors pGP-Tn7-Cm-P11mRuby and pGP-Tn7-Cm-P24mRuby to yield the eGFP Tn7 suicide vectors pGP-Tn7-Cm-P11eGFP and pGP-Tn7-Cm-P24eGFP. A 5' extension was included on the primer set for this amplification to restore the RBS and start/valine codon which was omitted by digestion with this enzyme set. The sequence of all the resulting plasmids was verified by Sanger sequencing prior to Tn7-mediated transposition of the constitutive fluorescent protein expression cassettes onto the *E. coli* chromosome.

Table 2.5. PCR Primers used for mini-Tn7 constitutive fluorescent protein expression cassette construction and chromosomal insertion detection. Restriction enzyme sites underlined. Fw, forward; Rv, reverse.

Primer Name	Sequence (5' to 3')	Purpose
mNeon_Fw	cagcagGAATTCACTAGTTTAACTTTAAGAAGGAGATATACATATGGTGAGCAAGGGCGAG	Forward primer for mNeonGreen cloning into pBBR1-P11/13/24 vector series. EcoRI site.
mNeon_Rv	cagcagGGATCCTTACTTGTACAGCTCGTCCATG	Reverse primer for mNeonGreen cloning into pBBR1- P11/13/24 vector series. BamHI site.
mRuby_Fw	cagcagGAATTCACTAGTTTAACTTTAAGAAGGAGATATACATATGGTGAGCAAGGGCGAG	Forward primer for mRuby2 cloning into pBBR1-P11/13/24 vector series. EcoRI site.
mRuby_Rv	cagcagGGATCCTTACTTGTACAGCTCGTCCATG	Reverse primer for mRuby2 cloning into pBBR1-P P11/13/24 vector series. BamHI site.
PxxFP_Fw	cagcagCTCGAGTTAAGGCTGAGGGAAAGTACC	Forward primer for amplification of P11/24 NeonGreen/mRuby cassettes from pBBR1 intermediate vectors for subcloning into Tn7 suicide vectors. XhoI site.
PxxFP_Rv	cagcagATGCATTTACTTGTACAGCTCGTCCAT	Reverse primer for amplification of P11/24 NeonGreen/mRuby cassettes from pBBR1 intermediate vectors for subcloning into Tn7 suicide vectors. XhoI site.
eGFP_Fw	cagACTAGTTTAACTTTAAGAAGGAGATATACATATGGTGAGCAAGGGCGAGGAGCTG	Forward primer for amplification of eGFP from pJH257-2 for subcloning into cut pGP-Tn7-Cm-P11/24 vectors. SpeI site.
eGFP-Rv	cagATGCATTTACTTGTACAGCTCGTCCATGCC	Reverse primer for amplification of eGFP from pJH257-2 for subcloning into cut pGP-Tn7-Cm-P11/24 vectors. NsiI site.
glmS_Fw	AGCTGCTGGCTTACCATGTC	glmS complementary primer for chromosomal amplification upstream of attTn7 site to detect Tn7 insertion.
pstT_Rv	AGGCTTGCTTCTGCAAACAC	pstT complementary primer for chromosomal amplification downstream of attTn7 site to detect Tn7 insertion.

2.2.5.2. Delivery of mini-Tn7 constitutive fluorescent protein expression cassettes into desired *E. coli* recipient strains

A classical biparental mating was performed using 3 x 10^7 CFU mL^{-1} of donor strain *E. coli* ST18 carrying the pGP-Tn7-Cm derivative vectors harbouring the mRuby2/mNeongreen/eGFP expression cassettes and 1 x 10^7 CFU mL^{-1} of the recipient strains carrying the transposase-encoding vector pSTNSK at 30 °C on LB agar plates for 18h. After incubation, the mating lawn was resuspended in sterile PBS and serially diluted to 10^{-3}, spread onto M9F Cm plates, incubated at 42 °C for 5h and then at 37 °C for 18 h. Colonies were then screened for resistance to Cm and sensitivity to Amp and Km. Since the Amp^R marker is located outside of the transposable mini-Tn7 cassette on the suicide vectors, sensitivity to Amp indicates the proper integration of the mini-Tn7 cassette at the intended chromosomal *att*Tn7 site instead of any unwanted chromosomal integration of the vector. Additionally, since the transposases are encoded on a temperature-sensitive helper plasmid, incubation at 42 °C was undertaken to promote the loss of these plasmids from the recipient strains, which is verified by loss of Km resistance. Furthermore, the use of M9F Cm plates selected for the growth of the recipient strains as the S17λ*pir* donors are *thi-, pro-* and hence are auxotrophic for these amino acids. Chromosomal integration of the mini-Tn7 transposons at the *att*Tn7 site downstream of *glmS* within various fluorescent clones was confirmed by PCR with the *glmS/pstS* primer pair listed in Table 2.5.

2.2.5.3. Fluorescence and Growth Analysis

Overnight cultures of the strains of interest were grown overnight in the M9F media. The optical density of the overnight culture was measured and used to inoculate 250 µL of fresh media in triplicate, normalised to a starting OD (600 nm) of 0.05 in a 96-well plate. The 96 well plate was incubated at 37 °C in a TECAN Infinite 200M Pro (Tecan) automated plate reader for 24 hours with optical density (600 nm) and fluorescence intensity (485/535 nm and 535/595 nm) recorded at 30 s intervals. Growth and fluorescence data was then analysed in Prism (GraphPad).

2.3. Results

2.3.1 Genomic deletion of *fim* operon regulatory apparatus and replacement with *tetR*-p$_{tetA}$

In order to eliminate the stochastic switching of the *fim* operon which is seen in wild type *E. coli* strains (Schwan, 2011; Schwan *et al.*, 1994) elimination of the *fim* switch and replacement with an inducible regulatory mechanism, as described in Chapter 2.5, was necessary. To this end, a synthetic construct was ordered containing the inducible *tetR*-P$_{tetA}$ system flanked by regions of homology (~500 bp) to the chromosomal regions of MG1655 flanking the *fimB* promoters and the start site of *fimA*. The plasmid containing this construct was pMKFimAE. This cassette was excised by digestion with XhoI/SpeI and ligated into the pDM4 suicide vector using standard restriction cloning techniques yielding pDM4FimAE. Identity of this suicide plasmid was confirmed by restriction digestion and Sanger sequencing with complete identity to the theoretical construct. Homology-mediated allelic exchange with the non-replicative suicide plasmid, pDM4Fim, resulted in the replacement of the native regulon of the *fim* operon with the inducible *tetR*-p$_{tetA}$ system which had been cloned into the pDM4 vector between the regions of homology to the *E coli* chromsome. A schematic of the genetic organisation of the *fim* operon before and after allelic exchange mutation as well as an agarose gel can be seen in Fig. 2.6. below.

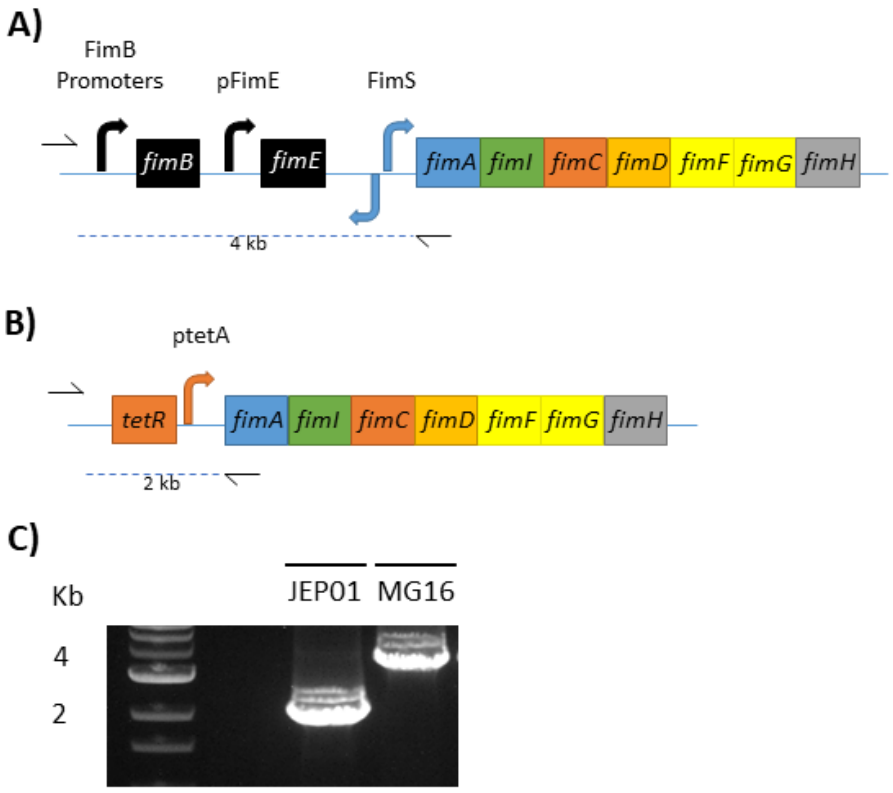

Figure 2.6. Construction of an ATc inducible *tetR*-P$_{tetA}$ regulatory mutant of the *fim* operon in *Escherichia coli* MG1655. A, schematic representation of the native *fim* operon in *E. coli* and associated regulatory elements. An invertible promoter element, *fimS*, regulates the downstream *fimAICDFGH* operon. Inversion is mediated by the actions of the two recombinases, FimB and FimE, which are encoded by genes upstream of the operon. Half arrows represent the primer pair FimF2/FimR2. The intergenic distance between these two sites in the native genomic context is 4 kb. **B**, schematic representation of the *fim* operon in the regulatory mutant JEP01, in which the native *fimS* regulatory system has been replaced by the inducible *tetR*-P$_{tetA}$ system. Half arrows represent the primer pair FimF2/FimR2. The intergenic distance between these two sites in the regulatory mutant genome is 2 kb. **C**, PCR of JEP01 and MG1655 with the mutation screening primer pair FimF2/FimR2, confirming the presence of the indel in JEP01.

Following the isolation of several Cm^S, Suc^R colonies following the double crossover homologous recombination allelic replacement process as described in Section 2.2.4. a PCR screen was performed to differentiate between those double crossover colonies which had reverted back to the wild type allele or which had replaced it by the engineered, regulated one.

A summation of this process is shown in Figure 2.6. The intergenic distance between the attachment sites for the interrogative primer pair is 4 kb in the wild type genomic context, however this intergenic distance is decreased to 2 kb in the inducible *tetR*-P_{tetA}-*fim* mutant. The region of chromosomal DNA which is deleted by this process is greater in size than the inserted regulatory element hence the decrease in overall intergenic distance (3.8 kb deleted, 1.8 kb inserted). PCR amplification of this region in the isolated mutant produced a ~2 kb band, compared with a ~4 kb band in the wild type (Figure 2.6, C), confirming the presence of the desired allelic replacement in the isolated JEP01 clone. To further validate the presence of this construct in the isolated JEP01 clone, the PCR product was isolated and sent for Sanger sequencing. The nucleotide sequence of this PCR fragment aligned with the expected sequence with full identity (Appendix 7.1.1.).

2.3.2. Effect of genomic mutation on bacterial growth compared to wild type

To ascertain whether the replacement of the native *fim* switch in *E. coli* MG1655 with the *tetR*-P_{tetA} regulatory system would result in any aberrant metabolic flux leading to decreased fitness of the non-native regulatory mutant, growth of this strain, in the presence and absence of the inducer compound ATc at maximal induction concentrations, was examined in parallel with the wild type strain and the afimbriate mutant JW4283-3 in rich media (LB). The resulting growth curves show that the *tetR*-P_{tetA} regulated mutant of the *fim* operon (JEP01) exhibits no difference in growth compared to the wild type strain (MG1655), regardless of induction state (Fig. 2.7.). Furthermore the Δ*fimH* mutant (JW4283-3) also does not

demonstrate any difference in growth compared to the wild type strain, or the regulatory mutant in the induced and uninduced states.

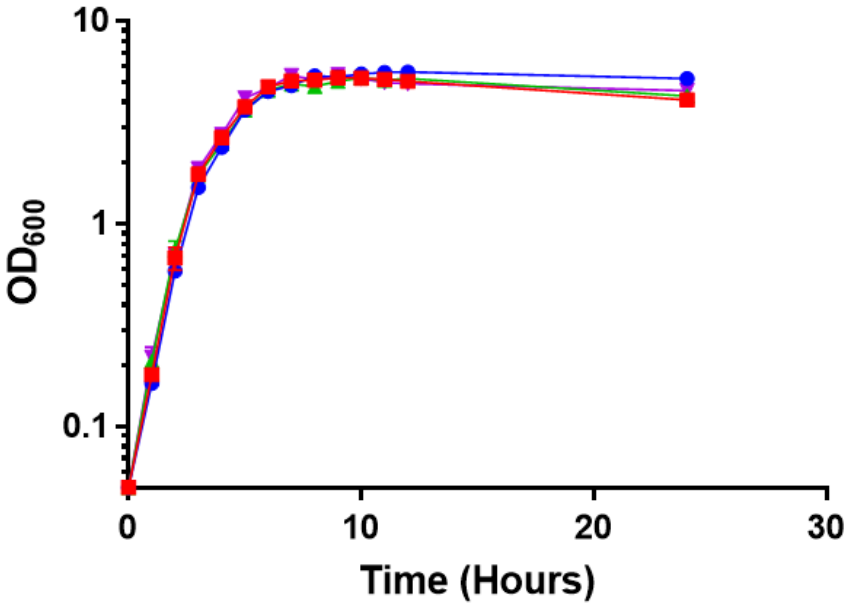

Figure 2.7. Growth of inducible *fim* mutant (JEP01). Cultures of JEP01 (red), JEP01 with 100 ng/mL ATc (blue), MG1655 (green) and JW4283-3 (magenta) were grown in conical flasks, and incubated at 37^{0}C with 200 rpm shaking. Samples were taken every hour for 12 hours, with an additional sample after 24 hours. Results represent the average of three independent replicates. Error bars represent one standard deviation about the mean. Presence of the genomic *fim* regulatory mutation, induced or otherwise, has no effect on strain growth under experimental conditions.

2.3.3. Confirmation of mutant phenotype by glycopolymer binding analysis

To confirm the inducible Type 1 fimbriae as constructed in Section 2.3.1 was able to bind to mannosylated polymers in the presence of the autoinducer, but not to other sugars, an initial binding assay was performed via confocal microscopy as described in Section 2.2.4.5. The glycomaterials used in this assay were kindly donated by Dr. Francesca Mastrotto and prepared by Atom Transfer Radical Polymerisation of a trimethylsilyl

propargyl methacrylate monomer, similar to the approach of Ladmiral and co-workers (Ladmiral *et al.*, 2006). Almost identical materials were produced by Mastrotto and co-workers, albeit with a different initiator, for binding the oral pathogen *S. mutans* (Magennis *et al.*, 2017). This synthetic route yielded a polymer which, after deprotection with TBAF and acetic acid, possessed a backbone displaying a free alkyne group per monomer unit. Copper(I)-catalysed azide-alkyne cycloaddition (CuAAC) with sugar azides produced by the methods Chernyak and co-workers allowed for addition of sugar units to the polymer backbone by (Chernyak *et al.*, 1992). Prior to the addition of the sugar moieties, a first CuAAC 'click' reaction was performed with an azide functionalised derivative of the dye Oregon green, at a 1% mol/mol compared to alkyne units, yielding fluorescent materials with excitation/emission maxima in the 488/526 nm range with minimal spectral overlap in emission with DAPI and FM4-64 fx (used to stain bacterial cell nuclei and membranes respectively).

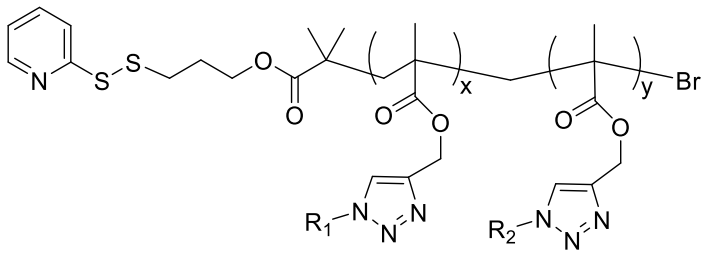

Figure 2.8. General structure of fluorescent glycopolymers used in *fim* mutant polymer binding assay by confocal microscopy. R_1=Oregon Green; R_2= Mannose or Galactose. Oregon green incorporated at 1% mol/mol for available alkyne units. $M_{n,SEC}$ = 25500 kDa, Đ = 1.38.

All strains were grown to the mid logarithmic stage and then fimbrial expression was induced with 100 ng/ml ATc as appropriate. The cells were

then stained with the red membrane dye (FM 4-64 Fx) and the blue nucleic acid dye DAPI and resuspended in 20 µL of a 1 mM solution of mannosylated or galactosylated polymer to facilitate binding prior to imaging on the confocal microscope.

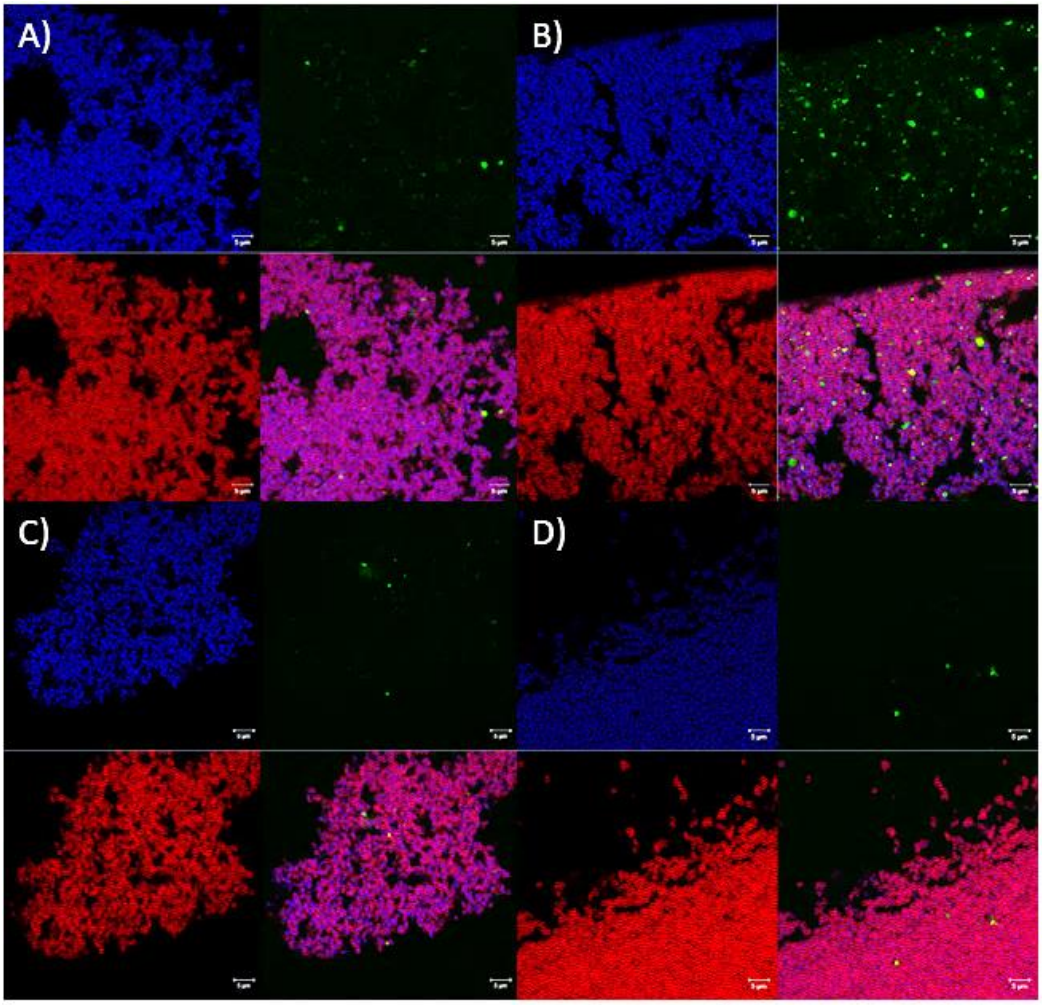

Figure 2.9. Representative confocal microscopy images of *E. coli* mannose polymer binding. *E. coli* cells are stained with DAPI (blue nucleic acid dye) and FM-464fx (red membrane dye) then incubated with 10 µM poly(mannose)@Oregon Green for 1 hour to facilitate lectin mediated binding. Scale bars represent 5 µm. A) Uninduced JEP01, B) JEP01 induced with ATc (100ng/ml), C) MG1655, D) JW4283-3 (Δ*fimH*). Binding of the mannose polymer only occurs when fimbrial expression is induced.

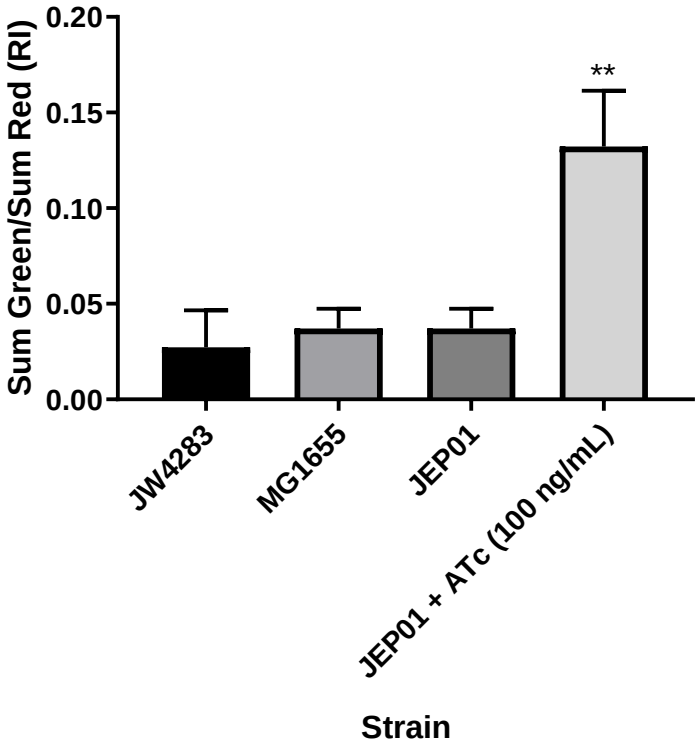

Figure 2. 10. Quantitation of mannose polymer binding by *E. coli* fimbriation mutants and wild type *E. coli*. Total polymer bound as measured by the sum green fluorescence intensity (polymer signal) divided by sum red intensity signal (membrane signal), error bars represent standard error of the mean (SEM), (n≥3 in all experiments). JW4283-3, afimbriate Keio mutant; MG1655, wild type K-12 *Escherichia coli*; JEP01, anhydrotetracycline inducible mutant of the Type 1 fimbriae expression cassette (*fim* operon) constructed in MG1655 (n≥3). Analysis performed by One-Way ANOVA with Tukey's Multiple Comparison Test. A significant difference in bound mannose polymer was observed between the induced mutant and all other strains (p=0.002-0.0022) but no significant difference was observed between the uninduced mutant and the other strains.

As demonstrated in Fig. 2.9. large amounts of green fluorescent material, in association with the red/blue labelled cells, is only observed in the case of the induced JEP01, the inducible Type 1 fimbriae mutant. To further validate this finding the total green fluorescence content of multiple confocal images was quantified in Volocity and normalised against the total red content of each images, which is directly proportional with the total cell content of each image, and analysed by ANOVA (Fig. 2.10). A statistically

significant difference in sum green divided by sum red intensity, giving an approximation of polymer binding as a function of cell density, was only observed in the case of induced JEP01 compared to the uninduced strain, the wild type (MG1655) and the afimbriate Keio mutant ($p=0.002$, 0.002 & 0.022 respectively). These data suggest that only JEP01, with induction by ATc, is able to bind significant quantities of mannosylated polymer and that this binding is mediated by expression of the Type 1 Fimbriae. In the absence of the inducer and, hence, absence of Type 1 fimbriae expression little bound polymer is detected.

In contrast when the same experiment is repeated with an identical fluorescent polymer which possesses galactose pendant groups, as opposed to mannose, little green fluorescence is observed (Fig 2.11). In addition the total green over total red fluorescence for each strain, and hence total galactose polymer bound as a function of cell density, is not seen to be significantly different for each strain (Fig 2.12). These data therefore further corroborate the specificity of the Type 1 fimbriae to mannose residues, but not galactose, despite their structural similarity.

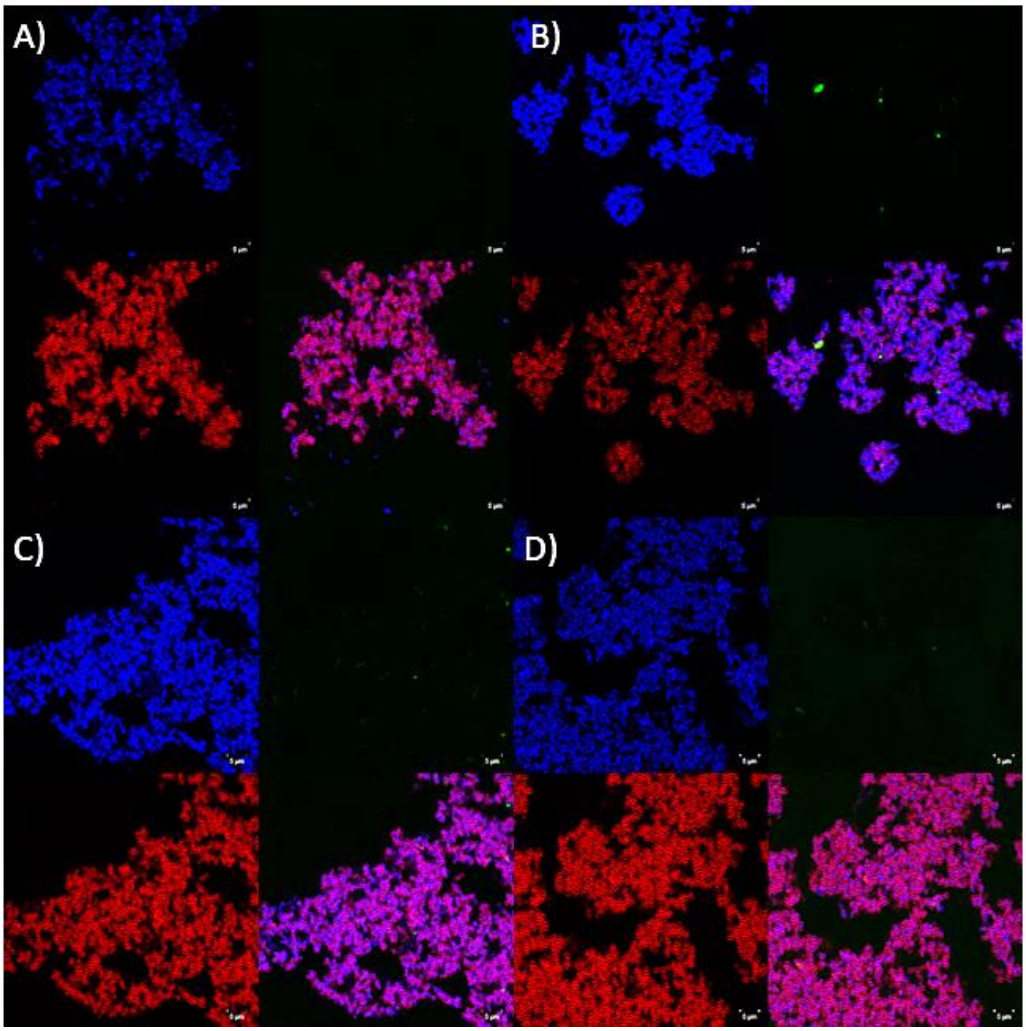

Figure 2.11. Representative confocal microscopy images of *E. coli* galactose polymer binding. E. coli cells are stained with DAPI (blue nucleic acid dye) and FM-464fx (red membrane dye) then incubated with 10μM poly(mannose)@Oregon Green for 1 hour to facilitate lectin mediated binding. Scale bars represent 5 μm. A) Uninduced JEP01, B) JEP01 induced with ATc (100ng/ml), C) MG1655, D) JW4283-3 (ΔfimH). Little to no polymer is seen spatially associated with the cells for any strain.

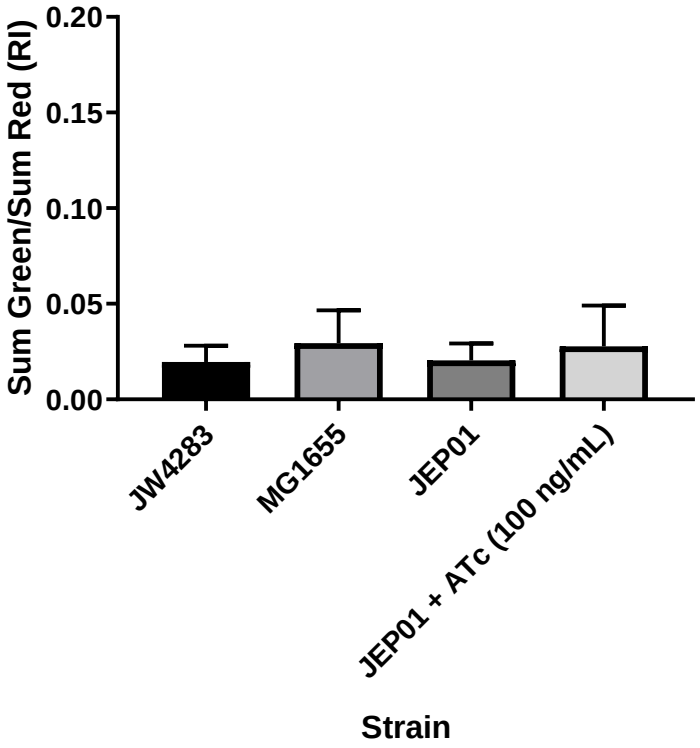

Figure 2. 12. Quantitation of galactose polymer binding by *E. coli* fimbriation mutants and wild type *E. coli*. Total polymer bound as measured by the sum green fluorescence intensity (polymer signal) divided by sum red intensity signal (membrane signal), error bars represent standard error of the mean (SEM), (N≥3 in all experiments). JW4283-3, afimbriate Keio mutant; MG1655, wild type K-12 *Escherichia coli*; JEP01, anhydrotetracycline inducible mutant of the Type 1 fimbriae expression cassette (*fim* operon) constructed in MG1655(n≥3). Analysis performed by One-Way ANOVA with Tukey's Multiple Comparison Test. There is no significant difference in total galactose polymer bound between each strain and condition.

To confirm that the ability of the induced *fim* mutant to specifically bind mannosylated polymers was not limited to small, individual clusters as observed via confocal microscopy tile scanning confocal microscopy was performed. This imaging technique allows for the generation of a large field of view images at high resolution, hence allowing for global scale analysis of bacteria phenotypes.

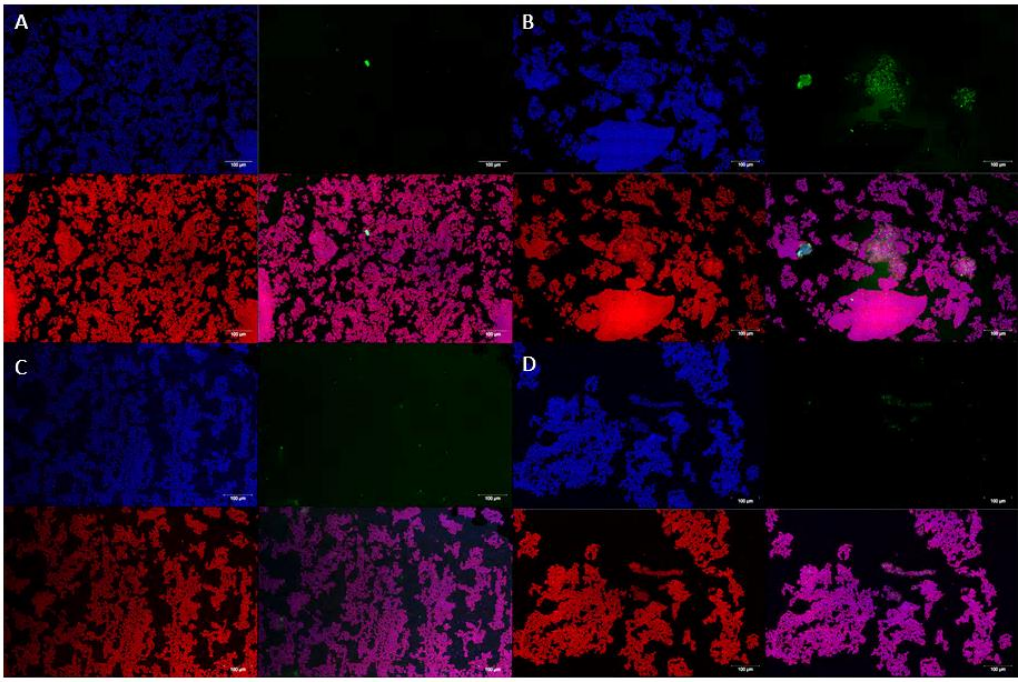

Figure 2.13. Representative confocal microscopy images of *E. coli* mannosylated polymer binding by tile scanning. *E. coli* cells are stained with DAPI (blue nucleic acid dye) and FM-464fx (red membrane dye) then incubated with 10μM poly(mannose)@Oregon Green for 1 hour to facilitate lectin mediated binding. Scale bars represent 100 μm. A) Uninduced JEP01, B) JEP01 induced with ATc (100ng/ml), C) MG1655, D) JW4283-3 (Δ*fimH*). Large clusters of polymer are seen associated with the induced *fim* mutant only.

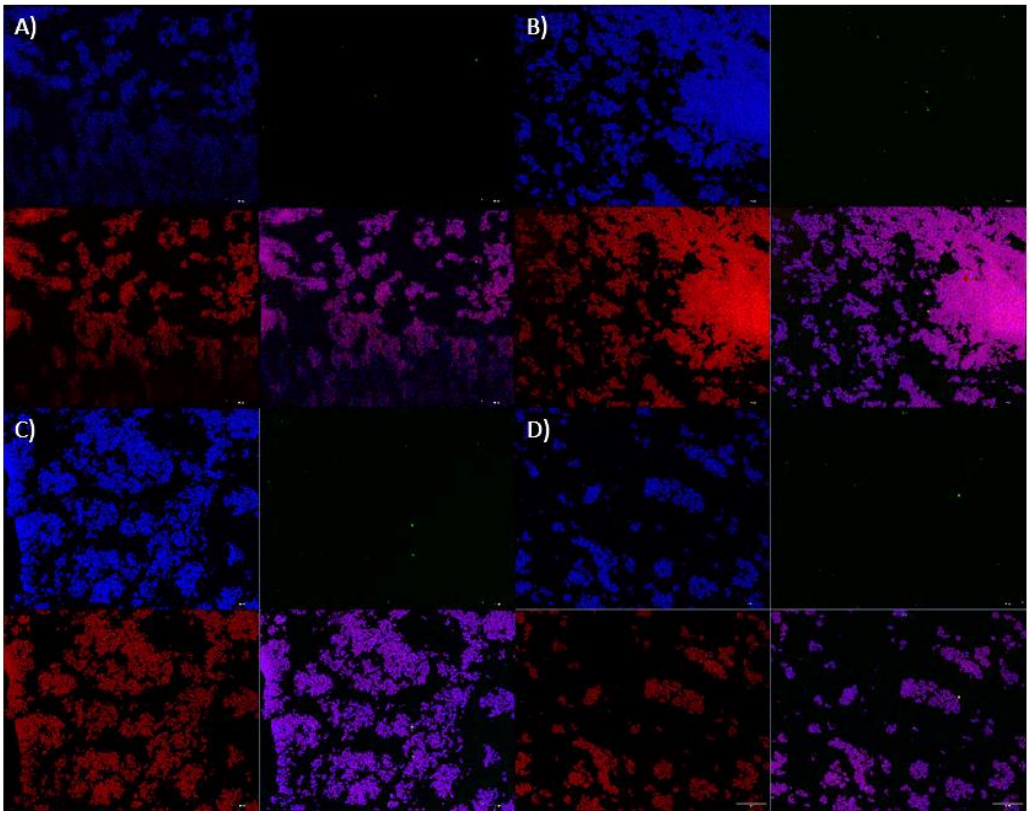

Figure 2.14. Representative confocal microscopy images of *E. coli* galactosylated polymer binding by tile scanning. *E. coli* cells are stained with DAPI (blue nucleic acid dye) and FM-464fx (red membrane dye) then incubated with 10μM poly(mannose)@Oregon Green for 1 hour to facilitate lectin mediated binding. Scale bars represent 100 μm. A) Uninduced JEP01, B) JEP01 induced with ATc (100ng/ml), C) MG1655, D) JW4283-3 (Δ*fimH*). No polymer is associated with cells regardless of strain.

As may be seen in Fig. 2.13 binding of mannosylated polymers is only observed for induced JEP01 and no other strains. Additionally all strains utilised, regardless of fimbriation, do not bind to galactosylated polymers as evidenced by the absence of fluorescence in the green channel in Fig 2.14. These data further corroborate the previous finding that induction of expression Type 1 fimbriae in JEP01 leads to selective binding of mannosylated polymers but not galactosylated polymers.

2.3.4. Transposon mutagenesis of strains for constitutive expression of fluorescent labels

Initially, the aim was to introduce a single copy of the genes encoding mRuby2 or mNeonGreen, two of the brightest monomeric red and respectively green fluorescent proteins described thus far in the literature, in the *E. coli* chromosome under the control of various insulated constitutive promoters as described by Alegesan and co-workers (Alagesan *et al.*, 2018; Wilton *et al.*, 2018). By inserting these constitutive expression systems as a single copy in the chromosome, it was hoped to minimise the variation and noise in fluorescence data which can commonly be observed in plasmid-based expression systems due to stochastic variance in copy number between cells in a clonal population (Ghozzi *et al.*, 2010; Ng *et al.*, 2010).

To achieve this aim, the chromosomal tagging system developed by Crépin and co-workers was modified to include expression cassettes for mRuby2, mNeonGreen and eGFP under the control of the strong, insulated, constitutive promoters, P_{11} and P_{24} (Crepin *et al.*, 2012). These systems exploits the mini-Tn7 transposon vehicle to integrate a desired cassette in the chromosome of a recipient strain at a single, evolutionarily conserved site by using the *tnsABCD* system while excluding the promiscuous recombinase *tns*E, which can facilitate transposition at multiple, non-determined chromosomal sites.

This system uses a classical conjugative approach, wherein a donor strain contains a mini-Tn7 vector (in which the cassette of interest is cloned

between the Tn7R and Tn7L elements) and is mobilised into a recipient strain in which it will be unable to replicate due to the non-native replicative machinery requirements of the R6K origin of replication. The recipient strain harbours a transposase vector which then be selected against following successful transposition due to the temperature sensitive origin of replication *ori* pSC101. Elegantly, the suicide vector which delivers the transposable cassette also contains selectable markers in the form of antibiotic resistance cassettes (Cm^R and Ap^R) both within and without of the transposable cassette allowing for screening of recipient transposon mutants by dual selection. A full list of all pGP-Tn7 derivatives constructed for this work are available in Section 2.1.1.5.

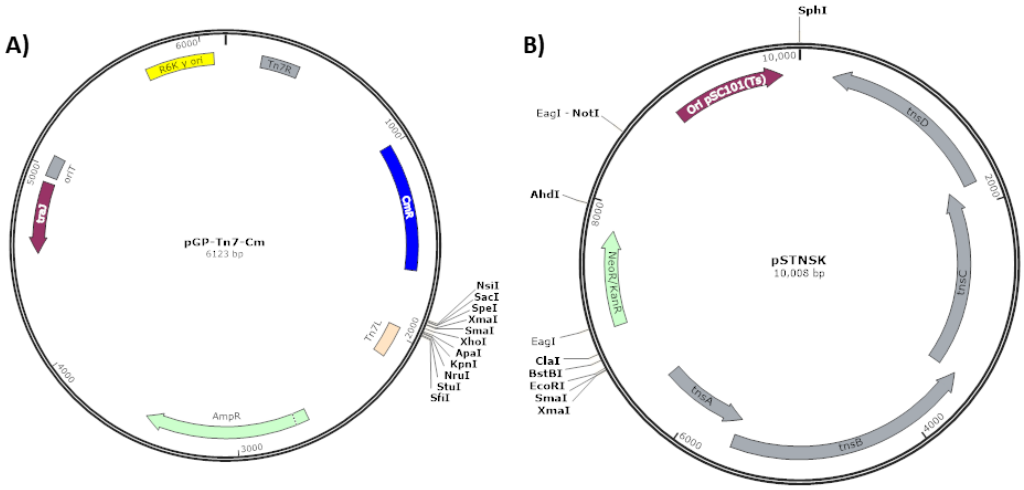

Figure 2.15. Features of the mini-Tn7 and transposase vectors from Crepin *et al.* (2012). A) The mobilisable suicide vector pGP-Tn7-Cm and derivatives contain the conjugative transfer elements *traJ* and *oriT* and *pir* dependant *ori* R6K. Cassettes of interest may be inserted in the MCS between the two ends of transposon. B) The thermosensitive vector pSNTSK contains the pSC101 origin and the transposases *tnsABCD*. Reproduced from: (Crepin *et al.*, 2012).

Correct integration of the constitutive fluorescent protein expression cassettes utilised in this study (P_{11}eGFP, P_{24}eGFP, P_{11}mRuby, P_{24}mRuby, P_{11}mNeongreen and P_{24}mNeongreen) can be interrogated by PCR using primers which bind to regions in the chromosome of *E. coli* which flank the attachment site *att Tn7* as shown in Fig 2.16. Tn7 transpositon mediated by *tnsABCD* integrates the element imediately downstream of the bacterial glutamine synthetase, *glmS*. The gene immediately proceeding *glmS* downstream is *pstS*, a periplasmic phosphate binding protein of the ATP dependent phosphate transport system in *E. coli*. The primer set *glmS*_Fw and *pstS*_Rv described in Section 2.2.5.1 bind to *glmS* and *pstS* respectively yielding an amplicon of ~500 bp from the chromosome of wild type *E. coli*. Conversely, upon the integration of the mini-Tn7 transposon element containing any of the aforementioned constitutive, insulated promoter-fluorescent protein fusions into this region, the intergenic distance is increased by ~2.5 kb – yielding a band of ~ 3 kb. It is important to note that both promoters, P11 and P24 are of indistinguishable lengths at 180 and 181 bp respectively. Similarly, the fluorescent protein genes used in this work are of such similar lengths that they too are indistinguishable by gel electrophoresis at 720, 711 and 711 bp respectively for eGFP, mNeonGreen and mRuby, respectively. Hence this PCR screen is only able to detect the presence of any of the modularly assembled cassettes utilised, but is unable to distinguish between them. Regardless, it is still an invaluable tool for the detection of the transposition of all of the constitutive promoter-fluorescent protein cassettes onto the *E. coli* genome.

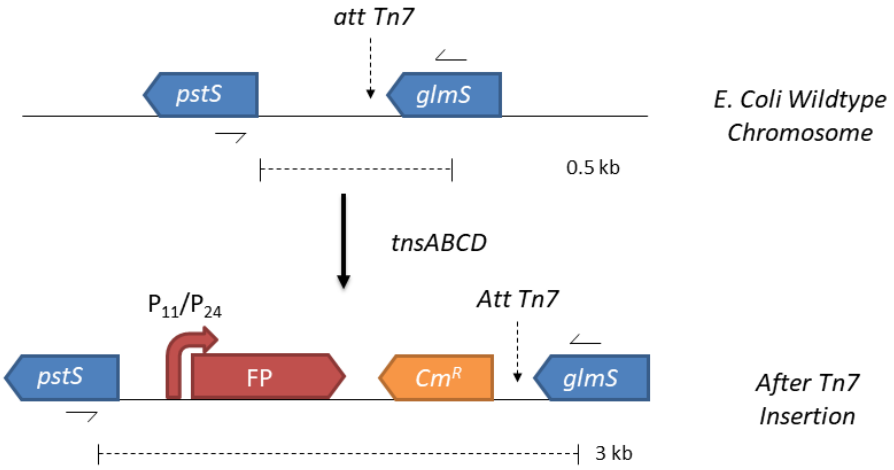

Figure 2.16. Construction of autofluorescent mutants of *E. coli* by tagging the chromosome with constitutive fluorescent protein expression cassettes. Schematic representation of the native Tn7 attachment site (*att Tn7*) in the wild type *E. coli* chromosome and after insertion of constitutive fluorescent protein expression cassettes containing a strong, insulated constitutive promoters (P_{11} or P_{24}) and a fluorescent protein gene (FP) (eGFP, mRuby2 or mNeonGreen). The half arrows represent the primer pair *glmS*F and pstSR. Successful transposition of expression cassettes onto the chromosome can be interrogated by PCR due to increase in distance between the primer binding sites.

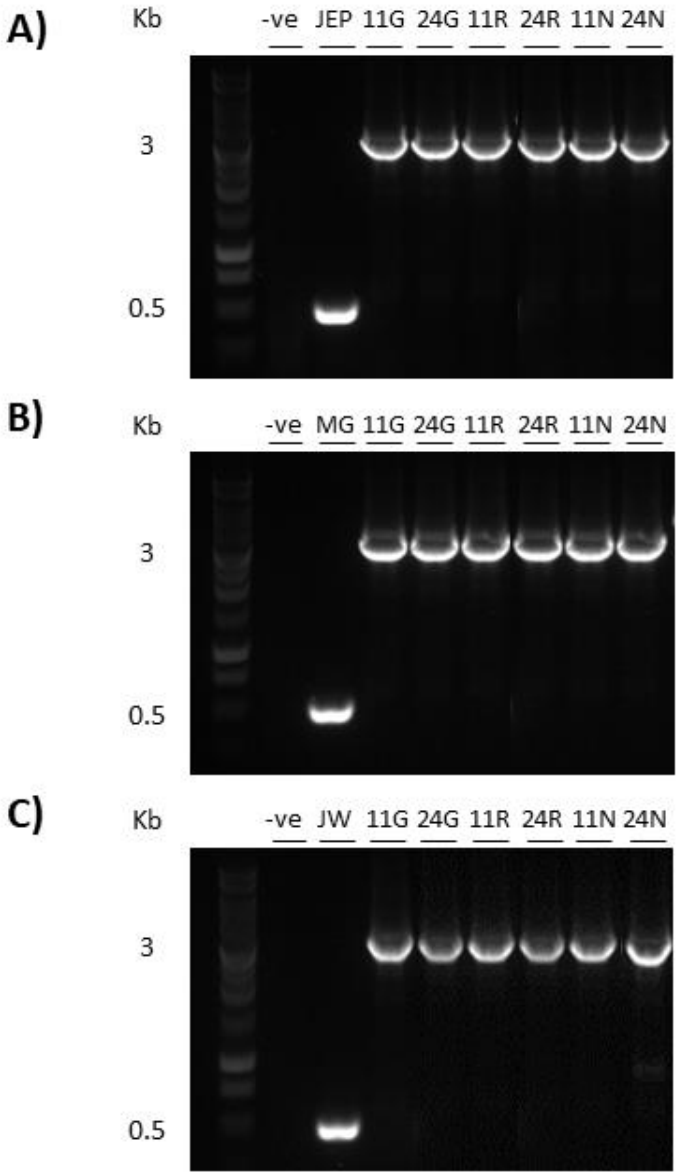

Figure 2.17. PCR confirmation of insertional mutation of constitutive fluorescent protein expression cassettes into *E. coli* strains by Tn7 transposon. Insertion of P_{11} (11) or P_{24} (24) controlled eGFP (G), mRuby2 (R) and mNeonGreen (N) cassettes into the strains JEP01 (Panel A), MG1655 (Panel B) and JW4283-3 (Panel C). A 3 kb band, consistent with insertion of the constitutive fluorescent protein cassettes into the *E. coli* genome, is observed in the case of all transposition mutants.

Each of the various mini-Tn7 transposition cassettes encoding for either eGFP, mRuby or mNeonGreen and regulated by either P_{11} or P_{24} were integrated into the chromosomes of *E. coli* strains JEP01, MG1655 and JW4283-3. A PCR screen interrogating clones resulting from these

constructions for the presence of the mini-transposons is shown in Fig 2.17. In all cases of mini-transposon insertion the obtained band is of 3 kb, whereas the non-transposed parent strain on each gel (JEP01, MG1655 of JW4283) yields a band of 0.5 kb. This observed difference in electrophoretic shift patterns is consistent with the integration of a 2.5 kb cassette into each of the derived strains; the size of the fluorescent protein-encoding transposition cassettes from the applicable pGP-Tn7-Cm derivatives used in this work.

However, while this screen does confirm the presence of the insulated, constitutive fluorescent protein expression cassettes within all derivative strains it does not guarantee the fluorescent phenotype. For eGFP and mRuby colony colour was consistent with the expression of coloured proteins but an altered colony phenotype was not observed for mNeongreen insertional transposition.

2.3.5. Validation of mini-Tn7 fluorescently tagged phenotypes

While all cassettes could be integrated in the chromosomes of all the *E. coli* strains, it was noticed that the fluorescence signal deriving from promoters P_{11} or P_{24} and the mNeonGreen gene when integrated in the chromosome was indistinguishable from that of the non-tagged parental strain despite strong fluorescence of these cassettes when on a multi-copy plasmid (data not shown). NeonGreen constructs were therefore deemed to be unsuitable for tracking population compositions and were excluded from further investigation despite sequencing analysis suggesting the chromosomal presence of mNeongreen expression cassettes with an absence of

nucleotide polymorphisms which could account for this loss of function in all isolated mNeongreen insertional mutants.

To confirm that the presence of a single constitutively active fluorescence protein cassette integrated in the *E. coli* chromosome at the specific Tn7 integration site downstream of the essential *glmS* gene, and that *glmS* was still functional and the insertion did not impede growth, a TECAN screening of both fluorescence in the red and green channels alongside optical density was performed in M9F mimimal media. For fluorescence analysis it is recommended to avoid rich media such as LB due to the green autofluorescence of such media.

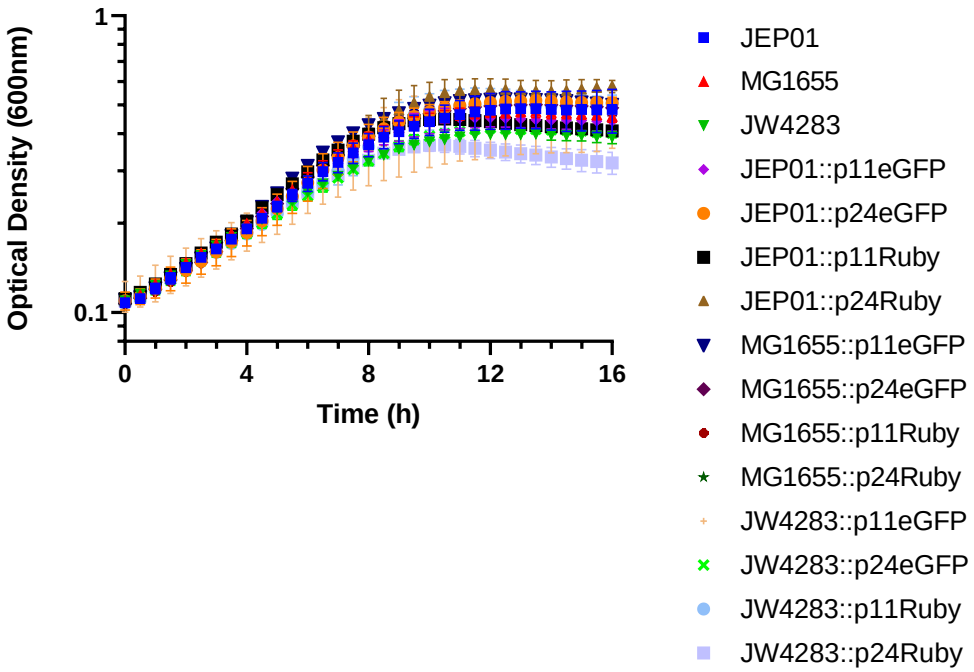

Figure 2.18. Growth curves of all mini-Tn7 transposition derived autofluorescent *E. coli.* Growth monitored over 24h period in TECAN automated plate reader in M9F media. Results represent the average of three independent replicates. Error bars represent one standard deviation about the mean. Presence of a single copy of P_{11} or P_{24} regulated mRuby2 or eGFP expression cassette on the chromosome appears to have little effect on strain growth.

Growth of all fluorescently tagged transposon strains generated in this study is shown in Fig. 2.18. There appears to be no difference in growth rate as monitored by optical density over 24h under these experimental conditions during the logarithmic growth phase. JW4283::P_{24}mRuby appears to reach the lowest maximal cell density when transitioning to the stationary phase after 10h, however mean optical density for the final time point does not exceed ±2 standard deviations from the mean optical density of any other strain after 24h suggesting a statistically insignificant difference between all tagged strains.

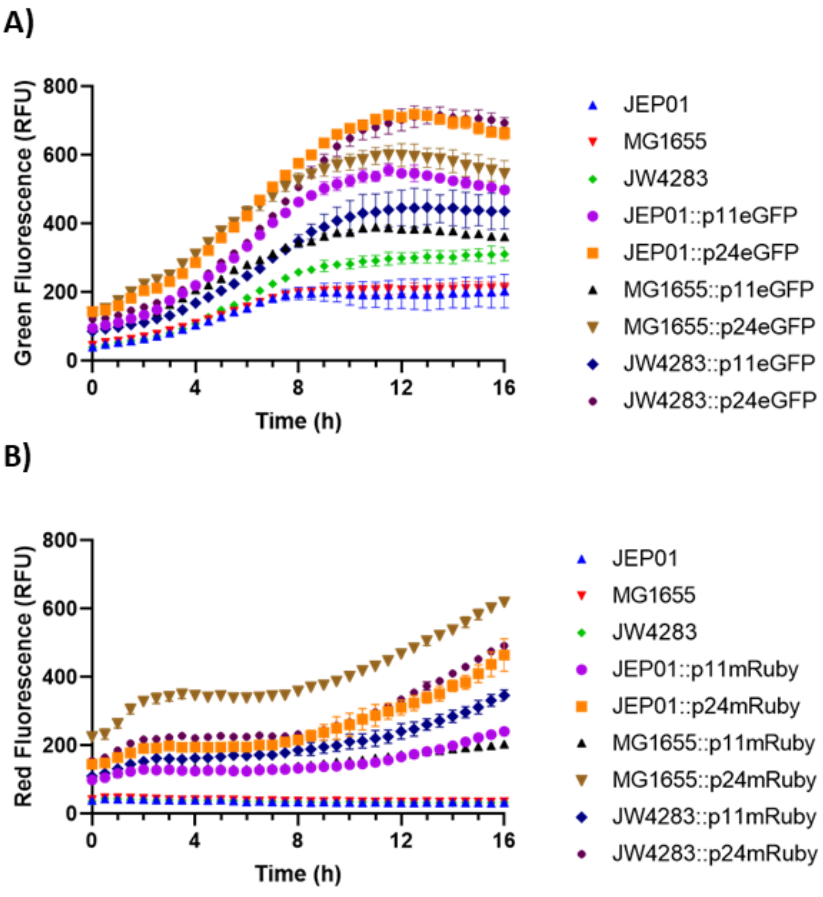

Figure 2.19. Evolution of relative fluorescence intensity over time for eGFP (A) and mRuby (B) transposon mutants. . Results represent the average of three independent replicates. Error bars represent one standard deviation about the mean.

Figure 2.19. shows the evolution of fluorescence output of all the transposon mutants generated in this study over time during the growth experiment. In general, all tagged strains show a fluorescence intensity hierarchy which correlates with promoter strength (P_{24}>P_{11}) and produce a significantly higher fluorescence output at all time- points compared to the untagged parental strains. While no autofluorescence is observed for the parent strains in the red bandwidth, some green autofluorescence is observed in the green bandwidth, however, this is sufficiently low to be distinguishable from all P_{11} and P_{24} regulated eGFP mutants by intensity gating as used during flow cytometry in Chapter 4. Green autofluorescence of *E coli* is a common observation and is likely linked to the biosynthesis of flavin/riboflavin compounds and maybe be empirically corrected if so desired (Mihalcescu *et al.*, 2015).

Intriguingly, the two fluorophores follow different fluorescent intensity evolution trends over time. eGFP-expressing strains follow a linear increase in fluorescence intensity up until ten hours, i.e. during the logarithmic growth phase, then stabilise or slowly decrease over time as the cells proceed into the stationary growth phase. In contrast, the mRuby-expressing cells exhibit a plateau in fluorescence intensity while the cells are in the logarithmic phase but fluorescence intensity increases linearly between 10-24 hours – as the cells proceed into the stationary phase.

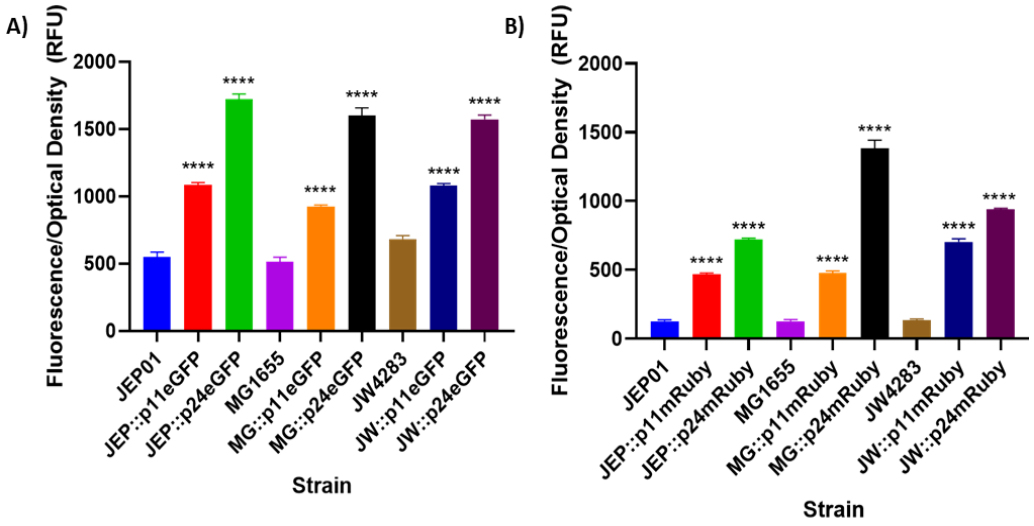

Figure 2.20. Fluorescence over optical density at 6h (mid-log phase) for eGFP (A) and mRuby (B) transposon mutants. . Results represent the average of three independent replicates. Error bars represent one standard deviation about the mean. Statistical analysis was performed by one-way ANOVA with Tukey's multiple comparisons test. All fluorescent strains are brighter than their parent strains and P_{24} was brighter than P_{11} for both fluorophores ($p<0.0001$).

To demonstrate the viability of the produced strains as a population monitoring tool during the logarithmic growth phase, during which Type 1 fimbriae expression may be induced in JEP01 and derivatives, analysis of fluorescence as a function of optical density was performed at 6 hours.

As may be seen in Fig. 2.20 all fluorescent protein expressing strains show a significant difference compared to their non-fluorescence parental strains (JEP01, MG1655 and JW4283) at the $p=0.0001$ level. Additionally, a significant difference in fluorescence intensity as a function of optical density was observed between each promoter for the same fluorophore at the $p=0.0001$ level.

2.4. Discussion

The results presented in this chapter demonstrate the successful construction of a *tetR*-P_{tetA} regulated inducible mutant of the Type 1 fimbriae and eGFP/mRuby expressing transposon-tagged strains.

As expression of the Type 1 fimbriae is stochastic in wildtype *E. coli*, the aim was to replace the regulatory apparatus in the native chromosome with a switchable regulatory system. The *tetR*-P_{tetA} system was selected for this due extensive characterisation and utilisation of this system, low levels of aberrant expression in the absence of the inducer ('leakiness' of the promoter), maximal expression of proteins from this system using relatively low concentrations of inducer compounds and the availability of an inducer analogue which is non-bactericidal and is not metabolised by *E. coli*. To insert this promoter onto the chromosome, delivery of an allelic exchange cassette on a non-replicative suicide vector was selected due to the availability of the necessary plasmids and experience with this technique involving classical double homologous recombination.

While the rate of mutant recovery compared to the wildtype achieved following secondary crossover of isolated merodiploids via a double crossover homologous recombination strategy should be in the order of a 1:1 ratio (Hmelo *et al.*, 2015), isolation of double-crossover mutants was a rarer occurrence in the employed strategy (data not shown). It is postulated that selection of the recipient strain from the donor strain via auxotrophy alone is insufficient to fully deplete the donor strain, hence leading to selection escape of the donor strain and persistence into the screening of

merodiploids for a secondary crossover event. As the donor strain would mimic the expected antibiotic resistance phenotype of any expected merodiploids, the Cm^R colonies isolated during the merodiploid screen may not be clonal for merodiploids. Furthermore the supposedly conditional lethality of the *sacB* counter-selectable element on the pDM4 (and derivatives) was not as schismatic as has been reported. Indeed Milton and co-workers, the original constructors of the pDM4 suicide vector series, noted that sucrose selection does not present a simple phenotype of growth or no growth. Instead, *sacB* and *sacB*-negative colonies demonstrate different morphologies on sucrose media and the lethal effect is delayed by 36 to 48 h (Milton *et al.*, 1996). Hence screens for double crossover mutants, may appear to yield fewer mutants than anticipated due to poor ability of the sucrose selection to discriminate between double crossover mutants and merodiploids and persistence of the donor strain in the screened population. In further biparent matings between *E. coli* donors and *E. coli* recipients, it was possible to minimise the presence of residual donor by exchanging S17-1 λ*pir* with ST18; a Δ*hemA* derivative of S17-1 λ*pir*, which requires exogenous 5-ALA (aminolevulinic acid) for growth (Thoma & Schobert, 2009). Fortunately PCR screens are sufficiently powerful to exquisitely differentiate between isolated mutant colonies or those of other genomic backgrounds, and multiple double crossover mutants candidates were routinely observed in a typical screen of 50-100 colonies following counter-selection.

Such PCR screens were able to confirm the presence of the desired mutation at the correct chromosomal location, with an electrophoretic profile consistent with the size of this insertion-deletion mutation. Furthermore, sequencing of the PCR product isolated from mutant clones reveals perfect identity with the designed construct.

Additionally, it was demonstrated by a confocal microscopy assay that the constructed inducible *fim* mutant was able to bind mannosylated glycopolymers but not galactosylated glycopolymers – consistent with previous reports on the binding preferences of FimH (Bouckaert *et al.*, 2006; Sperling *et al.*, 2006; Yan *et al.*, 2015b). This binding phenotype was exclusively displayed upon induction, suggesting tight, controllable regulation of Type 1 fimbriae expression by replacement of the native regulon by the *tetR*-P_{tetA} system.

It is noted that in the confocal microscopy binding assay complete coverage of all available mannose binding bacteria was not observed. It was not possible to determine fully with the amount of material available whether this was due to availability of the glycopolymer or incomplete expression of the Type 1 fimbriae, and the associated lectin FimH, from the inducible mutant. Alternatively an excess of a fluorescently labelled sugar could be utilised to visualise lectin expression on the surface of target bacteria. To guarantee maximal expression of the Type 1 fimbriae from the inducible promoter, an inducer titration could be performed and the confocal assay repeated with the most effective concentration. As previous studies have shown that maximal heterologous protein expression with the

concentration of inducer used in this study, it is more likely that insufficient concentration of glycopolymer is the culprit for this observation and inducer titration is not necessary. However, it is possible that the mutant construction strategy did not remove all transcriptional regulator binding sites upstream of the *fimA* transcriptional start site and the native regulon may still have some impact on expression of the Type 1 fimbriae in the inducible mutant.

Further confirmation of expression of the Type 1 fimbriae in the inducible mutant strain produced in this study could be interrogated with other molecular biology techniques. SDS-PAGE could be utilised to demonstrate the presence of the individual proteins expressed as part of the *fim* operon on a polyacrylamide gel. Furthermore, this method could be used to analyse expression levels based on titration of ATc and determine the optimal concentration of autoinducer for expression. However, it is important to note that SDS-PAGE is unable to distinguish proteins of similar size and that natively expressed proteins are also recovered, this may make determination of individual proteins which are expressed as part of the *fim* operon cumbersome.

Western blotting could also be utilised for analysis of *fim* operon expression while minimising the presence of confounding analytes by providing high specificity for *fim* proteins via an antibody. However, antibodies against neither FimA, the core subunit of the fimbriae, nor FimH, the mannose binding lectin on the distal tip, that would have enabled western blotting

analysis, are not commercially available. Hence this technique was omitted from the present study.

Some authors have previously reported the visualisation of Type 1 fimbriae on the surface of *E. coli* by TEM (Wright *et al.*, 2007). The data shown by Wright & co-workers, however, is not convincing for demonstration of Type 1 fimbriation as similar structures are seen in uninduced UTI189-*tetR*. Hence the structures identified as Type 1 fimbriae could feasibly be other filamentous appendages such as P pili, sex (F) pili or flagella (Costa *et al.*, 2016; Mu & Bullitt, 2006; Wright *et al.*, 2005). Furthermore, it was not possible to replicate this data in TEM studies performed with the inducible mutant produced in this study (data not shown).

To enable the monitoring of the extraction of bacteria from a mixed population via the magnetic glyconanoparticles produced in Chapter 3 an additional objective of this study was to generate autofluorescent derivatives of various *E. coli* strains. Expression cassettes for mRuby2 and mNeonGreen, the brightest and most photostable fluorescent proteins reported in the literature (Shaner *et al.*, 2013; Wilton *et al.*, 2018), were constructed. These mini-Tn7 cassettes were designed to be under the control of P_{11} and P_{24}, two strong, insulated promoters selected due to their constitutive function in numerous organisms, including *E. coli*, and the presence of an insulating feature to minimize polar effects due to transcription of genes proximal to the *att Tn7* insertional site in the *E. coli* chromosome (Alagesan *et al.*, 2018). For insertion of a single copy of these cassettes onto the chromosome, circumventing the population

heterogeneity demonstrated by plasmid-based fluorescence systems, the two-plasmid mini-Tn7 delivery system described by Crépin and co-workers was selected due to its elegance and viability in *E. coli*/*E. coli* biparental matings (Crepin *et al.*, 2012).

While screening for the transposon recombinants by PCR (Fig 2.17.) showed the correct integration in the *E. coli* chromosome for each strain utilised in this study, for reasons which cannot be explained, mNeonGreen appeared non-functional when integrated in the chromosome. Instead monomeric enhanced GFP (eGFP), an alternative bright, photostable green protein, was integrated in the chromosome under the control of P_{11} and P_{24} (Lam *et al.*, 2013; Zacharias *et al.*, 2002). mNeonGreen does not require any endogenous factors for folding or maturation and the maturation time is very fast (<10 min reported by the authors, compared with 25 mins for eGFP) (Shaner *et al.*, 2013). It may be possible that a critical intracellular concentration is required for the fluorescence of mNeonGreen and low expression from a single copy at a chromosomal location is insufficient to support this. Full genome sequencing and comparison with the wildtype would be necessary to determine whether abherrant chromosomal insertion, inversion or translocation of mNeonGreen expression cassettes could be a contributing factor in the observed loss of fluorescence phenotype during Tn7 mediated chromosomal tagging. Similarly in would be beneficial to perform whole genome sequencing and alignment on the inducible *fim* mutant produced by allelic exchange mutagenesis to monitor

for other chromosomal rearrangement events as a result of homologous recombination.

All eGFP- or mRuby2-expressing mini-Tn7 derivatives of JEP01, MG1655 and JW4283 grew with no statistically discernible growth differences over a period of 24 hours in M9F minimal media (Fig. 2.18), suggesting the absence of a fitness cost to the applicable cell population in terms of metabolic demand of hosting a single copy of the any of the fluorescent protein expression cassettes integrated in this study.

In terms of fluorescence, the eGFP-expressing strains follow a trend which correlates directly with that of OD_{600}. In contrast, the mRuby-expressing cells exhibit a plateau in fluorescence intensity while the cells are in the logarithmic phase but fluorescence increases steadily as cell density stabilises in the stationary phase. This difference in fluorescence intensity trends may stem from the maturation properties of the proteins themselves. While both proteins are of similar photostability with half-lives under arc lamp illumination of 150 s for EGFP and 123 s for mRuby2, there is a large difference in chromophore maturation times (Bajar *et al.*, 2016; Lam *et al.*, 2012). The maturation time (the time for fluorescence to obtain half-maximal value when exposed to oxygen) was determined to be 25 min and 150 min for eGFP and mRuby2, respectively, by Lam and co-workers (Lam *et al.*, 2012). As the requirement of molecular oxygen is six-fold greater for mRuby2 compared to eGFP the high metabolic and respiratory activity of a cell population in the logarithmic growth phase may deplete the intercellular molecular oxygen concentration such that it is insufficient

for rapid chromophore maturation in the case of mRuby2, but is sufficient for the maturation of eGFP. This may explain why eGFP expressing strains would display a fluorescence intensity trend that precisely follows growth patterns, whereas mRuby2 strains do not demonstrate an increase in fluorescence intensity until the stationary growth phase. This is a potential limitation of mRuby2 tagged strains when continuous monitoring of fluorescence during growth is required, as bright fluorescence is not observed until the stationary phase. However, this is not an issue for the flow cytometric assay to determine cell isolation by glycosylated nanoparticles as shown in Chapter 4 as bacterial populations were incubated with the materials overnight before analysis.

In summary, the data in this chapter demonstrate the construction of an ATc-inducible mutant of the *fim* operon in the *E. coli* MG1655 background which is able to bind mannosylated, but no galactosylated, materials in the presence of the inducer only. Additionally, mini-transposon-tags for all the key strains of interest, and their parental strains, which constitutively express either eGFP or mRuby2, were also produced. None of the generated strains appear to show any aberrant growth and hence should be suitable for the mediation of selective isolation of cells by magnetic glycomaterials as produced in Chapter 3, and monitoring of the extraction process as demonstrated in Chapter 4.

3. Synthesis of Glycopolymer Decorated Superparamagnetic Fe_3O_4 Nanoparticles

3.1. Introduction

3.1.1. Synthesis of polymers by controlled radical polymerisation (CRP)

Free radical polymerisation (FRP) is a critically important industrial process which is responsible for 40-50% of global synthetic polymer production corresponding to over 10^5 metric tonnes annually (Matyjaszewski & Davis, 2002; Nakamura & Yamago, 2015). Mechanistically, radical polymerisation involves reaction of radical intermediates with vinyl monomers, and can be split into three stages:

1. Initiation - Generation of radicals by the decomposition of radical initiators typically triggered thermally, by UV irradiation or by the presence of chemical activators.
2. Propagation – reaction of radical species with monomer double bonds, resulting in polymer chain extension ($r_p \propto [P\cdot]\,[M]$).
3. Termination – Irreversible reaction of two radical-terminated polymer chains, either by chain-chain coupling or disproportionation, yielding non-reactive ('dead') polymer chains which cannot be extended further ($r_t \propto [P\cdot]^2$).

Crucially however, traditional free radical polymerisation (FRP) techniques offer little control over key process elements such as propagation rates leading to poor control over polymer molecular weights, chain composition

and architecture, site-specific functionalities and, most importantly, dispersity (Matyjaszewski & Spanswick, 2005).

Since the 1990s significant effort has been invested in the development of new polymerisation techniques under the umbrella term controlled radical polymerisation (CRP) which aimed to improve conventional radical polymerisation techniques such that polymer chain length, molecular weight distribution, composition and macromolecular architecture could be adequately controlled (Braunecker & Matyjaszewski, 2007; Shipp, 2011).

The most commonly used controlled radical polymerisation techniques include Nitroxide Mediated Polymerisation (NMP) (Nicolas *et al.*, 2013), Atom Transfer Radical Polymerisation (ATRP) (Pintauer & Matyjaszewski, 2008), Reversible Addition Fragmentation Chain Transfer (RAFT) (Moad *et al.*, 2008). Mechanistically these systems still maintain the initiation, propagation, termination paradigm of FRP but crucially employ the establishment of a dynamic equilibrium between the propagating radicals (P·) and non-reactive (dormant) species. These equilibria are shifted largely towards dormant species which ensures that at any given time the concentration of radical species is very low. As termination is $\propto [P\cdot]^2$ while propagation is $\propto [P\cdot]$, the former is favoured over the latter at high concentrations of radical species. Thus, keeping the concentration of radical species low, one can minimise termination over propagation allowing for control over the evolution of polymer chain length (Mayadunne *et al.*, 2000; Moad & Rizzardo, 1995; Sawamoto & Kamigaito, 1997) (Fig 3.1).

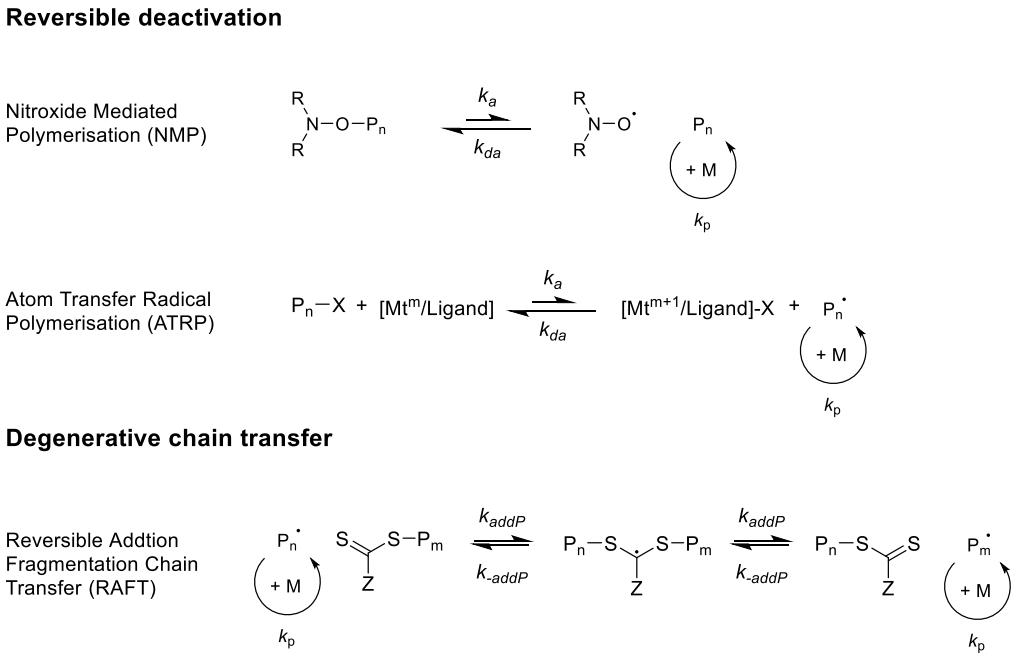

Figure 3.1. Main dynamic equilibria of different controlled radical polymerisation (CRP) processes. The most commonly used CRP techniques can be divided into two distinct mechanistic categories: reversible deactivation radical polymerisation (RDRP) and degenerative chain transfer. Establishment of a dynamic equilibrium between propagating radicals and a dormant species reduces the occurrence of termination to low levels, allowing for control of polymer molecular weight and distribution.

Since their advent, the use of CRP techniques has expanded significantly, with hundreds to thousands of papers published routinely every year (Matyjaszewski, 2012). The key to this popularity is in part related to the versatility of CRP techniques to generate a vast array of novel materials which desired properties. CRP-based polymerisation processes are also tolerant to a range of solvents and unprotected functional groups (Coessens *et al.*, 2001; Moad *et al.*, 2008). Specific functional groups can be inserted at one or both chain ends by using functional initiators in the case of ATRP and NMP, or CTA in the case of RAFT polymerisation (Tasdelen *et al.*, 2011).

CRP techniques also offer unprecedented control over the composition of polymers allowing for the synthesis of homopolymers (Li *et al.*, 2003;

Wever *et al.*, 2012), block copolymers (Albertin *et al.*, 2005; Lee *et al.*, 2003; Li *et al.*, 2003), gradient copolymers (Chen *et al.*, 2012; Lee *et al.*, 2003; Matyjaszewski *et al.*, 2000b), statistical copolymers (Lee *et al.*, 2003; Roka *et al.*, 2017; Shemper & Mathias, 2004), graft copolymers (Beers *et al.*, 1998; Crownover *et al.*, 2011; Jiang *et al.*, 2013b) and molecular brushes (Gao & Matyjaszewski, 2007; Li & Gao, 2013; Li *et al.*, 2009) – a distinct subspecies of graft copolymer in which multiple polymer chains are grafted onto a linear polymer resulting in a densely packed 'brush' like morphology (Fig. 3.2).

Furthermore, it is also possible to generate materials with a range of macromolecular architectures by CRP including linear (Wang *et al.*, 2018; Zhang & Chen, 2006), multi-armed/star (Angot *et al.*, 1998; Shemper & Mathias, 2004; Zhang & Chen, 2006), comb (Li *et al.*, 2018a; Ostmark *et al.*, 2007) and hyperbranched (Liu *et al.*, 2005; Tsarevsky *et al.*, 2009) polymers (Fig 3.2.)

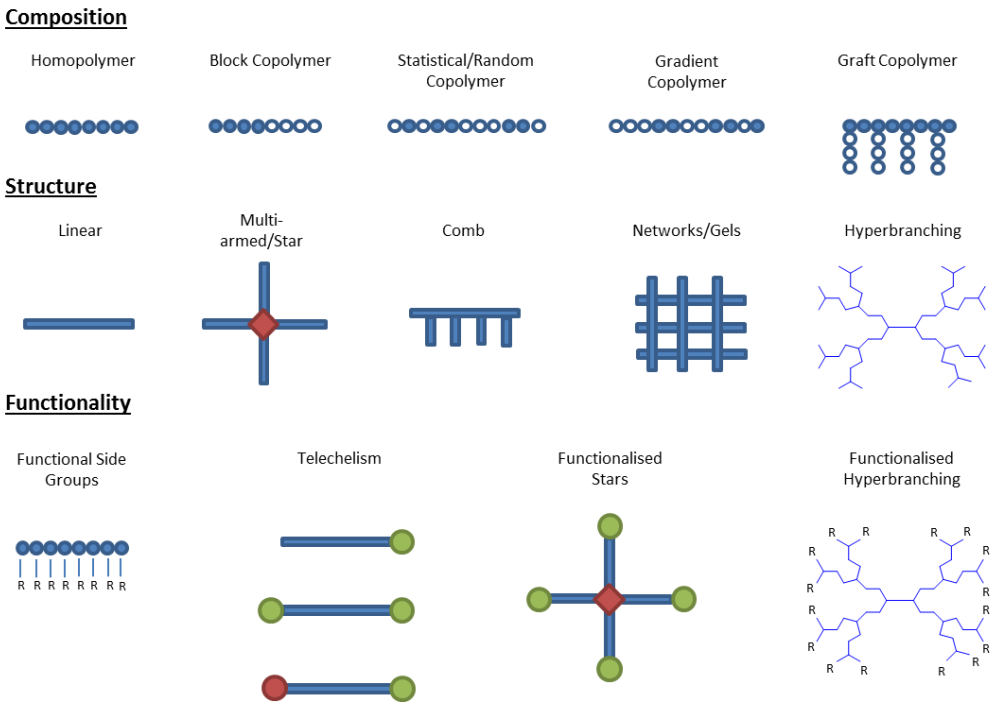

Figure 3.2. Overview of polymer composition, structure and functionality schemes achievable through CRP. CRP based polymers can be synthesised with defined ratios and composition of different monomers, shown here as blue and white circles. Additionally polymers can be synthesised with functional side groups (R groups in diagram) or reactive chain terminal groups (red and green circles). These end groups may be identical or different producing polymers with are hemitelechelic (one reactive terminus), homotelechelic (same reactive group at each terminus) or heterotelechelic (alternate reactive groups at either terminus). Adapted from Talesden et al, 2011 and Matyjaszewski & Spanswick, 2005.

Additionally, CRP based polymer synthesis schemes are very popular due to the ease of set up, readily available commercial catalyst systems and a wide variety of available monomers and initiators/CTAs; both commercially and described in the literature. The tolerance of these systems to myriad functional groups on both the monomers and initiators/CTAs lends CRP well to the rational design of a multitude of functional materials. These various facets have ensured CRP has become a ubiquitous and invaluable tool in material science, with unparalleled utility.

3.1.2. Synthesis of glycopolymers by CRP

In principle there are two distinct routes for the production of glycopolymers: direct polymerisation of glycomonomers or post-polymerisation functionalisation of reactive polymeric materials with carbohydrate groups (Becer, 2012). The first report of the synthesis of a well-defined glycopolymer by CRP was produced by Ohno *et al* in 1998 by NMP of an isopropylidene-protected glucose methacrylate monomer (Ohno *et al.*, 1998). Acidolysis of the protected homo and block copolymers synthesised yielded well-defined glucose functional polymers which were water soluble. Direct polymerisation of glycomonomers has also been reported for ATRP/SET-LRP (Single Electron Transfer Living Radical Polymerisation) (Albertin *et al.*, 2004; Albertin *et al.*, 2005; Ghadban & Albertin, 2013; Ke *et al.*, 2010; Miao *et al.*, 2019; Vazquez-Dorbatt *et al.*, 2009; Zhang *et al.*, 2013a; Zhang *et al.*, 2014) and RAFT (Adharis *et al.*, 2018; Albertin *et al.*, 2006; Cameron *et al.*, 2008; Deng *et al.*, 2009; Lowe *et al.*, 2003) based systems.

The development of 'click chemistry', a series of highly efficient organic reactions introduced by the Sharpless group has been invaluable in the development of synthetic chemistry for glycopolymer construction (Kolb *et al.*, 2001). In particular the copper catalysed azide-alkyne cycloaddition reaction (CuAAC) has been most widely applied (Fig. 3.3.) (Slavin *et al.*, 2011; Wang *et al.*, 2005).

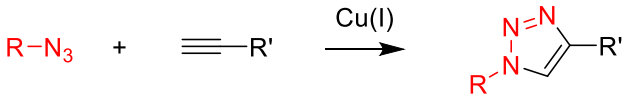

Figure 3.3. Copper(I)-catalysed azide alkyne cycloaddition (CuAAC).

Click reactions to yield vinyl glycomonomers have been well described, facilitating direct polymerisation of these monomers (Geng *et al.*, 2007; Hetzer *et al.*, 2010; Tanaka *et al.*, 2009). Furthermore, the use of click chemistry has allowed for the development of processes for post-polymerisation modification of polymers with a polyalkyne clickable scaffold with sugar azides (Ladmiral *et al.*, 2006). In this work, a trimethylsilyl propargyl methacrylate was polymerised by ATRP using CuBr/*N*-(ethyl)-2-pyridylmethanimine as the catalytic system. The resulting well-defined polymers were then quantitatively deprotected with tetra-*N*-butylammonium fluoride(TBAF)/acetic acid, to reveal an alkyne clickable backbone. Finally, this scaffold was used as a common starting material to produce a library of glycopolymers by CuAAC of the pedant alkyne groups with various sugar azides (Fig 3.4.) (Ladmiral *et al.*, 2006). In this way mannose modified particles have been synthesised and their ability to bind the lectin Concanavalin A tested (Chen *et al.*, 2007). Due to their sharing of a CuBr catalyst simultaneous one-pot CuAAC/ATRP techniques have also been described, streamlining the synthetic process to make well-defined glycopolymers (Geng *et al.*, 2008).

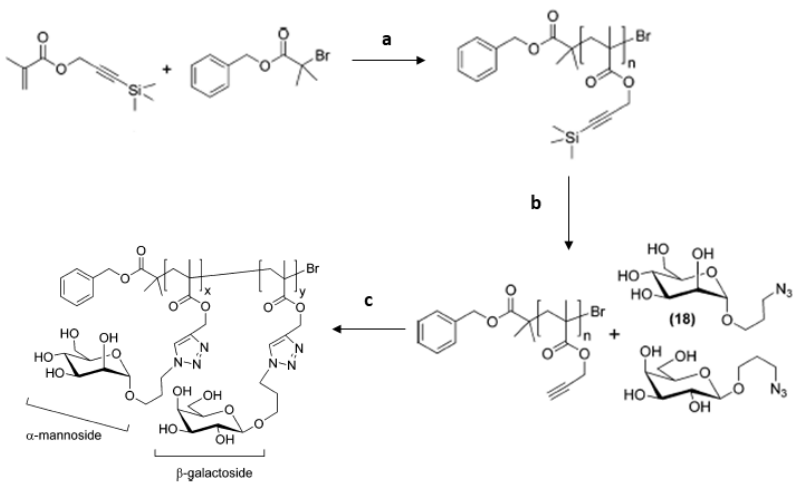

Figure 3.4. Synthesis of glycopolymers by combined ATRP/CuAAC approach as reported by Ladmiral *et al*, 2006. a) N-(n-ethyl)-2-pyridylmethanimine/CuBr, toluene, 70 °C; b) TBAF, acetic acid; c) (PPh3)3CuBr, DIPEA. Adapted from Ladmiral et al, 2006.

Another elegant approach for post polymerisation sugar-functionalisation was described by Boyer & Davis (Boyer & Davis, 2009). In this study a pentafluorophenyl acrylate was polymerised via RAFT in benzene using 3-(benzylsulfanylthiocarbonylsulfanyl)-propionic acid as a CTA. This polymer was then modified by nucleophilic addition of glucose or galactose amines in DMF with quantitative yields in less than one hour. *In situ* aminolysis of the RAFT end-group and addition of thiol to a biotin modified maleimide was then performed, yielding biotin-functionalised glycopolymers obtained in a one pot synthesis (Fig 3.5) (Boyer & Davis, 2009).

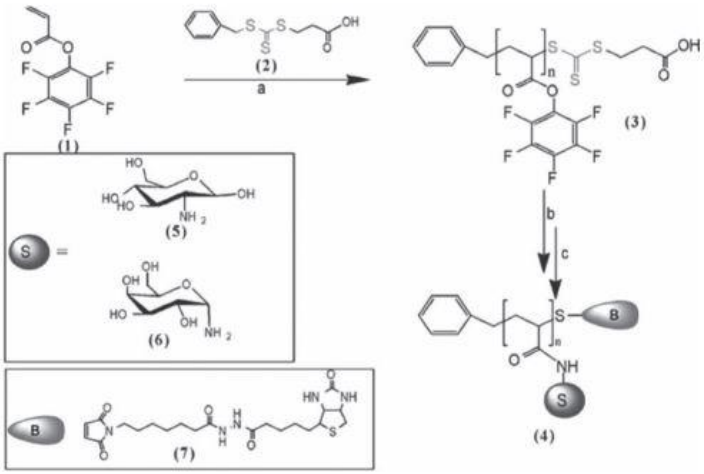

Figure 3. 5. Post-polymerisation glycosylation of RAFT derived polymers by Boyer & Davis Method. (a) RAFT polymerization with AIBN in benzene at 70 °C, (b) nucleophilic addition of amine in DMF–water (50/50 vol%) at room temperature, (c) in situ aminolysis of the RAFT end-group and the addition of thiol onto biotin modified maleimide. From Boyer & Davis (2009).

A particularly serendipitous discovery in the field of glycopolymer synthesis was the development of a single electron transfer living radical polymerisation (SET-LRP) procedure for glycopolymer synthesis by allowing disproportionation of the CuBr/Me_6TREN catalyst to Cu(0) powder and $CuBr_2$ in water prior to addition of both monomer and initiator (Anastasaki *et al.*, 2016; Nguyen *et al.*, 2010). Mechanistically SET-LRP is distinct to ATRP. In a model proposed by Percec & co-workers Cu(0) is the primary activator of the alkyl halide initiator (Levere *et al.*, 2013; Percec *et al.*, 2006). Highly reactive 'nascent' Cu(0) is spontaneously generated by disproportionation of Cu(I)X into Cu(0) and Cu(II)X_2 species in the presence of nitrosylated ligands with minimal comproportionation. Both activation and deactivation of propagating radicals by Cu(0) and Cu(II) species occurs by a low activation energy single outer sphere electron transfer (OSET) (Levere *et al.*, 2013; Percec *et al.*, 2006). However, there is

some controversy surrounding the mechanism of SET-LRP with other authors suggesting Cu(0) merely acts as a supplemental activator of alkyl halide initiators, with the core mechanistic traits of the polymerisation process being activation of propagating radicals by Cu(I) species and deactivation by Cu(II) species, in accordance with the paradigmatic ATRP mechanism (Konkolewicz *et al.*, 2013; Lorandi *et al.*, 2015). This alternative model has been named supplemental activator and reducing agent atom transfer radical polymerisation (SARA ATRP).

Regardless of mechanistic considerations, Cu(0) catalysed polymerisations can be performed at or below ambient temperatures, allowing for rapid conversions in biologically relevant solvents (water/phosphate buffered saline) with excellent control over molecular weight distributions ($Đ$<1.1) (Zhang *et al.*, 2013b). Indeed SET-LRP has been developed further by the Zhang & co-workers for the synthesis of well-defined hydrophilic fluorescent catechol terminal glycopolymers which may be conjugated to magnetic Fe_3O_4 nanoparticles generating novel bifunctional nanomaterials (Zhang *et al.*, 2016b).

SET-LRP is particularly amenable to the synthesis of glycopolymers as the disproportionation of Cu(I) species to Cu(0) and Cu(II) species is dependent upon highly polar reaction media, hence monomers for SET LRP must also be polar. Additionally this technique allows for exquisite control over molecular weight distributions and end-group fidelity even at conversions approaching 100% (Nystrom *et al.*, 2011; Simula *et al.*, 2015). This high maintenance of polymer end group leads itself well to the production of

copolymers due to retention of halide termini (Alsubaie *et al.*, 2015; Nystrom *et al.*, 2011; Soeriyadi *et al.*, 2011). However, extremely precise conditions are required for well controlled SET-LRP polymerisations and significant optimisation efforts must be expended by the investigator when using this technique.

RAFT polymerisation is particularly well suited to glycopolymer synthesis for a number of reasons. Firstly, RAFT may be conducted in homogenous aqueous media at ambient to moderate temperatures for the synthesis of water soluble glycopolymers (Albertin & Cameron, 2007; Albertin *et al.*, 2005; Lowe & McCormick, 2007). Also, by careful matching of CTA agent to monomer functionalities, well controlled RAFT polymerisation can achieved for practically all monomers which are amenable to radical polymerisation (Perrier, 2017). Secondly, RAFT polymerisation may be easily performed under heterogeneous conditions for the production of glycopolymer decorated nanoparticles with tunable core-shell morphologies (Kutcherlapati *et al.*, 2017b). Additionally, unlike Cu-catalysed techniques, RAFT polymerisation does not require removal of the metal catalyst from the final polymer. At the laboratory scale this can be achieved used silica or alumina columns or ion exchange resins but is still a major challenge for large scale polymerisations (Matyjaszewski *et al.*, 2000a).

For high end group retention, which is essential for multiblock polymer synthesis, ATRP based systems have typically had to be stopped at incomplete monomer conversion (Rabea & Zhu, 2014). In contrast RAFT

polymerisation block copolymers may be produced at high conversion and precise sequence with controlled polymers consisting of up to 20 blocks have been reported (Gody *et al.*, 2013, 2014). Indeed synthesis of periodic and alternating glycopolymers of maltose and lactose substituted vinyl ethers and maleimides using a RAFT based method has been reported, suggesting that RAFT based methods may be pivotal in the production of glycopolymers with precisely controlled sequences (Minoda *et al.*, 2019). Precise control over glycomonomer sequence is likely to be essential for the synthesis of glycomimetics for interrogation of the glycocode which is ubiquitous in biology and as high affinity lectin ligands (Becer, 2012; Yilmaz & Becer, 2014; Zhang & Ye, 2018).

Finally, the thiocarbonylthio group retained on RAFT-derived polymers may be exploited for further material functionalisation e.g. by conversion to a thiol group by reduction or aminolysis (Xu *et al.*, 2006) which may then be used for further couplings. Indeed reduction of RAFT polymers to thiolated materials was previously established as a versatile method for the decoration of transition metal nanoparticles in 2002 (Lowe *et al.*, 2002). Thiol terminal polymers may also be used in thiol-ene 'click' reactions to add new functionalities or architectures to RAFT polymers (Boyer *et al.*, 2009).

In this thesis work a RAFT strategy was employed for the production of glycopolymers with catechol functionalised end groups for the decoration of SPIONs.

3.1.3. Synthesis of superparamagnetic iron oxide nanoparticles (SPIONs)

Within recent years inverse spinel type superparamagnetic iron oxide nanoparticles (SPIONs) have been widely investigated in the fields of nanotechnology and nanomaterials due to their desirable properties: nanoscale size, large surface area to volume ratio, superparamagnetic behaviour, high magnetisation saturation level and biocompatibility (Demirer *et al.*, 2015; Gao *et al.*, 2009; Laurent *et al.*, 2008; Li *et al.*, 2016; Wu *et al.*, 2016). This class of nanomaterials, and derivatives thereof, have been investigated for many applications including tumour magnetic hypothermia for cancer therapies, magnetic resonance imaging contrast agents, targeted drug delivery, biosensors and cell/protein separation strategies (Brognaux *et al.*, 2013; Chen *et al.*, 2011; Dutz & Hergt, 2014; Frey *et al.*, 2009; Haun *et al.*, 2010; Kayal & Ramanujan, 2010; Li *et al.*, 2013; Ma *et al.*, 2012; Oz *et al.*, 2019; Sadhukha *et al.*, 2013). Some examples of SPION based therapies already on the market include: Feridex, a reticuloendothelial targeted MRI constrast agent for liver/spleen imaging (Reimer & Balzer, 2003); Feraheme, a macrophage targeted therapy for iron deficiency anaemia in patients with chronic kidney disease (Adkinson *et al.*, 2018) and NanoTherm, a therapy for magnetically induced thermal ablation of localised tumours in glioblastoma, prostate and pancreatic cancer (Maier-Hauff *et al.*, 2011; Ventola, 2017; Weissig *et al.*, 2014).

The properties of $Fe_3(_{II,III})O_4$ nanoparticles are exquisitely dependant on their production. To demonstrate superparamagnetism, iron oxide nanoparticles must be sufficiently small. A size of <20 nm has been

estimated to be critical for this (Jun *et al.*, 2005; Li *et al.*, 2017; Pereira *et al.*, 2012). Particle morphology and size distribution is also highly dependant on production process. Furthermore, if the designed particles are to be upscalled industrially, it is crucial that the production process is reproducible. As such, numerous methods have been devised for the synthesis of SPIONS including coprecipitation of ferric/ferrous salts, thermal decomposition, microemulsion and hydrothermal synthesis with varying degrees of control over size distribution and particle morphology, as well as reproducibility (Chin & Yaacob, 2007; Ge *et al.*, 2009; Maity & Agrawal, 2007; Park *et al.*, 2004).

3.1.1.1. Chemical Coprecipitation

The coprecipitation method is arguably the most commonly used and facile for the synthesis of magnetic nanoparticles, even for non-chemists. Iron oxides (either Fe_3O_4 or γFe_2O_3) may be prepared by aging a stoichiometric mixture of ferric and ferrous salts (2:1) in basic aqueous media under an inert atmosphere producing a black colloidal suspension as shown in equation 3.1. (Maity & Agrawal, 2007; Shen *et al.*, 1999; Vayssieres *et al.*, 1998). However magnetite (Fe_3O_4) is not very stable and prone to oxidation to maghemite (γFe_2O_3)(Schwaminger *et al.*, 2017).

$$Fe^{2+} + 2Fe^{3+} + 8OH^- \longrightarrow Fe_3O_4 + 4H_2O$$

Equation 3.1. SPION synthesis by coprecipitation method

Various factors affect the size and morphology of particles which can be obtained by the coprecipitation method. Maity & Agrawal demonstrated

that initial ratio of Fe(II) to Fe(III) altered particle size and composition (Maity & Agrawal, 2007). Furthermore, these authors demonstrated a decrease in mean particle size when incorporated into kerosene or dodecane based ferrofluids, suggesting better dispersion in non-aqueous media. Vayssieres & co-workers demonstrated that increasing pH and ionic strength of the media produced particles of decreasing mean size, thus allowing for some size targeting with this technique (Vayssieres *et al.*, 1998).

The popularity of coprecipitation for the synthesis of SPIONs belies two of its key advantages; simplicity and ability to perform synthesis on a large scale. However, control of particle size distribution and morphology is poor compared to other methods, and materials produced by coprecipitation are always polydisperse. Since the magnetic properties of SPIONs are intrinsically linked to size, materials with poorly uniform size distributions can exhibit non-uniform magnetic dipole moments and saturation magnetisation, which is undesirable for particles with precision applications and may contribute to aggregation after removal from a magnetic field (Batlle & Labarta, 2002; Demortiere *et al.*, 2011; Luigjes *et al.*, 2011).

3.1.1.2. Microemulsion

Microemulsions are clear, thermodynamically colloidal dispersions of two liquids which are immiscible (typically an oil phase and an aqueous phase) which are brought to coexist as a single phase due to the presence of surfactants (Lopez-Quintela, 2003). Structurally, microemulsions can be classified as either water in oil (o/w), oil in water (o/w), or bicontinuous (Lopez-Quintela, 2003; Zang *et al.*, 2018). Both water in oil and oil in water microemulsion systems have been utilised for the synthesis of SPIONs (Kekalo *et al.*, 2012; Nourafkan *et al.*, 2019). In their work Nourafkan & co-workers were able to produce SPIONs ranging from 5-30 nm but control of particle size and morphology was highly dependent upon oil to water ratio, temperature, concentration of iron precursor and the rate of alkali addition into the nanoreactor (Nourafkan *et al.*, 2019). In another example Chin & co-workers were able to produce SPIONs below 10 nm in size using a water in oil emulsion of ferrous chloride hexahydrate with hexadecyltrimethyl ammonium bromide and sodium hydroxide in butanol with improved polydispersity over chemical coprecipitation, however large variance in particle size and morphology was observed (Chin & Yaacob, 2007). While giving generally better properties than coprecipitation, preparation of monodisperse, uniform iron oxide nanoparticles via microemulsion is still an elusive goal. Furthermore, these particles tend to require significant work up and stabilisation prior to application.

3.1.1.3. Hydrothermal Synthesis

In hydrothermal synthesis the growth of crystals is dependent upon the solubility of precursors, which are not normally soluble in aqueous media, in hot water under elevated temperature and pressure (Wu *et al.*, 2016). This method is usually performed in an autoclave and can be used to grow iron oxide crystals with controlled size and shapes at sizes exceeding those that may be achieved by thermal decomposition or coprecipitation. Iron oxide nanoparticles of up to 150 nm have been synthesised by microwave assisted hydrothermal processes (Sayed & Polshettiwar, 2015). Control over shape and size of iron oxide nanoparticles produced by hydrothermal synthesis is dependent upon temperature, reaction time, iron precursor used and presence of surfactants or other metal ions (Ge *et al.*, 2009; Jensen *et al.*, 2014; Wu *et al.*, 2016; Wu *et al.*, 2014; Yang *et al.*, 2011).

In a facile synthesis Ge & co-workers were able to produce iron oxide nanoparticles in a range of diameters between 15 and 31 nm by autoclaving an aqueous solution of $Fe(II)Cl_2$ and ammonium hydroxide under air at 2 bar pressure (Ge *et al.*, 2009). The best size distribution reported in this study was 15.4 ± 2.4 nm. Particle size and magnetic properties could also be tuned be altering the concentration of iron(II) chloride and ammonium hydroxide (Ge *et al.*, 2009). Hydrothermal synthesis of metal oxide nanoparticles has also been performed in supercritical water, decreasing reaction times and giving good control over particle size and dispersity (Adschiri *et al.*, 2001; Hayashi & Hakuta, 2010; Takami *et al.*, 2007; Zhao *et al.*, 2007). Furthermore, by adequate design of a novel nozzle mixer within

their supercritical water reactor Lester *et al* were able to reproducibly manufacture a diverse panel of metal oxide nanoparticles ranging in 6-64 nm, paving the way for continuous nanoparticle production by hydrothermal synthesis with supercritical water (Lester *et al.*, 2006).

A key advantage of these syntheses is ease of the reaction and an absence of additional work up steps. The lack of need for an inert gas supply and requirements for specialised laboratory apparatus with the exception of an autoclave makes hydrothermal syntheses easier to perform than thermal decomposition or coprecipitation counterparts – however *in situ* surface modification remains elusive.

3.1.1.4. Thermal Decomposition

Many examples have been demonstrated in the literature for the synthesis of SPIONs via thermal decomposition. Nanoparticles with a high degree of monodispersity and size control may be obtained by the high temperature decomposition of a range of organometallic iron precursors including $Fe(CO)_5$, Fe(acetylacetonate)$_3$, Fe(cup)$_3$ (Cup = N-nitrosophenylhydroxylamine) , iron oleate complex, ferrocene and $Fe_3(CO)_{12}$ (Amara *et al.*, 2009; Bhalerao *et al.*, 2009; Hyeon *et al.*, 2001; Lassenberger *et al.*, 2016; Park *et al.*, 2004; Rockenberger *et al.*, 1999; Sun & Zeng, 2002). Typically these reactions are performed in high boiling point organic solvents, such as dioctyl ether or octadecene, with fatty acids or amines, such as oleic acid or oleylamine, included as stabilising agents (Laurent *et al.*, 2008; Wu *et al.*, 2016).

Particles produced by the thermal decomposition method are normally very small (up to around 20 nm) and their size may be precisely controlled by varying experimental conditions. In the method reported by Park & co-workers an iron oleate complex was produced using non-toxic and inexpensive precursors iron(III) chloride and sodium oleate. The iron oleate complex was then decomposed between 270 and 320^{o}C in varying organic solvents. This study showed that an increase in boiling point of the solvent, the diameter of the recovered particles increased from 5 nm for hexadecane (b.p. 274 °C) to ~22 nm for trioctylamine (b.p. 365 °C) (Park *et al.*, 2004). While this general trend was seen for all solvents tested, the presence of a potentially coordinating nitrogen centre in trioctylamine could have potentially affected the result for this solvent. Furthermore, this study also demonstrated that concentration of surfactant could also be modified to fine-tune particle diameter (Park *et al.*, 2004). Other authors also have shown that the ratio of surfactant to iron precursor was crucial for size control (Bixner *et al.*, 2015; Hufschmid *et al.*, 2015; Lassenberger *et al.*, 2016). It has previously been reported that for particles of increasing size beyond the normal ranges targeted, a trade off in terms of dispersity may be seen (Hufschmid *et al.*, 2015). However, in a relatively recent report Guardia & co-workers were able to produce monodisperse SPIONs up to 180 nm in size by using decanoic acid as a capping agent and meticulous control of the rate of heating (Guardia *et al.*, 2010).

The thermal decomposition method is the most effective for producing high quality, monodisperse nanoparticles with a narrow size distribution and

uniform morphology. As the performance of SPIONs in their intended applications is often strongly correlated with their morphology, size and magnetic anisotropy, thermal decomposition remains one of the preferred methods for nanoparticle synthesis. However thermal decomposition derived nanoparticles may only be redispersed in organic solvents due to high surface functionalisation with hydrophobic surfactants, which may limit their utility for biomedical applications without additional processing steps. Furthermore, the boiling of sometimes highly toxic organometallics can be more hazardous than other processes, which may deter researchers. The presence of a hazardous deterrent is particularly true in the case of iron carbonyl precursors, which liberate large quantities of gaseous CO when heated at elevated temperatures.

3.1.4. Strategies for coating SPIONs with polymeric materials

SPIONs without a surfactant or polymeric coating tend to be poorly stable in aqueous media or physiological fluids, tending towards aggregation and precipitation. For this reason either steric or electrostatic stabilisation is required to attain colloidal stability; hence fatty acids such as oleic acid are routinely added to SPION synthesis procedures. However, for more precise application, tailoring of specific surface chemistries of synthesised SPIONs is required. The presence of free hydroxyl groups on the surface of SPIONs provides a convenient synthetic handle for the attachment of an array different functionalities. Functionalities utilised for surface modification of SPIONs include: amines (Aslam *et al.*, 2007), cysteine (Shen *et al.*, 2014), carboxylic acids (Maity & Agrawal, 2007; Thomas *et al.*, 2009), phosphonic

acid (Gharbi *et al.*, 2017), trimethoxysilane (Mikhaylova *et al.*, 2004b) and dopamine (Boyer *et al.*, 2010; Xu *et al.*, 2004) (Fig. 3.6.)

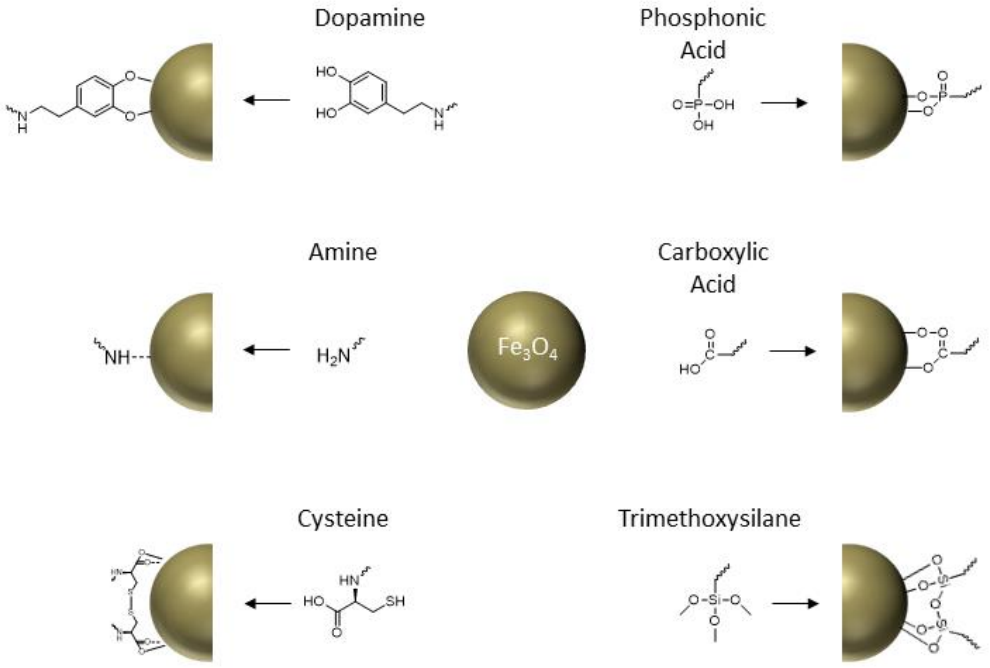

Figure 3.6. Functional groups utilised for SPION surface modification. Covalent bonds are shown as solid lines, electrostatic interactions/hydrogen bonding shown as dashed lines. Adapted from Boyer *et al*, 2010. More on bond type.

As such, polymeric materials which contain termini functionalised with the various anchor groups described above may be attached to SPIONs. Two main approaches to modifying the surface of SPIONs with polymeric materials exist in the literature: 'Grafting From' and 'Grafting To'.

3.1.2.1 'Grafting from'

In the case of 'grafting from' a polymer chain growth initiator (often a RAFT CTA or an ATRP alkyl-halide initiator) is fixed to a surface and the polymer chains are then grown from that surface *in situ*. Surface initiated RAFT and ATRP (si-RAFT/si-ATRP) functionalisation of inorganic materials has been reported using a variety of functional initiators and CTAs (Garcia *et al.*, 2007; Guo *et al.*, 2017; Hu *et al.*, 2006; Kang *et al.*, 2018; Lassenberger *et al.*, 2016; Li *et al.*, 2008; Majewski *et al.*, 2012; Ohno *et al.*, 2011; Oz *et al.*, 2019; Wang *et al.*, 2017; Zengin *et al.*, 2013).

In one work Kang & co-workers were able to functionalise SPIONs with a trimethoxysilane terminal alkyl bromide ATRP initiator, then grow a cationic polymer corona using si-ATRP (Fig. 3.7.). This cationic corona could complex ovalbumin, allowing for internalisation into macrophages (Kang *et al.*, 2018). Si-ATRP has also been utilised for grafting SPIONs with poly(methylmethacrylate) with a sulfonyl chloride initiator (Garcia *et al.*, 2007).

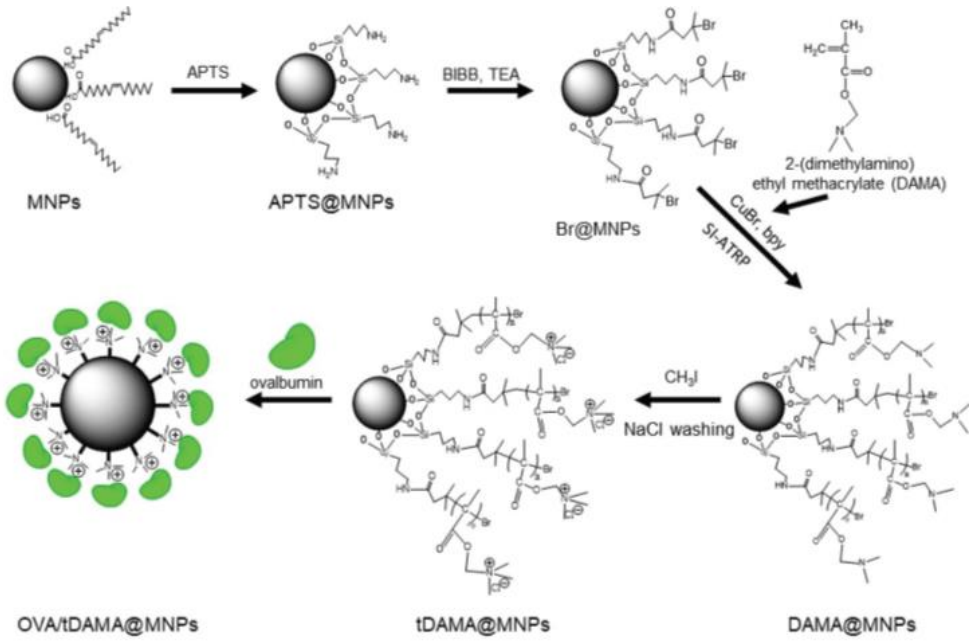

Figure 3.7. Functionalisation of magnetic nanoparticles with ovalbumin. Oleic-acid coated MNPs were first generated by aqueous co-precipiation of Fe(II) and Fe(III) salts. Nanoparticle surfaces were then amine functionalised with 2,2'-Bipyridyl 3-aminopropyltriethoxysilane (APTS@MNPs). Bromination of the primary amines presented on the silane functionalised MNPs by α-Bromoisobutyryl bromide with TEA in toluene yielded ATRP initiator functionalised NMPs (Br@NMPS). si-ATRP of 2-(dimethylamino) ethyl methacrylate by these initiatior funtionalised MNPs with catalytic amounts of CuBr and 2,2'-Bipyridine was then performed. The polymer coated NMPs (DAMA@MNPS) were trimethylated with iodomethane, before beinmg quenched with NaCl. Loading of ovalbumin onto the MNPs could be achieved by electrostatic interaction between the cationic polymer shell and net negative charge of the protein. Adapted from Kang *et al*, 2018.

For the surface modification of SPIONs with glycomaterials a key strategy has involved a 'grafting from' approach in combination with 'click' chemistry (Borase *et al.*, 2013; Farr *et al.*, 2014). In the one approach, Borase & co-workers functionalised SPIONs with 3-aminopropyl-triethoxysilane. Using these surface moieties as an initiator, ring opening polymerisation (ROP) of *N*-carboxyanhydrides was performed affording clickable alkyne groups. Azide-functionalised galactose was then attached to the nanoparticles by the canonical azide-alkyne 'click' reaction yielding glyconanoparticles which were water soluble and able to selectively bind lectins (Borase *et al.*, 2013). Alternatively, Farr & co-workers modified

silica-coated iron oxide nanoparticles with a trimethoxysilane terminal ester of N-hydroxysuccinimide. An amide linkage was created through coupling of amino-functionalised sugars to the activated NHS ester in DMF with triethylamine, yielding sugar functionalised magnetic iron oxide nanoparticles (Farr *et al.*, 2014).

Another strategy has involved using adamantane as a functionalisation medium. Oz & co-workers were able to functionalise SPIONs with a dopamine-terminal trithiocarbonate RAFT agent to allow the direct growth of PEG (Fig. 3.8.). Modification of the trithicarbonate with adamantane allowed for the functionalisation of the polymer brush with mannose or galactose containing β-cyclodextrins by non-covalent host-guest interactions. The glycosylated magnetic nanoparticles could then facilitate the selective magnetic purification of lectins (Oz *et al.*, 2019).

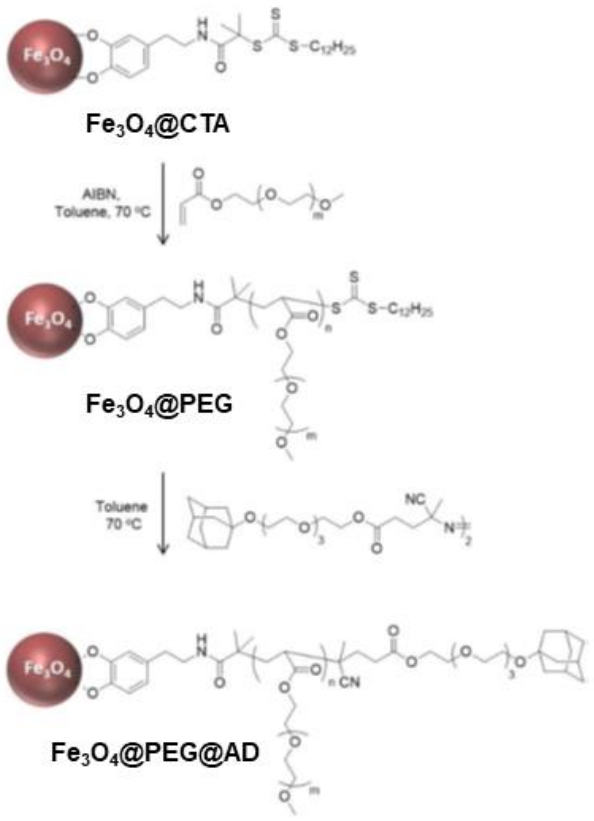

Figure 3.8. Funtionalisation of MNP surfaces with an adamantane terminal PEG. A catechol terminal RAFT chain transfer agent was first immobilised onto the Fe_3O_4 MNP surface. A polymer brush was then grown on the MNP surface by si-RAFT of poly(ethylene glycol) methyl ether acrylate in toluene with AIBN as the radical source. Radical transformation of the polymer brush was performed via a radical cross coupling reaction modification between the trithiocarbonate domain of the CTA and an adamantane functionalised azobis initiator. Subsequent glycosylation was then acheived by host-guest interactions between the adamantane functionalised MNPs and β-cyclodextrin functionalised sugars. Adapted from Oz *et al*, 2019.

Direct growth of glycopolymers on the surface of SPIONs may also be achieved using the grafting 'from' strategy and specific glycomonomers (Kutcherlapati *et al.*, 2017a; Yilmaz & Becer, 2015). Kutcherlapati & co-workers produced glyconanoparticles by grafting 4-cyanopentanoic acid dithiobenzoate to the nanoparticle surface and performing si-RAFT with the glycomonomers 2-(α-D-mannosyloxy)ethyl methacrylate (Kutcherlapati *et al.*, 2017a).

Jiao & co-workers have also demonstrated that a trimethoxysilane trithiocarbonate could be fixed to the surface of SPIONs (Jiao & Akcora, 2014). Intriguingly, faster polymer growth from the CTA affixed to the SPION surface was observed when compared RAFT polymerisation mediated by free CTA in solution (Jiao & Akcora, 2014). Furthermore, change transfer rates were found to be influenced by CTA density on the nanoparticle cores. The authors suggest radical transfer and exchange reactions become inefficient between grafts and free polymer, thus converting the surface-initiated RAFT mechanism to a free radical mechanism and increasing polydispersity of polymeric materials; a potentially significant limitation of this method (Jiao & Akcora, 2014). To minimise the impact this effect free sacrificial RAFT CTA or ATRP alkyl halide initiator may be added to these surface-initiated systems (Benetti *et al.*, 2017; Rowe *et al.*, 2008; Venkidasubramonian *et al.*, 2018; von Werne *et al.*, 2003; Wu *et al.*, 2015; Zheng *et al.*, 2014).

While the 'grafting from' route is able to generate high density grafts, characterisation of these materials can be challenging since the presence of iron oxide nanoparticles can confound analysis using conventional techniques such as NMR and SEC. If precise material architecture is required grafting 'to' remains preferable.

3.1.2.2. 'Grafting to'

In contrast to 'grafting from', in the 'grafting to' approach functional polymers with a chemically reactive terminus, as described above, are produced and characterised prior to surface modification. These materials may then be attached to the surface of SPIONs by molecular exchange of the reactive polymer with the surfactant coating. Synthesis of reactive polymers suitable for 'grafting to' modification of nanoparticles has been reported for a variety of functional CTA/initiators and a broad range of monomers (Asadi *et al.*, 2016; Bagaria *et al.*, 2013; Blin *et al.*, 2016; Guo *et al.*, 2017; Hemery *et al.*, 2015; Lassenberger *et al.*, 2016; Zhang *et al.*, 2016b). While 'grafting from' tends to produce higher density polymer coatings, 'grafting to' allows precise control of polymer architecture and functionality, as the polymers are synthesised and characterised in solution, prior to surface modification. Precise control over the architecture of coating materials and their prior characterisation makes the 'grafting to' approach potentially more versatile in application.

Blin & co-workers were able to demonstrate the viability of dimethoxyphosphonyl terminal dithiobenzoate RAFT agent to generate end-reactive polymers suitable for 'grafting to' iron oxide nanoparticles (Blin *et al.*, 2016). Bidentate poly(phosphorylcholine) (PC) and poly(ethylene glycol) (PEG) polymers could be produced with narrow dispersities (<1.2) and used to modify the surface of coprecipitation derived SPIONs (Fig. 3.9.). Interestingly the authors also showed improved

stability, water solubility, biocompatibility and cellular distribution of PC brush coated nanoparticles compared with PEG combs.

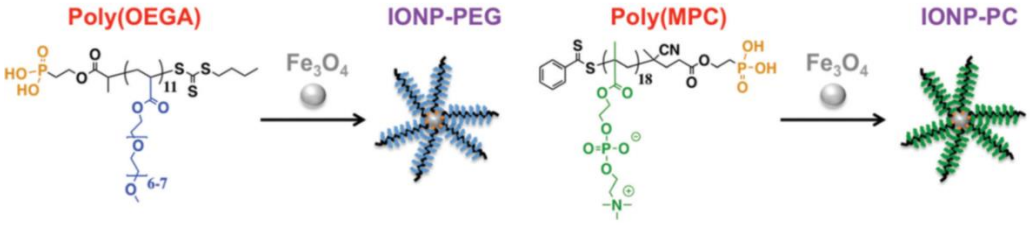

Figure 3.9. Grafting of poly(ethylene glycol) and poly(phosphorylcholine) brushes to iron oxide nanoparticles. Dimethylphosphonate polymers of oligo-ethylene glycol methyl ether acrylate and 2-(methacryloyloxy)ethyl phosphorylcholine were prepared by RAFT polymerisation with dimethylphosphonate CTAs. Functionalisation was achieved by sonication of a H_2O/MeOH dispersion of polymer brushes and nanoparticles followed by overnight incubation at 50 °C. Adapted from Blin *et al*, 2016.

For grafting glycopolymers, which are often highly hydrophilic, to SPIONs 'grafting to' processes for glycopolymers produced by SET-LRP and RAFT have been described. In the method of Pfaff & co-workers a galactose and pyrene containing glycocopolymer was synthesised via RAFT polymerisation using 2-cyano-2-propyl 4-cyanobenzodithioate (CPDB) as the chain-transfer agent. The magnetic nanoparticles were functionalised with 3-(trimethoxysilyl)propyl methacrylate (MPTS). Aminolysis of the glycopolymer terminal dithiobenzoate group with hexylamine yielded a chain terminal thiol group and subsequent thiol-ene reaction between the glycopolymers chains and the methacrylate carrying nanoparticles led to hydrophilic glycopolymers shell grafting (Fig. 3.10.)(Pfaff *et al.*, 2011).

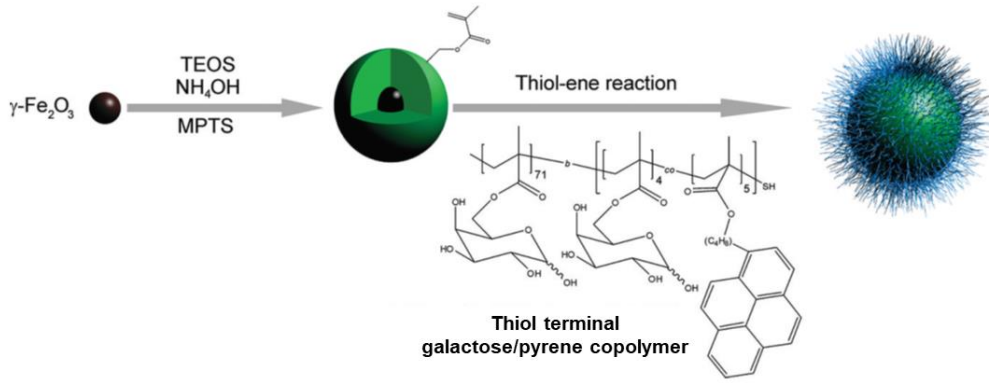

Figure 3.10. Grafting of fluorescent glycopolymers to MNPs by the thiol-ene reaction. γ-Fe_2O_3 MNPs were silanised using MPTS, resulting in silica coated MNPs functionalised with methacrylate groups. In tandem a pyrene/galactose containing glycocopolymer was synthesised via RAFT polymerisation using a dithiobenzoate chain transfer agent. Aminolysis of the purified glycocopolymer dithiobenzoate terminus yields a free thiol group. The thiolated glycopolymer could then be exploited for thiol-ene 'click' with the methacrylate C=C displayed by MPTS functionalised γ-Fe_2O_3 MNPs producing fluorescent, sugar polymer coated MNPs. Neither silica nor glycopolymer functionalisation impacted superparamagnetic properties of the recovered nanoparticles. Adapted from Pfaff *et al*, 2011.

Magnetic glyconanoparticles have also been produced by Basuki & co-workers by a combination of Cu(0) mediated SET-LRP polymerisation using a phosphonic ester initiator and alkyne-azide or thiol-epoxy 'click' chemistry (Basuki *et al.*, 2014). In this seminal work one-pot synthesis of diblock PEG-glycopolymers of α-D-mannose, α-D-glucose and β-D-glucose was reported and grafted to SPIONs. poly(oligo(ethyleneglycol) acrylate) was produced and chain extended with glycidyl acrylate. The glycopolymer derivatives were then produced by two divergent routes. The epoxy groups present in the copolymer were either reacted with sodium azide and then 'clicked' with propargyl-sugars via azide-alkyne cycloaddition or the epoxy groups on the copolymer were reacted with thiol functional sugars via a thiol-epoxy 'click' reaction. In the final step, the phosphonic ester groups of the polymers were cleaved to yield the phosphonic acid group, the multidentate terminus which can coordinate Fe_3O_4, allowing for surface modification.

Direct functionalisation of SPIONs with glycopolymers was achieved by Zhang & co-workers by the synthesis of glycopolymers with catecholic termini by Cu(0) mediated SET-LRP of glycomonomers with a dopamine functionalised alkyl bromide initiator (Fig. 3.11.)(Zhang *et al.*, 2016b). Stirring of the glycopolymers and oleic acid-stabilised SPIONs at 40^{o}C under nitrogen protection was sufficient for replacement of the oleic acid yielding hydrophilic, biocompatible fluorescent glyconanoparticles which could be uptaken by A549 cells, as qualitatively assessed by confocal microscopy. A similar 'grafting to' strategy using a dopamine terminal initiator was employed by Miao & co-workers to produce magnetic nanoparticles functionalised with a chitosan-mimicking cationic glycopolymer (Miao *et al.*, 2019).

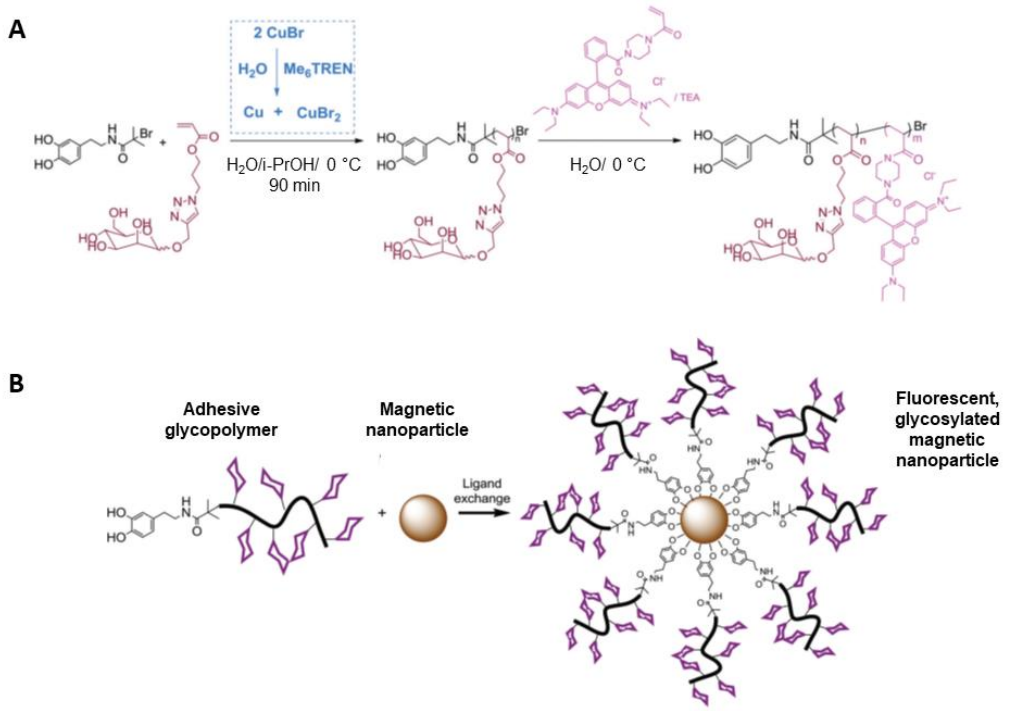

Figure 3.11. Decoration of magnetic Fe_3O_4 nanoparticles with fluorescent glycopolymers by a combined SET-LRP/'grafting to' approach. A) Block copolymerisation of sugar acrylates and Rhodamine B acrylamide was achieved using a SET-LRP system in water/isopropanol with catalytic amounts of CuBr/Me_6TREN. The bromo-initiator in this system features an unprotected dopamine terminus which has high affinity for metal oxides. B). Decoration of MNPs with dopamine-functionalised fluorescent glycopolymers. This ligand exchange reaction could be achieved by incubation of MNPs and the functional glycopolymers at 40 °C overnight under nitrogen protection.

However, the approaches described above for the grafting of highly hydrophilic materials, such as glycopolymers to SPIONs, only encompasses those synthesised by chemical co-precipitation or microemulsion. Grafting hydrophilic materials to the hydrophobic SPIONs derived from thermal decomposition, which have preferable morphology and size distributions, remains elusive. To date, the only method described in the literature we are aware of for the surface modification of thermal decomposition derived SPIONs with very hydrophilic materials was reported by Galli & co-workers. In this work efficient replacement of the oleic acid molecules on the SPION surface was achieved via a two-step replacement. An

intermediate molecule, tetramethylammonium hydroxide (TMAOH), was used as a phase transfer catalyst. The oleic acid was first replaced by TMAOH in an organic phase. TMAOH was then exchanged with the zwitterionic linear polyamidoamine (PAA) in a second stage in an aqueous phase (Galli *et al.*, 2019).

3.1.5. Chapter aims

This part of this project aimed to generate an array of glycopolymer-functionalised SPIONs. Glycopolymers of various chain lengths were generated by RAFT polymerisation using a novel dopamine-terminal CTA and characterised using NMR, SEC, and FTIR. Furthermore, greater control over polymer chain length could be achieved using this method thus also allowing the interrogation of the lectin binding capabilities of glycopolymers of varying length. SPIONs were also synthesised and characterised, prior to surface modification with glycopolymers. The lectin binding capacity of glycopolymer-coated SPIONs was also assessed.

3.2. Materials and Methods

3.2.1 Instrumentation and analysis

3.2.1.1. NMR spectroscopy

^{1}H and ^{13}C NMR spectra were recorded on a Bruker 400 Ultrashield spectrometer using deuterated solvents. High-resolution ^{1}H NMR for calculation of polymer DP was performed on a Bruker Av(III)500 spectrometer equipped with a dual $^{1}H/^{13}C$ helium-cooled cyroprobe.

3.2.1.2. Electrospray-ionisation time-of-flight mass spectrometry (ESI-TOF MS)

ESI-TOF mass spectrometry was performed on a Bruker microTOF II mass spectrometer in either HPLC grade MeCN, MeOH or milliQ H_2O with a sample concentration of ≤0.01 mg/mL.

3.2.1.3. Fourier transform infrared spectrometry (FTIR)

Fourier Transform Infrared Spectrometry was performed on an Agilent Cary630 FTIR with an ATR module between the wavelengths of 4000-650 cm^{-1} with a resolution of 2 cm^{-1} with 32 background scans and 64 sample scans per sample.

3.2.1.4. Thermogravimetric analysis

Thermogravimetric analysis was performed on a TA Instruments Q500 TGA in the temperature range 25-650 °C with a ramp of 10 K/min under inert gas. Platinum pans were filled with ~ 5 mg of sample and the total organic content was evaluated as the mass loss fraction at 500 °C by the horizontal setting.

3.2.1.5. Transmission electron microscopy

Imaging of coated and uncoated SPIONs was performed on a Tecnai G2 transmission electron microscope (Tecnai) with an acceleration voltage of 100 kV. 13 µl of aqueous sample was deposited on a Cu200 grid with a carbon support film and negatively stained with uranyl acetate (2%) where applicable. The suspension was allowed to settle onto the grid for ~10 minutes, excess liquid removed and the grid allowed to air dry prior to imaging. Particle sizing analysis was performed in ImageJ for >800 individual particles.

3.2.2. Synthetic procedures

3.2.2.1. Synthesis of mannose acrylamide monomer (ManAA)

3.2.1.1.1. 2′-acrylamidoethyl-2,3,4,6-tetra-O-acetyl-α-D-mannopyranoside (1)

In a 500 mL flask, α-D-Mannose pentaacetate (30.0 g, 76.9 mmol) and *N*-hydroxyethyl acrylamide (10.6 g, 9.55 mL, 93.3 mmol) were dissolved in anhydrous acetonitrile (300 mL). Using a dropping funnel, $BF_3{\cdot}Et_2O$ (65.5 g, 57.9 mL, 461 mmol) was added dropwise, and the reaction mixture was left under stirring at room temperature. The reaction was monitored by ^{13}C NMR ($CDCl_3$) by following the disappearance of the anomeric carbon of α-D-mannose pentaacetate starting material at 90.7 ppm, and the appearance of that of the desired 2′-acrylamidoethyl-galactopyranoside product at 97.9 ppm. Due to the high toxicity of the $BF_3{\cdot}Et_2O$ it was first necessary to neutralise this reagent prior to the workup. The reaction mixture was added dropwise to an aqueous saturated solution of sodium bicarbonate containing 116.3 g $NaHCO_3$ (1384mmol, 3 eq compared to to $BF_3{\cdot}Et_2O$). The organic phase was dried over $MgSO_4$, filtered, and the volatiles removed by rotary evaporation under reduced pressure. The crude yellow oil residue was purified by flash chromatography on SiO_2 (20 % - 60 % EtOAc in PetEt), to yield analytically pure 2′-acrylamidoethyl-2,3,4,6-tetra-O-acetyl-α-D-mannopyranoside **(1)** (18.61 g, 41.78 mmol, 52.59 %) as a colourless oil.

^{1}H NMR (400 MHz, DMSO) δ 8.33-8.19 (m, 1H), 6.29 - 6.22 (dd, *J* = 17.1, 10.1 Hz, 1H), 6.12 - 6.07 (dd, *J* = 17.1, 2.3 Hz, 1H), 5.62 - 5.58 (dd, 1H, *J* = 10.1 2.3

Hz), 5.18 - 5.07 (m, 3H), 4.90 (d, *J* = 1.4 Hz, 1H), 4.13 (dd, *J* = 12.3, 5.4 Hz, 1H), 4.02 - 3.96 (m, 2H), 3.72 – 3.50 (m, 2H), 3.38 - 3.34 (m, 2H), 2.12 (s, 3H), 2.03 (s, 3H), 2.02 (s, 3H), 1.95 (s, 3H).

^{13}C NMR (101 MHz, DMSO) δ 170.5, 170.08, 170.04, 169.9, 165.26, 132.05, 125.65, 97.15, 69.16, 69.15, 68.33, 66.74, 65.89, 38.83, 21.07, 20.94, 20.92, 20.88.

FT-IR (cm^{-1}) 3310, 1737, 1658, 1629, 1543, 1415, 1366, 1220, 1166, 1137, 1089, 1043, 942, 905, 850, 795.

ESI-MS *m/z*: calculated for $C_{19}H_{27}NO_{11}$ ($M+Na^+$): 468.15; found: 468.15.

3.2.1.1.2. 2′-acrylamidoethyl-α-D-mannopyranoside (ManAA) (2)

Compound **(1)** (4.60 g, 10.3 mmol) was dissolved in MeOH (20 mL) and KOH (0.120 g, 2.14 mmol) was added. The reaction mixture was left under stirring overnight at room temperature. The solvent was removed under reduced pressure, and the crude yellow oil residue was purified by flash chromatography on SiO_2 (25% MeOH in DCM) to give analytically pure 2′-acrylamidoethyl-α-D-mannopyranoside **(2)** (3.10 g, 11.2 mmol, 84.1 %) as a colourless oil.

^{1}H NMR (400 MHz, DMSO) δ 8.16 (t, 1H, *J* = 5.4), 6.25 (dd, 1H, *J* = 17.1 Hz, 10.1 Hz), 6.09 (dd, 1H, *J* = 17.1 Hz, 2.3 Hz), 5.59 (dd, 1H, *J* = 10.1 Hz, 2.3 Hz), 4.71 – 4.69 (2 s, 2H), 4.63 (d, 1H, *J* = 1.5 Hz), 4.56 (s, 1H), 4.49 (t, 1H, *J* = 5.8 Hz), 3.70 - 3.58 (m, 3H), 3.60 (s, 1H), 3.48 - 3.26 (m, 7H – overlapping H_2O signal).

^{13}C NMR (101 MHz, DMSO) δ 165.16, 132.14, 125.58, 100.45, 74.49, 71.36, 70.70, 67.43, 65.81, 61.24, 39.01.

FT-IR (cm^{-1}) 3283, 2927, 1655, 1624, 1544, 1409, 1369, 1316, 1247, 1049, 961, 878, 803.

ESI-MS *m/z*: calculated for $C_{11}H_{19}NO_7$ ($M+Na^+$), 300.10; found, 300.10

3.2.2.2. Synthesis of galactose acrylamide monomer (GalAA)

3.2.2.2.1. 2′-acrylamidoethyl-2,3,4,6-tetra-*O*-acetyl-α-D-galactopyranoside (3)

β-D-Galactose pentaacetate (50.0 g, 128 mmol) was dissolved in anhydrous CH_2Cl_2 (120 mL) and *N*-hydroxyethyl acrylamide (29.5 g, 256 mmol) was added under stirring. BF_3 Et_2O (36.3 g, 256 mmol) was slowly added to reaction mixture on ice drop-wise. The reaction was left under stirring at RT. After 6 days, TEA (28.5 g, 282 mmol) was added dropwise to the mixture cooled at 0°C. The organic phase was extracted with sat. $NaHCO_3$ (3x150 mL) and water (2x150mL), dried over $MgSO_4$ and evaporated under reduced pressure. The crude product was purified by flash chromatography (gradient elution from PetEt/Et_2O 90:10 to Et_2O/EtOAc 50:50) to yield 2′-acrylamidoethyl-2,3,4,6-tetra-*O*-acetyl-α-D-galactopyranoside **(3)** as a white solid (20.4 g, 45.8 mmol, 35.8%).

^{1}H NMR (400 MHz, $CDCl_3$) δ 6.28 (dd, 1H, *J* = 17.0, 1.4 Hz), 6.09 (dd, 2H, *J* = 17.0, 10.2 Hz), 5.64 (dd, J = 10.3, 1.3 Hz, 1H, COCHC*H*$_2$), 5.38 (d, 1H, *J* = 3.2 Hz), 5.17 (dd, 1H, *J* = 10.5, 7.9 Hz), 5.00 (dd, 1H, *J* = 10.5, 3.4 Hz), 4.46 (d, 1H,

J = 7.9 Hz), 4.13 (m, 2H), 3.89 (m, 2H), 3.77 – 3.67 (m, 1H), 3.65 – 3.53 (m, 1H), 3.52 – 3.43 (m, 1H), 2.14 (s, 3H), 2.03 (s, 3H), 2.03 (s, 3H), 1.97 (s, 3H).

^{13}C NMR (101 MHz, $CDCl_3$) δ 170.48, 170.25, 170.15, 169.86, 165.54, 130.80, 126.76, 101.56, 70.97, 70.79, 69.21, 69.05, 67.08, 61.49, 39.27, 20.95, 20.78, 20.76, 20.67.

FT-IR (cm^{-1}) 3258, 1744, 1648, 1610, 1547, 1409, 134, 1215, 1170, 1133, 1092, 1040, 932, 902, 738

ESI-MS *m/z*: calculated for $C_{19}H_{27}NO_{11}$ ($M+Na^+$): 468.15, found 468.15.

3.2.2.2.2. 2′-acrylamidoethyl-α-D-galactopyranoside (GalAA) (4)

2′-acrylamidoethyl-2,3,4,6-tetra-*O*-acetyl-α-D-galactopyranoside **(3)** (20.4 g, 45.8 mmol) was dissolved in 40 mL of MeOH and KOH (0.257 g, 4.58 mmol) was added. The reaction mixture was stirred overnight at room temperature. The solvent was removed under reduced pressure, and the crude yellow oil residue was purified by flash chromatography on SiO_2 (25% MeOH in DCM) to give analytically pure 2′-acrylamidoethyl-α-D-galactopyranoside **(4)** as a white powder (11.4 g, 41.1 mmol, 89.7%).

^{1}H NMR (400 MHz, DMSO-d_6) δ 8.09 (t, 1H, *J* = 5.3 Hz), 6.24 (dd, 1H, *J* = 17.1, 10.1 Hz,), 6.08 (dd, 1H, *J* = 17.1, 2.2 Hz), 5.58 (dd, 1H, *J* = 10.1, 2.2 Hz), 4.85 (s, 1H), 4.73 (s, 1H), 4.60 (s, 1H), 4.37 (s, 1H), 4.09 (d, 1H, *J* = 7.0 Hz), 3.80 – 3.69 (m, 1H), 3.62 (s, 1H), 3.51 (m, 3H), 3.43 – 3.23 (m, 5H).

^{13}C NMR (101 MHz, DMSO-d_6) δ 164.68, 131.70, 125.22, 103.77, 75.29, 73.30, 70.57, 68.16, 67.73, 60.50, 38.99.

FT-IR (cm^{-1}) 3295, 2885, 1655, 1621, 1543, 1409, 1376, 1316, 1245, 1036, 984, 891, 779.

ESI-MS *m/z* calculated for $C_{11}H_{19}NO_7$ ($M+Na^+$), 300.10; found, 300.10

3.2.2.3. Synthesis of dopamine terminal chain transfer agent (Dopa-PABTC) for RAFT polymerisation

3.2.2.3.1. 2-(((butylthio)carbonothioyl)thio)propanoic acid (PABTC) (5)

PABTC was synthesised as per the conditions reported by Ferguson et al (Ferguson *et al.*, 2005). A 50% w/w sodium hydroxide solution (4.84 g NaOH, 0.121 mol, 1.1 eq) in water was added to a mixture of butanethiol (10 g, 0.11 mol, 1 eq) dissolved in acetone (6 mL). Water (20 mL) was added and the solution was stirred for 30 min at room temperature. Carbon disulphide (8.68 g, 0.114 mol, 1.02 eq) was added dropwise and the orange solution was stirred for 30 min at room temperature, then cooled in an ice bath to below 10 °C. 2-Bromopropionic acid (17.4 g, 0.114 mol, 1.02 eq) was added dropwise, ensuring the temperature was maintained and subsequently a further 9.68 g of 50% w/w sodium hydroxide solution was added. The reaction mixture was left to stir for 18 h at ambient temperature. 200 mL of water was added to the reaction mixture, cooled in ice, and a 10 M solution of HCl was added dropwise until the pH reached between 2 and 3. The resulting precipitate was filtered, washed with water, and recrystallized in hot hexane yielding analytically pure PABTC **(5)** as a yellow solid (39.4 g, 0.165 mol , 75%).

^{1}H NMR (400 MHz, DMSO) δ 4.67 (q, *J* = 7.3 Hz, 1H), 3.41 – 3.36 (m, 2H), 1.62 (m, 2H), 1.51 (d, *J* = 7.3 Hz, 3H), 1.37 (sex, 2H), 0.88 (t, *J* = 7.4 Hz, 3H).

^{13}C NMR (101 MHz, DMSO) δ 222.53, 171.55, 48.21, 36.21, 29.6, 21.42, 16.81, 13.44.

FT-IR (cm^{-1}) 3329, 2958, 2927, 2857, 1617, 1442, 1421, 1258, 1240, 1106, 1072, 1049, 989, 915, 875, 587.

ESI-TOF MS *m/z* calculated for [M-H^+], 237.01; found, 237.01

3.2.2.3.2. 2,5-dioxopyrrolidin-1-yl-2-(((butylthio)carbonothioyl)thio)propanoate (NHS-PABTC) (6)

Synthesis of (6) was performed via a process adapted from Zobrist *et al* (Zobrist *et al.*, 2011). **(5)** (2.00 g, 8.38 mmol), N-hydroxysuccinimide (1.16 g, 10.0 mmol, 1.2 eq) and DMAP (0.10 g, 0.84 mmol, 0.1 eq) were dissolved in DCM (40 mL) under continuous stirring. In a separate vessel, DCC (2.08 g, 10.0 mmol, 1.2 eq) was dissolved in DCM (100 mL). The DCC solution was added dropwise to the reaction mixture and allowed to stir for 18 h at ambient temperature. The solvent was removed by rotary evaporation at reduced pressure and the crude product redissolved in Et_2O. The white precipitate was removed by precipitation and the organic phase was dried over $MgSO_4$, and filtered. The volatiles were removed under reduced pressure, and the resulting residue was purified by column chromatography on silica with ethyl acetate in hexane (20-50%) yielding analytically pure NHS-PABTC as an orange oil (2.16 g, 6.44 mmol, 76%)

^{1}H NMR (400 MHz, $CDCl_3$) δ 5.12 (q, *J* = 7.4 Hz, 1H), 3.37 (t, *J* = 7.4 Hz, 2H), 2.83 (s, 4H), 1.73 (d, *J* = 7.4 Hz, 3H), 1.70 – 1.60 (m, 2H), 1.47 – 1.36 (m, 2H), 0.92 (t, *J* = 9.6 Hz, 3H).

^{13}C NMR (101 MHz, $CDCl_3$) δ 220.35, 168.78, 167.35, 45.12, 37.34, 29.91, 25.69, 22.14, 16.77, 13.66.

FT-IR (cm^{-1}) 3496, 3463, 3313, 2958, 2930, 1784, 1605, 1446, 1362, 1278, 1200, 1067, 942, 912, 803, 647.

ESI-TOF MS *m/z* calculated for [M+Na^+], 358.02; found, 358.02

3.2.2.3.3. Butyl(1-((3,4-dihydroxyphenethyl)amino)-1-oxopropan-2-yl) carbonotrithioate (Dopa-PABTC) (7)

Synthesis of **(7)** was performed via a process adapted from Zobrist *et al* (Zobrist *et al.*, 2011). NHS-PABTC (2.1 g, 6.26 mmol), dopamine hydrochloride (1.30 g, 6.87 mmol, 1.1 eq) and TEA (0.76 g, 7.5 mmol, 1.1 mL, 1.2 eq) were stirred in MeOH at ambient temperature under a nitrogen atmosphere, in the dark, for 48 h. The solvent was removed by rotary evaporation and the product was redissolved in 50 mL Et_2O. The organic phase was washed with water (3 x 100 mL), saturated brine solution and then dried over $MgSO_4$ and filtered. The solvent was then removed by rotary evaporation at reduced pressure yielding Dopa-PABTC as a yellow solid (1.38 g, 3.70 mmol, 59%).

^{1}H NMR (400 MHz, DMSO) δ 8.72 (s, 1H), 8.64 (s, 1H), 8.34 (t, 1H, *J* = 5.5 Hz), 6.62 (d, 1H *J* = 8.0 Hz), 6.56 (d, 1h, *J* = 2.0 Hz), 6.42 (dd, 1H, *J* = 8.0, 2.0 Hz), 4.66 (q, 1H, *J* = 7.0 Hz), 3.36 (t, 2H, *J* = 7.2 Hz), 2.53-2.5 (m, overlapping

with DMSO signal), 3.19 (m, 2H), 1.62 (quin, 2H), 1.45 (d, 3H, *J* = 7.0 Hz), 1.37 (sext, 2H), 0.89 (t, 3H, *J* = 7.3 Hz).

^{13}C NMR (101 MHz, DMSO) δ 222.92, 169.0, 145.04, 143.52, 129.82, 119.25, 115.96, 115.42, 49.97, 40.82, 36.06, 34.02, 29.59, 21.41, 18.20, 13.43

FT-IR (cm^{-1}) 2953, 2926, 2865, 1699, 1450, 1413, 1374, 1232, 1205, 1105, 1086, 1064, 1041, 1007, 909, 823, 648, 461, 431.

ESI-MS m/*z* calculated for [M-H], 372.08; found, 372.08

3.2.2.4. General method for aqueous RAFT mediated polymerisation of acrylamide monomers

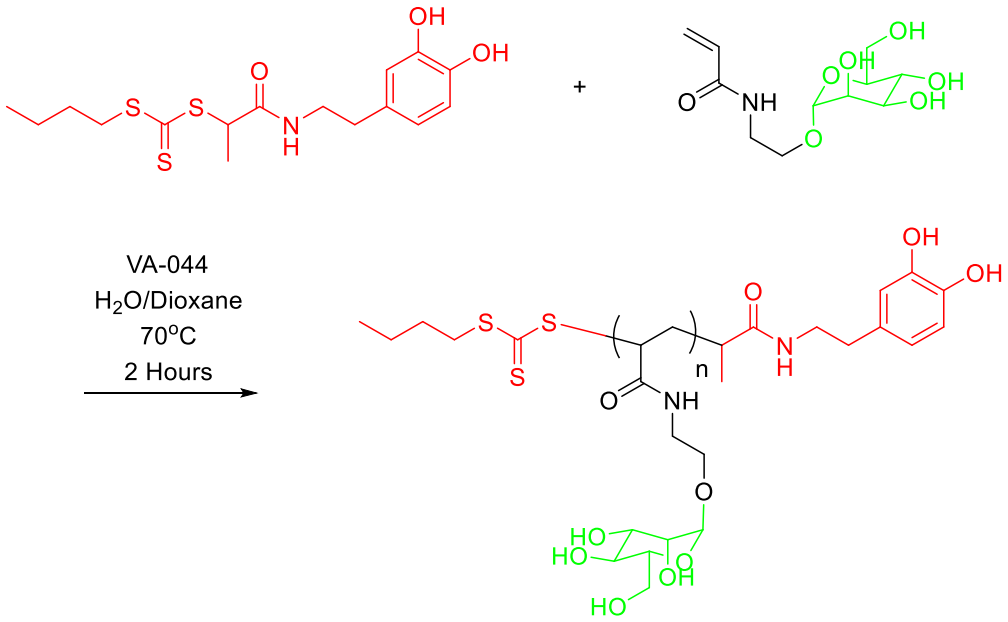

Figure 3.12. General scheme for Dopa-PABTC mediated RAFT polymerisation of glycomonomers.

In a typical polymerisation a glass vial was charged with mannose acrylamide (100 mg, 0.0363 mmol, 100 eq.), Dopa-PABTC (1.3 mg, 3.6 x10^{-3} mmol, 1 eq) (from a pre-made stock solution of 100 mg mL^{-1} in 1,4-dioxane) and VA-044 (0.0583 mg, 1.8x10^{-4} mmol, 0.05 eq.) (from a pre-made stock solution of 20 mg mL^{-1} in water). A stirrer bar and a water:1,4-dioxane (4:1) mix was added to a total volume of 360 µL. The reaction vessel was sealed with a rubber septum and degassed with N_2 for 15 min before being immersed in a preheated oil bath at 70 °C for 2 hours. DP targeting was controlled by altering the ratio of [ManAA]:[Dopa-PABTC] however [Dopa-PABTC]:[VA-044] was maintained at 20:1 in all reactions.

Monomer conversion was determined by ^{1}H NMR spectroscopy in d6-DMSO by comparison of the ratio of the monomer vinyl peak (δ =6.07 ppm)

to the CTA CH_3 z-group chain end group peak (δ =0.86 ppm), in all cases high conversion (≥97%) was obtained. All polymers were analysed by SEC with aqueous 0.1M $NaNO_3$ eluent at 35 °C. An exemplar spectrum is shown in Appendix 7.2.8. DP was calculated by comparing the integral ratio of the catecholic protons (δ 6.79 ppm, δ 6.56 ppm and δ 6.66 ppm) which had been normalised to 1 to the polymeric backbone -*CH* & -*CH_2* peaks (δ 2.17 ppm & δ 1.70 ppm respectively).

3.2.2.5. Synthesis of superparamagnetic iron oxide nanoparticles (SPIONs) via chemical coprecipitation method

Superparamagnetic iron oxide nanoparticles were prepared as per the methods of Maity *et al* and Braim *et al* (Braim *et al.*, 2016; Maity & Agrawal, 2007) with some modification. In a typical synthesis, $FeCl_3{\cdot}6H_2O$ (0.50 g, 1.84 mmol, 2 eqs) and $FeCl_2{\cdot}4H_2O$ were dissolved in H_2O which had been thoroughly degassed with N_2 for 30 minutes with vigorous stirring. The temperature was then raised to 80 °C and maintained for 30 minutes under N_2 with vigorous stirring. To this solution, 1 mL 25% ammonium hydroxide solution was added, resulting in the immediate formation of a black colloidal suspension. After 30 min, sodium oleate (0.36 g, 1.19 mmol, 1.3 eqs) was added under N_2 for particle coating. The solution was cooled to room temperature and the particles isolated by centrifugation at 15000 rpm and washed several times with distilled H_2O to remove the excess of oleic acid. The recovered particles were then resuspended in H_2O resulting in a stable black colloidal suspension.

3.2.2.6. Synthesis of SPIONs via the thermal decomposition method

Oleic acid stabilised magnetite (Fe_3O_4) nanoparticles were obtained as per the thermal decomposition method reported by (Lassenberger *et al.*, 2016) with some modification.

A mixture of dioctyl ether (50 mL) and oleic acid (29.66 mmol, 8.38 g, 4 eq., 9.36 mL) were heated to 100 °C in a two neck RBF under N_2 and allowed to stabilise for 15 min. Iron(0) pentacarbonyl (7.61 mmol, 1.49 g, 1 eq., 1 mL) was then injected rapidly into the oleic acid/dioctyl ether solution and was heated to 290 °C with a temperature ramp of 3 °C /min. After aging for 1 h the nanoparticle dispersion was allowed to cool to room temperature. The nanoparticles were precipitated 3x with acetone from toluene to remove the excess of oleic acid. The size and morphology of the isolated particles was observed by TEM as described in Section 3.2.1.5.

3.2.3. Decoration of SPIONs with RAFT-derived catechol-terminal hydrophilic polymers

3.2.3.1. Two-step ligand exchange catalysed by the phase transfer catalyst tetramethyl ammonium hydroxide (TMAOH)

Modification of the hexane soluble SPIONs stabilised with oleic acid synthesised as described in Section 3.2.2.6. was performed via a ligand exchange reaction with the catechol-terminal polymers by a two-step ligand exchange method adapted from Galli *et al.* with some modification (Galli *et al.*, 2019).

In a typical reaction, a suspension of 15 mg of SPIONs dissolved in approximately 3 ml hexane was dried via rotary evaporation. Subsequently 20 mL of a 0.125 M solution of TMAOH was added and the vial was sonicated for a few minutes to redisperse the SPIONs yielding a turbid mixture. To the water-dispersed SPION, DOPA-poly(HEAA)$_{50}$ (39 mg, 3 x weight by mass, 0.1 eq to Fe_3O_4) was added and left stirring for 48 hours. The particles were then purified from free polymer/oleic acid by dialysis against water for 3 days with 12 kDa MWCO RC dialysis. The particles were then lyophilised to yield a fine black powder which responded to an external magnetic field and was easily redispersible in water. A sample of the lyophilised powder was analysed by FTIR/TGA and TEM to confirm presence of the polymer coating and for size distribution analysis.

3.2.4. Lectin binding studies

3.2.4.1. Turbidimetry assay

All experiments were conducted with HEPES-buffered saline (HBS) (0.10 M HEPES, 0.9 M NaCl, 1 mM $MgCl_2$, 1 mM $CaCl_2$, and 1 mM $MnCl_2$ adjusted to pH 7.4 and filtered with 0.2 μm regenerated cellulose syringe filter. Absorbance was measured with a Cary 50 UV-Vis Spectrophotometer recorded at 420 nm every 0.12s. Turbidity measurements were performed by adding 2 mL of 50 μM polymer solution in HBS buffer to a dry 4.5 mL polystyrene cuvette. The cuvette was then inserted into the spectrophotometer and absorbance recorded for one minute. 50 μL of a 100 μM ConA solution in HBS buffer was quickly added into the cuvette *via* a pipette to induce aggregation. Absorbance was recorded for a further 3 min, then an excess of free mannose in HBS buffer was added to induce competitive binding with the glycopolymers. Absorbance was recorded for an additional minute and the results normalised so the baseline was zero by subtraction of the minimum value for each sample, then analysed via GraphPad.

3.2.4.2. Lectin binding and kinetics analysis via surface plasmon resonance (SPR)

The BIACore 300 SPR system (GE Healthcare) was used for interaction analysis for both lectins. DC-SIGN and Mannose Binding Lectin (MBL) (0.025 mg/mL) were immobilised onto a CM5 sensor chip (GE Healthcare) via a standard amino coupling protocol. The system was first equilibrated with HEPES buffer saline (HBS) (10 mM HEPES, 150 mM NaCl, 5 mM $CaCl_2$, pH 7.4) filter sterilised with a 0.22 μM filter. A 1:1 mixture of 0.1 M *N*-hydroxysuccinimide and 0.1 M 1-ethyl-3-(3-dimethylaminopropyl)carbodiimide was then flowed over the chip for 6 min at 25 °C at a flow rate of 20 μl/min, followed by the lectin solutions in acetate buffer (10 mM sodium acetate, pH 4) (GE Healthcare). Subsequently the channels were blocked by flowing a solution of ethanolamine (1M, pH 8.5) for 10 min at 5 μl/min to remove any remaining reactive groups on the surface. Sample solutions were prepared over a range of concentrations (10 nM to 0.6125 nM) in the HEPES buffer to calculate binding kinetics. Sensograms for each glycomaterial concentration were recorded for a 300 s injection of polymer solution followed by 150 s of buffer. Regeneration of the sensor chip surfaces was performed by flowing regeneration buffer (10 mM HEPES, 150 mM NaCl, 10 mM EDTA, 0.01% P20 surfactant, pH 7.4) for 40 seconds at 100 μl/min. Kinetic data was then analysed using the 1:1 Langmuir binding model in the BIAevaluation 3.1 software.

3.3. Results

3.3.1. Glycomonomer synthesis

3.3.1.1. Mannose acrylamide (2) synthesis

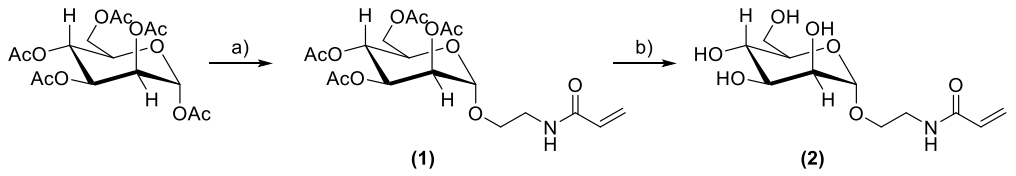

Scheme 3. 1. Synthesis of Mannose Acrylamide monomer. *Reagents and conditions*. a) *N*-hydroxyethyl acrylamide, $BF_3{\cdot}Et_2O$, acetonitrile, overnight; b) KOH, CH_3OH, overnight.

Synthesis of mannose acrylamide monomer **(2)** was performed similarly to the two-step strategy reported by Cameron and co-workers (Cameron *et al.*, 2008). The protected monomer was generated from a commercially available mannose pentaacetate, by selective deacetylation of the anomeric carbon by the strong Lewis acid $BF_3.OEt_2$ and subsequent nucleophilic attack by 2-hydroxyethyl acrylamide in acetonitrile. The remaining acetyl groups were then removed by hydrolysis with methanolic KOH to yield the final deprotected monomer **(2)**. Its chemical identity and purity, as well as those of intermediate **(1)**, were confirmed by ^{1}HNMR and ^{13}CNMR in d6-DMSO (assigned spectra available in Appendix 7.2.1 & 2), FTIR, and MS.

For the mannose monomer complete stereocontrol over the glycosylation step with 2-hydroxyethyl acrylamide was confirmed by ^{1}H and ^{13}C NMR analysis which showed the presence of only the α-anomer, in agreement with the results reported by Cameron & co-workers (Cameron *et al.*, 2008). Stereocontrol is believed to originate from anchimeric assistance

(assistance from a neighbouring group) provided by the acetate group at C2, that stabilises the carbocation intermediate that is formed following abstraction of the anomeric acetate group by $BF_3.OEt_2$ thus forcing the nucleophile to approach from the opposite side (Guo & Ye, 2010; Wang *et al.*, 2010). A computational study on the deacetylation of β-D-glucose pentaacetate showed that the energy for the attack from the above the anomeric carbon (the side which is not protected by a neighbouring acetate) is about 9.6 $kcalmol^{-1}$ higher than the total energy of the oxonium intermediate and water, whereas attack from the bottom (the protected side) is 3.5 $kcalmol^{-1}$ lower than the total energy of the oxonium intermediate and water combined (Wang *et al.*, 2010). This suggests formation of the α-anomer is kinetically favoured. Thus, for the deacetylation of sugar pentacetates, formation of the α or β-anomer is determined by the spatial orientation of the acetate at C2.

The yield of the protected monomer **(1)** was lower than anticipated, which can be attributed to partial hydrolysis of the product during the neutralisation of $BF_3.OEt_2$. Indeed a proportion of starting material selectively deacetylated at C1 was isolated following flash column chromatography of the acetyl-group protected glycomonomers. These product clearly showed two peaks δ 8.53 and 8.31 ppm (doublet and triplet respectively) on the ^1H NMR spectrum, corresponding to the coupling of a hydroxyl group to the anomeric proton. The signal for these peaks was lost upon addition of D_2O to the NMR sample, providing further evidence for the presence of the expected partially hydrolysed by-product.

3.3.1.2. Galactose acrylamide (4) synthesis

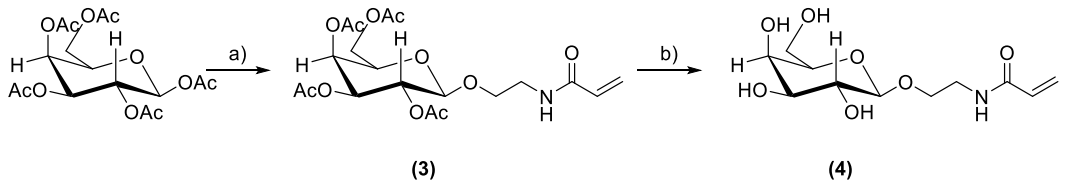

(3) (4)

Scheme 3.2. Synthesis of Galactose Acrylamide monomer **(4)**. *Reagents and conditions*. a) *N*-hydroxyethyl acrylamide, $BF_3{\cdot}Et_2O$, anhydrous DCM, overnight; b) KOH, CH_3OH, overnight.

Synthesis of galactose acrylamide **(4)** monomer was performed similarly to the two-step strategy reported by Cameron and co-workers (Cameron *et al.*, 2008). The protected monomer **(3)** was generated from a commercially available β-D-galactose pentaacetate by selective deacetylation of the anomeric carbon by the strong Lewis acid $BF_3.OEt_2$ and subsequent nucleophilic attack by 2-hydroxyethyl acrylamide in anhydrous DCM. The remaining acetyl groups were then removed by hydrolysis with methanolic KOH to yield the deprotected monomer. The structure and purity of the protected and deprotected monomer was confirmed by ^{1}HNMR and ^{13}CNMR in $CDCl_3$ (assigned spectra available in Appendix 7.2.3 & 4).

In contrast to the synthesis of the mannose monomer described in section 3.3.1.2., synthesis of the galactose monomer leads to the selective formation of the β-anomer because the acetate on C2 in the starting sugar pentaacetate is in the opposite spatial orientation – equatorial for galactose, as opposed to axial for mannose.

3.3.2. Catechol-terminal RAFT agent (7) synthesis

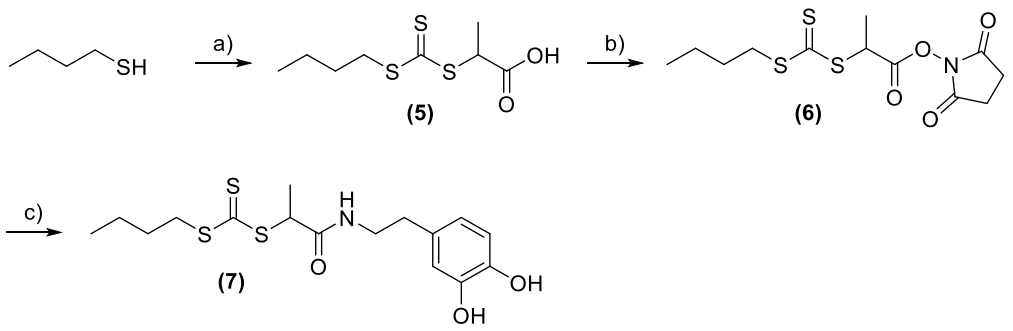

Scheme 3.3. Synthesis of catechol-terminal RAFT agent Dopa-PABTC **(7)**. *Reagents and conditions*. a) NaOH, CS_2, 10^{oC}; then 2-bromopropionic acid, overnight; b) NHS, DMAP, DCC, DCM, overnight; c) Dopamine HCl, triethylamine, MeOH, overnight.

Synthesis of a catechol-terminal RAFT agent was desired to allow the polymerisation of the glycomonomers described in Section 3.2.3.1. while ensuring a singular catecholic terminus for coating SPIONs. To this end a carboxylic acid terminal RAFT **(5)** was synthesised as per the procedure reported by Ferguson and co-workers (Ferguson *et al.*, 2005). Confirmation of this compound was determined by the appearance of diagnostic peaks for the carbonyl adjacent methyl group and–CH groups (δ 1.51 ppm, doublet and δ 4.67 ppm respectively) originating from 2-bromopropionic acid. (Assigned spectra available in Appendix 7.2.5.).

For functionalisation with dopamine, a catechol-terminal amine, amide bond formation was attempted. Amide bonds can be synthesised by the union of amines and carboxylic acids; however unification of these functional groups does not take place at ambient temperature with elimination of water, the mechanistic driver of the reaction, typically only occurring at ≥200 °C (Jursic & Zdravkovski, 1993). These reactions may

instead be mediated by a range of so called 'coupling agents' which function by activating the carboxylic acid by converting the hydroxyl group of the acid into a good leaving group such as an ester (Valeur & Bradley, 2009). These coupling agents are typically carbodiimides or salts of uronium, aminium, phosphonium or immonium (Valeur & Bradley, 2009).

Despite the use of several different conventional amide coupling agents, including EDC, DCC, BOP and pyBOP direct coupling of dopamine to PABTC was not able to be achieved. In these reactions typically the doublet at δ1.51 ppm corresponding to the free methyl group and the δ222 ppm peak for the C=S moiety within the trithiocarbonate centre were lost (Fig. 3.13.)). This may result from the nucleophilic attack of these coupling agents, or the amine itself, upon the SC(=S)S centre of the trithiocarbonate domain and hence the loss of these diagnostic NMR peaks.

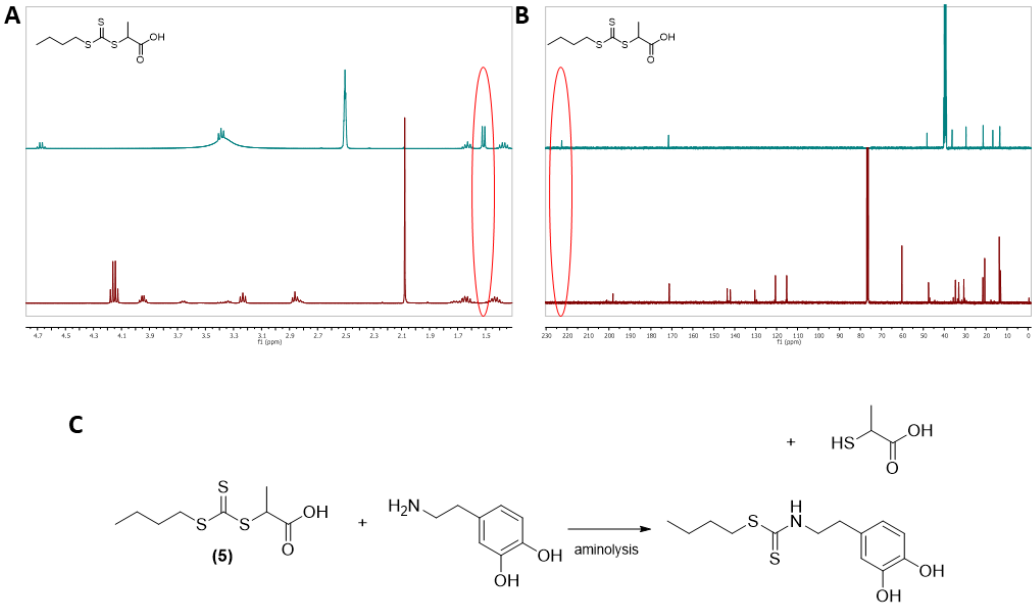

Figure 3.13. Degradation of PABTC (5) by coupling agents. A) ^{1}H NMR and B) ^{13}C NMR of PABTC before (above) and after (below) coupling with dopamine HCl mediated by pyBOP. Loss of the free methyl group at δ1.51 ppm and the trithiocarbonate centre at δ222 ppm (circled in red) may be diagnostic of degradation. C) Possible aminolysis mechanism for degradation of PABTC in presence of dopamine HCl.

To circumvent this issue, the formation of an NHS ester of PABTC was attempted using an approach similar to those reported by Larnaudie & co-workers and Oyeneye & co-workers (Larnaudie *et al.*, 2016; Oyeneye *et al.*, 2015). Confirmation of the synthesis of the NHS ester was provided by the appearance of a singlet at δ 2.83 ppm which integrated to 4 protons, corresponding to the two symmetrical –*CH₂* groups on the five membered ring of succinimide (Fig. 3.14.). Furthermore, the doublet from the free methyl group shifted downfield in comparison to the carboxylic acid (from δ1.51 ppm to δ 1.73 ppm) suggesting deshielding from the electron withdrawing effect of the succinimide, consistent with formation of the desired ester **(6)** (Fig. 3.14.)(assigned spectra available in Appendix 7.2.6.).

Nucleophilic attack to the ester of NHS-PABTC by dopamine could then be achieved under ambient conditions in MeOH by prior deprotonation of Dopamine HCl with TEA. Confirmation of formation of Dopa-PABTC could then be provided by the appearance of two doublets of doublets at δ 6.79 ppm and δ 6.56 ppm as well as a doublet at δ 6.66 ppm which correspond to the aromatic protons from the catechol terminus (Fig. 3.14.). Additionally, the appearance of a triplet at δ 6.45 corresponding to the amide group proton as well as triplets (δ ~3.26 ppm and 2.66 ppm) for the –CH_2 groups on the $NHCH_2CH_2$(Catechol) backbone of the amide, provide good credence to the synthesis of **(7)** (Fig. 3.14.)(assigned spectra available in Appendix 7.2.7.).

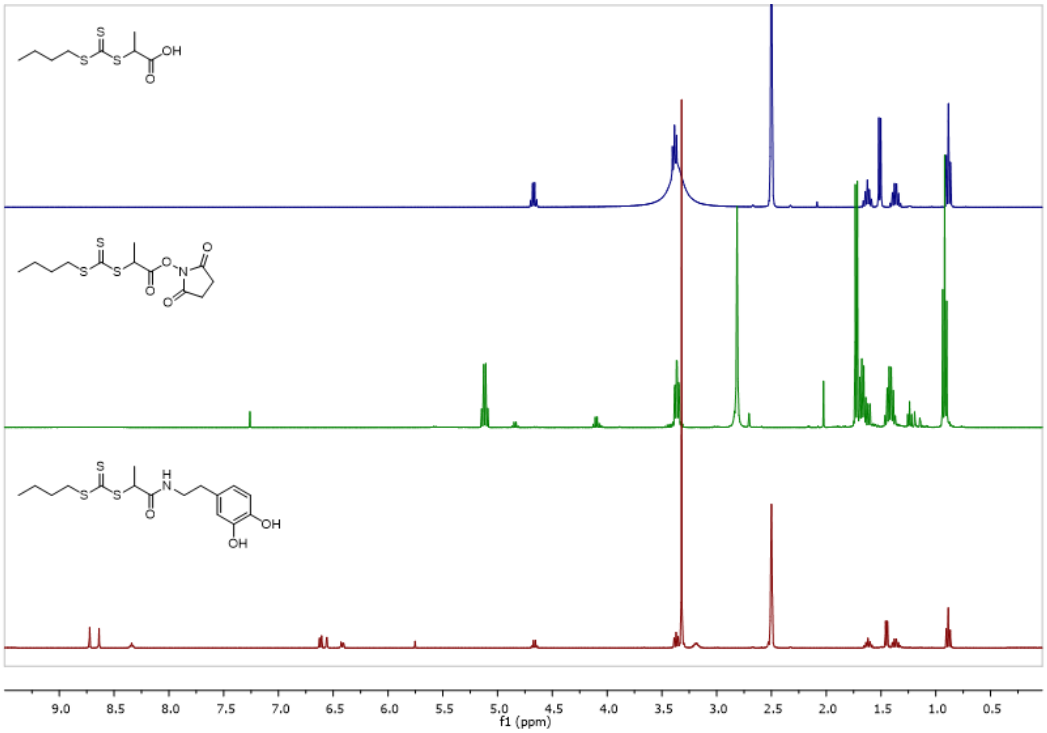

Figure. 3.14. Stacked ^{1}H NMR spectra of PABTC, PABTC-NHS and Dopa-PABTC. The emergence of a singlet at δ 2.83 ppm is diagnostic for the succinimide ring for the NHS ester of PABTC (panel 2). Downshift of the free methyl group from δ1.51 ppm to δ 1.73 ppm compared with the carboxylic acid also suggests the identity of the NHS ester. The emergence of diagnostic peaks for the aromatic protons (δ 6.79 ppm, δ 6.56 ppm and δ 6.66 ppm) and amide group (δ 6.45 ppm) suggests successful coupling and formation of Dopa-PABTC from the NHS ester (panel 3).

3.3.3. RAFT polymerisation of glycomonomers

In order to synthesise catechol-terminal glycopolymers of HEAA and the sugar acrylamides as produced in sections 3.2.3.1. RAFT polymerisation with the catecholic chain transfer agent produced in section 3.2.3.2. was performed. This catecholic domain has a high affinity for SPIONs and would allow for future surface modification of SPIONs (Shultz *et al.*, 2007; Xu *et al.*, 2004).

For these RAFT polymerisations the relevant acrylamide monomer, Dopa-PABTC and VA-044 were homogenised in a water:dioxane solution (4:1), degassed with Argon and subsequently heated to 70 °C for 2h under vigorous stirring. Dioxane was added to improve the solubility of Dopa-PABTC, which demonstrated poor solubility in water alone. All syntheses were performed at 1M monomer concentration with a [CTA]/[I] = 20. For the polymerisations of ManAA four different $[M]_0/[CTA]_0$ ratios (20, 50, 100 and 200) were performed to generate increasing chain length mannosylated polymers. For the control materials (HEAA/GalAA) a single $[M]_0/[CTA]_0$ of 50 was utilised to allow comparison to the DP 50 mannosylated material.

Table 3.1. Characterisation data for catechol-terminal polymers produced in this study

Polymer	DP_{target}	$M_{n,th}$ (g mol^{-1})[a]	$M_{n,NMR}$ (g mol^{-1})[b]	$M_{n,SEC}$ (g mol^{-1})[c]	$M_{w,SEC}$ (g mol^{-1})[c]	$Đ$[c]
Dopa-$(HEAA)_{50}$	50	6100	6300	10500[d]	12100[d]	1.15[d]
Dopa-$(ManAA)_{20}$	20	6000	8900	9400	11800	1.25
Dopa-$(ManAA)_{50}$	50	14200	16400	12800	15300	1.19
Dopa-$(ManAA)_{100}$	100	28100	20000	17300	20700	1.19
Dopa-$(ManAA)_{200}$	200	55800	42400	31100	38400	1.24
Dopa-$(GalAA)_{50}$	50	14200	13100	14000	17300	1.23

[a]Determined using equation 3.2. [b]Determined using ^{1}H NMR spectroscopy via end group analysis. [c]Determined using Aqueous SEC using conventional calibration from linear PEG standards. [d]Determined using DMF-SEC.

A

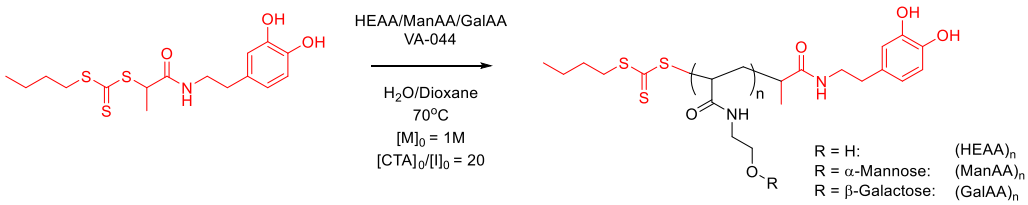

B

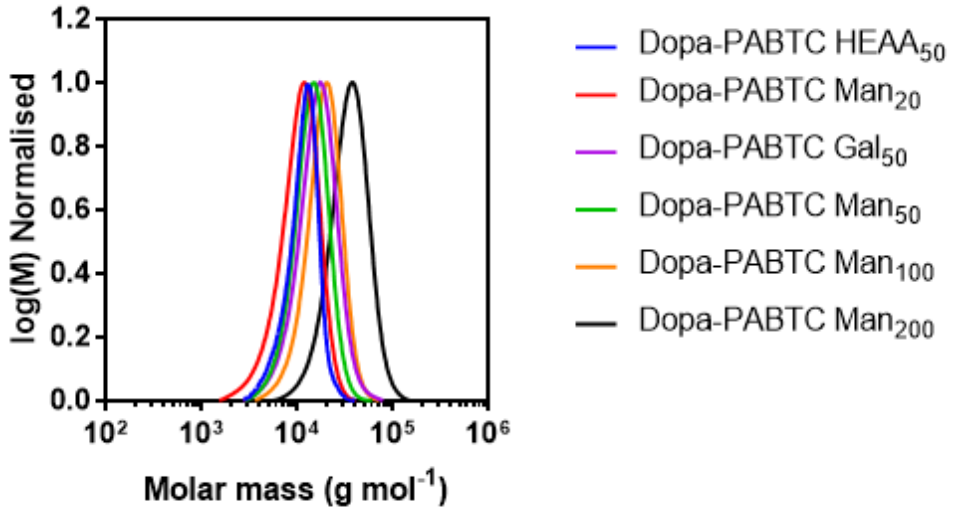

Figure 3.15.Characterisation of Dopa-PABTC mediated polymerisations. A) Polymerisation of acrylamide monomers mediated by Dopa-PABTC. B) SEC chromatogram traces for catechol-terminal polyacrylamide polymers.

$$M_{n,th} = \frac{[M]_0 p M_M}{[CTA]_0} + M_{CTA}$$

Equation 3.2. Calculation of theoretical number average molar mass ($M_{n,th}$) where $[M]_0$ and $[CTA]_0$ are the initial concentrations (in mol dm-3) of monomer and chain transfer agent respectively. p is the monomer conversion as determined by ^{1}H NMR spectroscopy. M_M and M_{CTA} are the molar masses (g mol^{-1}) of the monomer and chain transfer agent respectively.

All polymerisations rapidly achieved >90% conversion within 2 hours as monitored by the depletion of the vinyl peaks of the acrylamide monomers at around δ 6.3, 6.1 and 5.6 ppm and the emergence of broad doublet and triplet peaks centred around δ 2.2 and 1.7 ppm corresponding to the –CH and –CH_2 groups present on the polymer backbone. Furthermore, all polymers demonstrated doublet peaks at around δ 6.9, 6.8 and 6.7 ppm in D_2O, consistent with those expected from the aromatic protons of the dopamine terminus suggesting retention of the catecholic terminus which is essential for SPION decoration. An exemplar spectrum is shown in Apppendix 7.2.8.

SEC analysis demonstrated narrow dispersities ($Đ$ = 1.15-1.25) (Table 3.1) and the chromatograms displayed narrow, symmetrical, unimodal molar mass distributions consistent with well controlled radical polymerisation free from significant termination events (Fig 3.15.B). Molar mass size increase also correlated with the targeted DP, i.e. longer polymers had a greater molar mass. The observed molar masses via NMR ($M_{n,NMR}$) showed good agreement between the theoretical molar masses ($M_{n,th}$) for the shorter chain materials (DP 20/50 for HEAA, mannose or galactose) (Table 3.1). However the longer chain mannose materials show some deviation

from the expected molar mass ($M_{n,NMR}$ 20,000 vs $M_{n,th}$ 28000 for Dopa-$(ManAA)_{100}$; $M_{n,NMR}$ 42,400 vs $M_{n,th}$ 55,800 for Dopa-$(ManAA)_{200}$. These deviations may be somewhat accounted for by errors in measurement of CTA or initiator, thereby altering $[M]_0/[CTA]_0$ to a greater extent than for shorter chain materials and thus altering the true degree of polymerisation.

The discrepancy observed between $M_{n,SEC}$ and $M_{n,th}$ is likely to be due to the difference in hydrodynamic volume of size standards used to calibrate the instrument with those of the analysed polymers during size exclusion chromatography. This observation is further exacerbated in the case of the Dopa-$(HEAA)_{50}$ material, due to the swelling of HEAA in DMF.

While it appears that the molar mass achieved deviate somewhat from the expected molar mass, for continuity the produced material nomenclature based on targeted DP shall be retained in further sections.

3.3.4. Kinetics of acrylamide polymerisation mediated by PABTC and Dopa-PABTC

To investigate the kinetic properties of RAFT polymerisation of acrylamide monomers with the Dopamine-containing RAFT agent Dopa-PABTC in comparison to the unmodified RAFT agent (PABTC). Kinetics was monitored over a 4 hour period for the polymerisation of NAM, a model acrylamide monomer, using the conditions described in 3.2.2.4 substituting dioxane for DMSO to solubilise the monomer. However, as aqueous polymerisation of acrylamides via CTA mediated RAFT using the initiator VA-044 at 70 °C occurs very fast, the reaction was seen to proceed to completion in less than 20 minutes, insufficient time points could be collected in this time frame to yield good kinetic plots. To reduce radical flux the temperature of the polymerisations was lowered to 44 °C, the ten hour half-life of the initiator. Reducing the number of propagating radicals was sufficient to reduce the rate of propagation such that complete monomer consumption took ≥2 hours when mediated by Dopa-PABTC and PABTC, thus allowing for monitoring of kinetics. A summary of this data is shown in table 3.2 and figures 3.16-8.

Table 3.2. Kinetic data for polymerisation of NAM using PABTC or Dopa-PABTC as the CTA.

Time (h)	% conv	$M_{n,th}$ (g mol^{-1})[a]	$M_{n,SEC}$ (g mol^{-1})[b]	$Đ$
PABTC				
02.5	15	4200	2500	1.69
0.5	31	8800	13900	1.09
0.75	41	11600	19300	1.06
1	49	13900	21900	1.06
1.5	81	23000	24200	1.06
2	95	27000	23900	1.07
3	96	27300	24500	1.06
4	97	27500	24500	1.09
Dopa-PABTC				
0.25	3	900	700	1.2
0.5	3	900	800	1.35
0.75	4	1100	900	1.6
1	6	1700	1600	1.77
1.5	25	7100	10600	1.12
2	40	11400	19400	1.07
3	90	25700	25600	1.18
4	93	26600	26000	1.07

[a]Determined using equation 3.2. [b]Determined using THF-SEC by conventional calibration with linear PMMA standards

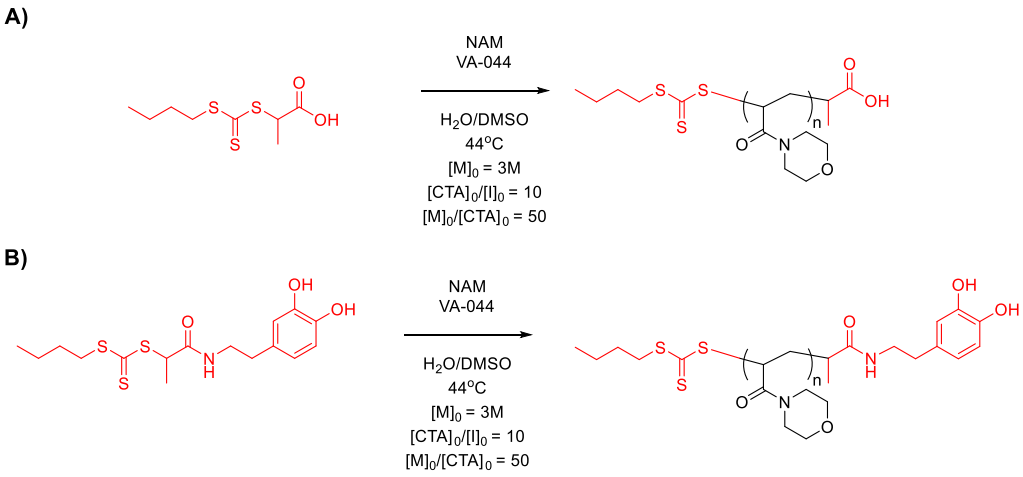

Figure 3.16. Polymerisations of NAM performed in kinetic study. A) mediated by PABTC, B) mediated by the Dopamine-containing derivative Dopa-PABTC

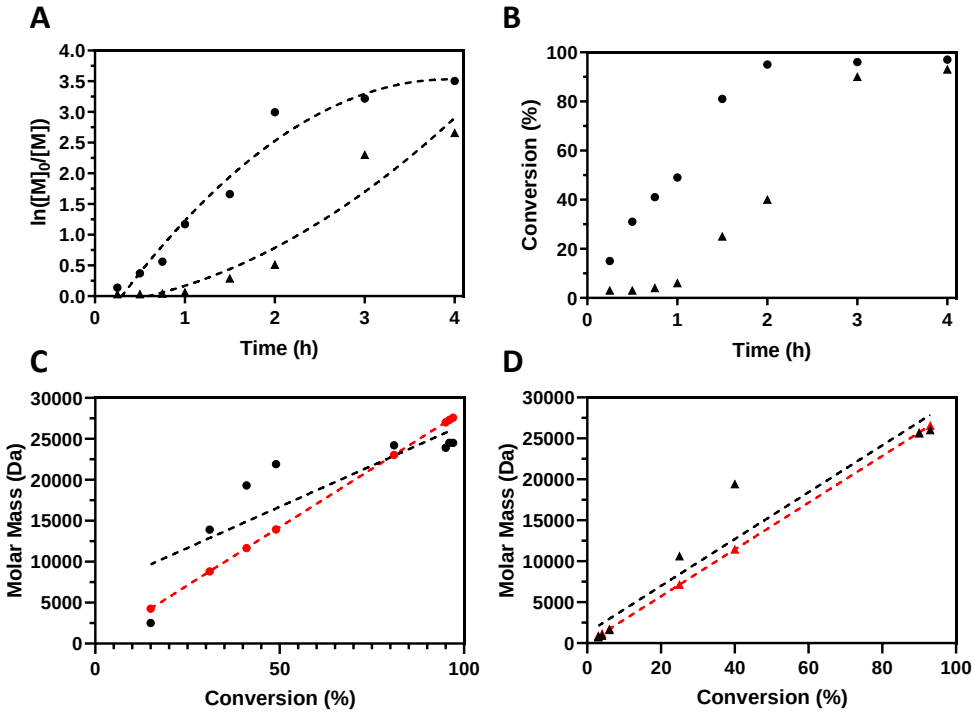

Figure 3.17. Polymerisation kinetics of model acrylamide NAM monomer with PABTC and Dopamine-containing chain-transfer agents. PABTC (Circles) vs Dopa-PABTC (Triangles). A) Pseudo First Order Plot. B) Conversion against time. C) Conversion against $M_{n,sec}$ and $M_{n,th}$ (black and red respectively) with linear regression for PABTC D) Conversion against $M_{n,sec}$ and $M_{n,th}$ (black and red respectively) with linear regression for Dopa-PABTC.

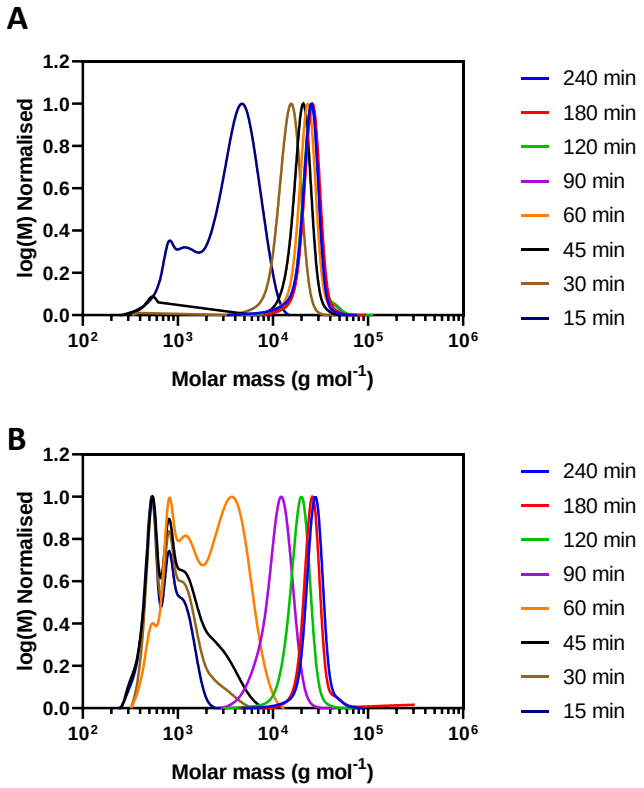

Figure 3.18. Evolution of SEC chromatograms over time for polymerisation of NAM mediated by A) PABTC, B) Dopa-PABTC chain-transfer agents.

$M_{n,\,SEC}$ showed a mostly linear increase with monomer conversion reaching 97% conversion and 93% conversion for polymerisations mediated by PABTC and Dopa-PABTC chain-transfer agents, respectively (Fig 3.17.C and D). In principle, for fully controlled radical polymerisation this linear mass increase should begin at the molar mass of the RAFT agent (238 g mol^{-1} for PABTC and 374 g mol^{-1} for Dopa-PABTC). For the conditions tested a molar mass of 4200 and 900 g mol^{-1} are seen after 15-30 min for PABTC and Dopa-PABTC respectively. These increased early molecular weights suggest that during the initial stages of polymerisation these RAFT agents are unable to perform efficient chain transfer and a small amount of free radical polymerisation may be taking place, producing larger observed molar

masses than those predicted theoretically. This finding is further corroborated by the high dispersity of materials analysed between 15-30 min, maximally 1.69 and 1.35 for PABTC and Dopa-PABTC respectively. In the first order plot (Fig 3.17.A) PABTC generally conforms to a linear fit up until 2 hours, when conversion has already reached 95%, suggesting that for PABTC mediated aqueous polymerisation of acrylamides the concentration of propagating radicals mostly remains constant; an indicative feature of a controlled radical polymerisation. The SEC evolution curves for PABTC (fig. 3.18.A.) demonstrate an increase in molecular weight over time with narrow molecular weight distributions ($Đ$ =1.06-1.09) and symmetrical elution curves for all time points except 15 min where a low molecular weight shoulder is seen, likely attributable to early free radical polymerisation. Unusually, the presence of a high molecular weight tail is at 90 and 120 min which is not observed at other time points. This is difficult to rationalise, as a high molecular weight tail would be expected to be observed across later time points, particularly when high conversion has already been reached, and may be an artefact of SEC.

In contrast for Dopa-PABTC little to no polymerisation is seen prior to 1 hour (Fig. 3.17.B). Additionally, in the first order plot (Fig. 3.10.A) an upward curve is seen until 2 hours prior to linearizing. The increasing gradient of the first order plot suggests that the concentration of propagating radicals increases up until this point, indicative of slow initiation. The SEC evolution plot for the first 4 time points (0.25-1 hour) show non-uniform elution curves which may suggest the occurrence of

some free radical polymerisation, however as conversion remains low this may have little impact on the final materials. Indeed, the evolution of M_w distributions over time, monitored by SEC (fig 3.18.B.) shows an increase in molecular weight over time for all times points past one hour with reasonably symmetrical elution curves and narrow molecular weight distributions ($Đ$ =1.07-1.18) which would suggest good control despite the earlier induction period, suggesting that this chain transfer agent may be applicable for polymerisation of acrylamide monomers in an aqueous system.

However a slight high molecular weight shoulder is seen for the final time point, 240 min (Fig. 3.18.B.). The presence of this shoulder suggests the occurrence of some termination at this time, either by bimolecular termination or disproportionation which could impact polydispersity of materials produced. However, as the high molecular weight tail only appears to occur at high conversion for Dopa-PABTC termination, at this time may only be due to depletion of the monomer. While termination is an important consideration in a polymerisation system, as it can impede control over molecular weight distributions, this could be counteracted by stopping the reaction prior to reaching complete conversion or by minimising the concentration of radicals in the system.

It is surprising that an induction period is observed for Dopa-PABTC as no induction period was reported by Oyeneye & co-workers for an analogous dopamine terminal RAFT CTA (Oyeneye *et al.*, 2015). While the mechanism of the observed induction period is not investigated herein, several

hypotheses are offered to explain its origin. Incomplete depletion of oxygen in the reaction by degassing or abstraction of radicals by the catecholic terminus could lead to the quenching of initiator derived radicals. Initiator derived radical depletion by these phenomena may delay monomer consumption until sufficient initiator has decomposed to deplete the oxygen or overcome radical abstract by the phenol.

Furthermore, it is also possible that stabilisation of the RAFT intermediate could delay monomer consumption, leading to an induction period. As the 'acrylamide like' reinitiating group of Dopa-PABTC is similar to the acrylamide domain of NAM it may be possible that neither radical is favoured and the pre-equilibrium tends towards the centre – formation of the RAFT adduct (Scheme 3.4.A). As a result, formation and cycling of radicals between the central RAFT intermediate and initiator derived chains may be favoured over propagation. Once sufficient initiator decomposition has occurred sufficient radicals may be present in the system to fully saturate the RAFT agent and push the equilibrium towards the generation of propagating radicals.

In contrast no induction period is observed for PABTC mediated reactions. The 'carbonyl-like' reinitiating group of the carboxylic acid RAFT agent, PABTC, is less stable than the acrylamide like initiator derived radicals of NAM therefore pushing the equilibrium to the left favouring RAFT agent consumption and generation of propagating radicals by reinitiation by R-group radicals (Scheme 3.4.B). This in turn would result in faster, well-controlled polymerisation of acrylamides by mediated by this RAFT agent.

While common in other CTAs, such as dithiobenzoates and dithiocarbamates, induction periods have been rarely observed in trithiocarbonates (Rizzardo *et al.*, 2007; Schilli *et al.*, 2002; Zhang *et al.*, 2010). However induction periods have been observed for trithiocarbonate CTAs where reinitiation by the R-group is poor, but with little impact on material polydispersity (Houillot *et al.*, 2007; Li & Benicewicz, 2005).

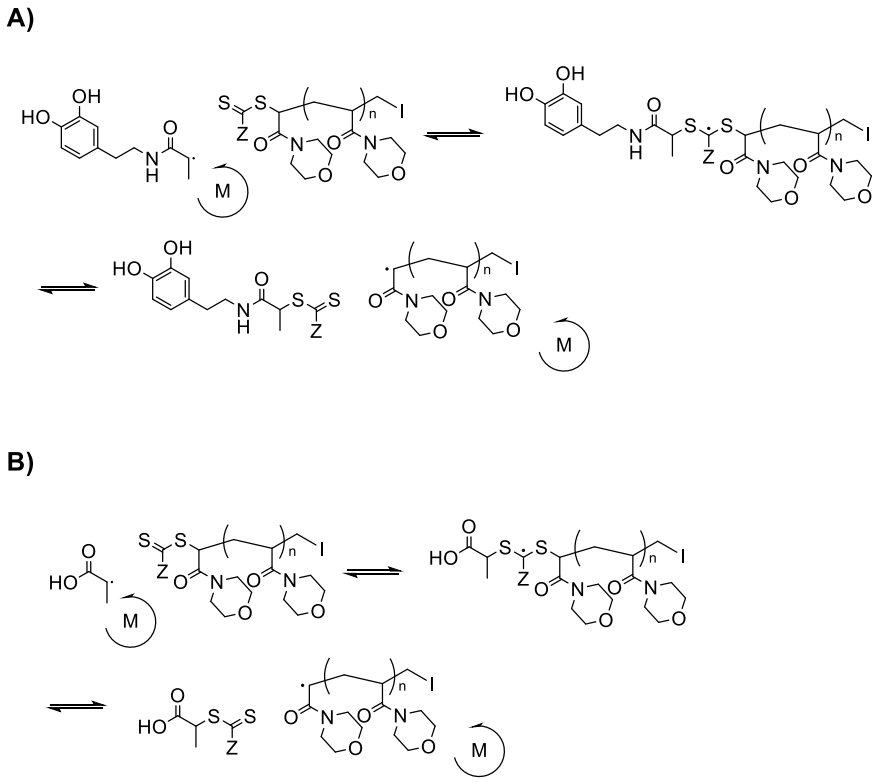

Scheme 3.4. Pre-equilibrium of a RAFT polymerisation of NAM mediated by A) Dopa-PABTC or B) PABTC. Z = n-Bu.

3.3.5. Assessing lectin binding activity of RAFT-derived catechol-terminal glycopolymers

To determine the effect of mannose polymer chain length on lectin binding, lectin binding assays were performed on variable length Dopa-(ManAA) polymers, as well as control non-Con A-binding control polymers Dopa-$(HEAA)_{50}$ and Dopa-$(GalAA)_{50}$.

3.3.5.1. ConA turbidity assay

To demonstrate that dopamine-containing glycopolymers were able to interact reversibly with lectins a UV-vis turbidity assay was performed with Concanavalin A, a model lectin which is capable of binding α-D-mannosyl and, less strongly, α-D-glucosyl residues (Goldstein *et al.*, 1973) . ConA exists in a tetrameric form at neutral pH and demonstrates tetravalency with respect to specific sugar binding sites (Edelman & Wang, 1978; Saito *et al.*, 1983). Due to the tetravalency of ConA, it is able to bind multiple polymer chains resulting in the formation of large insoluble aggregates, leading to an increase in turbidity.

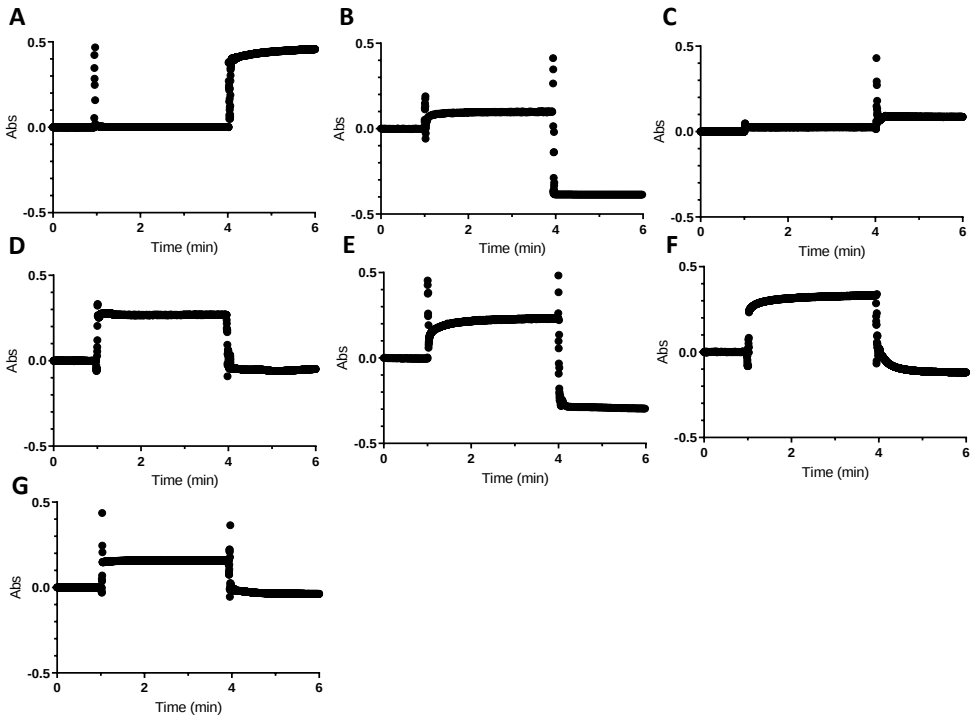

Figure 3. 19. Catecholic glycopolymer-ConA aggregation by turbidimetric analysis. ConA solution was injected at 1 min; excess of free D-mannose injected at 4 min. A) Buffer only; B) Dopa- $(HEAA)_{50}$ (non-glycopolymers control polymer); C) Dopa-$(GalAA)_{50}$; D) Dopa-$(ManAA)_{20}$; E) Dopa-$(ManAA)_{50}$; F) Dopa- $(ManAA)_{100}$; G) Dopa- $(ManAA)_{200}$. Absorbance recorded at λ=420 nm.

As shown in Fig 3.19. all mannosylated polymers showed a reversible interaction with the lectin ConA demonstrated by an increase in turbidity upon the addition of the lectin and a decrease in turbidity to at or below the baseline upon addition of an excess of free D-mannose, used here as a competitive monovalent ligand for ConA. In contrast, little to no increase in turbidity is seen upon lectin addition for the galactosylated polymer Dopa-$(GalAA)_{50}$. Surprisingly, there does appear to be some minimal interaction between the non-sugar acrylamide polymer (Dopa-$(HEAA)_{50}$) and ConA, as evidenced by a small increase in turbidity upon addition of the lectin which may be reversed by addition of free sugar, for this material. Lectins can demonstrate some promiscuity when it comes to sugar binding (Agostino

et al., 2015; Jeyaprakash *et al.*, 2005; Otten & Gibson, 2015), it may be that the combination of free hydroxyl groups on the poly(acrylamide) backbone with the presence of catechol termini may mimic the ligand of ConA sufficiently to lead to an interaction but there is little precedence in the literature to support this hypothesis.

It is important to note that these experiments demonstrate that there is no correlation between DP and absolute turbidity. This is likely because secondary interactions can occur between glycopolymer-lectin clusters thus increasing aggregate size and perturbing turbidity. Furthermore, turbidity measurements are greatly affected by the light scattering ability of particles in solution and the dilution effect upon solution injection. Hence this technique can should mainly be used as a qualitative measure of aggregation.

For a more quantitative measure of lectin capture by glycopolymers some authors have attempted to determine the rate of clustering by measuring the initial slope as precipitation occurs (Cairo *et al.*, 2002; Ladmiral *et al.*, 2006). This method could not be utilised in our case due to injection and pipetting of the ConA solution into the cuvette which obscured the intial increase in turbidty.

3.3.5.2. Kinetics of catecholic glycopolymer lectin binding determined by surface plasmon resonance (SPR).

To confirm the results obtained from the turbidimetric assay performed in Section 3.3.5.1. additional analysis was performed using SPR with two model mannose binding lectins, DC-SIGN and MBL.

Table 3.3. Kinetic binding data of glycopolymers and DC-SIGN as calculated by SPR

Polymer	k_a (1/M s)	k_d (1/s)	K_a (1/M)	K_d (nM)	R_{max} (RU)
DopaPABTC-(HEAA)50	3.06×10^{8}	0.0922	3.32×10^{9}	0.301	107
DopaPABTC-(GalAA)50	1.49×10^{5}	1.38×10^{-3}	1.08×10^{8}	9.24	53.9
DopaPABTC-(ManAA)20	5.78×10^{5}	2.21×10^{-3}	2.62×10^{8}	3.82	134
DopaPABTC-(ManAA)50	3.88×10^{5}	2.75×10^{-4}	1.41×10^{9}	0.709	269
DopaPABTC-(ManAA)100	2.26×10^{5}	1.89×10^{-4}	1.20×10^{9}	0.836	282
DopaPABTC-(ManAA)200	8.32×10^{5}	4.24×10^{-5}	1.96×10^{10}	0.051	271

Table 3.4. Kinetic binding data of glycopolymers and MBL as calculated by SPR

Polymer	k_a (1/M s)	k_d (1/s)	K_a (1/M)	K_d (nM)	R_{max} (RU)
DopaPABTC-(HEAA)50	5.50×10^{7}	0.297	1.85×10^{8}	5.41	431
DopaPABTC-(GalAA)50	5.34×10^{5}	6.38×10^{-3}	8.36×10^{7}	12.0	112
DopaPABTC-(ManAA)20	4.93×10^{5}	1.18×10^{-3}	4.20×10^{8}	2.38	392
DopaPABTC-(ManAA)50	5.68×10^{5}	5.34×10^{-4}	1.06×10^{9}	0.941	751
DopaPABTC-(ManAA)100	1.92×10^{5}	5.31×10^{-4}	3.63×10^{8}	2.76	1050
DopaPABTC-(ManAA)200	9.66×10^{5}	2.00×10^{-4}	4.8×10^{9}	0.207	901

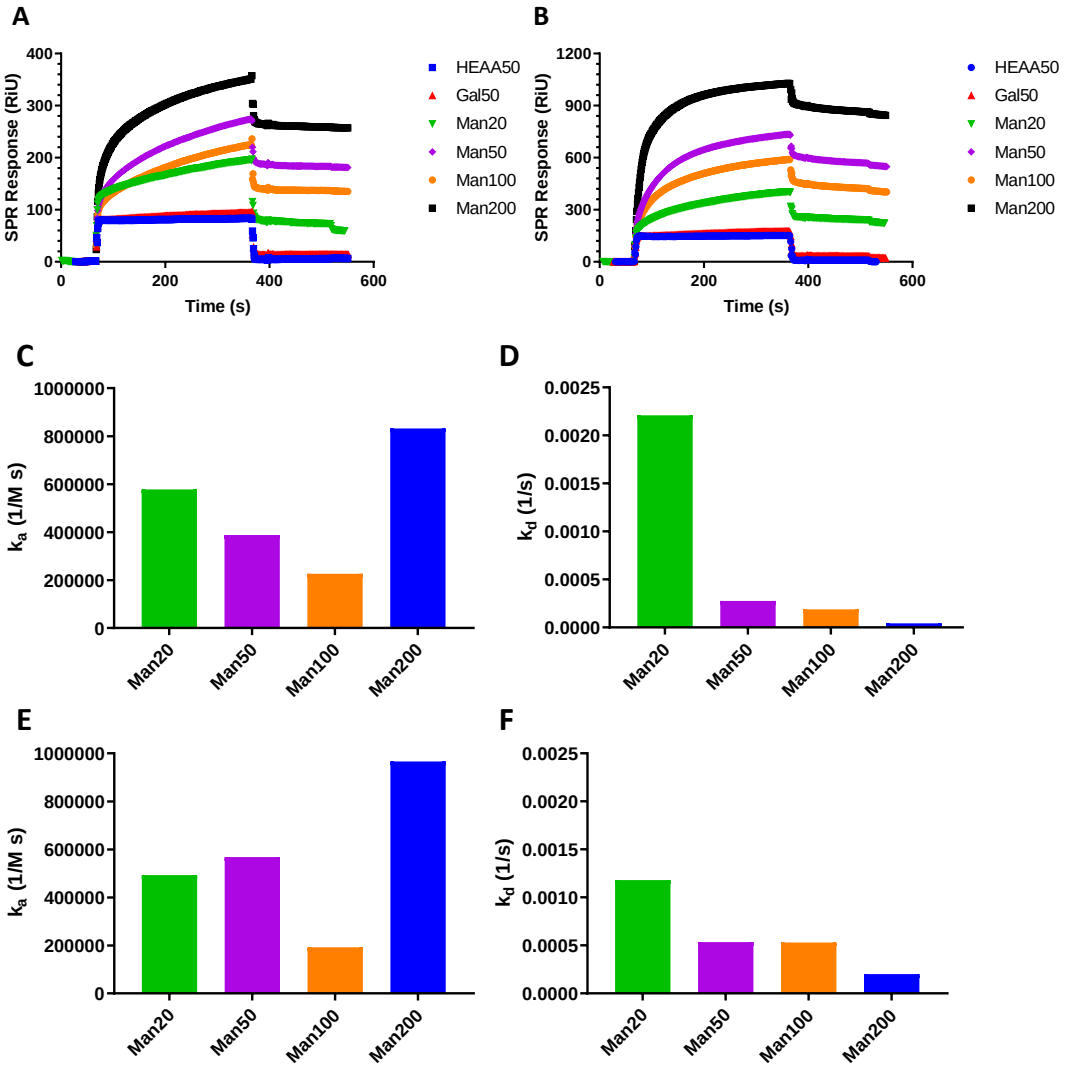

Figure 3.20. Comparison of variable chain length glycopolymer binding with DC-SIGN and MBL. A) SPR sensogram of catechol-terminal polymers with DC-SIGN at 10 nM; B) SPR sensogram of catechol-terminal polymers with MBL at 10 nM; C) DC-SIGN association rate constants for various chain mannosylated materials; D) DC-SIGN dissociation rate constants for various chain mannosylated materials; E) MBL association rate constants for various chain mannosylated materials; F) MBL dissociation rate constants for various chain mannosylated materials.

All kinetic data and determined rate constants for DC-SIGN and MBL are shown in Tables 3.3. and 3.4. respectively. From the SPR response curves (Fig 3.20.A & B) little deposition of the HEAA or galatosylated material onto the chip is observed; suggesting little interaction of these materials with mannose binding lectins. Since SPR response is proportional to the mass of material deposited upon the chip it may be expected that SPR response to material molecular weight and, hence DP. SPR sensograms (Fig 3.20.A & B) for the mannosylated materials of various chain lengths shows that the amount of material deposited onto the chip surface is dependent on the polymer length in the order $DP_{200} > DP_{50} > DP_{100} > DP_{20}$, for both lectins (Fig. 3.20.A&B). This imperfect correlation between DP and SPR response may suggest a more complex relationship between lectin affinity and glycopolymer chain length than expected.

Dissociation rate constants (k_d) for both lectins progresses in decreasing magnitude in the order $DP_{20} > DP_{50} > DP_{100} > DP_{200}$ suggesting that glycopolymer dissocation rates are inversely proportional to chain length; i.e. interaction of lectins to glycomaterials of increasing length are harder to disrupt (Fig 3.20.D&F). Slow dissociation rates are seen for all mannosylated materials which would be expected in the case of multivalent binding interactions (Lee & Lee, 2000; Munoz *et al.*, 2009; Munoz *et al.*, 2013) .

The relationship between association rate constants (k_a) and glycopolymer chain length is harder to interpret. Association rate constants for DC SIGN progresses in decreasing magnitude in the order $DP_{200} > DP_{20} > DP_{50} >$

DP_{100}; whereas for MBL the association proceeds in the following order: DP_{200} > DP_{50} > DP_{20} > DP_{100} (Fig.3.20.C&E). These data may suggest that association rates of lectins to glycopolymers is not directly correlated to glycopolymer chain length.

In summation these data suggest that the DP_{200} mannosylated glycomaterial is the strongest binding material, showing greatest adsorption to the chip as well as the highest association rate constant with lowest dissociation constant. The DP_{100} material demonstrated a lower adsorption onto the chip than DP_{50} surprisingly, however this may somewhat be explained by the kinetics constants. While the DP_{100} material had the second smallest dissociation constant (i.e. second hardest to remove) it also had the smallest association constant (i.e. it was the least able to bind of the materials). In contrast, the DP_{50} material attached to the surface in greater amounts than the DP_{100} material. However this material showed a greater rate of association, while having a very similar dissociation constant to DP_{100}. These rate constants suggest that the DP_{50} material attached more rapidly, but was similar in detachment to the DP_{100} mannose polymer. Finally, the DP_{20} material, while able associate to both lectins very fast, was also the easiest to detach from both lectins having the highest k_d rate constant of all analysed materials.

Consequently Dopa-$(ManAA)_{50}$ and Dopa-$(ManAA)_{200}$ were taken forward to use in coating of SPIONs as these two materials had the highest association rate constants and lowest dissociation rate constants of all mannosylated catechol-terminal glycomaterials analysed. That Dopa-

$(HEAA)_{50}$ and Dopa-$(GalAA)_{50}$ demonstrated little deposition onto the lectin functionalised chip also further validates these materials as non-binding controls for use in subsequent Type 1 fimbriae facilitated magnetic pulldown experiments.

However, it is important to recognise that sugar specificity and binding affinities are specific for each lectin (Becer, 2012; Lis & Sharon, 1998; Schnaar, 2016; Sharon & Lis, 2004) . The results demonstrated in this Chapter may not be respective of glycopolymers binding by FimH, the lectin tip on *E. coli* Type 1 fimbriae, due to the usage of alternate lectins as the purified FimH protein was not commercially available. Use of non-target lectins as models is a key limitation of the present study. However, as FimH has previously been demonstrated to have a high affinity for mannose but not galactose, polysaccharides the binding affinities determined in this chapter are likely to be representative of FimH glycopolymer interaction (Chervenak & Toone, 1995; Mandal *et al.*, 1994; Naismith & Field, 1996).

3.3.6. Synthesis and coating of SPIONs

3.3.6.1. Synthesis of SPIONs: comparison of chemical co-precipitation and thermal decomposition methods

Initially two methods were trialled for the synthesis of superparamagnetic iron oxide nanoparticles: the co-precipitation method and the thermal decomposition method.

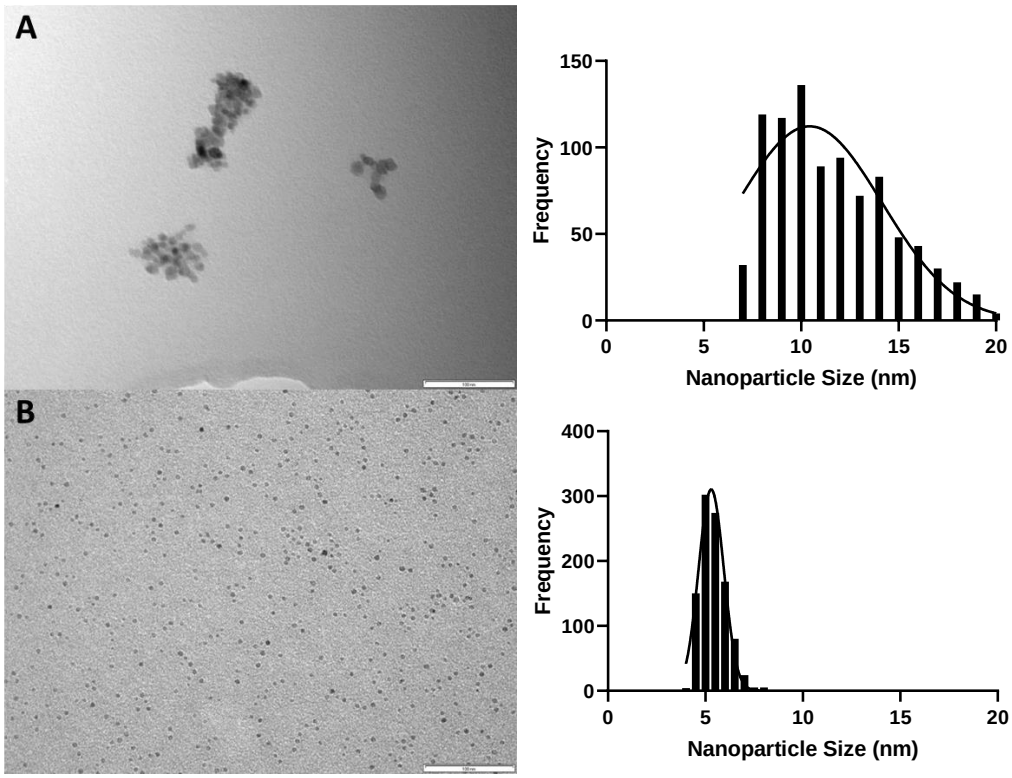

Figure 3.21. Representation TEM micrograph of SPIONs produced by (A) coprecipitation and (B) thermal decomposition method, with size distribution histograms. Coprecipitation yields disperse, irregularly shaped nanoparticles which appear to aggregate in aqueous media ($\bar{x}$ = 11.63 ± 3.03 nm, n= 906, R^2= 0.854). Thermal decomposition yields monodisperse size distributions of nanoparticles with a consistent, spherical morphology and as distinct entities as opposed to aggregates method ($\bar{x}$ = 5.42 ± 0.65 nm, n= 1008, R^2= 0.968). Scale bars = 100 nm. Size analysis performed in ImageJ. Size distribution analysis and non-linear fit was performed in GraphPad Prism.

Particles derived from the co-precipitation method appeared to have an irregular morphology on TEM micrographs (Fig 3.21.) which also formed aggregates in aqueous media. In contrast nanoparticles produced via the thermal decomposition method had more consistently spherical morphology with a distinct absence of multiple particle conglomerates (Fig 3.21.). Additionally, particle size analysis from TEM micrographs revealed better control of particle size; 5.42 ± 0.65 nm for thermal decomposition derived particles and 11.63 ± 3.03 nm for co-precipitation derived particles (Fig 3.14.). Both of these nanoparticles lie within the size range for superparamagnetism; generally believed to be <20 nm (Jun *et al.*, 2005; Li *et al.*, 2017; Pereira *et al.*, 2012). Furthermore, previous analysis of SPIONs produced by chemical co-precipitation and thermal decomposition generally present monodisperse, uniform particles of <10 nm for thermal decomposition and disperse particle size and lack of uniformity, with particles >10 nm, in the case of chemical co-precipitation which is consistent with the above findings (Hyeon *et al.*, 2001; Lassenberger *et al.*, 2016; Maity & Agrawal, 2007; Oz *et al.*, 2016; Park *et al.*, 2004; Vayssieres *et al.*, 1998; Vikram *et al.*, 2015).

Due to the greater degree of control afforded to particle size distribution and morphology, the thermal decomposition method was utilised to generate nanoparticles for coating in later sections.

3.3.6.2. Coating of thermal decomposition derived SPIONs with catechol-terminal glycopolymers

Nanoparticles synthesised as per Section 3.3.6.1. were coated during synthesis with oleic acid for nanoparticle stabilisation. Few methods have been reported in the literature for grafting very hydrophilic materials to SPIONs which have been stabilised with oleic acid, primarily due to solvent incompatibility of the two materials. Fortuitously, a method was reported very recently by Galli & co-workers which was able to replace the oleic acid ligand of SPIONs with a catechol-functionalised polyamidoamine in an aqueous system using the phase transfer catalyst TMAOH (Galli *et al.*, 2019). As the catechol-functionalised glycopolymers produced in section 3.3.3. were also highly hydrophilic, similar to the polyamidoamine, this method was adapted for the coating of oleic acid coated SPIONs with the glycomaterials produced in this study (Fig 3.22).

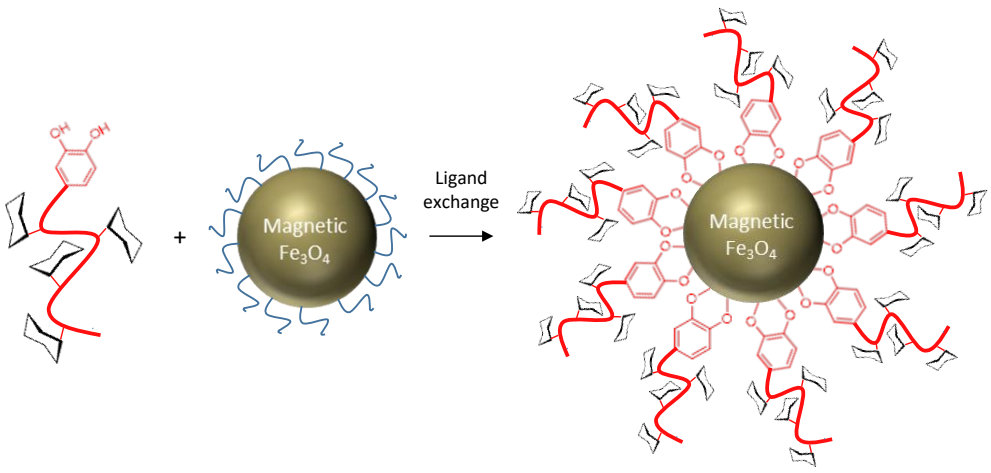

Fig 3.22. Ligand replacement of oleic acid by catechol terminal glycopolymers. Catechol-terminal materials have a high affinity for the under-coordinated Fe surface sites of magnetic nanoparticles resulting in tight binding of the bidentate ligand and replacement of the oleic acid (blue lines) producing a glycosylated iron oxide shell:core nanoparticle.

To confirm the presence of the various catechol-terminal polymers on the surface of functionalised SPIONs FTIR analysis was performed.

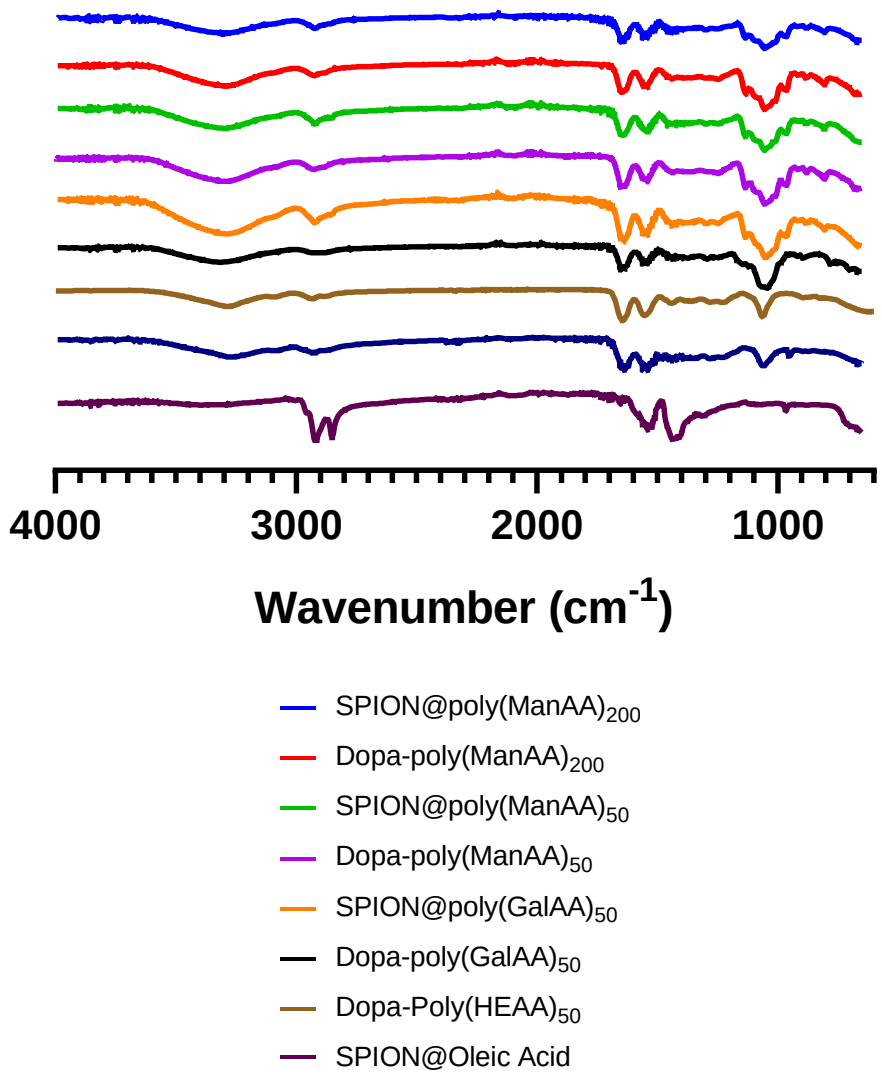

Fig 3.23. FTIR spectra of polymer-functionalised SPIONs, compared to the corresponding free polymers, and oleic acid coated SPIONs

In the case of all polymer functionalised materials a depletion of the two sharp peaks at ~2900 and ~2800 cm^{-1} from the stretching from the CH_2 groups of oleic acid and emergence of a broad peak at around 3300 cm^{-1} are seen which could correspond to the hydroxyl groups on all polymer repeating units (Fig. 3.23.). Furthermore all coated materials show the

appearance of sharp peaks at ~1660 and ~1550 cm^{-1}, which are also present on the polymeric materials, which could correspond to the amide C=O stretch and N-H bending from the polymer amide groups. The polyHEAA-coated SPION shows a peak at ~1060 cm^{-1}, also present on the polymeric material, likely derived from the C-N stretch on the amide. All glycopolymer- functionalised SPIONs, as well as free glycopolymers, show broad overlapping peaks centred around 1000 cm^{-1}, likely from the various C-O bonds present on the sugars. The summation of these data provide good qualitative evidence of the presence of the polymeric materials on the functionalised nanoparticles which were recovered from dialysis.

To determine the weight percentage of the polymeric coating compared to the SPION core of nanoparticle:polymer conjugates thermogravimetric analysis was performed as described in Section 3.2.1.4. Results of this analysis are shown in Figure 3.24. below.

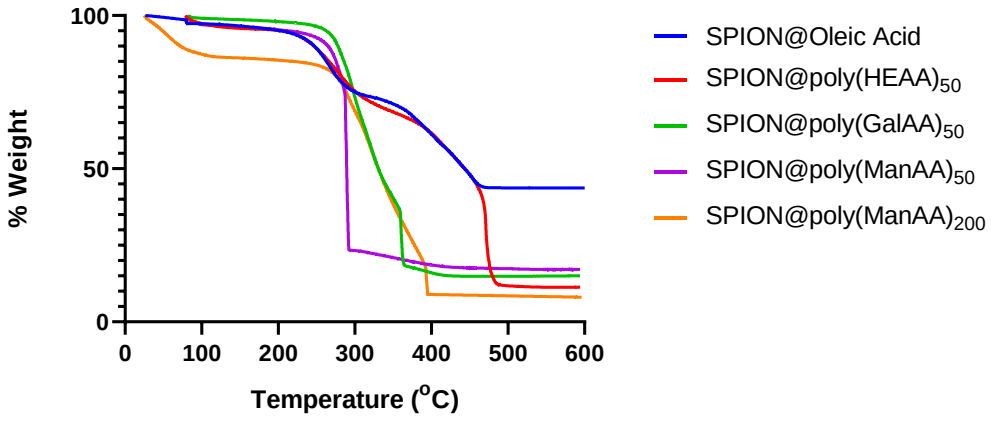

Figure 3.24. Thermal analysis of dopamine-containing polymer functionalised SPIONs. High coating efficiency is seen for all materials.

Below 400°C a two-step TGA profile is obtained for the oleic acid capped SPIONs. Similar biphasic profiles have been observed by other authors for oleic acid capped SPIONs (Bixner *et al.*, 2015; Lassenberger *et al.*, 2016; Roonasi & Holmgren, 2009; Sahoo *et al.*, 2001). Sahoo & co-workers suggest that this biphasic transition is due to a quasi-two layer adsorption of oleic acid onto SPION surfaces, where the two layers have differing binding strengths (Sahoo *et al.*, 2001). Alternatively Roonasi & Holmgren attributed this biphasic shift to the partial cleavage of the capping agent during temperature ramping (Roonasi & Holmgren, 2009).

This biphasic shift pattern is also observed in the case of poly(HEAA) coated nanoparticles in this study. Additionally, the final temperature at which no further weight loss is observed is also similar for this material and the oleic acid capped SPIONs, at around 595 °C. This may suggest that incomplete ligand exchange is achieved between Dopa-poly(HEAA)$_{50}$ and oleic acid using the TMAOH mediated exchange method, leading to some retention of oleic acid on the particle surface. However the total iron oxide weight of the HEAA functionalised material is similar to that of other coatings (11.31% IO (Iron Oxide), 88.69% TOC (Total Organic Content).

Alternatively, complete vaporisation of the coating material is seen by 400 °C for mannose and galactose polymer functionalised SPIONs, suggesting high replacement of oleic acid using the TMAOH mediated ligand exchange method. Furthermore, TGA plots do not reveal biphasic shift patterns for these materials suggesting a monophasic coating architecture which would be consistent with all polymers forming a bidentate

interaction between the catechol terminus and SPION surface. Polymer weight percentage by total organic content was determined to be 85.0%, 82.9% and 91.9%, respectively, for SPION@poly(GalAA)$_{50}$, SPION@poly(ManAA)$_{50}$ and SPION@poly(ManAA)$_{200}$, demonstrating high functionalisation for all coatings. This difference in weight percentage between the short and long chain length material could be attributed to the difference in molecular weights of these materials and may not be indicative of differing levels of functionalisation.

Interestingly, polymer weight percentage is higher than other authors have reported for decorated SPIONs via a 'grafting to' approach (Babiuch *et al.*, 2011; Lassenberger *et al.*, 2016; Li *et al.*, 2014; Munoz-Bonilla *et al.*, 2012; Zhang *et al.*, 2016b). However in all of these studies, the diameter of iron oxide particle cores were greater than those reported in this study. Furthermore, in the case of co-precipitation derived SPIONs, as utilised by Zhang & co-workers, these particles are prone to aggregation. These factors could limit the surface area available for functionalisation in these materials, reducing polymer load. In the nanoparticles produced herein are very small (~ 6 nm) thus increasing the surface area available for functionalisation and potentially increasing polymer weight percentage after ligand exchange. This strategy may rival the weight percentage of glycopolymer which can be achieved via a 'grafting from' process (Kutcherlapati *et al.*, 2017a; Oz *et al.*, 2016).

Polymer chain grafting density per nm^2 maybe be calculated using the method reported by Benoit & co-workers using a combination of TGA and

TEM (Benoit *et al.*, 2012). However, this analysis was omitted as this model requires many fundamental assumptions (perfectly spherical particles, precise knowledge of polymer weight, knowledge of particle density, no impact of steric effects, etc). These calculations give a hypothetical approximation of nanoparticle grafting density at best, but do not reflect real measurements.

3.3.6.3. Size analysis of coated SPIONs by TEM

To determine the effect of catechol-terminal glycopolymer coating on SPION core size, size distribution analysis via TEM as described in section 3.2.1.5 was performed.

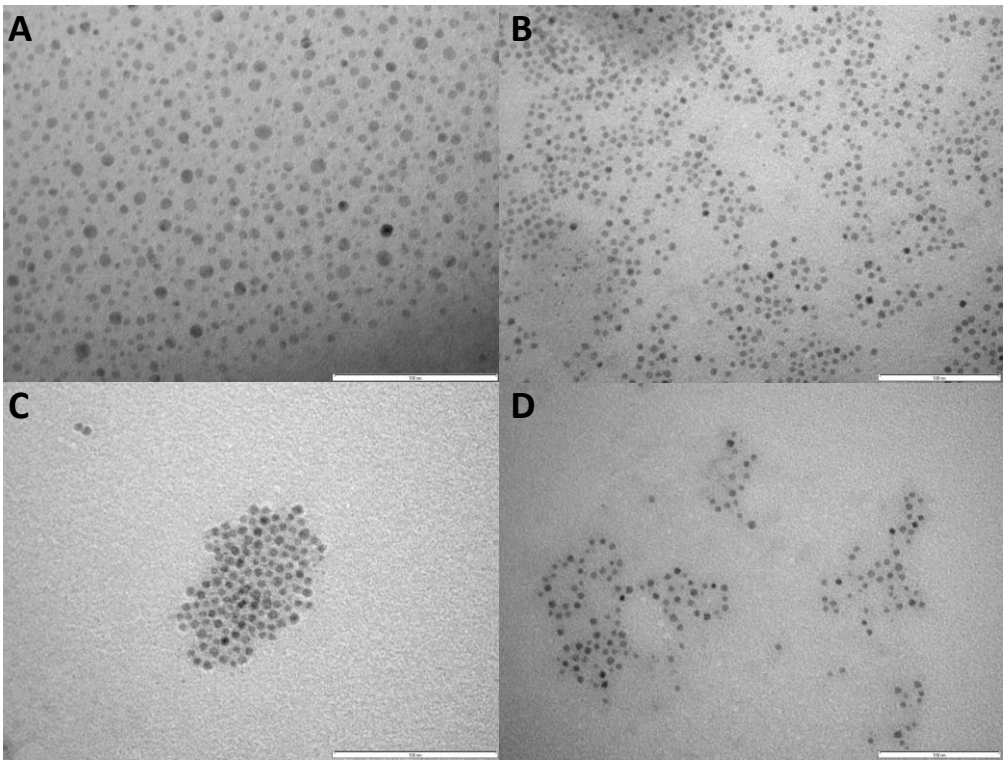

Figure 3.25. Representative TEM micrographs of catechol-terminal polymer functionalised SPIONs. A) SPION@Dopa-poly(HEAA)$_{50}$; B) SPION@Dopa-poly(Gal)$_{50}$; C) SPION@Dopa-poly(ManAA)$_{50}$; D) SPION@Dopa-poly(ManAA)$_{200}$. Scale bars represent 100 nm. All coated materials demonstrate monodisperse nanoparticle core with a consistent, spherical morphology and as distinct entities as opposed to aggregates.

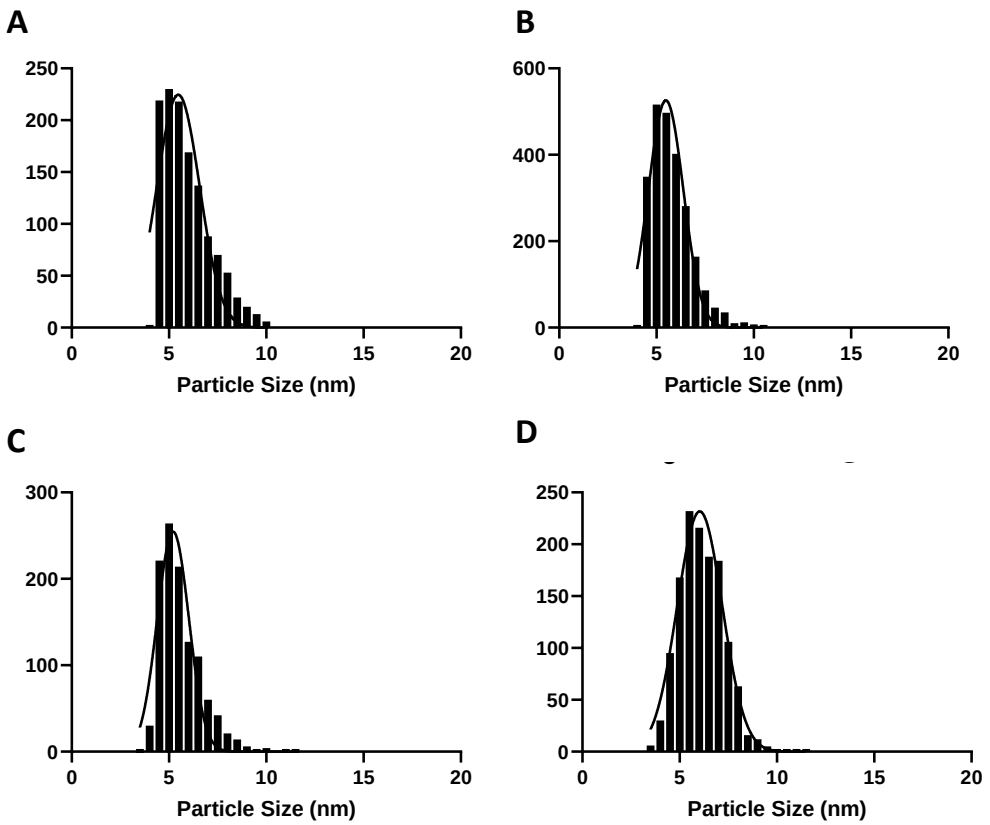

Figure 3.26. Nanoparticle size distribution for glycopolymer coated SPIONs as assessed by TEM. A) SPION@Dopa-p(HEAA)$_{50}$ ($\bar{x}$ = 5.9 ± 1.2 nm, n= 1252, R^2= 0.81); B) SPION@Dopa-(GalAA)$_{50}$ ($\bar{x}$ = 5.8 ± 1.0 nm, n= 2406, R^2= 0.93); C) SPION@Dopa-(ManAA)$_{50}$ ($\bar{x}$ = 5.6 ± 1.1 nm, n=1118, R^2= 0.9); D) SPION@Dopa-(ManAA)$_{200}$ ($\bar{x}$ = 6.1 ± 1.1 nm, n=1332, R^2= 0.98) Size analysis performed in ImageJ. Size distribution analysis and non-linear fit was performed in GraphPad Prism.

The data in Figs. 3.25-6. suggest that this method of coating, and sugar composition of catechol-terminal polymers used in coating, does not affect the diameter of the SPION core of SPION:polymer core:shell nanoparticles. There appears to be no statistically relevant difference in coated SPION between these particles and the oleic acid coated nanoparticles produced via the thermal decomposition method as analysed by TEM described in Section 3.2.1.5. It is also noted that in some TEM micrographs captured a zone of lesser electron density was observed in a corona around the

nanoparticle core, which may correlate to the presence of the less dense polymer shell of the polymer:nanoparticle conjugates (Fig 3.27).

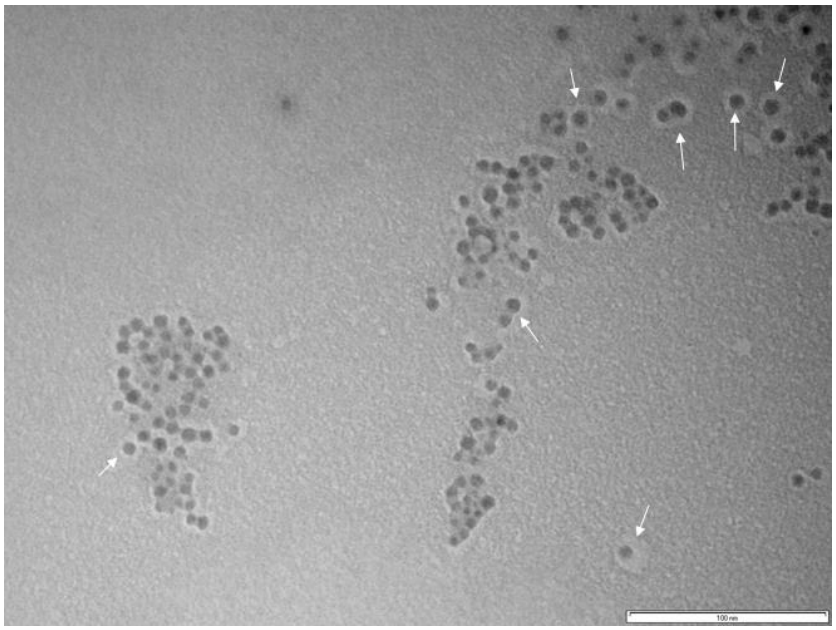

Figure 3.27. Representative TEM micrograph of SPION@Dopa-(ManAA)$_{200}$ with polymer corona. Scale bars represent 100 nm. White arrows indicate particles which demonstrate corona of lesser electron density around iron oxide core which may correspond to polymer shell.

A similar observation has been noted in the case of metal oxide nanoparticle:polymer conjugates (Abedin *et al.*, 2018; Brazzale *et al.*, 2017; Liu *et al.*, 2014; Munoz-Bonilla *et al.*, 2012; Zhang *et al.*, 2016b) However, due to the lack of consistent observation of this phenomenon, it was not possible to determine if this was a true observation of polymer surrounding the nanoparticle core or an artefact of contrast between the highly electron dense SPION core and the thin carbon film on the TEM grids.

3.3.6.4. Lectin binding capability of magnetic glyconanoparticles (MGNPs).

To determine if the SPIONs which had been functionalised with catechol-terminal poly(HEAA/ManAA/GalAA) polymers a lectin binding turbidimetric assay was performed as described in Section 3.2.4.1. As concentration of polymer available on the functionalised nanoparticles could not be determined a 1 mg/mL solution of each MGNP was utilised for comparison.

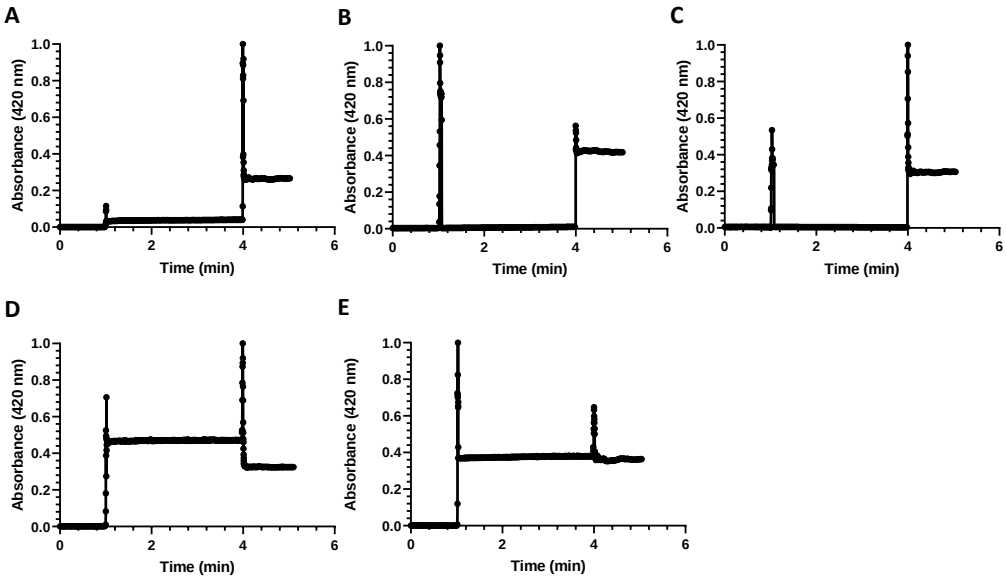

Figure 3.28. MGNP ConA aggregation by turbidimetric analysis. ConA solution was injected at 1 min; excess of free sugar injected at 4 min. A) Buffer only; B) SPION@Dopa-p(HEAA)$_{50}$; C) SPION@Dopa-p(GalAA)$_{50}$; D) SPION@Dopa-p(ManAA)$_{50}$; E) SPION@Dopa-p(ManAA)$_{200}$

As demonstrated in Fig 3.28. no increase in turbidity is observed when ConA is added to the poly(HEAA) and poly(GalAA) functionalised materials. Furthermore, an increase in turbidity is only observed upon the addition of free mannose competitive ligand for these two materials suggesting that SPION@Dopa-p(HEAA)$_{50}$ and SPION@Dopa-p(GalAA)$_{50}$ are unable to

complex ConA. In contrast, a sharp increase in turbidity is observed upon the addition of ConA solution to both mannosylated SPION materials which suggests that the mannosylated polymer coating on these materials is sufficient for multivalent interaction with the lectin under the conditions tested. However, addition of free mannose solution is unable to fully reduce turbidity in the case of the p(ManAA)$_{50}$ material and little change in turbidity was observed upon free sugar addition for the p(ManAA)$_{200}$ material.

This suggests that lectin binding of glycopolymer conjugated nanoparticles may be less reversible than the lectin binding of the same free, linear glycopolymers in solution. As multivalent sugar ligands are displayed on particles with a very small surface area an enhanced cluster glycoside effect leading to high affinity binding of lectins may be presence in the case of the produced MGNP.

Further investigation into the avidity of MGNPs described herein for target lectins could be performed by SPR analysis, as with the free glycopolymers in solution described in Section 3.3.4. However, due to the risk of damage to or contamination of the instrument by the magnetic nanoparticles this analysis was omitted.

Intriguingly, other reports have suggested that lectin binding to MGNPs can be reversed by the addition of an excess of a competitive monosaccharide ligand. Kavunja & co-workers were able to use galactosylated MNPs for the isolation of lectins from eukaryotic cell lysates (Kavunja *et al.*, 2015). Both exogenously added soy bean agglutinin and endogenously expressed

galectin could be captured by these particles and, after incubation with an excess of galactose, both of these lectins could be detected in the supernatant by Western blot (Kavunja *et al.*, 2015). However, these MNPs only displayed monovalent ligands for their target lectins, which have a lower affinity for lectins than polyvalent materials such as plycopolymers. Hence competitive inhibiton of lectin capture by free galactose can be expected to be facile in this case.

In contrast, Oz & coworkers used MGNPs decorated with either heptyl mannose or a DP_{280} mannose polymer and demonstrated they ability of these materials to capture and release FITC labelled ConA (Oz *et al.*, 2019). These polyvalent materials are more representative of the MNGPs produced in our study. In this work ConA could be released both heptyl-mannose and $p(Man)_{280}$ decorated MNPs as demonstrated by the release of fluorescent material from MNPs-lectin clusters and reversion of nanoparticle clusters to discrete particles upon addition of free mannose monitored by TEM (Oz *et al.*, 2019). However, a more than 20-fold excess of free mannose was added to achieve this release. A similar effect may be observed with the materials analysed herein with if a similar excess of mannose was applied. Substitution of free mannose with a higher affinity competitive ligand, such as heptyl-mannose, in this assay may help to determine if ConA binding is reversible in the case of the reported MGNPs. Additionally, direct observation of MGNP clusters by TEM could also provide further insight to lectin release by MGNPs.

Importantly neither of these studies investigated the iron oxide/glycomaterial compostion of their respective MGNPs. It may be that the high mass proportion of polyvalent glycomaterial present in SPION@Dopa-p(ManAA)$_{200}$ particles may contribute to the irreversibility of this binding due to high density of binding epitopes and the ability to form many interparticle lectin-ligand interactions leading to clustering which is not readily reversed.

Irreversible lectin binding by SPION@Dopa-p(ManAA)$_{200}$ may impede the ability of this material to capture, and then release, fimbriated bacteria. As a result the choice of MGNPs utilised for bacterial separation will have to be led by both efficiency and application. Where simply removal of bacteria from a mixed population is required SPION@Dopa-p(ManAA)$_{200}$ may be the most efficient tool. However, if capture and release into a different environment or analytical device is required SPION@Dopa-p(ManAA)$_{50}$ or indeed materials with shorter chain length glycopolymers with lower lectin avidities may be preferential.

3.4. Conclusions

In this Chapter the viability of a synthesis strategy for producing catechol-terminal glycopolymers via RAFT polymerisation, and subsequent grafting 'to' SPIONs synthesised via the thermal decomposition method was demonstrated. To the best of our knowledge, this is the first strategy for highly efficient coating of SPIONs produced by the thermal decomposition with highly hydrophilic materials such as glycopolymers.

Acrylamide monomers of mannose, the sugar bound by FimH, and a non-binding sugar analogue, galactose, were synthesised in a similar strategy to that described by Cameron & co-workers, with precise stereocontrol around the anomeric carbon. (Cameron *et al.*, 2008).

For the synthesis of catechol-terminal glycopolymers a RAFT polymerisation strategy, mediated by a catechol-terminal CTA, was devised. To this end a synthetic scheme was devised to produce the desired CTA by amide coupling of dopamine to the carboxylic acid terminal CTA **(5)** produced via the method reported by Ferguson & co-workers (Ferguson *et al.*, 2005). Direct amide coupling of dopamine to PABTC proved ineffective despite the trialling of several difference coupling agents and conditions. To circumvent this issue an addition step in the synthetic pathway was incorporated – replacement of the carboxylic acid terminus of PABTC with a good leaving group, N-hydroxysuccinimide, similar to the strategies reported by Larnaudie & co-workers and Oyeneye & co-workers (Larnaudie *et al.*, 2016; Oyeneye *et al.*, 2015). Nucleophillic attack by

dopamine against this NHS- ester of PABTC proved efficient to produce the desired catechol-terminal trithiocarbonate CTA (Dopa-PABTC).

RAFT polymerisation of sugar acrylamide monomers, and the non-sugar control monomer HEAA, mediated by Dopa-PABTC yielded polymers with narrow molecular weight distributions ($Đ$ = 1.15-1.25) (Table 3.1.) and the chromatograms displayed narrow, symmetrical, unimodal molar mass distributions. Generally good agreement was seen between theoretical molecular weights ($M_{n,th}$) and those derived from SEC. Some deviation in molecular weight from theoretical was observed but this is likely due to difference in hydrodynamic volume between the PEG standards and synthesised glycopolymers. All Dopa-PABTC mediated polymerisations yielded materials which displayed characteristic catecholic proton shifts by ^{1}HNMR, suggesting maintenance of dopamine termini on these materials which was essential for SPION decoration using our devised strategy.

An investigation into polymerisation kinetics of acrylamides by PABTC and Dopa-PABTC revealed an induction period, under the tested conditions, for Dopa-PABTC. Following this induction period, a linear dependence of $\ln([M]_0 / [M]_t)$ with time demonstrated the rate of the polymerization to be pseudo-first order with respect to monomer conversion, an essential feature of a well-controlled radical polymerisation.

The lectin binding characteristics of the catechol-terminal glycopolymers produced via RAFT were also analysed. By turbidimetric analysis with ConA, glycopolymer binding rates could be estimated for mannosylated glycopolymers while, as expected, galactosylated materials could not bind

to ConA (Fig 3.12.). This finding is consistent with previous reports (Liu *et al.*, 2019; Xie *et al.*, 2017).

Epitope binding by mannose specific lectins has previously been shown to be dependent upon glycopolymers chain length and epitope density (Cairo *et al.*, 2002; Gou *et al.*, 2013; Lin & Kasko, 2015; Papp *et al.*, 2011; Xie *et al.*, 2017; Yilmaz *et al.*, 2016). A correlation between glycopolymer length and lectin affinity is consistent with the increase in mannose avidity with increasing chain length observed in SPR studies (fig. 3.8.). Gou & co-workers suggest that there is little increase in lectin avidity for mannose glycopolymers above ~50 pendant sugars (Gou *et al.*, 2013). Such diminishing returns in avidity increase were not observed for the materials described herein. A greater than tenfold increase in avidity for DC-SIGN and fivefold for MBL between DP50 and DP200 materials was observed ($K_{d,\ DC\text{-}SIGN}$ 0.709 to 0.051 nM; $K_{d,\ MBL}$ 0.941 to 0.207 nM). As the DP50 and DP200 material showed the highest avidity for mannose binding lectins, these two materials were chosen to take forward as coatings for nanoparticles for use in trial bacterial separation studies in Chapter 4.

Furthermore, clustering of sugar ligands in high densities onto the surface of nanoparticles has been shown to increase lectin binding avidities compared to the free ligands (Boden *et al.*, 2017; Lin *et al.*, 2003; Selvaprakash & Chen, 2018). As such the binding avidity of the produced MGNPs to FimH may be greater than indicated by SPR of the free glycopolymers. Indeed, interaction of ConA with the MGNPs as determined by UV-vis turbidity demonstrated fast aggregation which could not be fully

reversed by the addition of free mannose (Fig 3.20). However, further characterisation of lectin-MGNP interaction dynamics could be performed using SPR or isothermal calorimetry or the use of a higher avidity competitive ligand.

Decoration of thermal decomposition derived SPIONs with dopamine-containing glycopolymers was demonstrated to be successful by FTIR and TGA. Functionalisation of SPIONs with glycopolymers was very efficient with greater than 82% total organic content weight percentage for all glyconanoparticles (Fig. 3.17.). This is akin to coating efficiencies reported for 'grafting from' strategies.

Additionally, TEM showed that nanoparticle iron oxide core size was not affected by the presence of polymeric coating (fig. 3.18.). All coated materials displayed monodisperse nanoparticle cores with a consistent, spherical morphology and an absence of aggregation. Regretfully, the polymeric shell could not be visualised consistently using the techniques in this report. Further investigation may be of interest to confirm the presence of polymer shell for sake of completeness of this work. However presence of the polymer shell can be suitably inferred by biological interactions and TGA/FTIR analysis.

Finally, lectin capture was shown to be partly reversible in the case of SPION@Dopa-p(ManAA)$_{50}$ but not SPION@Dopa-p(ManAA)$_{200}$ under the experimental conditions described . This is likely to have implications in the ability of these two materials to selectively isolate, and then release, lectin expressing bacteria.

4. Specific Cellular Isolation of Bacteria from Mixed Populations Mediated by Magnetic Glyconanoparticles (MGNPs)

4.1. Introduction and Chapter Aims

As demonstrated in Chapter 1 magnetic glyconanoparticles (MGNPs) appear to be a potent strategy for the capture and depletion of specific bacteria from aqueous suspension (Chen *et al.*, 2016b; El-Boubbou *et al.*, 2007; Malakootikhah *et al.*, 2017; Miao *et al.*, 2019; Pera *et al.*, 2010).

Crucially though, no reports currently exist which analyse the ability of MGNPs to selectively capture and isolate specific bacteria from mixed populations; a significant limitation which must be addressed prior to advancement of these technologies to specific application.

To this end, this Chapter aims to utilise the MGNPs functionalised with different glycopolymer coatings produced in Chapter 3 for the magnetic separation of chromosomally tagged *E. coli* strains as produced and described in Chapter 2 from a mixed population. Equiproportional mixtures of *E. coli* strains chromosomally tagged with red and green fluorescent proteins will be prepared and treated with MGNPs under a magnetic field to deplete Type 1 fimbriated strains from the mixture culture (Fig. 4.1). The efficacy of selective separation shall be analysed by flow cytometry to monitor the mixed populations before and after extraction. Additionally, the adoption of an afimbriated strain as the non-extractable target shall compared to wildtype *E. coli*.

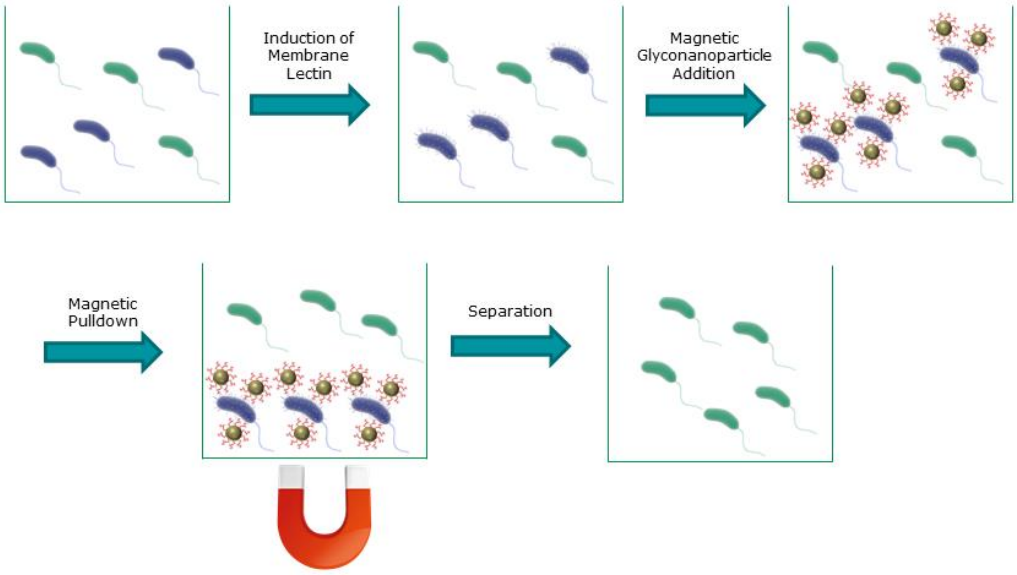

Figure 4.1. Schematic representation of selective separation of bacteria from a mixed population. A mixture of two bacterial strains from which isolation is desired is established. One of these strains is genetically modified such that expression of a surface associated lectin can be controlled by the addition of an inducer compound (blue), while the other strain is lectin deficient (green). Magnetic glyconanoparticles bearing carbohydrate ligands which have an affinity for the surface associated lectin is then added. Magnetic extraction of the glycomaterial:bacteria aggregate facilitates selective separation and isolation of fimbriated cells from their afimbriate neighbours.

4.2. Materials and Methods

4.2.1. Bacterial strains and growth conditions

All bacterial strains used in magnetic pulldown assays were grown in $LBCm_{25}$ media overnight prior to pulldown as described in Section 2.2.1.1. eGFP chromosomally tagged JEP01 and mRuby tagged wildtype or afimbriate strains (MG1655/JW4283 parental) were used as the fishable and non-fishable strains respectively in the magnetic pulldown assay. The utilised strains are described in section 2.2.1.4.

4.2.2. Magnetic isolation of bacteria from mixed populations by MGNPs.

A total of 5 ml cultures of each JEP01::p24eGFP and non-fishable controls (JW4283::p24mRuby/MG1655::p24mRuby) were grown in LB media overnight supplemented with chloramphenicol (25 μg/ml). The following morning the OD_{600} of these cultures was measured and used to inoculate 5 ml of fresh LB for individual cultures and the two mixed cultures, with OD_{600} normalised to 0.05. These day cultures were then incubated at 37 °C for 2 hours, prior to the addition of ATc (50ng/ml), where appropriate, and further incubation for another 3 hours to induce expression of the fimbriae in one of the mixed cultures. After 5 hours of growth, 100 μL of each culture (JEP01::p24eGFP alone, JW::p24mRuby alone, mixed culture with ATc, mixed culture without ATc) were transferred into 1.5 mL Eppendorf tube. The cell pellet was collected by centrifugation and washed twice with sterile PBS. The cell pellet was then resuspended in 200 μL of nanoparticle solution for each coated nanoparticle sample (SPION@Dopa-$(HEAA)_{50}$,

SPION@Dopa-(GalAA)$_{50}$, SPION@Dopa-(ManAA)$_{50}$, SPION@Dopa-(Man200)$_{50}$; all at 5 mg/ml in sterile PBS) and left on a magnetic extraction rack overnight at 4 °C. The following morning, the supernatant and pellet were recovered for each sample. Cells from both pellet and supernatant were then collected by centrifugation, washed twice with sterile PBS and resuspended in 500 µL sterile PBS. The relative proportion of each strain was then analysed by flow cytometry.

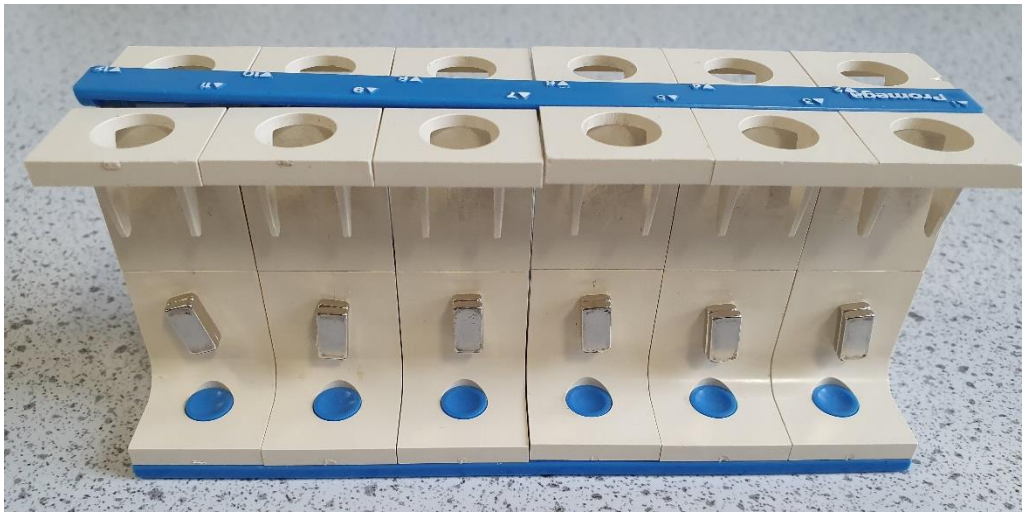

Figure 4.2. Magnetic extraction rack using in magnetic isolation experiments. Each slot can accommodate a 1.5 ml centrifuge tube and was installed with Nickel plated N42 grade neodymium 10mm x 5mm x 2mm magnets (eMagnets).

4.2.3. Magnetic isolation of Bbcteria from mixed populations by MGNPs using Miltenyi Biotec MACS MS column kit

A total of 5 ml cultures of JEP01::p24eGFP and non-fishable control (JW4283::p24mRuby) were grown in LB media overnight supplemented with chloramphenicol (25 µg/ml). The following morning the OD_{600} of these cultures was measured and used to inoculate 5 ml of fresh LB for individual cultures and the mixed cultures, with OD_{600} normalised to 0.05. These day

cultures were then incubated at 37 °C for 2 hours, prior to the addition of ATc (50ng/ml), where appropriate, and further incubation for another 3 hours to induce expression of the fimbriae in one of the mixed cultures. After 5 hours of growth 100 µL of each culture (JEP01::p24eGFP alone, JW::p24mRuby alone, mixed culture with ATc, mixed culture without ATc) was transferred into 1.5 mL Eppendorf tube. The cell pellet was collected by centrifugation and washed twice with sterile PBS. The cell pellet was then resuspended in 200 µL of nanoparticle solution for each coated nanoparticle sample (SPION@Dopa-$(HEAA)_{50}$, SPION@Dopa-$(GalAA)_{50}$, SPION@Dopa-$(ManAA)_{50}$, SPION@Dopa-$(Man200)_{50}$; all at 5 mg/ml in sterile PBS). PBS was added to 1 mL. Miltenyi MS columns were fitted to an OCTOMacs Separator (Miltenyi Biotec) and each nanoparticle/cell solution was passed through a column and the supernatant collected. This first supernatant was the unbound cell sample. Each column was then removed from the magnetic apparatus and 1 mL of sterile PBS passed through the column and collected. This second supernatant was the bound cell sample. The collected cell fractions were stored at 4 °C overnight. The following morning, the cell pellet for each sample was collected by centrifugation, washed twice with sterile PBS and then resuspended in 500 µL sterile PBS. The relative proportion of each strain was then analysed by flow cytometry.

4.2.4. Flow cytometry

Flow cytometric analysis of bacterial populations recovered from the magnetic isolation procedure were then analysed using a Beckman Coulter Astrios EQ cell sorter. Forward and side scatter data was recorded with both 405 and 488 nm laser lines. eGFP fluorescence output was recorded using a 488 nm laser line, a 513/26 nm bandpass emission filter and emission bandwidth of 500-526 nm. mRuby fluorescence output was recorded using a 561 nm laser line, a 614/20 nm bandpass emission filter and emission bandwidth of 604-624 nm. A primary cell gate was constructed using the side scatter and forward scatter data for a clonal, fluorescent protein-tagged cell population. At least 100,000 events within the primary cell gate were recorded for each sample. Composition of each recovered fraction was analysed by plotting density histograms for each fluorophore to give relative percentage of red and green fluorescent protein labelled cells.

4.2.5. Microscopic analysis

Confirmation of bacterial population depletion by magnetic isolation with MGNPs was performed using a Zeiss Elyra Super Resolution Confocal Microscope. Samples of the starting mixtures of red and green tagged cells as well as those after extraction by MGNPs were washed in PBS and then resuspended in 20 µl FluoroGel Mounting Media (GeneTex). A 10 µL aliquot of each sample was dispensed onto a high performance coverglass (D = 0.17mm, RI = 1.5255)(Zeiss). The cover glasses containing the stained cells in mounting medium were then mounted onto a Super Premium Microscopy slide (VWR) by inversion. The slides were left to cure overnight and imaged via confocal microscopy the following day using the 63 X oil immersion lens. Fields of view were established that contained 20-50 individual bacteria. Total numbers of green and red cells were counted for each condition and analysed in Prism (Graphpad).

4.2.6. Release of sequestered bacteria from MGNPs by addition of excess sugar

To assess the ability of the MGNPs used for magnetic isolation as described in 4.2.2. to release bacteria upon the addition of free sugar a release assay was performed. The cell/MGNP pellet collected as described in 4.2.2. was collected in a 1.5 ml Eppendorf tube for the each MGNP species in the presence of the autoinducer. To each pellet 750 µl of a sterile, saturated mannose solution in PBS was added. The pellet was vortexed briefly and allowed to sit at room temperature for 5 min before being analysed by flow cytometry as described in Section 4.2.3. The relative percentage of red and green fluorescent protein labelled cells was compared for the initial starting mixture to the relative percentage of each pellet sample with the addition of free sugar.

4.3. Results and Discussion

4.3.1. Extraction of ATc-inducible Type 1 fimbriae mutant from wildtype *E. coli* using magnetic glyconanoparticles

Initial magnetic separation trials were performed using an equal mixture of the ATc-inducible Type 1 Fimbriae chromosomally tagged with eGFP (JEP01::p24eGFP) and wildtype *E. coli* tagged with mRuby (MG1655::p24mRuby) as described in Chapter 2. Population proportions were determined by monitoring the percentage of each label before and after magnetic isolation with MGNPs coated with a non-sugar control polymer (Dopa-$(HEAA)_{50}$), a binding sugar polymer of multiple chain lengths (Dopa-$(ManAA)_{50}$) and Dopa-$(ManAA)_{200}$) and a non-binding control sugar polymer (Dopa-$(GalAA)_{50}$).

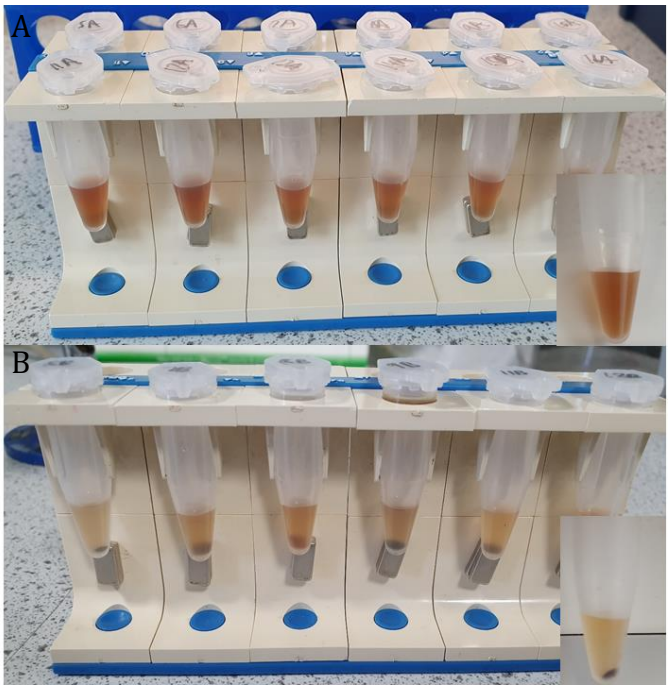

Figure 4.3. Setup of magnetic extraction experiments using magnetic extraction rack. A) Initial mixtures of MGNPs and mixed bacterial populations. Inset, singular sample. B) MGNP/bacteria solution after incubation on magnetic rack overnight. Inset, singular sample. Overnight incubation leads to the formation of MGNP/bacteria pellet and depletion of bacteria from supernatant depending on MGNP composition and fimbriation state of population.

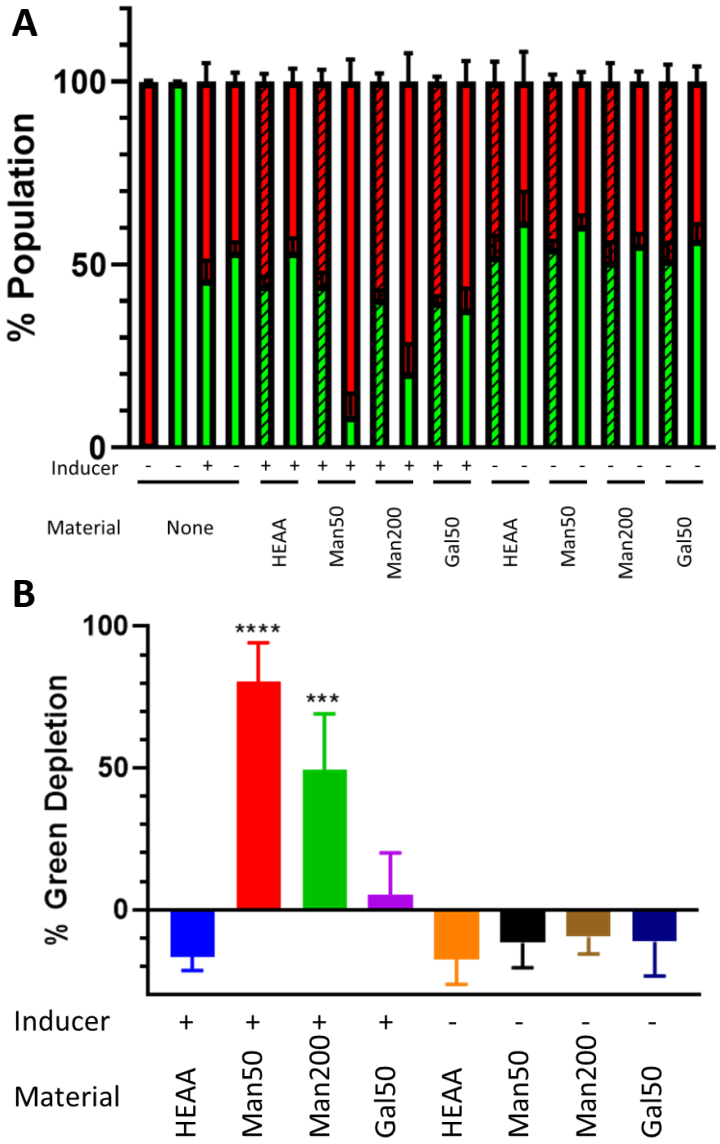

Figure 4.4. Magnetic Extraction of JEP01::p24eGFP from equal JEP01::p24eGFP/MG1655::p24mRuby mixture using magnetic glyconanoparticles in presence and absence of inducer. A) Flow cytometric analysis of mixed populations before (dashed bars) and after (smooth bars) extraction with magnetic glyconanoparticles. Green bars indicate eGFP labelled cell population percentage, red bars indicate mRuby labelled cell population percentage. B) % depletion of eGFP labelled ATc-inducible Type 1 fimbriae mutant from mixed culture by magnetic glyconanoparticles. Data shown as mean of three independent experiments with standard deviation. **** $p<0.0001$; *** $p=0.001$ compared to non-sugar material control in one way ANOVA with Tukey's multiple comparisons test. Material field indicates composition of magnetic glyconanoparticle polymeric coating.

As demonstrated in Fig 4.4.A. isolation of the ATc-inducible fimbriated strain (JEP01) after incubation with MGNPS under a magnetic field was primarily achieved in the presence of the inducer and with mannosylated MGNPs as demonstrated by a decrease in green labelled cells under these conditions. Depletion of fimbriate bacteria from these populations by mannosylated nanoparticles suggests that selective isolation is mediated by cell surface presentation of the Type 1 Fimbriae, which is mannose specific. SPION@Dopa-p(HEAA)$_{50}$ particles were unable to deplete labelled JEP01 under any conditions, confirming the interaction is glycan dependent. Some depletion of the labelled JEP01 target from the population was also observed in the case of galactosylated materials however this effect was both small (5% on average) and highly variable. Consequently, capture of fimbriated bacteria by galactosylated nanoparticles was statistically insignificant compared to the non-glycan decorated control, SPION@Dopa-p(HEAA)$_{50}$. However, a lack of a statistically distinguishable difference between target cell depletion by Dopa-p(HEAA)$_{50}$ and Dopa-p(GalAA)$_{50}$ does not necessarily preclude cell capture by galactosylated materials, which could impact the selectivity of this system.

Increasing mannose polymer chain length does not appear to correlate with improved isolation of the Type 1 fimbriated *E. coli*. MGNPs coated with Dopa-(ManAA)$_{50}$ were able to deplete 80.5% of the green labelled strain from the starting mixture, whereas MGNPs coated with the DP$_{200}$ mannosylated polymers were only able to deplete 49.3% of the green labelled (Fig 4.4.B). This result is somewhat surprising considering the

increased binding affinity of longer mannosylated polymers for mannose specific lectins reported in Section 3.2.3.3. of this report and other studies (Cairo *et al.*, 2002; Gou *et al.*, 2013; Lin & Kasko, 2015; Papp *et al.*, 2011; Xie *et al.*, 2017; Yilmaz *et al.*, 2016). However, the observed difference in fimbriated *E. coli* depletion by the two mannosylated materials could be attributable to the increased proportion by weight of the magnetic iron oxide core in Dopa-$(ManAA)_{50}$ coated MGNPs compared to Dopa-$(ManAA)_{200}$ coated MGNPs, thus increasing the attractive magnetic force exerted on these nanoparticles. While the presence of coatings on SPIONs does not by itself appear to diminish superparamagnetic properties, some studies have shown a decrease in saturation magnetisation with the presence of coating materials or increasing polymer graft densities (Lachowicz *et al.*, 2017; Maver *et al.*, 2009; Mikhaylova *et al.*, 2004a; Taresco *et al.*, 2015; Wan *et al.*, 2006). Kim & co-workers suggest that coatings decrease the uniformity of SPIONs due to quenching of surface moments, thus reducing the magnetic moment of these particles (Kim *et al.*, 2003). It is possible that reduced magnetic saturation of Dopa-$(ManAA)_{200}$ coated SPIONs may have an effect on the efficiency of magnetic bacterial separation but this should be investigated further. SQUID magnetometry would offer further insight into the effect of the different polymer coating upon the magnetic properties of the produced MGNPs.

It is also possible that variance in the hydrodynamic radii of Dopa-$(ManAA)_{50}$ and Dopa-$(ManAA)_{200}$ may have some impact on the lectin interaction as this parameter could alter the spatial availability of glycan

epitopes presented by nanoparticles in solution. For linear, brush and star glycopolymers those of greater size which display multiple sugar domains tend to have a higher affinity to target lectins than smaller, less valent materials, presumably due to an increase in binding epitope density (Chen *et al.*, 2015; de la Calle *et al.*, 2019; Gestwicki *et al.*, 2002; Gou *et al.*, 2013; Shamout *et al.*, 2020; Tanaka *et al.*, 2017). This effect is remarkably pronounced when the size of polymers in solution matches the distance between binding sites on target lectins (Jono *et al.*, 2018; Nagao *et al.*, 2019). The relationship between hydrodynamic radius/volume of MGNPs and their affinity to target lectins has not been explored in existing literature. DLS based size analysis of the MGNPs described herein would be useful to relate the effect of particle morphology in solution to lectin affinity in tandem with SPR or ITC analysis.

Intriguingly, when expression of Type 1 fimbriae in JEP01::p24eGFP was not induced it appears that some of the red labelled wildtype *E. coli* (MG1655::p24mRuby) was depleted by MGNPs (Fig 4.4. A & B). Depletion of the wildtype strain could be attributed to the stochastic expression of mannose binding Type 1 fimbriae in the this background (Schwan, 2011), leading to a small, fimbriated subpopulation which can be bound by mannosylated MGNPs. However, it is also noted that this depletion effect is not significantly distinct to depletion of red labelled cells by the control materials and hence may be of little practical significance.

4.3.2. Extraction of ATc-inducible Type 1 fimbriae mutant from afimbriate *E. coli* using magnetic glyconanoparticles

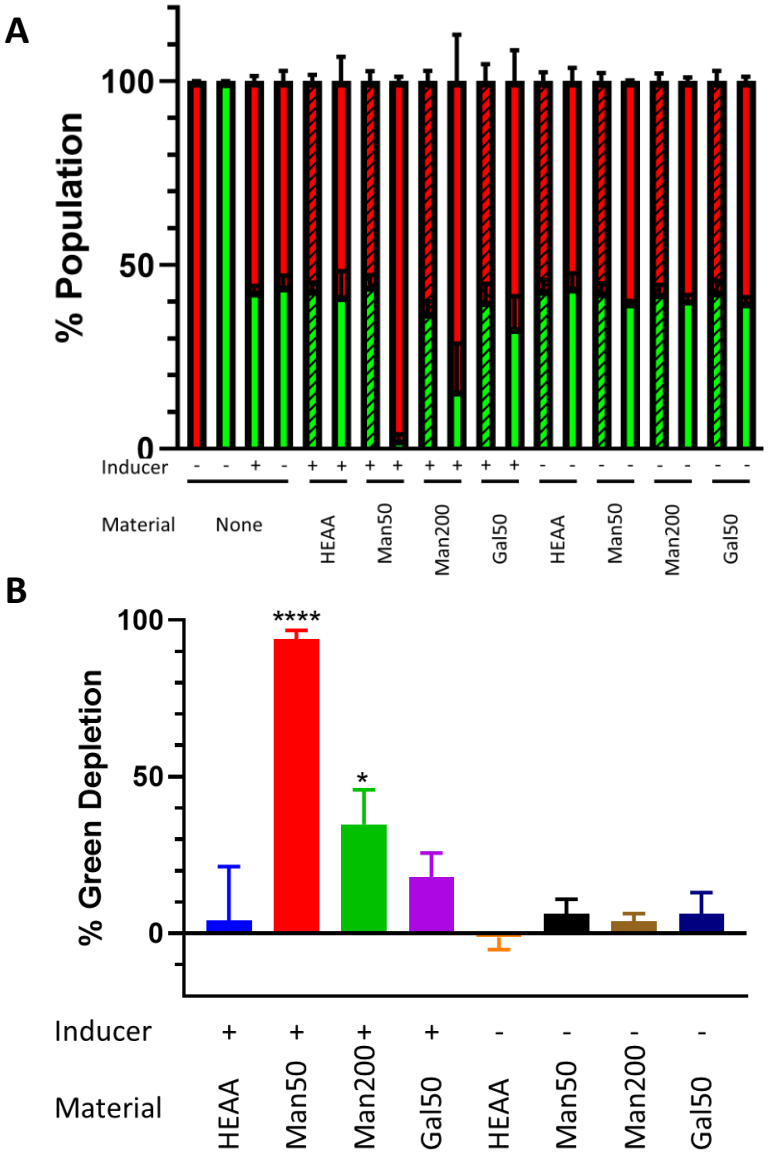

Figure 4.5. Magnetic Extraction of JEP01::p24eGFP from equal JEP01::p24eGFP / JW4283::p24mRuby mixture using magnetic glyconanoparticles in presence and absence of inducer. A) Flow cytometric analysis of mixed populations before (dashed bars) and after (smooth bars) extraction with magnetic glyconanoparticles. Green bars indicate eGFP labelled cell population percentage, red bars indicate mRuby labelled cell population percentage. B) % depletion of eGFP labelled ATc-ATc-inducible Type 1 fimbriae mutant from mixed culture by magnetic glyconanoparticles. Data shown as mean of three independent experiments with standard deviation. **** $p<0.0001$; * $p<0.05$ compared to non-sugar material control in one way ANOVA with Tukey's multiple comparisons test. Material field indicates composition of magnetic glyconanoparticle polymeric coating.

In order to attempt to improve the specificity of magnetic isolation mediated by MGNPs a further battery of magnetic isolation experiments was performed using an initial starting mixture of JEP01::p24eGFP, the eGFP tagged ATc-inducible mutant of the Type 1 fimbriae, and JW4283::p24mRuby – an mRuby2 tagged knockout mutant deficient in *fimH*, the lectin on the distal tip of the fimbriae which is responsible for mannose adhesion.

As demonstrated in Fig 4.5.A. isolation of the ATc-inducible fimbriated strain (JEP01) after incubation with MGNPs under a magnetic field was primarily achieved in the presence of the inducer and with mannosylated MGNPs as demonstrated by a decrease in green labelled cells, similar to the effect seen for the JEP01/MG1655 extraction experiments (Fig. 4.5.A). MGNPs coated with Dopa-$(ManAA)_{50}$ polymers were able to deplete 94 % of the green labelled strain from the starting mixture, whereas MGNPs coated with the Dopa-$(ManAA)_{200}$ were only able to deplete 34.8 % of the green labelled (Fig 4.5.B). These improved capture dynamics suggests a greater specificity of the mannosylated MGNPs to fimbriated cells when the counterpart strain does not harbour the genetic apparatus for expression of a lectin with competing specificity to the binding-sugar coated nanoparticles. However a 17.9% depletion of green labelled cells was observed upon the induction of Type 1 fimbriation during incubation with Dopa-$(GalAA)_{50}$. While not statistically distinguishable from Dopa-$(HEAA)_{50}$ led depletion or from all materials in the absence of the inducer, this finding may suggest that galactosylated materials could also be capable

of fimbriated cell depletion. Fimbriated cell depletion by galactose decorated nanoparticles raises additional questions about the specificity of tunable lectin expression in tandem with magnetic nanoparticles as a specific depletion mechanism.

Again, higher depletion efficiency is demonstrated by the mannosylated MGNPs with the shorter chain length mannose polymer coating. As previously discussed, this may be attributable to the lesser weight proportion of the iron oxide nanoparticle core as corroborated by TGA data (Fig. 3.17). However, the possible impact of differing hydrodynamic radii between Dopa-$(ManAA)_{50}$ and Dopa-$(ManAA)_{200}$ was not analysed and could be a contributory factor as discussed above.

Additionally, in the absence of the inducer, no depletion of the afimbriate strain from the starting heterogeneous population is observed by mannosylated glyconanoparticles (Fig. 4.5.B.). Lack of depletion in the absence of the inducer further supports the conclusion that the specificity of the magnetic isolation of fimbriated bacteria from a mixed population is improved when the counterpart strain is afimbriated.

To confirm the findings of these two series of experiments, analysis was also performed by LSCM. An aliquot of the starting mixture of both JEP01/MG1655 and JEP01/JW4283 experiments and after extraction with each polymer coated nanoparticle in the presence of the inducer was mounted onto glass slide and imaged according to Section 4.2.5. The proportion of red and green cells for each tested condition is shown in Figure 4.6.

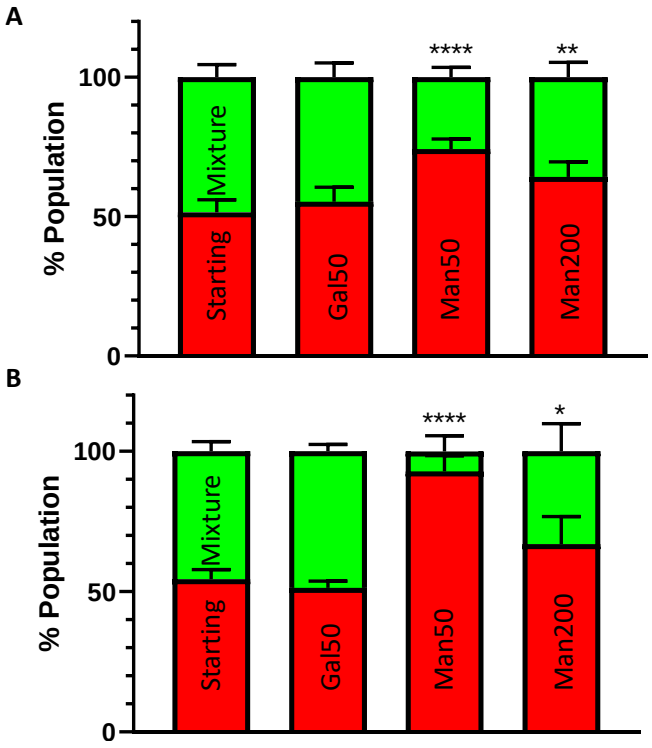

Figure 4.6. Analysis of bacterial populations after magnetic separation with MGNPs in presence of inducer as analysed by confocal microscopy. A) Extraction of JEP01::p24eGFP from MG1655::p24mRuby. B) Extraction of JEP01::p24eGFP from JW4283::p24mRuby. Data shown as mean population of each fluorophore per field of view with standard deviation (n≥5). Bars labelled with polymeric material component of MGNPs. Difference from starting mixture analysed by 2-way ANOVA using Dunnett's Multiple Comparison Test. **** = $p<0.0001$, ** = $p<0.01$, * $p<0.05$.

As shown in Fig 4.6.A & B there is no statistically significant difference in population composition of JEP01/wildtype or JEP01/afimbriate *E. coli* mixtures after magnetic extraction with galactosylated MGNPs.

In the case of a mixture of ATc-inducible fimbriae mutant and wildtype *E. coli*, magnetic extraction with Dopa-$(ManAA)_{50}$ coated MGNPs led to a decrease in in green labelled strain population proportion from 45.4% to 25.8%, constituting a 43.4% depletion. For the Dopa-$(ManAA)_{200}$ coated

MGNPs reduction of JEP01::p24eGFP from 45.4% to 35.7% is observed, constituting a 21.3% depletion (Fig 4.6.A.).

In contrast, for the mixture of the ATc-inducible fimbriae and afimbriate *E. coli* mutants, magnetic extraction with Dopa-$(ManAA)_{50}$ coated MGNPs a decrease in green labelled strain population proportion from 45.6% to 7.2% is observed, constituting an 84.3% depletion. For Dopa-$(ManAA)_{200}$ coated MGNPs a reduction of JEP01::p24eGFP from 45.6% to 33.1% is observed, constituting a 27.4% depletion (Fig 4.6.B.).

These results correlate with the findings presented in the flow cytometry experiments shown in Sections 4.3.1&2, confirming their validity. These data suggest mannosylated polymer coated MGNPs are sufficient for the selective isolation of fimbriated *E. coli*, with the Dopa-$(ManAA)_{50}$ coated MGNPs more efficient than the Dopa-$(ManAA)_{200}$ coated nanoparticles for both mixed populations. Similarly, extraction efficiency is improved by using an afimbriate counterpart to the JEP01 target strain, adding further credence to this finding.

Importantly the data presented in Fig. 4.6 also shows that the non-sugar and non-binding sugar control (HEAA/GalAA) coated MGNPs are unable to deplete fimbriated *E. coli* from wildtype or afimbriate strains. While an absence of depletion mediated by SPION@Dopa$(HEAA)_{50}$ is consistent with the findings presented in Figs. 4.4-5, a mild but statistically insignificant fimbriated cell depletion effect by galactosylated MNGPs was observed in the flow cytometry experiments but is absent from these imaging experiments. While this finding could suggest that fimbriated cell depletion

by galactosylated nanoparticles is an artefact of flow cytometric analysis, flow cytometry is far more statistically powerful than imaging workflows. As such, additional investigation would be necessary to ascertain the ability of galactosylated nanoparticles to capture fimbriated cells.

4.3.3. Extraction of ATc-inducible Type 1 fimbriae mutant from an afimbriate mutant by MGNPs using a commercially available system

Since commercial magnetic cell sorting platforms are widely available, typically using antibody coupled magnetic nanoparticles, an attempt to compare the efficiency of one of these platforms to the MGNP system for fimbriated cell isolation described in this report was attempted. The column based magnetically assisted cell sorting (MACS) platform developed and available commercially from Miltenyi Biotec was utilised using the MGNPs produced in this study as described in Section 4.2.3. Results of this experiment are shown in Fig 4.7. below.

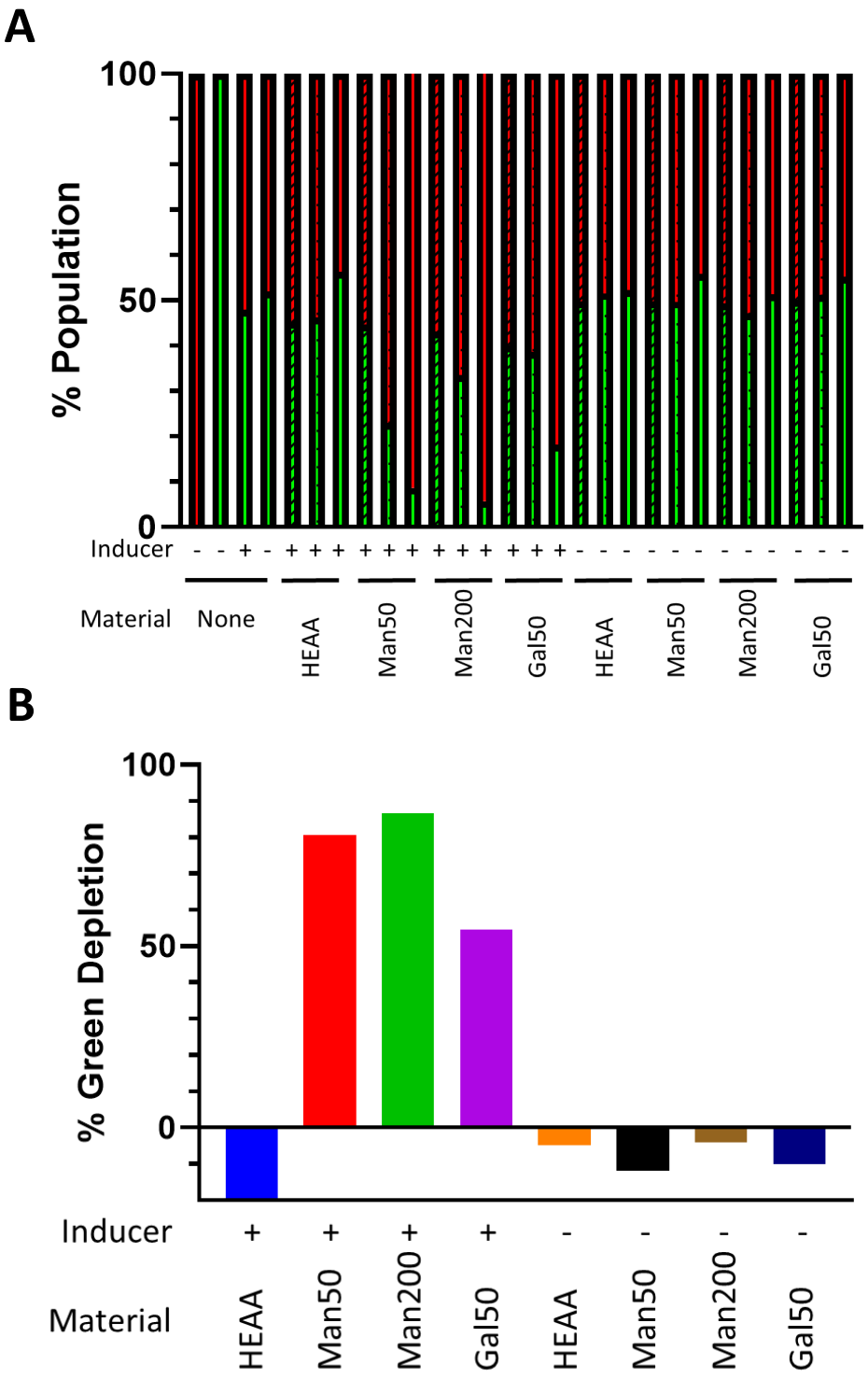

Figure 4.7. Magnetic Extraction of JEP01::p24eGFP from equal JEP01::p24eGFP / JW4283::p24mRuby mixture by magnetic glyconanoparticles in presence and absence of inducer using Miltenyi MS Columns. A) Flow cytometric analysis of mixed populations at start (dashed bars), cells released from the column under magnetic field (dotted bars) and cells released from column when the magnetic field was removed (smooth bars). Green bars indicate eGFP labelled cell population percentage, red bars indicate mRuby labelled cell population percentage. B) % depletion of eGFP labelled ATc-inducible Type 1 fimbriae mutant from mixed culture by magnetic glyconanoparticles using Miltenyi MS columns.

Separation of the green labelled fimbriated mutant from the afimbriated mutant is seen with all MGNPs, (Fig 4.7.). 80.7%, 86.77% and 54.7% depletion of the green labelled strain is seen with Dopa-$(ManAA)_{50}$, Dopa-$(ManAA)_{200}$ and Dopa-$(GalAA)_{50}$ coated MGNPs respectively is achieved using the MS column MACS system (Fig 4.7.B.). These results suggest that using MGNPs with this commercially available cell separation system exacerbates fimbriated cell depletion by galactosylated nanoparticles which could impede the ability to selectively isolate fimbriated cells with this system. Since the Miltenyi MS column system uses a ferromagnetic matrix in the columns which enhances the magnetic field, the weak interaction of the galactosylated materials with mannose binding lectins as demonstrated by SPR (Table 3.3. & 4.; Fig. 3.13) may be sufficiently supplemented by increased interparticle magnetic attraction such that glycomaterial/fimbriated bacteria aggregates can form and become entrapped within the column matrix. However, due to time constraints and exhaustion of MGNPs this panel of experiments could not be repeated, reducing the robustness of associated findings. Despite this, these preliminary findings may suggest the suitability of existing commercial magnetic extraction systems to adaption for use with the magnetic glyconanoparticles and lectin expression modified *E. coli* strains described in this report, with supplementary investigation and optimisation.

4.3.4. Release of sequestered bacteria from MGNPs by addition of excess sugar

For some applications release of bacterial cells sequestered by MGNPs may be required. To this end the ability of mannosylated MGNPs to release captured fimbriated *E. coli* in both JEP01 and MG1655/JW4283 mixtures by the addition of free sugar was tested as described in Section 4.2.6. A summary of these results in shown in Figure 4.8. below.

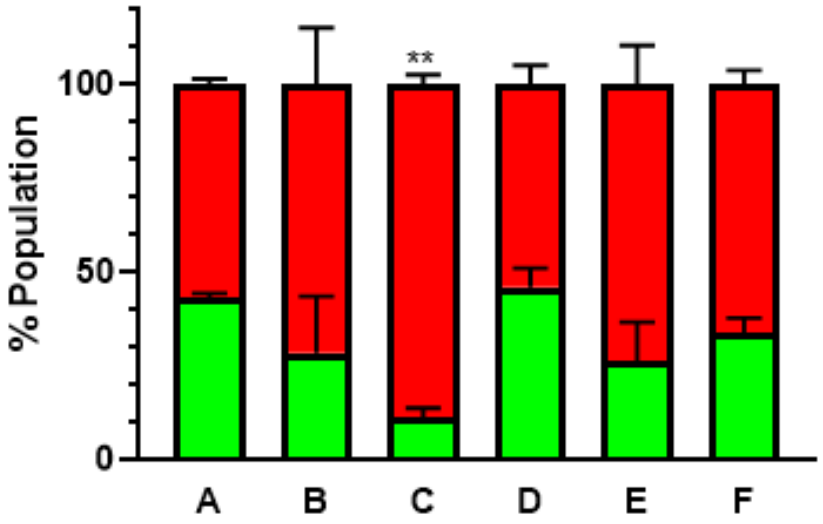

Figure 4.8. Release of sequestered cells from pellet after magnetic separation using MGNPs. A) JEP01::p24eGFP/JW4283::p24mRuby starting mixture; B) A + SPION@ManAA$_{50}$ pellet with excess mannose; C) A + SPION@ManAA$_{200}$ pellet with excess mannose; D) JEP01::p24eGFP/MG1655::p24mRuby starting mixture; E) D + SPION@ManAA$_{50}$ pellet with excess mannose; F) D + SPION@ManAA$_{200}$ pellet with excess mannose. Green bars indicate eGFP labelled cell population percentage, red bars indicate mRuby labelled cell population percentage. Data shown as mean of three independent experiments with standard deviation ** = $p<0.01$ compared to starting mixture as determined by 2way ANOVA with Tukey's multiple comparisons test.

The bacterial composition of the supernatant after addition of free mannose was only significantly different from the starting mixture in the case of the JEP01/JW4283 mixture with Dopa-poly(ManAA)$_{200}$ coated MGNPs suggesting captured bacterial cells could be released from the Dopa-poly(ManAA)$_{50}$ coated MGNPs but not their Dopa-poly(ManAA)$_{200}$ coated counterpart. Limited release of fimbriated cells is consistent with the lectin binding characteristics of polymer decorated MGNPs as determined by ConA aggregation (Fig. 3.21). Agglomeration of Dopa-(ManAA)$_{50}$ functionalised MGNPs by ConA could be partially reversed by the addition of an excess of sugar ligand but agglomeration of DP$_{200}$ mannosylated MGNPs could not. The higher affinity of mannose binding lectins for the Dopa-(ManAA)$_{200}$ compared to the Dopa-(ManAA)$_{50}$ material as determined by SPR also supports this finding (Tables 3.3 & 3.4; Fig. 3.13). This suggests that the multivalent binding of Dopa-(ManAA)$_{200}$ MGNPs to the multiple FimH epitopes available on induced JEP01 bacterial surfaces may be too strong to be inhibited by an excess of free sugar, perhaps due to the density of mannose epitopes on this material. In contrast, Dopa-(ManAA)$_{50}$ coated nanoparticles demonstrate a lower polymer weight proportion by mass which may equate to lower mannose epitope density allowing better inhibition of FimH binding by free sugar addition.

Indeed it may be expected that only eGFP tagged cells would be recovered upon dissociation of MGNP/bacteria pellet from JEP01::p24eGFP/JW4283::p24mRuby upon addition of free mannose as the red tagged cells do not express the necessary Type 1 fimbriae for

attachment to mannosylated materials. However, this hypothesis is incompatible with the findings described above (Fig 4.8.).In all cases a greater release of red labelled cells, which should be afimbriate, from the MGNP/bacteria clusters was observed. Release of supposedly afimbriate bacteria from agglomerates could indicate non-specific bacterial capture or release by these nanoparticles. It is postulated that the red-tagged cells may either become entrapped within aggregates formed by the multivalent interactions of mannosylated MGNPs with JEP01 associated fimbriae, or as residual cells from the incomplete removal of supernatant following pellet formation. The supernatant could not be completely depleted from the pellet by pipetting without disruption of the pellet and constitutes a key limitation of this method. However, no evidence was generated to show that red labelled, non-target bacteria were not a major component of MGNPs/bacterial clusters.

While no statistically significant difference was observed between the JEP01/MG1655 starting mixture and cell populations removed from MGNP pellets by the addition of free mannose this result may be difficult to interpret due to confounding entrapment of red-labelled cells which are stochastically fimbriated, thus skewing the recovered population composition. Once again this could also be related to incomplete depletion of the supernatant prior to conducting this experiment and should be investigated further.

Development of alternative methods to analyse the composition of bacteria entrapped within the MGNP pellet after extraction may prove useful to

interrogate bacterial interactions with the described MGNPs further. Microscopic imaging and quantitative analysis by comparison of relative fluorophore prevalent within MGNPs/bacterial clusters could provide further insight into bacterial capture by the MGNPs described herein. Similar experiments were performed in Section 2.3.3. to demonstrate capture of the inducible *fim* mutant by fluorescent glycopolymers, however, due to time constraints, could not performed for these glyconanoparticles. Disruption of the individual clusters by competitive ligand addition and analysis of the released bacteria by microscopic analysis could prove vital in understanding the reversibility of bacterial capture by these MNGPs.

Furthermore simple optical density monitoring or colony-forming unit counts of the bacterial populations before and after incubation with MGNPs, and following aggregate disruption by competitive ligand addition, could provide additional insight into capture and release efficiency.

4.4 Conclusions

The results in this chapter suggest the viability of a mannose glycopolymer coated magnetic nanoparticle system for the depletion of Type 1 fimbriated bacteria from a mixed population. Extraction of *E. coli* from a mixed population using magnetic glyconanoparticles is dependent on the expression of the mannose specific Type 1 fimbriae, which could be controlled in a regulatory mutant of the Type 1 fimbriae. Fimbriated bacteria could be depleted from wildtype *E. coli* (maximal 80.5% depletion under conditions tested) or from an afimbriated counterpart (maximal 94% depletion under conditions tested) suggesting that this system may be most appropriate for the depletion of a fimbriate strain from another which does not have the genetic apparatus to express a surface associated lectin with competing sugar preferences.

However the selectivity of this system still requires additional investigation as some, limited capture of fimbriated *E coli* was consistently observed by galactosylated nanoparticles. Utilisation of an existing, commercial column based system for cellular isolation after magnetic nanoparticle labelling exacerbated fimbriated bacteria depletion by galactosylated nanoparticles. Due to time constraints, this experiment could not be repeated,, but greater understanding of galactose mediated cellular capture would be required before this system could be adapted for specific application.

It was also noted that depletion was more efficient for Dopa-$(ManAA)_{50}$ coated nanoparticles compared to Dopa-$(ManAA)_{200}$ counterparts. Improved bacterial depletion by nanoparticles decorated with shorter

chain glycomaterials is puzzling due to the higher affinity of the higher molecular weight material for mannose specific lectins (Tables 3.3 & 3.4; Fig. 3.13). However, this may be due to the higher magnetic nanoparticle content of the MGNPs coated with the lower molecular weight glycopolymer (Fig. 3.17), resulting in greater attraction to the magnets and improved isolation dynamics. The morphology of these materials in solution and subsequent changes in the presentation of lectin binding epitopes could also be a factor, but was not examined in the current report due to a lack of time.

Release of extracted bacteria from the magnetic pellet by the addition of an excess of a competitive ligand could not be adequately demonstrated.Restoration of population composition to pre-extraction levels, was not observed for either mannosylated nanomaterial tested. Additionally, in all cases, a greater proportion of red-labelled bacteria was detected in the supernatant from release experiments (Fig. 4.8.) This may suggest that either bacterial capture by or release from mannosylated nanoparticles is not specific. Importantly though, this investigation could be skewed due to incomplete depletion of supernatant containing the bacterial suspension from MGNP pellets after magnetic extraction. Other methods may be required to fully explore the composition of bacteria populations sequestered by MGNPs and to confirm release dynamics. Essential further works could include microscopic analysis of MGNP/bacteria clusters or microbiological monitoring of bacterial load before and after both capture and release by optical density analysis or

colony forming unit counts. An absence of the ability to release captured bacteria from these MGNPs could limit applications to those where depletion alone is sufficient. More complete understanding of captured bacteria release dynamics is essential before the described system can be applied to specific applications.

For applications where release of bacteria is desired, these results suggest nanoparticles coated with shorter chain mannosylated glycomaterials may be more appropriate. Shorter chain mannosylated materials had improved dissociation parameters as evidenced by SPR (Section 3.2.4.2.), investigation of MGNPs coated with mannosylated polymers of less than DP_{50} may be beneficial for improved release dynamics

While impressive bacterial capture from a mixed population containing fimbriate and afimbriate bacteria was achieved, the results described in this Chapter suggest additional work would be required to characterise the limitations of this system before replacement of existing immunomagnetic separation pipelines could be considered. For example, the experiments described in this Chapter were performed using normalised masses of MGNPs; this may not correlate to equal nanoparticle availability. Further experiments should be performed normalised to nanoparticle concentration, iron oxide concentration (of the nanoparticle core) and surface displayed glycopolymer concentration to fully understand these effects. Additionally, titration of ATc for the induction of expression of the Type 1 fimbriae in mixed population extraction should also be attempted as this may provide further control over the efficiency of extraction.

Furthermore, the results presented herein only describe the selective extraction of two distinct, genomically modified strains of the same bacterial species (*E. coli*). Further investigation of this system to selectively isolate fimbriated *E. coli* from a different bacterial strain (*C. necator*) was attempted but due to time constraints could not be completed. Completion of these experiments in the future would determine whether this system could be applied to the selective isolation of bacteria from mixed species populations.

5. Conclusions and Future Directions

In the initial chapter the current state of strategies for the selective confinement of bacteria from mixed populations was explored. This extensive review revealed that methods based on spatial entrapment (hydrogels, microfluidics, flow cytometry) were limited to small volumes and may lack the capacity to distinguish between cell types. Immunomagnetic separation, while effective and specific, appears very expensive hence not cost-effective. Other specific capture technique featuring aptamers and affintins are still in their infancy and some cross-reactivity has been observed. In contrast, MGNPs as a platform for capture specific targeted bacteria by lectin mediated attachment appeared promising. However, no reports have appeared in the literature up to this point describing the use of MGNPs for the capture and isolation of bacteria from mixed populations. The aim of this thesis work was therefore to investigate the unexplored potential of MGNPs to achieve this aim.

In chapter 2 an ATc-inducible mutant of the *fim* operon was constructed by allelic exchange of the native *fim* regulon by the *tetR*-p_{tetA} promoter system in *E. coli*. Control over Type 1 fimbriae expression was demonstrated and allowed for programmable binding of *E. coli* to mannosylated glycopolymers but not galactosylated polymers as shown in CLSM studies. Control of fimbrial expression was tightly regulated, with no glycopolymer capture observed in the absence of the inducer compound. Importantly though, while the LCMS data presented chapter infers the expression of Type 1 fimbriae, this should also be confirmed at the molecular level by

interrogation of protein expression using SDS-PAGE or Western blotting. Chromosomal tagging of *E. coli* strains by Tn7 transposition with constitutive expression cassettes for eGFP and mRuby yielded strains which were autofluorescent in the red and green spectral bandwidths with little impact on strain growth, suggesting no detrimental metabolic strain when hosting these non-native expression cassettes. Chromosomally labelled strains were desired to allow for the monitoring of bacterial population dynamics by flow cytometry so that the efficiency of magnetic isolation could be determined.

In Chapter 3 the aim was to produce magnetic glyconanoparticles coated with mannose and galactose polymers of various chain lengths. After in depth review of existing techniques a 'grafting to' synthetic route was devised, whereby glycopolymers could be produced via RAFT polymerisation and used to coat nanoparticle produced via thermal decomposition of organometallic precursor. To this end a novel RAFT agent, Dopa-PABTC was produced, with a catecholic terminus. The functionality of this compound as a CTA with acrylamides was proven via a kinetic study. An induction period was observed, which is unusual for trithiocarbonates, but could be attributed to the 'acrylamide-like' character of the reinitiating group, radical abstraction by the catecholic domain on this CTA or incomplete deoxygenation. However, little impact upon polymerisation control was observed as Dopa-PABTC was able to mediate the polymerisation of glycoacrylamides with narrow molecular weight distributions. Lectin binding analysis of produced glycopolymers via SPR

and ConA turbidity assay showed little to no interaction between mannose specific lectins and the control (HEAA) or non-binding (GalAA) polymer. Importantly though, these SPR studies were limited to model mannose binding lectins, MBL and DC-SIGN, instead of FimH which was not commercially available as a purified protein. The highest avidity mannose polymers, Dopa-$(ManAA)_{50}$ and Dopa-$(ManAA)_{200}$, were taken forward for nanoparticle decoration. Nanoparticle decoration was shown to be highly efficient by TGA and FTIR, however the Dopa-poly$(ManAA)_{200}$ coated material showed a lower weight percentage of iron oxide compared to other materials. To date this is the only study to describe the coating of thermal decomposition derived magnetic nanoparticles with adhesive-group terminal glycopolymers produced via RAFT polymerisation. Future functionalisation of MGNPs with non-mannose sugar polymers could also improve the scope for targeting other bacterial lectins.

Chapter 4 demonstrated that mannosylated MGNPs could be utilised to successfully deplete bacteria from a heterogeneous population. Isolation of fimbriated *E. coli* from afimbriate *E. coli* was near complete under the best conditions tested and this isolation was most efficient when non-target strain did not harbour the genetic apparatus for express of Type 1 fimbriae, suggesting genetic manipulation of microbial chassis may improve selectivity by MGNPs. Interestingly, the Dopa-$(ManAA)_{50}$ functionalised MGNPs proved more effective than Dopa-$(ManAA)_{200}$ coated particles for the depletion of fimbriated *E. coli* from solution, despite SPR and ConA binding studies suggesting a higher avidity for mannose specific lectins in

the case of Dopa-$(ManAA)_{200}$ coated MGNPs. This could be attributed to the lower iron oxide content of Dopa-$(ManAA)_{200}$ coated MGNPs as shown by TGA. Changes in the hydrodynamic radii between these two materials was not investigated, but could have an impact of binding epitope presentation and should be investigated.

Importantly though, some minor depletion of target bacteria by galactosylated nanoparticles was consistently observed. In particular, depletion of the target fimbriate strain by galactosylated materials was almost analogous to depletion by mannosylated counterparts during the adaption of an existing, column-based magnetic extraction system. Additionally, release of the target bacteria from nanoparticle clusters could not be adequately demonstrated by the addition of a competive ligand. Release of non-target bacteria was also consistently observed in these experiments. Cumulatively, these findings may suggest that either capture or release of bacteria was non-specific. While experimental design and execution could have contributed to this finding, it is essential that the specificity of bacterial capture and release by mannosylated glyconanoparticles is better understood before usage can be translated to specific applications.

It is proposed that the system described herein could be utilised for the selective isolation of bacteria from mixed populations at large scales, analogous to conventional immunomagnetic separation but without the prohibitive cost of upscaling antibody-based methods. However we have

identified that substantial investigation of the limitations of this system will be required before industrial adoption can begin.

This system has some significant advantages over other separation techniques. Principally these include multiplex separation and ability to distinguish genotypically distinct but morphologically identical cells. *E. coli* harbours the genetic apparatus for multiple surface associated lectins with differing sugar preferences. Putting these distinct operons under the control of different promoters would allow the construct of a single chassis which be programmed to respond to different external stimuli (inducers) thus allowing discrete control over lectin expression which could be targeted for extraction by distinct MGNPs for use in bioindustry or fundamental scientific research. Cautious design could ensure that these MGNPs are specific to one particular lectin, thus allowing selective isolation as demonstrated in this work but in sequential rounds.

Similarly, the lectins of other bacterial species could be targeted by MGNPs with differing sugar functionality to expand this system to targeting practically any bacteria species which expresses surface associated sugar binging proteins. It may also be possible to heterologously express non-native surface associated lectins in other organisms (Martinez-Alarcon *et al.*, 2018), thus mediating their selective isolation by MGNPs.

Furthermore, it is predicted that MGNPs for bacterial isolation may not be limited to the biotechnological industries and could be utilised for the specific capture of bacteria from mixed populations as a replacement for immunomagnetic/targeted nanoparticles in diagnostics (Intorasoot *et al.*,

2016; Li *et al.*, 2018b), treatment of contaminated drinking water (Bohara *et al.*, 2017; Malakootikhah *et al.*, 2017), pathogen detection agent in the food industry (Lim *et al.*, 2017; Zhang *et al.*, 2017), bioremediation (Chakraborty *et al.*, 2011), extraction of biosensing strains from microbial consortia (Xiu *et al.*, 2017) and in other fundamental microbial research. Potential applications may only be limited to the ingenuity of future users and the expression of surface associated lectins in organisms of interest, but would require significant future investigation and development.

6. References

Abedin, M. R., Umapathi, S., Mahendrakar, H., Laemthong, T., Coleman, H., Muchangi, D*., et al.* (2018). Polymer coated gold-ferric oxide superparamagnetic nanoparticles for theranostic applications. *Journal of Nanobiotechnology, 16*, 13.

Abraham, S. N., Babu, J. P., Giampapa, C. S., Hasty, D. L., Simpson, W. A., & Beachey, E. H. (1985). Protection against Escherichia coli-induced urinary tract infections with hybridoma antibodies directed against type 1 fimbriae or complementary D-mannose receptors. *Infect Immun, 48*(3), 625-628.

Adharis, A., Vesper, D., Koning, N., & Loos, K. (2018). Synthesis of (meth)acrylamide-based glycomonomers using renewable resources and their polymerization in aqueous systems. *Green Chemistry, 20*(2), 476-484.

Adkinson, N. F., Strauss, W. E., Macdougall, I. C., Bernard, K. E., Auerbach, M., Kaper, R. F*., et al.* (2018). Comparative safety of intravenous ferumoxytol versus ferric carboxymaltose in iron deficiency anemia: A randomized trial. *American Journal of Hematology, 93*(5), 683-690.

Adler, A., Forster, N., Homann, M., & Goringer, H. U. (2008). Post-SELEX chemical optimization of a trypanosome-specific RNA aptamer. *Combinatorial Chemistry & High Throughput Screening, 11*(1), 16-23.

Adschiri, T., Hakuta, Y., Sue, K., & Arai, K. (2001). Hydrothermal synthesis of metal oxide nanoparticles at supercritical conditions. *Journal of Nanoparticle Research, 3*(2-3), 227-235.

Agostino, M., Velkov, T., Dingjan, T., Williams, S. J., Yuriev, E., & Ramsland, P. A. (2015). The carbohydrate-binding promiscuity of Euonymus europaeus lectin is predicted to involve a single binding site. *Glycobiology, 25*(1), 101-114.

Agrahari, A. K., Singh, A. S., Singh, A. K., Mishra, N., Singh, M., Prakash, P*., et al.* (2019). Click inspired synthesis of hexa and octadecavalent peripheral galactosylated glycodendrimers and their possible therapeutic applications. *New Journal of Chemistry, 43*(31), 12475-12482.

Ajish, J. K., Kumar, K. S. A., Ruhela, A., Subramanian, M., Ballal, A. D., & Kumar, M. (2018). AIE based fluorescent self assembled glycoacrylamides for E.coli detection and cell imaging. *Sensors and Actuators B-Chemical, 255*, 1726-1734.

Alagesan, S., Hanko, E. K. R., Malys, N., Ehsaan, M., Winzer, K., & Minton, N. P. (2018). Functional genetic elements for controlling gene expression in Cupriavidus necator H16. *Applied and Environmental Microbiology*.

Albertin, L., & Cameron, N. R. (2007). RAFT polymerization of methyl 6-O-Methacryloyl-alpha-D-glucoside in homogeneous aqueous medium. A detailed kinetic study at the low molecular weight limit of the process. *Macromolecules, 40*(17), 6082-6093.

Albertin, L., Stenzel, M., Barner-Kowollik, C., Foster, L. J. R., & Davis, T. P. (2004). Well-defined glycopolymers from RAFT polymerization: Poly(methyl 6-O-methacryloyl-alpha-D-glucoside) and its block copolymer with 2-hydroxyethyl methacrylate. *Macromolecules, 37*(20), 7530-7537.

Albertin, L., Stenzel, M. H., Barner-Kowollik, C., & Davis, T. P. (2006). Effect of an added base on (4-cyanopentanoic acid)-4-dithiobenzoate mediated RAFT polymerization in water. *Polymer, 47*(4), 1011-1019.

Albertin, L., Stenzel, M. H., Barner-Kowollik, C., Foster, L. J. R., & Davis, T. P. (2005). Well-defined diblock glycopolymers from RAFT polymerization in homogeneous aqueous medium. *Macromolecules, 38*(22), 9075-9084.

Alsubaie, F., Anastasaki, A., Wilson, P., & Haddleton, D. M. (2015). Sequence-controlled multi-block copolymerization of acrylamides via aqueous SET-LRP at 0 degrees C. *Polymer Chemistry, 6*(3), 406-417.

Amara, D., Felner, I., Nowik, I., & Margel, S. (2009). Synthesis and characterization of Fe and Fe3O4 nanoparticles by thermal decomposition of triiron dodecacarbonyl. *Colloids and Surfaces a-Physicochemical and Engineering Aspects, 339*(1-3), 106-110.

Ambriz-Avina, V., Contreras-Garduno, J. A., & Pedraza-Reyes, M. (2014). Applications of Flow Cytometry to Characterize Bacterial Physiological Responses. *Biomed Research International*, 14.

Ambrosi, M., Cameron, N. R., & Davis, B. G. (2005). Lectins: tools for the molecular understanding of the glycocode. *Organic & Biomolecular Chemistry, 3*(9), 1593-1608.

Anastasaki, A., Nikolaou, V., & Haddleton, D. M. (2016). Cu(0)-mediated living radical polymerization: recent highlights and applications; a perspective. *Polymer Chemistry, 7*(5), 1002-1026.

Anderson, R. A., Paquette, S., & Lovrien, R. (2002). Lectin-erythrocyte interaction with external transmembrane glycophorin saccharides controlling membrane internal cytoskeleta. *Journal of Agricultural and Food Chemistry, 50*(22), 6599-6604.

Angot, S., Murthy, K. S., Taton, D., & Gnanou, Y. (1998). Atom transfer radical polymerization of styrene using a novel octafunctional initiator: Synthesis of well-defined polystyrene stars. *Macromolecules, 31*(21), 7218-7225.

Aronson, M., Medalia, O., Schori, L., Mirelman, D., Sharon, N., & Ofek, I. (1979). Prevention of Colonization of the Urinary Tract of Mice with Escherichia coli by Blocking of Bacterial Adherence with Methyl α-d-Mannopyranoside. *Journal of Infectious Diseases*.

Asadi, H., Khoee, S., & Deckers, R. (2016). Polymer-grafted superparamagnetic iron oxide nanoparticles as a potential stable system for magnetic resonance imaging and doxorubicin delivery. *Rsc Advances, 6*(87), 83963-83972.

Aslam, M., Schultz, E. A., Sun, T., Meade, T., & Dravid, V. P. (2007). Synthesis of amine-stabilized aqueous colloidal iron oxide nanoparticles. *Crystal Growth & Design, 7*(3), 471-475.

Aspholm, M., Olfat, F. O., Norden, J., Sonden, B., Lundberg, C., Sjostrom, R.*, et al.* (2006). SabA is the H. pylori hemagglutinin and is polymorphic in binding to sialylated glycans. *Plos Pathogens, 2*(10), 989-1001.

Atack, J. M., Day, C. J., Poole, J., Brockman, K. L., Bakaletz, L. O., Barenkamp, S. J.*, et al.* (2018). The HMW2 adhesin of non-typeable Haemophilus influenzae is a human-adapted lectin that mediates high-affinity binding to 2-6 linked N-acetylneuraminic acid glycans. *Biochemical and Biophysical Research Communications, 503*(2), 1103-1107.

Audfray, A., Claudinon, J., Abounit, S., Ruvoen-Clouet, N., Larson, G., Smith, D. F.*, et al.* (2012). Fucose-binding Lectin from Opportunistic Pathogen Burkholderia ambifaria Binds to Both Plant and Human Oligosaccharidic Epitopes. *Journal of Biological Chemistry, 287*(6), 4335-4347.

Aziz, R. K., Breitbart, M., & Edwards, R. A. (2010). Transposases are the most abundant, most ubiquitous genes in nature. *Nucleic Acids Research, 38*(13), 4207-4217.

Baba, T., Ara, T., Hasegawa, M., Takai, Y., Okumura, Y., Baba, M.*, et al.* (2006). Construction of Escherichia coli K-12 in-frame, single-gene knockout mutants: the Keio collection. *Molecular Systems Biology, 2*, 11.

Babiuch, K., Wyrwa, R., Wagner, K., Seemann, T., Hoeppener, S., Becer, C. R., *et al.* (2011). Functionalized, Biocompatible Coating for Superparamagnetic Nanoparticles by Controlled Polymerization of a Thioglycosidic Monomer. *Biomacromolecules, 12*(3), 681-691.

Backhed, F., Alsen, B., Roche, N., Angstrom, J., von Euler, A., Breimer, M. E., *et al.* (2002). Identification of target tissue glycosphingolipid receptors for uropathogenic, F1C-fimbriated Escherichia coli and its role in mucosal inflammation. *Journal of Biological Chemistry, 277*(20), 18198-18205.

Baeshen, M. N., Al-Hejin, A. M., Bora, R. S., Ahmed, M. M. M., Ramadan, H. A. I., Saini, K. S., *et al.* (2015). Production of Biopharmaceuticals in E. coli: Current Scenario and Future Perspectives. *Journal of Microbiology and Biotechnology, 25*(7), 953-962.

Bagaria, H. G., Xue, Z., Neilson, B. M., Worthen, A. J., Yoon, K. Y., Nayak, S., *et al.* (2013). Iron Oxide Nanoparticles Grafted with Sulfonated Copolymers are Stable in Concentrated Brine at Elevated Temperatures and Weakly Adsorb on Silica. *Acs Applied Materials & Interfaces, 5*(8), 3329-3339.

Bajar, B. T., Wang, E. S., Lam, A. J., Kim, B. B., Jacobs, C. L., Howe, E. S., *et al.* (2016). Improving brightness and photostability of green and red fluorescent proteins for live cell imaging and FRET reporting. *Scientific Reports, 6*, 12.

Basuki, J. S., Esser, L., Duong, H. T. T., Zhang, Q., Wilson, P., Whittaker, M. R., *et al.* (2014). Magnetic nanoparticles with diblock glycopolymer shells give lectin concentration-dependent MRI signals and selective cell uptake. *Chemical Science, 5*(2), 715-726.

Batlle, X., & Labarta, A. (2002). Finite-size effects in fine particles: magnetic and transport properties. *Journal of Physics D-Applied Physics, 35*(6), R15-R42.

Becer, C. R. (2012). The Glycopolymer Code: Synthesis of Glycopolymers and Multivalent Carbohydrate-Lectin Interactions. *Macromolecular Rapid Communications, 33*(9), 742-752.

Becer, C. R., Gibson, M. I., Geng, J., Ilyas, R., Wallis, R., Mitchell, D. A., *et al.* (2010). High-Affinity Glycopolymer Binding to Human DC-SIGN and Disruption of DC-SIGN Interactions with HIV Envelope Glycoprotein. *Journal of the American Chemical Society, 132*(43), 15130-15132.

Becker, N. A., Peters, J. P., Lionberger, T. A., & Maher, L. J. (2013). Mechanism of promoter repression by Lac repressor-DNA loops. *Nucleic Acids Research, 41*(1), 156-166.

Beers, K. L., Gaynor, S. G., Matyjaszewski, K., Sheiko, S. S., & Moller, M. (1998). The synthesis of densely grafted copolymers by atom transfer radical polymerization. *Macromolecules, 31*(26), 9413-9415.

Behra, M., Azzouz, N., Schmidt, S., Volodkin, D. V., Mosca, S., Chanana, M., *et al.* (2013). Magnetic Porous Sugar-Functionalized PEG Microgels for Efficient Isolation and Removal of Bacteria from Solution. *Biomacromolecules, 14*(6), 1927-1935.

Beloin, C., Renard, S., Ghigo, J. M., & Lebeaux, D. (2014). Novel approaches to combat bacterial biofilms. *Current Opinion in Pharmacology, 18*, 61-68.

Benetti, E. M., Kang, C. J., Mandal, J., Divandari, M., & Spencer, N. D. (2017). Modulation of Surface-Initiated ATRP by Confinement: Mechanism and Applications. *Macromolecules, 50*(15), 5711-5718.

Benoit, D. N., Zhu, H. G., Lilierose, M. H., Verm, R. A., Ali, N., Morrison, A. N., *et al.* (2012). Measuring the Grafting Density of Nanoparticles in Solution by Analytical Ultracentrifugation and Total Organic Carbon Analysis. *Analytical Chemistry, 84*(21), 9238-9245.

Berlec, A., Skrlec, K., Kocjan, J., Olenic, M., & Strukelj, B. (2018). Single plasmid systems for inducible dual protein expression and for CRISPR-Cas9/CRISPRi gene regulation in lactic acid bacterium Lactococcus lactis. *Scientific Reports, 8*, 11.

Bernardi, A., Jimenez-Barbero, J., Casnati, A., De Castro, C., Darbre, T., Fieschi, F*., et al.* (2013). Multivalent glycoconjugates as anti-pathogenic agents. *Chemical Society Reviews, 42*(11), 4709-4727.

Bernstein, H. C., Brislawn, C., Renslow, R. S., Dana, K., Morton, B., Lindemann, S. R*., et al.* (2017). Trade-offs between microbiome diversity and productivity in a stratified microbial mat. *Isme Journal, 11*(2), 405-414.

Bhalerao, G. M., Sinha, A. K., Srivastava, H., & Srivastava, A. K. (2009). Synthesis and studies of growth kinetics of monodispersed iron oxide nanoparticles using ferrocene as novel precursor. *Applied Physics a-Materials Science & Processing, 95*(2), 373-380.

Bicart-See, A., Rottman, M., Cartwright, M., Seiler, B., Gamini, N., Rodas, M*., et al.* (2016). Rapid Isolation of Staphylococcus aureus Pathogens from Infected Clinical Samples Using Magnetic Beads Coated with Fc-Mannose Binding Lectin. *Plos One, 11*(6), 12.

Bixner, O., Lassenberger, A., Baurecht, D., & Reimhult, E. (2015). Complete Exchange of the Hydrophobic Dispersant Shell on Monodisperse Superparamagnetic Iron Oxide Nanoparticles. *Langmuir, 31*(33), 9198-9204.

Blattner, F. R., Plunkett, G., Bloch, C. A., Perna, N. T., Burland, V., Riley, M*., et al.* (1997). The complete genome sequence of Escherichia coli K-12. *Science, 277*(5331), 1453-&.

Blin, T., Kakinen, A., Pilkington, E. H., Ivask, A., Ding, F., Quinn, J. F*., et al.* (2016). Synthesis and in vitro properties of iron oxide nanoparticles grafted with brushed phosphorylcholine and polyethylene glycol. *Polymer Chemistry, 7*(10), 1931-1944.

Blind, M., & Blank, M. (2015). Aptamer Selection Technology and Recent Advances. *Molecular Therapy-Nucleic Acids, 4*, 7.

Blomfield, I. C., Calie, P. J., Eberhardt, K. J., McClain, M. S., & Eisenstein, B. I. (1993). Lrp stimulates phase variation of type 1 fimbriation in Escherichia coli K-12.

Blomfield, I. C., Kulasekara, D. H., & Eisenstein, B. I. (1997). Integration host factor stimulates both FimB- and FimE-mediated site-specific DNA inversion that controls phase variation of type 1 fimbriae expression in Escherichia coli. *Mol Microbiol, 23*(4), 705-717.

Blomfield, I. C., Vaughn, V., Rest, R. F., & Eisenstein, B. I. (1991). Allelic Exchange in Escherichia Coli Using the Bacillus Subtilis SacB Gene and a Temperature Sensitive pSC101 Replicon. *Mol Microbiol, 5*(6), 1447-1457.

Boden, S., Wagner, K. G., Karg, M., & Hartmann, L. (2017). Presenting Precision Glycomacromolecules on Gold Nanoparticles for Increased Lectin Binding. *Polymers, 9*(12), 27.

Boedicker, J. Q., Li, L., Kline, T. R., & Ismagilov, R. F. (2008). Detecting bacteria and determining their susceptibility to antibiotics by stochastic confinement in nanoliter droplets using plug-based microfluidics. *Lab on a Chip, 8*(8), 1265-1272.

Boedicker, J. Q., Vincent, M. E., & Ismagilov, R. F. (2009). Microfluidic Confinement of Single Cells of Bacteria in Small Volumes Initiates High-Density Behavior of Quorum Sensing and Growth and Reveals Its Variability. *Angewandte Chemie-International Edition, 48*(32), 5908-5911.

Bohara, R. A., & Pawar, S. H. (2015). Innovative Developments in Bacterial Detection with Magnetic Nanoparticles. *Applied Biochemistry and Biotechnology, 176*(4), 1044-1058.

Bohara, R. A., Throat, N. D., Mulla, N. A., & Pawar, S. H. (2017). Surface-Modified Cobalt Ferrite Nanoparticles for Rapid Capture, Detection, and Removal of Pathogens: a Potential Material for Water Purification. *Applied Biochemistry and Biotechnology, 182*(2), 598-608.

Bolotin, A., Ouinquis, B., Sorokin, A., & Ehrlich, S. D. (2005). Clustered regularly interspaced short palindrome repeats (CRISPRs) have spacers of extrachromosomal origin. *Microbiology-Sgm, 151*, 2551-2561.

Borase, T., Ninjbadgar, T., Kapetanakis, A., Roche, S., O'Connor, R., Kerskens, C.*, et al.* (2013). Stable Aqueous Dispersions of Glycopeptide-Grafted Selectably Functionalized Magnetic Nanoparticles. *Angewandte Chemie-International Edition, 52*(11), 3164-3167.

Bouchard, P. R., Hutabarat, R. M., & Thompson, K. M. (2010). Discovery and Development of Therapeutic Aptamers *Annual Review of Pharmacology and Toxicology* (Vol. 50, pp. 237-257). Palo Alto: Annual Reviews.

Bouckaert, J., Berglund, J., Schembri, M., De Genst, E., Cools, L., Wuhrer, M.*, et al.* (2005). Receptor binding studies disclose a novel class of high-affinity inhibitors of the Escherichia coli FimH adhesin. *Mol Microbiol, 55*(2), 441-455.

Bouckaert, J., Mackenzie, J., de Paz, J. L., Chipwaza, B., Choudhury, D., Zavialov, A.*, et al.* (2006). The affinity of the FimH fimbrial adhesin is receptor-driven and quasi-independent of Escherichia coli pathotypes. *Mol Microbiol, 61*(6), 1556-1568.

Bourque, G., Burns, K. H., Gehring, M., Gorbunova, V., Seluanov, A., Hammell, M.*, et al.* (2018). Ten things you should know about transposable elements. *Genome Biology, 19*, 12.

Bowater, R., & Doherty, A. J. (2006). Making ends meet: Repairing breaks in bacterial DNA by non-homologous end-joining. *Plos Genetics, 2*(2), 93-99.

Boyer, C., & Davis, T. P. (2009). One-pot synthesis and biofunctionalization of glycopolymers via RAFT polymerization and thiol-ene reactions. *Chemical Communications*(40), 6029-6031.

Boyer, C., Granville, A., Davis, T. P., & Bulmus, V. (2009). Modification of RAFT-Polymers via Thiol-Ene Reactions: A General Route to Functional Polymers and New Architectures. *Journal of Polymer Science Part a-Polymer Chemistry, 47*(15), 3773-3794.

Boyer, C., Whittaker, M. R., Bulmus, V., Liu, J. Q., & Davis, T. P. (2010). The design and utility of polymer-stabilized iron-oxide nanoparticles for nanomedicine applications. *Npg Asia Materials, 2*(1), 23-30.

Braim, S. A., Shakesheff, K. M., Saunders, B. R., & Alexander, C. (2016). Thermoresponsive magnetic colloidal gels via surface-initiated polymerisation from functional microparticles. *Journal of Materials Chemistry B, 4*(5), 962-972.

Braunecker, W. A., & Matyjaszewski, K. (2007). Controlled/living radical polymerization: Features, developments, and perspectives. *Progress in Polymer Science, 32*(1), 93-146.

Brazzale, C., Mastrotto, F., Moody, P., Watson, P. D., Balasso, A., Malfanti, A.*, et al.* (2017). Control of targeting ligand display by pH-responsive polymers on gold nanoparticles mediates selective entry into cancer cells. *Nanoscale, 9*(31), 11137-11147.

Brognaux, A., Han, S. S., Sorensen, S. J., Lebeau, F., Thonart, P., & Delvigne, F. (2013). A low-cost, multiplexable, automated flow cytometry procedure for the characterization of microbial stress dynamics in bioreactors. *Microbial Cell Factories, 12*, 14.

Brosius, J., Erfle, M., & Storella, J. (1985). Spacing of the -10 and -35 regions in the Tac promoter - effects on its *in vivo* activity. *Journal of Biological Chemistry, 260*(6), 3539-3541.

Brouns, S. J. J., Jore, M. M., Lundgren, M., Westra, E. R., Slijkhuis, R. J. H., Snijders, A. P. L.*, et al.* (2008). Small CRISPR RNAs guide antiviral defense in prokaryotes. *Science, 321*(5891), 960-964.

Browning, D. F., & Busby, S. J. W. (2004). The regulation of bacterial transcription initiation. *Nature Reviews Microbiology, 2*(1), 57-65.

Bruno, J. G., Phillips, T., Carrillo, M. P., & Crowell, R. (2009). Plastic-Adherent DNA Aptamer-Magnetic Bead and Quantum Dot Sandwich Assay for Campylobacter Detection. *Journal of Fluorescence, 19*(3), 427-435.

Cai, G. Z., Wang, S. Y., Zheng, L. Y., & Lin, J. H. (2018). A Fluidic Device for Immunomagnetic Separation of Foodborne Bacteria Using Self-Assembled Magnetic Nanoparticle Chains. *Micromachines, 9*(12), 11.

Cairo, C. W., Gestwicki, J. E., Kanai, M., & Kiessling, L. L. (2002). Control of multivalent interactions by binding epitope density. *Journal of the American Chemical Society, 124*(8), 1615-1619.

Cameron, N. R., Spain, S. G., Kingham, J. A., Weck, S., Albertin, L., Barker, C. A.*, et al.* (2008). Synthesis of well-defined glycopolymers and some studies of their aqueous solution behaviour. *Faraday Discussions, 139*, 359-368.

Campuzano, S., Orozco, J., Kagan, D., Guix, M., Gao, W., Sattayasamitsathit, S.*, et al.* (2012). Bacterial Isolation by Lectin-Modified Microengines. *Nano Letters, 12*(1), 396-401.

Cao, Y., Liang, X. F., Li, L., Pan, R. J., Wang, K., Xiao, C. G.*, et al.* (2017). High-Efficiency EpCAM/EGFR-PLGA Immunomagnetic Beads with Specific Recognition on Circulating Tumor Cells in Colorectal Cancer. *Journal of Biomedical Nanotechnology, 13*(7), 758-766.

Carnes, E. *e. a.* (2010). Confinement-induced quorum sensing of individual*Staphylococcus aureus* bacteria. *Nature Chemical Biology, 6*, 41-45.

Chakraborty, R., Hazen, T. C., Joyner, D. C., Kusel, K., Singer, M. E., Sitte, J.*, et al.* (2011). Use of immunomagnetic separation for the detection of Desulfovibrio vulgaris from environmental samples. *Journal of Microbiological Methods, 86*(2), 204-209.

Chen, B., Wu, W., & Wang, X. (2011). Magnetic Iron Oxide Nanoparticles for Tumor-Targeted Therapy. *Current Cancer Drug Targets, 11*(2), 184-189.

Chen, G. J., Tao, L., Mantovani, G., Geng, J., Nystrom, D., & Haddleton, D. M. (2007). A modular click approach to glycosylated polymeric beads: Design, synthesis and preliminary lectin, recognition studies. *Macromolecules, 40*(21), 7513-7520.

Chen, L., Wu, L. L., Zhang, Z. L., Hu, J., Tang, M., Qi, C. B.*, et al.* (2016a). Biofunctionalized magnetic nanospheres-based cell sorting strategy for efficient isolation, detection and subtype analyses of heterogeneous circulating hepatocellular carcinoma cells. *Biosensors & Bioelectronics, 85*, 633-640.

Chen, X., Wu, B., Jayawardana, K. W., Hao, N. J., Jayawardena, H. S. N., Langer, R.*, et al.* (2016b). Magnetic Multivalent Trehalose Glycopolymer Nanoparticles for the Detection of Mycobacteria. *Advanced Healthcare Materials, 5*(16), 2007-2012.

Chen, Y., Lord, M. S., Piloni, A., & Stenzel, M. H. (2015). Correlation between Molecular Weight and Branch Structure of Glycopolymers Stars and Their Binding to Lectins. *Macromolecules, 48*(2), 346-357.

Chen, Y. J., Luo, W., Wang, Y. F., Sun, C., Han, M., & Zhang, C. C. (2012). Synthesis and self-assembly of amphiphilic gradient copolymer via RAFT emulsifier-free emulsion polymerization. *Journal of Colloid and Interface Science, 369*, 46-51.

Chernyak, A. Y., Sharma, G. V. M., Kononov, L. O., Krishna, P. R., Levinsky, A. B., Kochetkov, N. K.*, et al.* (1992). 2-Azidoethyl glycosides - glycosides potentially useful for the preparation of neoglycoconjugates. *Carbohydrate Research, 223*, 303-309.

Chervenak, M. C., & Toone, E. J. (1995). Calorimertic analysis of the binding of lectins with overlapping carbohydrate-binding ligand specificities. *Biochemistry, 34*(16), 5685-5695.

Chin, A. B., & Yaacob, II. (2007). Synthesis and characterization of magnetic iron oxide nanoparticles via w/o microemulsion and Massart's procedure. *Journal of Materials Processing Technology, 191*(1-3), 235-237.

Choi, K. H., Gaynor, J. B., White, K. G., Lopez, C., Bosio, C. M., Karkhoff-Schweizer, R. R.*, et al.* (2005). A Tn7-based broad-range bacterial cloning and expression system. *Nature Methods, 2*(6), 443-448.

Chrispeels, M. J., & Raikhel, N. V. (1991). Lectins, lectin genes, and their role in plant defense. *Plant Cell, 3*(1), 1-9.

Claverys, J. P., Martin, B., & Polard, P. (2009). The genetic transformation machinery: composition, localization, and mechanism. *FEMS Microbiology Reviews, 33*(3), 643-656.

Cobb, R. E., Wang, Y. J., & Zhao, H. M. (2015). High-Efficiency Multiplex Genome Editing of Streptomyces Species Using an Engineered CRISPR/Cas System. *Acs Synthetic Biology, 4*(6), 723-728.

Coessens, V., Pintauer, T., & Matyjaszewski, K. (2001). Functional polymers by atom transfer radical polymerization. *Progress in Polymer Science, 26*(3), 337-377.

Cong, L., Ran, F. A., Cox, D., Lin, S. L., Barretto, R., Habib, N.*, et al.* (2013). Multiplex Genome Engineering Using CRISPR/Cas Systems. *Science, 339*(6121), 819-823.

Connell, I., Agace, W., Klemm, P., Schembri, M., Mărild, S., & Svanborg, C. (1996). Type 1 fimbrial expression enhances Escherichia coli virulence for the urinary tract. *Proc Natl Acad Sci U S A, 93*(18), 9827-9832.

Connell, J. L., Wessel, A. K., Parsek, M. R., Ellington, A. D., Whiteley, M., & Shear, J. B. (2010). Probing Prokaryotic Social Behaviors with Bacterial "Lobster Traps". *Mbio, 1*(4), 8.

Coppens, F., Iyyathurai, J., Ruer, S., Fioravanti, A., Taganna, J., Vereecke, L.*, et al.* (2015). Structural and adhesive properties of the long polar fimbriae protein LpfD from adherent-invasive Escherichia coli. *Acta Crystallographica Section D-Structural Biology, 71*, 1615-1626.

Correa, A., Pacheco, S., Mechaly, A. E., Obal, G., Behar, G., Mouratou, B.*, et al.* (2014). Potent and Specific Inhibition of Glycosidases by Small Artificial Binding Proteins (Affitins). *Plos One, 9*(5), 12.

Cossarizza, A., Chang, H. D., Radbruch, A., Akdis, M., Andra, I., Annunziato, F.*, et al.* (2017). Guidelines for the use of flow cytometry and cell sorting in immunological studies. *European Journal of Immunology, 47*(10), 1584-1797.

Costa, T. R. D., Ilangovan, A., Ukleja, M., Redzej, A., Santini, J. M., Smith, T. K.*, et al.* (2016). Structure of the Bacterial Sex F Pilus Reveals an Assembly of a Stoichiometric Protein-Phospholipid Complex. *Cell, 166*(6), 1436-+.

Craig, N. L. (1991). Tn7 - A target site-specific transposon. *Mol Microbiol, 5*(11), 2569-2573.

Crepin, S., Harel, J., & Dozois, C. M. (2012). Chromosomal Complementation Using Tn7 Transposon Vectors in Enterobacteriaceae. *Applied and Environmental Microbiology, 78*(17), 6001-6008.

Crownover, E., Duvall, C. L., Convertine, A., Hoffman, A. S., & Stayton, P. S. (2011). RAFT-synthesized graft copolymers that enhance pH-dependent membrane destabilization and protein circulation times. *Journal of Controlled Release, 155*(2), 167-174.

Darwin, A. J., & Stewart, V. (1995). Expression of *narX*, *narL, narP* and *narQ* genes of *Escherichia coli* K12 - regulation of the regulators. *J Bacteriol, 177*(13), 3865-3869.

Datsenko, K. A., & Wanner, B. L. (2000). One-step inactivation of chromosomal genes in Escherichia coli K-12 using PCR products. *Proceedings of the National Academy of Sciences of the United States of America, 97*(12), 6640-6645.

De Boer, H. A., Comstock, L. J., & Vasser, M. (1983). The tac promoter: a functional hybrid derived from the trp and lac promoters. *Proc Natl Acad Sci USA, 80*(1), 21-25.

de la Calle, A. C., Gerke, C., Chang, X. J., Grafmuller, A., Hartmann, L., & Schmidt, S. (2019). Multivalent Interactions of Polyamide Based Sequence-Controlled Glycomacromolecules with Concanavalin A. *Macromolecular Bioscience, 19*(6), 9.

De Mey, M., Maertens, J., Lequeux, G. J., Soetaert, W. K., & Vandamme, E. J. (2007). Construction and model-based analysis of a promoter library for E-coli: an indispensable tool for metabolic engineering. *Bmc Biotechnology, 7*, 14.

Degenkolb, J., Takahashi, M., Ellestad, G. A., & Hillen, W. (1991). Structural requirements of the tetracycline Tet repressor interaction - determination of the equilibrium binding constants for the tetracycline analogs with the tet repressor. *Antimicrobial Agents and Chemotherapy, 35*(8), 1591-1595.

Degiorgi, C. F., Pizarro, R. A., Smolko, E. E., Lora, S., & Carenza, M. (2002). Hydrogels for immobilization of bacteria used in the treatment of metal-contaminated wastes. *Radiation Physics and Chemistry, 63*(1), 109-113.

DeLisa, M. P., Li, J. C., Rao, G., Weigand, W. A., & Bentley, W. E. (1999). Monitoring GFP-operon fusion protein expression during high cell density cultivation of Escherichia coli using an on-line optical sensor. *Biotechnology and Bioengineering, 65*(1), 54-64.

Deltcheva, E., Chylinski, K., Sharma, C. M., Gonzales, K., Chao, Y. J., Pirzada, Z. A*., et al.* (2011). CRISPR RNA maturation by trans-encoded small RNA and host factor RNase III. *Nature, 471*(7340), 602-+.

Demirer, G. S., Okur, A. C., & Kizilel, S. (2015). Synthesis and design of biologically inspired biocompatible iron oxide nanoparticles for biomedical applications. *Journal of Materials Chemistry B, 3*(40), 7831-7849.

Demortiere, A., Panissod, P., Pichon, B. P., Pourroy, G., Guillon, D., Donnio, B*., et al.* (2011). Size-dependent properties of magnetic iron oxide nanocrystals. *Nanoscale, 3*(1), 225-232.

Deng, Z. C., Ahmed, M., & Narain, R. (2009). Novel Well-Defined Glycopolymers Synthesized via the Reversible Addition Fragmentation Chain Transfer Process in Aqueous Media. *Journal of Polymer Science Part a-Polymer Chemistry, 47*(2), 614-627.

Deniaud, D., Julienne, K., & Gouin, S. G. (2011). Insights in the rational design of synthetic multivalent glycoconjugates as lectin ligands. *Organic & Biomolecular Chemistry, 9*(4), 966-979.

Disney, M. D., & Seeberger, P. H. (2004). The use of carbohydrate microarrays to study carbohydrate-cell interactions and to detect pathogens. *Chemistry & Biology, 11*(12), 1701-1707.

Doudna, J. A., & Charpentier, E. (2014). The new frontier of genome engineering with CRISPR-Cas9. *Science, 346*(6213), 1077-+.

Dove, S. L., Smith, S. G., & Dorman, C. J. (1997). Control of Escherichia coli type 1 fimbrial gene expression in stationary phase: a negative role for RpoS. *Mol Gen Genet, 254*(1), 13-20.

Dundas, C. M., Demonte, D., & Park, S. (2013). Streptavidin-biotin technology: improvements and innovations in chemical and biological applications. *Applied Microbiology and Biotechnology, 97*(21), 9343-9353.

Dutz, S., & Hergt, R. (2014). Magnetic particle hyperthermia-a promising tumour therapy? *Nanotechnology, 25*(45), 28.

Dwivedi, H. P., Smiley, R. D., & Jaykus, L. A. (2013). Selection of DNA aptamers for capture and detection of Salmonella Typhimurium using a whole-cell SELEX approach in conjunction with cell sorting. *Applied Microbiology and Biotechnology, 97*(8), 3677-3686.

Edelman, G. M., & Wang, J. L. (1978). Binding and functional properties of Concanavalin A and its derivatives. 3. Interactions with indoleacetic acid and other hydrophobic ligands *Journal of Biological Chemistry, 253*(9), 3016-3022.

El-Boubbou, K., Gruden, C., & Huang, X. (2007). Magnetic glyco-nanoparticles: A unique tool for rapid pathogen detection, decontamination, and strain differentiation. *Journal of the American Chemical Society, 129*(44), 13392-+.

Ellington, A. D., & Szostak, J. W. (1990). *In vitro* selection of RNA molecules that bind specific ligands. *Nature, 346*(6287), 818-822.

Elmore, J. R., Furches, A., Wolff, G. N., Gorday, K., & Guss, A. M. (2017). Development of a high efficiency integration system and promoter library for rapid modification of Pseudomonas putida KT2440. *Metabolic Engineering Communications, 5*, 1-8.

Ernst, B., & Magnani, J. (2009). From Carbohydrate Leads To Glycomimetic Drugs. *Nature Reviews Drug Discovery*, 661-677.

Fang, W. J., Han, C., Zhang, H. B., Wei, W. M., Liu, R., & Shen, Y. X. (2016). Preparation of amino-functionalized magnetic nanoparticles for enhancement of bacterial capture efficiency. *Rsc Advances, 6*(72), 67875-67882.

Farr, T. D., Lai, C. H., Grunstein, D., Orts-Gil, G., Wang, C. C., Boehm-Sturm, P.*, et al.* (2014). Imaging Early Endothelial Inflammation Following Stroke by Core Shell Silica Superparamagnetic Glyconanoparticles That Target Selectin. *Nano Letters, 14*(4), 2130-2134.

Feng, L. J., Zhong, M. J., Zhang, S. Z., Wang, M., Sun, Z. Y., & Chen, Q. (2019). Synthesis of water-soluble fluorescent polymeric glycoconjugate for the detection of cholera toxin. *Designed Monomers and Polymers, 22*(1), 150-158.

Ferguson, C. J., Hughes, R. J., Nguyen, D., Pham, B. T. T., Gilbert, R. G., Serelis, A. K.*, et al.* (2005). Ab initio emulsion polymerization by RAFT-controlled self-assembly. *Macromolecules, 38*(6), 2191-2204.

Figueredo, F., Saavedra, A., Corton, E., & Diz, V. E. (2018). Hydrophobic Forces Are Relevant to Bacteria-Nanoparticle Interactions: Pseudomonas putida Capture Efficiency by Using Arginine, Cysteine or Oxalate Wrapped Magnetic Nanoparticles. *Colloids and Interfaces, 2*(3), 16.

Flickinger, S. T., Copeland, M. F., Downes, E. M., Braasch, A. T., Tuson, H. H., Eun, Y. J., *et al.* (2011). Quorum Sensing between Pseudomonas aeruginosa Biofilms Accelerates Cell Growth. *Journal of the American Chemical Society, 133*(15), 5966-5975.

Foster, L. L., Yusa, S., & Kuroda, K. (2019). Solution-Mediated Modulation of Pseudomonas aeruginosa Biofilm Formation by a Cationic Synthetic Polymer. *Antibiotics-Basel, 8*(2), 16.

Frey, N. A., Peng, S., Cheng, K., & Sun, S. H. (2009). Magnetic nanoparticles: synthesis, functionalization, and applications in bioimaging and magnetic energy storage. *Chemical Society Reviews, 38*(9), 2532-2542.

Fu, Y. F., Foden, J. A., Khayter, C., Maeder, M. L., Reyon, D., Joung, J. K., *et al.* (2013). High-frequency off-target mutagenesis induced by CRISPR-Cas nucleases in human cells. *Nature Biotechnology, 31*(9), 822-+.

Fujimoto, R., Osakabe, T., Saito, M., Kurosawa, N., & Isobe, M. (2009). Minimum Length of Homology Arms Required for Effective Red/ET Recombination. *Bioscience Biotechnology and Biochemistry, 73*(12), 2783-2786.

Galli, M., Rossotti, B., Arosio, P., Ferretti, A. M., Panigati, M., Ranucci, E., *et al.* (2019). A new catechol-functionalized polyamidoamine as an effective SPION stabilizer. *Colloids and Surfaces B-Biointerfaces, 174*, 260-269.

Gallo, J., Garcia, I., Genicio, N., Padro, D., & Penades, S. (2011). Specific labelling of cell populations in blood with targeted immuno-fluorescent/magnetic glyconanoparticles. *Biomaterials, 32*(36), 9818-9825.

Gally, D. e. a. (2007). Comparative analysis of FimB and FimE recombinase activity. *Microbiology, 153*, 4138-4149.

Gally, D. L., Bogan, J. A., Eisenstein, B. I., & Blomfield, I. C. (1993). Environmental regulation of the fim switch controlling type 1 fimbrial phase variation in Escherichia coli K-12: effects of temperature and media. *J Bacteriol, 175*(19), 6186-6193.

Gao, H. F., & Matyjaszewski, K. (2007). Synthesis of molecular brushes by "grafting onto" method: Combination of ATRP and click reactions. *Journal of the American Chemical Society, 129*(20), 6633-6639.

Gao, J. H., Gu, H. W., & Xu, B. (2009). Multifunctional Magnetic Nanoparticles: Design, Synthesis, and Biomedical Applications. *Accounts of Chemical Research, 42*(8), 1097-1107.

Gao, X. L., Shao, M. F., Xu, Y. S., Luo, Y., Zhang, K., Ouyang, F., *et al.* (2016). Non-selective Separation of Bacterial Cells with Magnetic Nanoparticles Facilitated by Varying Surface Charge. *Frontiers in Microbiology, 7*, 10.

Garcia, I., Zafeiropoulos, N. E., Janke, A., Tercjak, A., Eceiza, A., Stamm, M., *et al.* (2007). Functionalization of iron oxide magnetic nanoparticles with poly(methyl methacrylate) brushes via grafting-from atom transfer radical polymerization. *Journal of Polymer Science Part a-Polymer Chemistry, 45*(5), 925-932.

Gay, N. J., Tybulewicz, V. L. J., & Walker, J. E. (1986). INSERTION OF TRANSPOSON TN7 INTO THE ESCHERICHIA-COLI-GLMS TRANSCRIPTIONAL TERMINATOR. *Biochemical Journal, 234*(1), 111-117.

Ge, S., Shi, X. Y., Sun, K., Li, C. P., Uher, C., Baker, J. R., *et al.* (2009). Facile Hydrothermal Synthesis of Iron Oxide Nanoparticles with Tunable Magnetic Properties. *Journal of Physical Chemistry C, 113*(31), 13593-13599.

Gedi, V., & Kim, Y. P. (2014). Detection and Characterization of Cancer Cells and Pathogenic Bacteria Using Aptamer-Based Nano-Conjugates. *Sensors, 14*(10), 18302-18327.

Geng, J., Lindqvist, J., Mantovani, G., & Haddleton, D. M. (2008). Simultaneous copper(I)-catalyzed azide-alkyne cycloaddition (CuAAC) and living radical polymerization. *Angewandte Chemie-International Edition, 47*(22), 4180-4183.

Geng, J., Mantovani, G., Tao, L., Nicolas, J., Chen, G. J., Wallis, R.*, et al.* (2007). Site-directed conjugation of "Clicked" glycopolymers to form glycoprotein mimics: Binding to mammalian lectin and induction of immunological function. *Journal of the American Chemical Society, 129*(49), 15156-15163.

Gening, L. V., Klincheva, S. A., Reshetnjak, A., Grollman, A. P., & Miller, H. (2006). RNA aptamers selected against DNA polymerase beta inhibit the polymerase activities of DNA polymerases beta and kappa. *Nucleic Acids Research, 34*(9), 2579-2586.

Gerchman, Y., & Weiss, R. (2004). Teaching bacteria a new language. *Proceedings of the National Academy of Sciences of the United States of America, 101*(8), 2221-2222.

Gestwicki, J. E., Cairo, C. W., Strong, L. E., Oetjen, K. A., & Kiessling, L. L. (2002). Influencing receptor-ligand binding mechanisms with multivalent ligand architecture. *Journal of the American Chemical Society, 124*(50), 14922-14933.

Ghadban, A., & Albertin, L. (2013). Synthesis of Glycopolymer Architectures by Reversible-Deactivation Radical Polymerization. *Polymers, 5*(2), 431-526.

Gharbi, K., Salles, F., Mathieu, P., Amiens, C., Colliere, V., Coppel, Y.*, et al.* (2017). Alkyl phosphonic acid-based ligands as tools for converting hydrophobic iron nanoparticles into water soluble iron-iron oxide core-shell nanoparticles. *New Journal of Chemistry, 41*(20), 11898-11905.

Ghozzi, S., Ng, J. W., Chatenay, D., & Robert, J. (2010). Inference of plasmid-copy-number mean and noise from single-cell gene expression data. *Physical Review E, 82*(5), 8.

Gody, G., Maschmeyer, T., Zetterlund, P. B., & Perrier, S. (2013). Rapid and quantitative one-pot synthesis of sequence-controlled polymers by radical polymerization. *Nature Communications, 4*, 9.

Gody, G., Maschmeyer, T., Zetterlund, P. B., & Perrier, S. (2014). Pushing the Limit of the RAFT Process: Multiblock Copolymers by One-Pot Rapid Multiple Chain Extensions at Full Monomer Conversion. *Macromolecules, 47*(10), 3451-3460.

Golden, J. P., Verbarg, J., Howell, P. B., Shriver-Lake, L. C., & Ligler, F. S. (2013). Automated processing integrated with a microflow cytometer for pathogen detection in clinical matrices. *Biosensors & Bioelectronics, 40*(1), 10-16.

Goldstein, I. J., Reichert, C. M., Misaki, A., & Gorin, P. A. J. (1973). Extension of carbohydrate binding specificity of Concanavalin A. *Biochimica et biophysica acta, 317*(2), 500-504.

Gou, Y. Z., Geng, J., Richards, S. J., Burns, J., Becer, C. R., & Haddleton, D. M. (2013). A detailed study on understanding glycopolymer library and Con A interactions. *Journal of Polymer Science Part a-Polymer Chemistry, 51*(12), 2588-2597.

Gouin, S. G., Wellens, A., Bouckaert, J., & Kovensky, J. (2009). Synthetic Multimeric Heptyl Mannosides as Potent Antiadhesives of Uropathogenic Escherichia coli. *Chemmedchem, 4*(5), 749-755.

Gourikutty, S. B. N., Chang, C. P., & Puiu, P. D. (2016). Microfluidic immunomagnetic cell separation from whole blood. *Journal of Chromatography B-Analytical Technologies in the Biomedical and Life Sciences, 1011*, 77-88.

Gratz, S. J., Ukken, F. P., Rubinstein, C. D., Thiede, G., Donohue, L. K., Cummings, A. M.*, et al.* (2014). Highly Specific and Efficient CRISPR/Cas9-Catalyzed Homology-Directed Repair in Drosophila. *Genetics, 196*(4), 961-+.

Guardia, P., Perez-Juste, J., Labarta, A., Batlle, X., & Liz-Marzan, L. M. (2010). Heating rate influence on the synthesis of iron oxide nanoparticles: the case of decanoic acid. *Chemical Communications, 46*(33), 6108-6110.

Guo, J. A., & Ye, X. S. (2010). Protecting Groups in Carbohydrate Chemistry: Influence on Stereoselectivity of Glycosylations. *Molecules, 15*(10), 7235-7265.

Guo, S. T., Zhang, Q., Wang, D. H., Wang, L., Lin, F., Wilson, P.*, et al.* (2017). Bioinspired coating of TiO2 nanoparticles with antimicrobial polymers by Cu(0)-LRP: grafting to vs. grafting from. *Polymer Chemistry, 8*(42), 6570-6580.

Gupta, A., Gupta, R., & Gupta, G. (2009). Targetting cells for drug and gene delivery: Emerging applications of mannans and mannan binding lectins. *Journal of Scientific & Industrial Research, 68*, 465-483.

Guzman, L. M., Belin, D., Carson, M. J., & Beckwith, J. (1995). Tight regulation, modulation, and high-level expression by vectors containing the arabinose P_{BAD} promoter. *J Bacteriol, 177*(14), 4121-4130.

Haft, D. H., Selengut, J., Mongodin, E. F., & Nelson, K. E. (2005). A guild of 45 CRISPR-associated (Cas) protein families and multiple CRISPR/Cas subtypes exist in prokaryotic genomes. *Plos Computational Biology, 1*(6), 474-483.

Hamula, C. L. A., Zhang, H. Q., Li, F., Wang, Z. X., Le, X. C., & Li, X. F. (2011). Selection and analytical applications of aptamers binding microbial pathogens. *Trac-Trends in Analytical Chemistry, 30*(10), 1587-1597.

Hansen, R. R., Hinestrosa, J. P., Shubert, K. R., Morrell-Falvey, J. L., Pelletier, D. A., Messman, J. M.*, et al.* (2013). Lectin-Functionalized Poly(glycidyl methacrylate)-block-poly(vinyldimethyl azlactone) Surface Scaffolds for High Avidity Microbial Capture. *Biomacromolecules, 14*(10), 3742-3748.

Hansson, L., Wallbrandt, P., Andersson, J. O., Bystrom, M., Backman, A., Carlstein, A.*, et al.* (1995). Carbohydrate Specificity of the *Escherichia coli* P-Pilus PapG Protein is Mediated by its N-terminal Part. *Biochimica Et Biophysica Acta-General Subjects, 1244*(2-3), 377-383.

Harper, J. C., Brozik, S. M., Brinker, C. J., & Kaehr, B. (2012). Biocompatible Microfabrication of 3D Isolation Chambers for Targeted Confinement of Individual Cells and Their Progeny.

Haun, J. B., Yoon, T. J., Lee, H., & Weissleder, R. (2010). Magnetic nanoparticle biosensors. *Wiley Interdisciplinary Reviews-Nanomedicine and Nanobiotechnology, 2*(3), 291-304.

Hayashi, H., & Hakuta, Y. (2010). Hydrothermal Synthesis of Metal Oxide Nanoparticles in Supercritical Water. *Materials, 3*(7), 3794-3817.

He, Q., Hemme, C. L., Jiang, H. L., He, Z. L., & Zhou, J. Z. (2011). Mechanisms of enhanced cellulosic bioethanol fermentation by co-cultivation of Clostridium and Thermoanaerobacter spp. *Bioresource Technology, 102*(20), 9586-9592.

Hemery, G., Garanger, E., Lecommandoux, S., Wong, A. D., Gillies, E. R., Pedrono, B.*, et al.* (2015). Thermosensitive polymer-grafted iron oxide nanoparticles studied by in situ dynamic light backscattering under magnetic hyperthermia. *Journal of Physics D-Applied Physics, 48*(49), 13.

Hetzer, M., Chen, G. J., Barner-Kowollik, C., & Stenzel, M. H. (2010). Neoglycopolymers Based on 4-Vinyl-1,2,3-Triazole Monomers Prepared by Click Chemistry. *Macromolecular Bioscience, 10*(2), 119-126.

Hevey, R. (2019). Strategies for the Development of Glycomimetic Drug Candidates. *Pharmaceuticals, 12*(2), 26.

Hmelo, L. R., Borlee, B. R., Almblad, H., Love, M. E., Randall, T. E., Tseng, B. S.*, et al.* (2015). Precision-engineering the Pseudomonas aeruginosa genome with two-step allelic exchange. *Nature Protocols, 10*(11), 1820-1841.

Hoang, T. T., Karkhoff-Schweizer, R. R., Kutchma, A. J., & Schweizer, H. P. (1998). A broad-host-range Flp-FRT recombination system for site-specific excision of chromosomally-located DNA sequences: application for isolation of unmarked Pseudomonas aeruginosa mutants. *Gene, 212*(1), 77-86.

Holden, N., Blomfield, I. C., Uhlin, B. E., Totsika, M., Kulasekara, D. H., & Gally, D. L. (2007). Comparative analysis of FimB and FimE recombinase activity. *Microbiology-Sgm, 153*, 4138-4149.

Hoshino, K., Huang, Y. Y., Lane, N., Huebschman, M., Uhr, J. W., Frenkel, E. P.*, et al.* (2011). Microchip-based immunomagnetic detection of circulating tumor cells. *Lab on a Chip, 11*(20), 3449-3457.

Hospenthal, M. K., Costa, T. R. D., & Waksman, G. (2017). A comprehensive guide to pilus biogenesis in Gram-negative bacteria. *Nature Reviews Microbiology, 15*(6), 365-379.

Houillot, L., Bui, C., Save, M., Charleux, B., Farcet, C., Moire, C.*, et al.* (2007). Synthesis of well-defined polyacrylate particle dispersions in organic medium using simultaneous RAFT polymerization and self-assembly of block copolymers. A strong influence of the selected thiocarbonylthio chain transfer agent. *Macromolecules, 40*(18), 6500-6509.

Hu, F. X., Neoh, K. G., Cen, L., & Kang, E. T. (2006). Cellular response to magnetic nanoparticles "PEGylated" via surface-initiated atom transfer radical polymerization. *Biomacromolecules, 7*(3), 809-816.

Huang, Y. F., Wang, Y. F., & Yan, X. P. (2010). Amine-Functionalized Magnetic Nanoparticles for Rapid Capture and Removal of Bacterial Pathogens. *Environmental Science & Technology, 44*(20), 7908-7913.

Hufschmid, R., Arami, H., Ferguson, R. M., Gonzales, M., Teeman, E., Brush, L. N.*, et al.* (2015). Synthesis of phase-pure and monodisperse iron oxide nanoparticles by thermal decomposition. *Nanoscale, 7*(25), 11142-11154.

Hyeon, T., Lee, S. S., Park, J., Chung, Y., & Bin Na, H. (2001). Synthesis of highly crystalline and monodisperse maghemite nanocrystallites without a size-selection process. *Journal of the American Chemical Society, 123*(51), 12798-12801.

Imberty, A., Chabre, Y. M., & Roy, R. (2008). Glycomimetics and glycodendrimers as high affinity microbial anti-adhesins. *Chemistry-a European Journal, 14*(25), 7490-7499.

Imberty, A., & Varrot, A. (2008). Microbial recognition of human cell surface glycoconjugates. *Current Opinion in Structural Biology, 18*(5), 567-576.

Intorasoot, S., Tharinjaroen, C. S., Phunpae, P., Butr-Indr, B., Anukool, U., Intachai, K.*, et al.* (2016). Novel potential diagnostic test for Mycobacterium tuberculosis complex using combined immunomagnetic separation (IMS) and PCR-CTPP. *J Appl Microbiol, 121*(2), 528-538.

Ishino, Y., Shinagawa, H., Makino, K., Amemura, M., & Nakata, A. (1987). Nucleotide sequence of the iap gene responsible for the alkaline-phosphatase isozyme conversion in *Escherichia coli* and identification of the gene product. *J Bacteriol, 169*(12), 5429-5433.

Jan, M., Chao, M. P., Cha, A. C., Alizadeh, A. A., Gentles, A. J., Weissman, I. L.*, et al.* (2011). Prospective separation of normal and leukemic stem cells based on differential expression of TIM3, a human acute myeloid leukemia stem cell marker. *Proceedings of the National Academy of Sciences of the United States of America, 108*(12), 5009-5014.

Jasinska, U. T., Skapska, S., Owczarek, L., Dekowska, A., & Lewinska, D. (2018). Immobilization of Bifidobacterium infantis Cells in Selected Hydrogels as a

Method of Increasing Their Survival in Fermented Milkless Beverages. *Journal of Food Quality*, 11.

Jensen, K. M. O., Andersen, H. L., Tyrsted, C., Bojesen, E. D., Dippel, A. C., Lock, N.*, et al.* (2014). Mechanisms for Iron Oxide Formation under Hydrothermal Conditions: An in Situ Total Scattering Study. *Acs Nano, 8*(10), 10704-10714.

Jeyaprakash, A. A., Jayashree, G., Mahanta, S. K., Swaminathan, C. P., Sekar, K., Surolia, A.*, et al.* (2005). Structural basis for the energetics of jacalin-sugar interactions: Promiscuity versus specificity. *Journal of Molecular Biology, 347*(1), 181-188.

Jia, X. Q., Liu, C., Song, H., Ding, M. Z., Du, J., Ma, Q.*, et al.* (2016). Design, analysis and application of synthetic microbial consortia. *Synthetic and Systems Biotechnology, 1*(2), 109-117.

Jiang, W., Bikard, D., Cox, D., Zhang, F., & Marraffini, L. A. (2013a). CRISPR-assisted editing of bacterial genomes. *Nature Biotechnology, 31*(3), 233-239.

Jiang, X. Y., Li, Y. J., Lu, G. L., & Huang, X. Y. (2013b). A novel poly(N-vinylcaprolactam)-based well-defined amphiphilic graft copolymer synthesized by successive RAFT and ATRP. *Polymer Chemistry, 4*(5), 1402-1411.

Jiang, Y. J., Wu, R. F., Zhou, J., He, A. Y., Xu, J. X., Xin, F. X.*, et al.* (2019). Recent advances of biofuels and biochemicals production from sustainable resources using co-cultivation systems. *Biotechnology for Biofuels, 12*, 12.

Jiao, Y., & Akcora, P. (2014). Accelerated Brush Growth on Nanoparticle Surfaces by Reversible Addition-Fragmentation Chain Transfer Polymerization. *Journal of Polymer Science Part a-Polymer Chemistry, 52*(12), 1700-1705.

Jinek, M., Chylinski, K., Fonfara, I., Hauer, M., Doudna, J. A., & Charpentier, E. (2012). A Programmable Dual-RNA-Guided DNA Endonuclease in Adaptive Bacterial Immunity. *Science, 337*(6096), 816-821.

Jittawuttipoka, T., Buranajitpakorn, S., Fuangthong, M., Schweizer, H. P., Vattanaviboon, P., & Mongkolsuk, S. (2009). Mini-Tn7 vectors as genetic tools for gene cloning at a single copy number in an industrially important and phytopathogenic bacteria, Xanthomonas spp. *FEMS Microbiol Lett, 298*(1), 111-117.

Johnson, A. O., Gonzalez-Villanueva, M., Tee, K. L., & Wong, T. S. (2018). An Engineered Constitutive Promoter Set with Broad Activity Range for Cupriavidus necator H16. *Acs Synthetic Biology, 7*(8), 1918-1928.

Jono, K., Nagao, M., Oh, T., Sonoda, S., Hoshino, Y., & Miura, Y. (2018). Controlling the lectin recognition of glycopolymers via distance arrangement of sugar blocks. *Chemical Communications, 54*(1), 82-85.

Jun, Y. W., Huh, Y. M., Choi, J. S., Lee, J. H., Song, H. T., Kim, S.*, et al.* (2005). Nanoscale size effect of magnetic nanocrystals and their utilization for cancer diagnosis via magnetic resonance imaging. *Journal of the American Chemical Society, 127*(16), 5732-5733.

Jursic, B. S., & Zdravkovski, Z. (1993). A simple preparation of amides from acids by heating thier mixture. *Synthetic Communications, 23*(19), 2761-2770.

Kalas, V., Hibbing, M. E., Maddirala, A. R., Chugani, R., Pinkner, J. S., Mydock-McGrane, L. K.*, et al.* (2018). Structure-based discovery of glycomimetic FmlH ligands as inhibitors of bacterial adhesion during urinary tract infection. *Proceedings of the National Academy of Sciences of the United States of America, 115*(12), E2819-E2828.

Kalichuk, V., Behar, G., Renodon-Corniere, A., Danovski, G., Obal, G., Barbet, J.*, et al.* (2016). The archaeal "7 kDa DNA-binding" proteins: extended characterization of an old gifted family. *Scientific Reports, 6*, 10.

Kang, M. K., Mao, W., & Yoo, H. S. (2018). Surface-initiated atom transfer radical polymerization of cationic corona on iron oxide nanoparticles for magnetic sorting of macrophages. *Biomaterials Science, 6*(8), 2248-2260.

Kavunja, H. W., Voss, P. G., Wang, J. L., & Huang, X. F. (2015). Identification of Lectins from Metastatic Cancer Cells through Magnetic Glyconanoparticles. *Israel Journal of Chemistry, 55*(3-4), 423-436.

Kayal, S., & Ramanujan, R. V. (2010). Doxorubicin loaded PVA coated iron oxide nanoparticles for targeted drug delivery. *Materials Science & Engineering C-Materials for Biological Applications, 30*(3), 484-490.

Ke, B. B., Wan, L. S., Zhang, W. X., & Xu, Z. K. (2010). Controlled synthesis of linear and comb-like glycopolymers for preparation of honeycomb-patterned films. *Polymer, 51*(10), 2168-2176.

Kekalo, K., Koo, K., Zeitchick, E., & Baker, I. (2012). Microemulsion Synthesis of Iron Core/Iron Oxide Shell Magnetic Nanoparticles and Their Physicochemical Properties. *Materials Research Society symposia proceedings. Materials Research Society, 1416*.

Kennedy, D., & Wilkinson, M. G. (2017). Application of Flow Cytometry to the Detection of Pathogenic Bacteria. *Current Issues in Molecular Biology, 23*, 21-38.

Kim, D. K., Mikhaylova, M., Zhang, Y., & Muhammed, M. (2003). Protective coating of superparamagnetic iron oxide nanoparticles. *Chemistry of Materials, 15*(8), 1617-1627.

Kim, J., Webb, A. M., Kershner, J. P., Blaskowski, S., & Copley, S. D. (2014). A versatile and highly efficient method for scarless genome editing in Escherichia coli and Salmonella enterica. *Bmc Biotechnology, 14*.

Kim, U., & Soh, H. T. (2009). Simultaneous sorting of multiple bacterial targets using integrated Dielectrophoretic-Magnetic Activated Cell Sorter. *Lab on a Chip, 9*(16), 2313-2318.

Kim, Y. S., Song, M. Y., Jurng, J., & Kim, B. C. (2013). Isolation and characterization of DNA aptamers against Escherichia coli using a bacterial cell-systematic evolution of ligands by exponential enrichment approach. *Analytical Biochemistry, 436*(1), 22-28.

Kirkeby, S., Hansen, A. K., d'Apice, A., & Moe, D. (2006). The galactophilic lectin (PA-IL, gene LecA) from Pseudomonas aeruginosa. Its binding requirements and the localization of lectin receptors in various mouse tissues. *Microbial Pathogenesis, 40*(5), 191-197.

Kleinstiver, B. P., Prew, M. S., Tsai, S. Q., Topkar, V. V., Nguyen, N. T., Zheng, Z. L*., et al.* (2015). Engineered CRISPR-Cas9 nucleases with altered PAM specificities. *Nature, 523*(7561), 481-U249.

Kolb, H. C., Finn, M. G., & Sharpless, K. B. (2001). Click chemistry: Diverse chemical function from a few good reactions. *Angewandte Chemie-International Edition, 40*(11), 2004-+.

Konkolewicz, D., Wang, Y., Zhong, M. J., Krys, P., Isse, A. A., Gennaro, A*., et al.* (2013). Reversible-Deactivation Radical Polymerization in the Presence of Metallic Copper. A Critical Assessment of the SARA ATRP and SET-LRP Mechanisms. *Macromolecules, 46*(22), 8749-8772.

Korea, C. G., Ghigo, J. M., & Beloin, C. (2011). The sweet connection: Solving the riddle of multiple sugar-binding fimbrial adhesins in Escherichia coli. *Bioessays, 33*(4), 300-311.

Kouki, A., Haataja, S., Loimaranta, V., Pulliainen, A. T., Nilsson, U. J., & Finne, J. (2011). Identification of a novel streptococcal adhesin P (SadP) protein recognizing

galactosyl-alpha 1-4-galactose-containing glycoconjugates. Convergent evolution of bacterial pathogens to binding to the same host receptor *Journal of Biological Chemistry, 286*(45), 38854-38864.

Krogfelt, K., Bergman, B., & Klemm, P. (1990). Direct Evidence that the FimH Protein Is the Mannose-Specific Adhesin of Escherichia coli Type 1 Fimbriae. *Infect Immun, 58*(6), 1995-1998.

Krushkal, J., Leang, C., Barbe, J., Qu, Y. H., Yan, B., Puljic, M.*, et al.* (2009). Diversity of promoter elements in a Geobacter sulfurreducens mutant adapted to disruption in electron transfer. *Functional & Integrative Genomics, 9*(1), 15-25.

Kulbachinskiy, A. V. (2007). Methods for selection of aptamers to protein targets. *Biochemistry-Moscow, 72*(13), 1505-1518.

Kumar, V., Nath, G., Kotnala, R. K., Saxena, P. S., & Srivastava, A. (2013). Biofunctional magnetic nanotube probe for recognition and separation of specific bacteria from a mixed culture. *Rsc Advances, 3*(34), 14634-14641.

Kutcherlapati, S. N. R., Koyilapu, R., Boddu, U. M. R., Datta, D., Perali, R. S., Swamy, M. J.*, et al.* (2017a). Glycopolymer-Grafted Nanoparticles: Synthesis Using RAFT Polymerization and Binding Study with Lectin. *Macromolecules, 50*(18), 7309-7320.

Kutcherlapati, S. N. R., Yeole, N., Gadi, M. R., Perali, R. S., & Jana, T. (2017b). RAFT mediated one-pot synthesis of glycopolymer particles with tunable core-shell morphology. *Polymer Chemistry, 8*(8), 1371-1380.

Lachowicz, D., Szpak, A., Malek-Zietek, K. E., Kepczynski, M., Muller, R. N., Laurent, S.*, et al.* (2017). Biocompatible and fluorescent superparamagnetic iron oxide nanoparticles with superior magnetic properties coated with charged polysaccharide derivatives. *Colloids and Surfaces B-Biointerfaces, 150*, 402-407.

Ladmiral, V., Mantovani, G., Clarkson, G. J., Cauet, S., Irwin, J. L., & Haddleton, D. M. (2006). Synthesis of neoglycopolymers by a combination of "click chemistry" and living radical polymerization. *Journal of the American Chemical Society, 128*(14), 4823-4830.

Lakhin, A. V., Tarantul, V. Z., & Gening, L. V. (2013). Aptamers: Problems, Solutions and Prospects. *Acta Naturae, 5*(4), 34-43.

Lam, A. J., St-Pierre, F., Gong, Y. Y., Marshall, J. D., Cranfill, P. J., Baird, M. A.*, et al.* (2012). Improving FRET dynamic range with bright green and red fluorescent proteins. *Nature Methods, 9*(10), 1005-+.

Lam, A. J., St-Pierre, F., Gong, Y. Y., Marshall, J. D., McKeown, M. R., Schnitzer, M. J.*, et al.* (2013). Improving FRET Dynamic Range with Bright Green and Red Fluorescent Proteins. *Biophysical Journal, 104*(2), 683A-683A.

Lambertsen, L., Sternberg, C., & Molin, S. (2004). Mini-Tn7 transposons for site-specific tagging of bacteria with fluorescent proteins. *Environmental Microbiology, 6*(7), 726-732.

Lander, E. S., Int Human Genome Sequencing, C., Linton, L. M., Birren, B., Nusbaum, C., Zody, M. C.*, et al.* (2001). Initial sequencing and analysis of the human genome. *Nature, 409*(6822), 860-921.

Langermann, S., Möllby, R., Burlein, J. E., Palaszynski, S. R., Auguste, C. G., DeFusco, A.*, et al.* (2000). Vaccination with FimH Adhesin Protects Cynomolgus Monkeys from Colonization and Infection by Uropathogenic Eschevichia coli.

Lara, A. R., Galindo, E., Ramirez, O. T., & Palomares, L. A. (2006). Living with heterogeneities in bioreactors. *Molecular Biotechnology, 34*(3), 355-381.

Larnaudie, S. C., Brendel, J. C., Jolliffe, K. A., & Perrier, S. (2016). Cyclic Peptide-Polymer Conjugates: Grafting-to vs Grafting-From. *Journal of Polymer Science Part a-Polymer Chemistry, 54*(7), 1003-1011.

Lassenberger, A., Bixner, O., Gruenewald, T., Lichtenegger, H., Zirbs, R., & Reimhult, E. (2016). Evaluation of High-Yield Purification Methods on Monodisperse PEG-Grafted Iron Oxide Nanoparticles. *Langmuir, 32*(17), 4259-4269.

Laughlin, S. T., & Bertozzi, C. R. (2009). Imaging the glycome. *Proceedings of the National Academy of Sciences of the United States of America, 106*(1), 12-17.

Laurent, S., Forge, D., Port, M., Roch, A., Robic, C., Elst, L. V.*, et al.* (2008). Magnetic iron oxide nanoparticles: Synthesis, stabilization, vectorization, physicochemical characterizations, and biological applications. *Chemical Reviews, 108*(6), 2064-2110.

Lee, D. J., Minchin, S. D., & Busby, S. J. W. (2012). Activating Transcription in Bacteria. In S. Gottesman, C. S. Harwood & O. Schneewind (Eds.), *Annual Review of Microbiology, Vol 66* (Vol. 66, pp. 125-152). Palo Alto: Annual Reviews.

Lee, R. T., & Lee, Y. C. (2000). Affinity enhancement by multivalent lectin-carbohydrate interaction. *Glycoconjugate Journal, 17*(7-9), 543-551.

Lee, S. B., Russell, A. J., & Matyjaszewski, K. (2003). ATRP synthesis of amphiphilic random, gradient, and block copolymers of 2-(dimethylamino)ethyl methacrylate and n-butyl methacrylate in aqueous media. *Biomacromolecules, 4*(5), 1386-1393.

Leelavatcharamas, V., Emery, A. N., & AlRubeai, M. (1997). Use of flow cytometry for the monitoring of growth and productivity in batch culture of Chinese Hamster Ovary cells. *Animal Cell Technology: Basic & Applied Aspects, Vol 8*, 55-60.

Leire, E., Amaral, S. P., Louzao, I., Winzer, K., Alexander, C., Fernandez-Megia, E.*, et al.* (2016). Dendrimer mediated clustering of bacteria: improved aggregation and evaluation of bacterial response and viability. *Biomaterials Science, 4*(6), 998-1006.

Lester, E., Blood, P., Denyer, J., Giddings, D., Azzopardi, B., & Poliakoff, M. (2006). Reaction engineering: The supercritical water hydrothermal synthesis of nano-particles. *Journal of Supercritical Fluids, 37*(2), 209-214.

Levere, M. E., Nguyen, N. H., Leng, X. F., & Percec, V. (2013). Visualization of the crucial step in SET-LRP. *Polymer Chemistry, 4*(5), 1635-1647.

Li, C. Z., & Benicewicz, B. C. (2005). alpha-Cyanobenzyl dithioester reversible addition-fragmentation chain-transfer agents for controlled radical polymerizations. *Journal of Polymer Science Part a-Polymer Chemistry, 43*(7), 1535-1543.

Li, H. F., Lin, J. M., Su, R. G., Cai, Z. W., & Uchiyama, K. (2005). A polymeric master replication technology for mass fabrication of poly(dimethylsiloxane) microfluidic devices. *Electrophoresis, 26*(9), 1825-1833.

Li, L., Jiang, W., Luo, K., Song, H. M., Lan, F., Wu, Y.*, et al.* (2013). Superparamagnetic Iron Oxide Nanoparticles as MRI contrast agents for Non-invasive Stem Cell Labeling and Tracking. *Theranostics, 3*(8), 595-615.

Li, L., Kang, E., & Neoh, K. (2008). Preparation of well-defined polymer-silicon wafer hybrids via surface-initiated RAFT-mediated process. *Applied Surface Science, 254*(9), 2600-2604.

Li, L. N., Huang, J. J., & Zhang, Y. W. (2018a). Synthesis of Comb-Like Macromolecules via Semi-Batch Miniemulsion RAFT Polymerizations. *Macromolecular Chemistry and Physics, 219*(18), 6.

Li, L. Y., Li, Q. J., Liao, Z. Y., Sun, Y., Cheng, Q. S., Song, Y.*, et al.* (2018b). Magnetism-Resolved Separation and Fluorescence Quantification for Near-Simultaneous Detection of Multiple Pathogens. *Analytical Chemistry, 90*(15), 9621-9628.

Li, Q., Kartikowati, C. W., Horie, S., Ogi, T., Iwaki, T., & Okuyama, K. (2017). Correlation between particle size/domain structure and magnetic properties of highly crystalline Fe3O4 nanoparticles. *Scientific Reports, 7*, 7.

Li, S. P., & Gao, C. (2013). Dendritic molecular brushes: synthesis via sequential RAFT polymerization and cage effect for fluorophores. *Polymer Chemistry, 4*(16), 4450-4460.

Li, X., Bao, M. M., Weng, Y. Y., Yang, K., Zhang, W. D., & Chen, G. J. (2014). Glycopolymer-coated iron oxide nanoparticles: shape-controlled synthesis and cellular uptake. *Journal of Materials Chemistry B, 2*(34), 5569-5575.

Li, X. M., Wei, J. R., Aifantis, K. E., Fan, Y. B., Feng, Q. L., Cui, F. Z.*, et al.* (2016). Current investigations into magnetic nanoparticles for biomedical applications. *Journal of Biomedical Materials Research Part A, 104*(5), 1285-1296.

Li, Y. T., Armes, S. P., Jin, X. P., & Zhu, S. P. (2003). Direct synthesis of well-defined quaternized homopolymers and diblock copolymers via ATRP in protic media. *Macromolecules, 36*(22), 8268-8275.

Li, Z., Zhang, K., Ma, J., Cheng, C., & Wooley, K. L. (2009). Facile Syntheses of Cylindrical Molecular Brushes by a Sequential RAFT and ROMP "Grafting-Through" Methodology. *Journal of Polymer Science Part a-Polymer Chemistry, 47*(20), 5557-5563.

Li, Z. H., Wang, X. N., & Zhang, H. R. (2019a). Balancing the non-linear rosmarinic acid biosynthetic pathway by modular co-culture engineering. *Metabolic Engineering, 54*, 1-11.

Li, Z. M., Ma, J. Y., Ruan, J., & Zhuang, X. (2019b). Using Positively Charged Magnetic Nanoparticles to Capture Bacteria at Ultralow Concentration. *Nanoscale Research Letters, 14*, 8.

Liang, P. P., Xu, Y. W., Zhang, X. Y., Ding, C. H., Huang, R., Zhang, Z.*, et al.* (2015). CRISPR/Cas9-mediated gene editing in human tripronuclear zygotes. *Protein & Cell, 6*(5), 363-372.

Lim, M. C., Park, J. Y., Park, K., Ok, G., Jang, H. J., & Choi, S. W. (2017). An automated system for separation and concentration of food-borne pathogens using immunomagnetic separation. *Food Control, 73*, 1541-1547.

Limoli, D. H., Sladek, J. A., Fuller, L. A., Singh, A. K., & King, S. J. (2011). BgaA acts as an adhesin to mediate attachment of some pneumococcal strains to human epithelial cells. *Microbiology-Sgm, 157*, 2369-2381.

Lin, C. C., Yeh, Y. C., Yang, C. Y., Chen, G. F., Chen, Y. C., Wu, Y. C.*, et al.* (2003). Quantitative analysis of multivalent interactions of carbohydrate-encapsulated gold nanoparticles with concanavalin A. *Chemical Communications*(23), 2920-2921.

Lin, K., & Kasko, A. M. (2015). Multivalent 3D Display of Glycopolymer Chains for Enhanced Lectin Interaction. *Bioconjugate Chemistry, 26*(8), 1504-1512.

Lis, H., & Sharon, N. (1998). Lectins: Carbohydrate-specific proteins that mediate cellular recognition. *Chemical Reviews, 98*(2), 637-674.

Liu, B. L., Kazlauciunas, A., Guthrie, J. T., & Perrier, S. (2005). One-pot hyperbranched polymer synthesis mediated by reversible addition fragmentation chain transfer (RAFT) polymerization. *Macromolecules, 38*(6), 2131-2136.

Liu, G. Q., Cai, M. R., Wang, X. L., Zhou, F., & Liu, W. M. (2014). Core-Shell-Corona-Structured Polyelectrolyte Brushes-Grafting Magnetic Nanoparticles for Water Harvesting. *Acs Applied Materials & Interfaces, 6*(14), 11625-11632.

Liu, S. X., Liu, J. B., Hou, J. Y., Chao, N., Gai, Y., & Jiang, X. N. (2017). Three steps in one pot: biosynthesis of 4-hydroxycinnamyl alcohols using immobilized whole cells

of two genetically engineered Escherichia coli strains. *Microbial Cell Factories, 16*, 12.

Liu, Z. F., Zhu, Y., Ye, W. L., Wu, T., Miao, D. Y., Deng, W.*, et al.* (2019). Synthesis of well-defined glycopolymers with highly ordered sugar units in the side chain via combining CuAAC reaction and ROMP: lectin interaction study in homo- and hetero-glycopolymers. *Polymer Chemistry, 10*(29), 4006-4016.

Lopez-Quintela, M. A. (2003). Synthesis of nanomaterials in microemulsions: formation mechanisms and growth control. *Current Opinion in Colloid & Interface Science, 8*(2), 137-144.

Lorandi, F., Fantin, M., Isse, A. A., & Gennaro, A. (2015). RDRP in the presence of Cu-0: The fate of Cu(I) proves the inconsistency of SET-LRP mechanism. *Polymer, 72*, 238-245.

Louzao, I., Sui, C., Winzer, K., Fernandez-Trillo, F., & Alexander, C. (2015). Cationic polymer mediated bacterial clustering: Cell-adhesive properties of homo- and copolymers. *European Journal of Pharmaceutics and Biopharmaceutics, 95*, 47-62.

LoVullo, E. D., Molins-Schneekloth, C. R., Schweizer, H. P., & Pavelka, M. S. (2009). Single-copy chromosomal integration systems for Francisella tularensis. *Microbiology-Sgm, 155*, 1152-1163.

Lowe, A. B., & McCormick, C. L. (2007). Reversible addition-fragmentation chain transfer (RAFT) radical polymerization and the synthesis of water-soluble (co)polymers under homogeneous conditions in organic and aqueous media. *Progress in Polymer Science, 32*(3), 283-351.

Lowe, A. B., Sumerlin, B. S., Donovan, M. S., & McCormick, C. L. (2002). Facile preparation of transition metal nanoparticles stabilized by well-defined (Co)polymers synthesized via aqueous reversible addition-fragmentation chain transfer polymerization. *Journal of the American Chemical Society, 124*(39), 11562-11563.

Lowe, A. B., Sumerlin, B. S., & McCormick, C. L. (2003). The direct polymerization of 2-methacryloxyethyl glucoside via aqueous reversible addition-fragmentation chain transfer (RAFT) polymerization. *Polymer, 44*(22), 6761-6765.

Lui, L. T., Xue, X., Sui, C., Brown, A., Pritchard, D. I., Halliday, N.*, et al.* (2013). Bacteria clustering by polymers induces the expression of quorum-sensing-controlled phenotypes. *Nature Chemistry, 5*(12), 1058-1065.

Luigjes, B., Woudenberg, S. M. C., de Groot, R., Meeldijk, J. D., Galvis, H. M. T., de Jong, K. P.*, et al.* (2011). Diverging Geometric and Magnetic Size Distributions of Iron Oxide Nanocrystals. *Journal of Physical Chemistry C, 115*(30), 14598-14605.

Lundquist, J. J., & Toone, E. J. (2002). The cluster glycoside effect. *Chemical Reviews, 102*(2), 555-578.

Luo, Y., Gu, Y., Feng, R. Y., Brash, J., Eissa, A. M., Haddleton, D. M.*, et al.* (2019). Synthesis of glycopolymers with specificity for bacterial strains via bacteria-guided polymerization. *Chemical Science, 10*(20), 5251-5257.

Lutz, R., & Bujard, H. (1997). Independent and tight regulation of transcriptional units in Escherichia coli via the LacR/O, the TetR/O and AraC/I-1-I-2 regulatory elements. *Nucleic Acids Research, 25*(6), 1203-1210.

Ma, X. X., Tao, H. Q., Yang, K., Feng, L. Z., Cheng, L., Shi, X. Z.*, et al.* (2012). A functionalized graphene oxide-iron oxide nanocomposite for magnetically targeted drug delivery, photothermal therapy, and magnetic resonance imaging. *Nano Research, 5*(3), 199-212.

Machens, F., Balazadeh, S., Mueller-Roeber, B., & Messerschmidt, K. (2017). Synthetic Promoters and Transcription Factors for Heterologous Protein Expression in

Saccharomyces cerevisiae. *Frontiers in Bioengineering and Biotechnology, 5*, 11.

Magennis, E. P., Fernandez-Trillo, F., Sui, C., Spain, S. G., Bradshaw, D. J., Churchley, D.*, et al.* (2014). Bacteria-instructed synthesis of polymers for self-selective microbial binding and labelling. *Nature Materials, 13*(7), 748-755.

Magennis, E. P., Francini, N., Mastrotto, F., Catania, R., Redhead, M., Fernandez-Trillo, F.*, et al.* (2017). Polymers for binding of the gram-positive oral pathogen Streptococcus mutans. *Plos One, 12*(7), 23.

Maier-Hauff, K., Ulrich, F., Nestler, D., Niehoff, H., Wust, P., Thiesen, B.*, et al.* (2011). Efficacy and safety of intratumoral thermotherapy using magnetic iron-oxide nanoparticles combined with external beam radiotherapy on patients with recurrent glioblastoma multiforme. *Journal of Neuro-Oncology, 103*(2), 317-324.

Maity, D., & Agrawal, D. C. (2007). Synthesis of iron oxide nanoparticles under oxidizing environment and their stabilization in aqueous and non-aqueous media. *Journal of Magnetism and Magnetic Materials, 308*(1), 46-55.

Majewski, A. P., Schallon, A., Jerome, V., Freitag, R., Muller, A. H. E., & Schmalz, H. (2012). Dual-Responsive Magnetic Core-Shell Nanoparticles for Nonviral Gene Delivery and Cell Separation. *Biomacromolecules, 13*(3), 857-866.

Malakootikhah, J., Rezayan, A. H., Negandari, B., Nasseri, S., & Rastegar, H. (2017). Glucose reinforced Fe3O4@cellulose mediated amino acid: Reusable magnetic glyconanoparticles with enhanced bacteria capture efficiency. *Carbohydrate Polymers, 170*, 190-197.

Mali, P., Yang, L. H., Esvelt, K. M., Aach, J., Guell, M., DiCarlo, J. E.*, et al.* (2013). RNA-Guided Human Genome Engineering via Cas9. *Science, 339*(6121), 823-826.

Mallikaratchy, P. R., Ruggiero, A., Gardner, J. R., Kuryavyi, V., Maguire, W. F., Heaney, M. L.*, et al.* (2011). A multivalent DNA aptamer specific for the B-cell receptor on human lymphoma and leukemia. *Nucleic Acids Research, 39*(6), 2458-2469.

Mandal, D. K., Bhattacharyya, L., Koenig, S. H., Brown, R. D., Oscarson, S., & Brewer, C. F. (1994). Studies of the binding-specificity of Concanavalin A - Nature of extended binding-site for asparagine-linked carbohydrates. *Biochemistry, 33*(5), 1157-1162.

Martinez-Alarcon, D., Blanco-Labra, A., & Garcia-Gasca, T. (2018). Expression of Lectins in Heterologous Systems. *International Journal of Molecular Sciences, 19*(2), 16.

Marton, S., Cleto, F., Krieger, M. A., & Cardoso, J. (2016). Isolation of an Aptamer that Binds Specifically to E. coli. *Plos One, 11*(4), 17.

Matyjaszewski, K. (2012). Atom Transfer Radical Polymerization (ATRP): Current Status and Future Perspectives. *Macromolecules, 45*(10), 4015-4039.

Matyjaszewski, K., & Davis, T. P. (2002). *Handbook of Radical Polymerisation*. Hoboken: John Wiley & Sons.

Matyjaszewski, K., Pintauer, T., & Gaynor, S. (2000a). Removal of copper-based catalyst in atom transfer radical polymerization using ion exchange resins. *Macromolecules, 33*(4), 1476-1478.

Matyjaszewski, K., & Spanswick, J. (2005). Controlled/living radical polymerisation. *Materials Today, 8*(3), 26-33.

Matyjaszewski, K., Ziegler, M. J., Arehart, S. V., Greszta, D., & Pakula, T. (2000b). Gradient copolymers by atom transfer radical copolymerization. *Journal of Physical Organic Chemistry, 13*(12), 775-786.

Maver, U., Bele, M., Makovec, D., Campelj, S., Jamnik, J., & Gaberscek, M. (2009). Incorporation and release of drug into/from superparamagnetic iron oxide

nanoparticles. *Journal of Magnetism and Magnetic Materials, 321*(19), 3187-3192.

Mayadunne, R. T. A., Rizzardo, E., Chiefari, J., Krstina, J., Moad, G., Postma, A.*, et al.* (2000). Living polymers by the use of trithiocarbonates as reversible addition-fragmentation chain transfer (RAFT) agents: ABA triblock copolymers by radical polymerization in two steps. *Macromolecules, 33*(2), 243-245.

McCarty, N. S., & Ledesma-Amaro, R. (2019). Synthetic Biology Tools to Engineer Microbial Communities for Biotechnology. *Trends in Biotechnology, 37*(2), 181-197.

McClain, M. S., Blomfield, I. C., & Eisenstein, B. I. (1991). Roles of fimB and fimE in site-specific DNA inversion associated with phase variation of type 1 fimbriae in Escherichia coli.

McDonald, J. C., Duffy, D. C., Anderson, J. R., Chiu, D. T., Wu, H. K., Schueller, O. J. A.*, et al.* (2000). Fabrication of microfluidic systems in poly(dimethylsiloxane). *Electrophoresis, 21*(1), 27-40.

Melnyk, R. A., Clark, I. C., Liao, A., & Coates, J. D. (2014). Transposon and Deletion Mutagenesis of Genes Involved in Perchlorate Reduction in Azospira suillum PS. *Mbio, 5*(1), 12.

Meredith, T. C., Wang, H., Beaulieu, P., Grundling, A., & Roemer, T. (2012). Harnessing the power of transposon mutagenesis for antibacterial target identification and evaluation. *Mobile genetic elements, 2*(4), 171-178.

Miao, Z. Y., Li, D., Zheng, Z. Q., & Zhang, Q. (2019). Synthesis of chitosan-mimicking cationic glycopolymers by Cu(0)-LRP for efficient capture and killing of bacteria. *Polymer Chemistry, 10*(29), 4059-4066.

Mihalcescu, I., Gateau, M. V., Chelli, B., Pinel, C., & Ravanat, J. L. (2015). Green autofluorescence, a double edged monitoring tool for bacterial growth and activity in micro-plates. *Physical Biology, 12*(6), 11.

Mikhaylova, M., Jo, Y. S., Kim, D. K., Bobrysheva, N., Andersson, Y., Eriksson, T.*, et al.* (2004a). The effect of biocompatible coating layers on magnetic properties of superparamagnetic iron oxide nanoparticles. *Hyperfine Interactions, 156*(1), 257-263.

Mikhaylova, M., Kim, D. K., Berry, C. C., Zagorodni, A., Toprak, M., Curtis, A. S. G.*, et al.* (2004b). BSA immobilization on amine-functionalized superparamagnetic iron oxide nanoparticles. *Chemistry of Materials, 16*(12), 2344-2354.

Miltenyi, S., Muller, W., Weichel, W., & Radbruch, A. (1990). High-Gradient magentic cell separation with MACS. *Cytometry, 11*(2), 231-238.

Milton, D. L., Otoole, R., Horstedt, P., & WolfWatz, H. (1996). Flagellin A is essential for the virulence of Vibrio anguillarum. *J Bacteriol, 178*(5), 1310-1319.

Minoda, M., Otsubo, T., Yamamoto, Y., Zhao, J. X., Honda, Y., Tanaka, T.*, et al.* (2019). The First Synthesis of Periodic and Alternating Glycopolymers by RAFT Polymerization: A Novel Synthetic Pathway for Glycosaminoglycan Mimics. *Polymers, 11*(1), 14.

Mitchell, E., Houles, C., Sudakevitz, D., Wimmerova, M., Gautier, C., Perez, S.*, et al.* (2002). Structural basis for oligosaccharide-mediated adhesion of Pseudomonas aeruginosa in the lungs of cystic fibrosis patients. *Nature Structural Biology, 9*(12), 918-921.

Moad, G., & Rizzardo, E. (1995). Alkoxyamine-initiated living radical polymerization: Factors affecting alkoxyamine homolysis rates. *Macromolecules, 28*(26), 8722-8728.

Moad, G., Rizzardo, E., & Thang, S. H. (2008). Radical addition-fragmentation chemistry in polymer synthesis. *Polymer, 49*(5), 1079-1131.

Mojica, F. J. M., Diez-Villasenor, C., Soria, E., & Juez, G. (2000). Biological significance of a family of regularly spaced repeats in the genomes of Archaea, bacteria and mitochondria. *Mol Microbiol, 36*(1), 244-246.

Moon, J., Kim, G., Park, S. B., Lim, J., & Mo, C. (2015). Comparison of Whole-Cell SELEX Methods for the Identification of Staphylococcus Aureus-Specific DNA Aptamers. *Sensors, 15*(4), 8884-8897.

Morel, P., Stasiak, A., Ehrlich, S. D., & Cassuto, E. (1994). Effect of Length and Location of Heterologous Sequences on RecA-Mediated Strand Exchange. *Journal of Biological Chemistry, 269*(31), 19830-19835.

Mu, X. Q., & Bullitt, E. (2006). Structure and assembly of P-pili: A protruding hinge region used for assembly of a bacterial adhesion filament. *Proceedings of the National Academy of Sciences of the United States of America, 103*(26), 9861-9866.

Mulvey, M. A., Schilling, J. D., & Hultgren, S. J. (2001). Establishment of a persistent Escherichia coli reservoir during the acute phase of a bladder infection. *Infect Immun, 69*(7), 4572-4579.

Munoz-Bonilla, A., Marcelo, G., Casado, C., Teran, F. J., & Fernandez-Garcia, M. (2012). Preparation of glycopolymer-coated magnetite nanoparticles for hyperthermia treatment. *Journal of Polymer Science Part a-Polymer Chemistry, 50*(24), 5087-5096.

Munoz-Lopez, M., & Garcia-Perez, J. L. (2010). DNA Transposons: Nature and Applications in Genomics. *Current Genomics, 11*(2), 115-128.

Munoz, E. M., Correa, J., Fernandez-Megia, E., & Riguera, R. (2009). Probing the Relevance of Lectin Clustering for the Reliable Evaluation of Multivalent Carbohydrate Recognition. *Journal of the American Chemical Society, 131*(49), 17765-17767.

Munoz, E. M., Correa, J., Riguera, R., & Fernandez-Megia, E. (2013). Real-Time Evaluation of Binding Mechanisms in Multivalent Interactions: A Surface Plasmon Resonance Kinetic Approach. *Journal of the American Chemical Society, 135*(16), 5966-5969.

Nagao, M., Matsubara, T., Hoshino, Y., Sato, T., & Miura, Y. (2019). Topological Design of Star Glycopolymers for Controlling the Interaction with the Influenza Virus. *Bioconjugate Chemistry, 30*(4), 1192-1198.

Naismith, J. H., & Field, R. A. (1996). Structural basis of trimannoside recognition by concanavalin A. *Journal of Biological Chemistry, 271*(2), 972-976.

Nakamura, Y., & Yamago, S. (2015). Termination Mechanism in the Radical Polymerization of Methyl Methacrylate and Styrene Determined by the Reaction of Structurally Well-Defined Polymer End Radicals. *Macromolecules, 48*(18), 6450-6456.

Nam, K. H., Haitjema, C., Liu, X. Q., Ding, F., Wang, H. W., DeLisa, M. P.*, et al.* (2012). Cas5d Protein Processes Pre-crRNA and Assembles into a Cascade-like Interference Complex in Subtype I-C/Dvulg CRISPR-Cas System. *Structure, 20*(9), 1574-1584.

Narayanaswamy, V. P., Giatpaiboon, S. A., Uhrig, J., Orwin, P., Wiesmann, W., Baker, S. M.*, et al.* (2018). In Vitro activity of novel glycopolymer against clinical isolates of multidrug-resistant Staphylococcus aureus. *Plos One, 13*(1), 16.

Nebe-von-Caron, G., Stephens, P. J., Hewitt, C. J., Powell, J. R., & Badley, R. A. (2000). Analysis of bacterial function by multi-colour fluorescence flow cytometry and single cell sorting. *Journal of Microbiological Methods, 42*(1), 97-114.

Neurauter, A. A., Bonyhadi, M., Lien, E., Nokleby, L., Ruud, E., Camacho, S.*, et al.* (2007). Cell isolation and expansion using Dynabeads((R)). In A. Kumar, I. Y.

Galaev & B. Mattiasson (Eds.), *Cell Separation: Fundamentals, Analytical and Preparative Methods* (Vol. 106, pp. 41-73). Berlin: Springer-Verlag Berlin.

Newman, J. V., Burghoff, R. L., Pallesen, L., Krogfelt, K. A., Kristensen, C. S., Laux, D. C.*, et al.* (1994). Stimulation of Escherichia coli F-18Col- type-1 fimbriae synthesis by leuX. *FEMS Microbiol Lett, 122*(3), 281-287.

Ng, J. W., Chatenay, D., & Robert, J. (2010). Plasmid copy number noise in monoclonal populations of bacteria. *Physical Review E, 81*(1), 8.

Nguyen, N. H., Rosen, B. M., & Percec, V. (2010). SET-LRP of N,N-Dimethylacrylamide and of N-Isopropylacrylamide at 25 degrees C in Protic and in Dipolar Aprotic Solvents. *Journal of Polymer Science Part a-Polymer Chemistry, 48*(8), 1752-1763.

Nicolas, J., Guillaneuf, Y., Lefay, C., Bertin, D., Gigmes, D., & Charleux, B. (2013). Nitroxide-mediated polymerization. *Progress in Polymer Science, 38*(1), 63-235.

Nielson, R., Koehr, B., & Shear, J. B. (2009). Microreplication and Design of Biological Architectures Using Dynamic-Mask Multiphoton Lithography. *Small, 5*(1), 120-125.

Nourafkan, E., Gardy, J., Asachi, M., Ahmed, W., & Wen, D. S. (2019). Nanoparticle Formation in Stable Microemulsions for Enhanced Oil Recovery Application. *Industrial & Engineering Chemistry Research, 58*(28), 12664-12677.

Nystrom, F., Soeriyadi, A. H., Boyer, C., Zetterlund, P. B., & Whittaker, M. R. (2011). End-Group Fidelity of Copper(0)-Meditated Radical Polymerization at High Monomer Conversion: An ESI-MS Investigation. *Journal of Polymer Science Part a-Polymer Chemistry, 49*(24), 5313-5321.

Oh, S., Jung, S. H., Seo, H., Min, M. K., Kim, B., Hahn, Y. K.*, et al.* (2018). Magnetic activated cell sorting (MACS) pipette tip for immunomagnetic bacteria separation. *Sensors and Actuators B-Chemical, 272*, 324-330.

Ohno, K., Ma, Y., Huang, Y., Mori, C., Yahata, Y., Tsujii, Y.*, et al.* (2011). Surface-Initiated Reversible Addition-Fragmentation Chain Transfer (RAFT) Polymerization from Fine Particles Functionalized with Trithiocarbonates. *Macromolecules, 44*(22), 8944-8953.

Ohno, K., Tsujii, Y., & Fukuda, T. (1998). Synthesis of a well-defined glycopolymer by atom transfer radical polymerization. *Journal of Polymer Science Part a-Polymer Chemistry, 36*(14), 2473-2481.

Olsen, P. B., & Klemm, P. (1994). Localization of promoters in the fim gene cluster and the effect of H-NS on the transcription of fimB and fimE. *FEMS Microbiol Lett, 116*(1), 95-100.

Olsen, P. B., Schembri, M. A., Gally, D. L., & Klemm, P. (1998). Differential temperature modulation by H-NS of the fimB and fimE recombinase genes which control the orientation of the type 1 fimbrial phase switch. *FEMS Microbiol Lett, 162*(1), 17-23.

Osman, O., Toru, S., Dumas-Bouchiat, F., Dempsey, N. M., Haddour, N., Zanini, L.-F.*, et al.* (2013). Microfluidic immunomagnetic cell separation using integrated permanent micromagnets. *Biomicrofluidics, 7*(5).

Ostmark, E., Harrisson, S., Wooley, K. L., & Malmstrom, E. E. (2007). Comb polymers prepared by ATRP from hydroxypropyl cellulose. *Biomacromolecules, 8*(4), 1138-1148.

Otten, L., & Gibson, M. I. (2015). Discrimination between lectins with similar specificities by ratiometric profiling of binding to glycosylated surfaces; a chemical 'tongue' approach. *Rsc Advances, 5*(66), 53911-53914.

Oyeneye, O. O., Xu, W. Z., & Charpentier, P. A. (2015). Adhesive RAFT agents for controlled polymerization of acrylamide: effect of catechol-end R groups. *Rsc Advances, 5*(94), 76919-76926.

Oz, Y., Abdouni, Y., Yilmaz, G., Becer, C. R., & Sanyal, A. (2019). Magnetic glyconanoparticles for selective lectin separation and purification. *Polymer Chemistry, 10*(24), 3351-3361.

Oz, Y., Arslan, M., Gevrek, T. N., Sanyal, R., & Sanyal, A. (2016). Modular Fabrication of Polymer Brush Coated Magnetic Nanoparticles: Engineering the Interface for Targeted Cellular Imaging. *Acs Applied Materials & Interfaces, 8*(30), 19813-19826.

Paddon, C., & Keasling, J. (2014). Semi-synthetic artemisinin: a model for the use of synthetic biology in pharmaceutical development. *Nature Reviews Microbiology, 12*(5), 355-367.

Paddon, C. *e. a.* (2013). High-level semi-synthetic production of the potent antimalarial artemisinin. *Nature, 469*(7446), 528-532.

Papp, I., Dernedde, J., Enders, S., Riese, S. B., Shiao, T. C., Roy, R.*, et al.* (2011). Multivalent Presentation of Mannose on Hyperbranched Polyglycerol and their Interaction with Concanavalin A Lectin. *Chembiochem, 12*(7), 1075-1083.

Park, E. Y., Naruse, K., & Kato, T. (2012). One-pot bioethanol production from cellulose by co-culture of Acremonium cellulolyticus and Saccharomyces cerevisiae. *Biotechnology for Biofuels, 5*, 11.

Park, J., An, K. J., Hwang, Y. S., Park, J. G., Noh, H. J., Kim, J. Y.*, et al.* (2004). Ultra-large-scale syntheses of monodisperse nanocrystals. *Nature Materials, 3*(12), 891-895.

Park, S., Wolanin, P. M., Yuzbashyan, E. A., Lin, H., Darnton, N. C., Stock, J. B.*, et al.* (2003). Influence of topology on bacterial social interaction. *Proceedings of the National Academy of Sciences of the United States of America, 100*(24), 13910-13915.

Parkkinen, J., Rogers, G. N., Korhonen, T., Dahr, W., & Finne, J. (1986). Identification of the O-linked Sialyloligosaccharides of GlycophorinA as the Erythrocyte Receptors for S-fimbriated *Escherichia coli*. *Infect Immun, 54*(1), 37-42.

Paruchuri, D. K., Seifert, H. S., Ajioka, R. S., Karlsson, K. A., & So, M. (1990). Identification and characterization of a *Neisseria gonorrhoeae* gene encoding a glycolipid-binding adhesin. *Proceedings of the National Academy of Sciences of the United States of America, 87*(1), 333-337.

Pasparakis, G., Cockayne, A., & Alexander, C. (2007). Control of bacterial aggregation by thermoresponsive glycopolymers. *Journal of the American Chemical Society, 129*(36), 11014-+.

Paul, T. J., Rubel, S., Hildebrandt, M., Strzelczyk, A. K., Spormann, C., Lindhorst, T. K.*, et al.* (2019). Thermosensitive Display of Carbohydrate Ligands on Microgels for Switchable Binding of Proteins and Bacteria. *Acs Applied Materials & Interfaces, 11*(30), 26674-26683.

Pelicic, V., Reyrat, J. M., & Gicquel, B. (1996). Expression of the Bacillus subtilis sacB gene confers sucrose sensitivity on mycobacteria. *J Bacteriol, 178*(4), 1197-1199.

Pera, N. P., Kouki, A., Haataja, S., Branderhorst, H. M., Liskamp, R. M. J., Visser, G. M.*, et al.* (2010). Detection of pathogenic Streptococcus suis bacteria using magnetic glycoparticles. *Organic & Biomolecular Chemistry, 8*(10), 2425-2429.

Percec, V., Guliashvili, T., Ladislaw, J. S., Wistrand, A., Stjerndahl, A., Sienkowska, M. J.*, et al.* (2006). Ultrafast synthesis of ultrahigh molar mass polymers by metal-catalyzed living radical polymerization of acrylates, methacrylates, and vinyl

chloride mediated by SET at 25 degrees C. *Journal of the American Chemical Society, 128*(43), 14156-14165.

Pereira, B., Zhang, H. R., De Mey, M., Lim, C. G., Li, Z. J., & Stephanopoulos, G. (2016). Engineering a Novel Biosynthetic Pathway in Escherichia coli for Production of Renewable Ethylene Glycol. *Biotechnology and Bioengineering, 113*(2), 376-383.

Pereira, C., Pereira, A. M., Fernandes, C., Rocha, M., Mendes, R., Fernandez-Garcia, M. P.*, et al.* (2012). Superparamagnetic MFe2O4 (M = Fe, Co, Mn) Nanoparticles: Tuning the Particle Size and Magnetic Properties through a Novel One-Step Coprecipitation Route. *Chemistry of Materials, 24*(8), 1496-1504.

Perez-Soto, N., Creese, O., Fernandez-Trillo, F., & Krachler, A. M. (2018). Aggregation of Vibrio cholerae by Cationic Polymers Enhances Quorum Sensing but Overrides Biofilm Dissipation in Response to Autoinduction. *Acs Chemical Biology, 13*(10), 3021-3029.

Perrier, S. (2017). 50th Anniversary Perspective: RAFT Polymerization-A User Guide. *Macromolecules, 50*(19), 7433-7447.

Perroud, T. D., Meagher, R. J., Kanouff, M. P., Renzi, R. F., Wu, M., Singh, A. K.*, et al.* (2009). Isotropically etched radial micropore for cell concentration, immobilization, and picodroplet generation.

Peternel, S., Grdadolnik, J., Gaberc-Porekar, V., & Komel, R. (2008). Engineering inclusion bodies for non denaturing extraction of functional proteins. *Microbial Cell Factories, 7*, 9.

Peters, J. E., & Craig, N. L. (2001). Tn7: Smarter than we thought. *Nature Reviews Molecular Cell Biology, 2*(11), 806-814.

Pfaff, A., Schallon, A., Ruhland, T. M., Majewski, A. P., Schmalz, H., Freitag, R.*, et al.* (2011). Magnetic and Fluorescent Glycopolymer Hybrid Nanoparticles for Intranuclear Optical Imaging. *Biomacromolecules, 12*(10), 3805-3811.

Philippe, N., Alcaraz, J. P., Coursange, E., Geiselmann, J., & Schneider, D. (2004). Improvement of pCVD442, a suicide plasmid for gene allele exchange in bacteria. *Plasmid, 51*(3), 246-255.

Pintauer, T., & Matyjaszewski, K. (2008). Atom transfer radical addition and polymerization reactions catalyzed by ppm amounts of copper complexes. *Chemical Society Reviews, 37*(6), 1087-1097.

Porter, J., Robinson, J., Pickup, R., & Edwards, C. (1998). An evaluation of lectin-mediated magnetic bead cell sorting for the targeted separation of enteric bacteria. *J Appl Microbiol, 84*(5), 722-732.

Pranantyo, D., Xu, L. Q., Hou, Z., Kang, E. T., & Chan-Park, M. B. (2017). Increasing bacterial affinity and cytocompatibility with four-arm star glycopolymers and antimicrobial alpha-polylysine. *Polymer Chemistry, 8*(21), 3364-3373.

Qiu, J. M., Zhou, Y., Chen, H., & Lin, J. M. (2009). Immunomagnetic separation and rapid detection of bacteria using bioluminescence and microfluidics. *Talanta, 79*(3), 787-795.

Quenee, L., Lamotte, D., & Polack, B. (2005). Combined sacB-based negative selection and cre-lox antibiotic marker recycling for efficient gene deletion in Pseudomonas aeruginosa. *Biotechniques, 38*(1), 63-67.

Rabea, A. M., & Zhu, S. P. (2014). Achieving High-Conversion Bulk ATRP with Good Livingness and Well Controlled by Design and Optimization of Polymerization Temperature Profile. *Macromolecular Reaction Engineering, 8*(11), 771-776.

Raee, M. J., Ebrahiminezhad, A., Gholami, A., Ghoshoon, M. B., & Ghasemi, Y. (2018). Magnetic immobilization of recombinant E-coli producing extracellular

asparaginase: An effective way to intensify downstream process. *Separation Science and Technology, 53*(9), 1397-1404.

Ramstrom, O., & Yan, M. D. (2015). Glyconanomaterials for Combating Bacterial Infections. *Chemistry-a European Journal, 21*(46), 16310-16317.

Reimer, P., & Balzer, T. (2003). Ferucarbotran (Resovist): a new clinically approved RES-specific contrast agent for contrast-enhanced MRI of the liver: properties, clinical development, and applications. *European Radiology, 13*(6), 1266-1276.

Richards, S. J., & Gibson, M. I. (2014). Optimization of the Polymer Coating for Glycosylated Gold Nanoparticle Biosensors to Ensure Stability and Rapid Optical Readouts. *Acs Macro Letters, 3*(10), 1004-1008.

Richards, S. J., Isufi, K., Wilkins, L. E., Lipecki, J., Fullam, E., & Gibson, M. I. (2018). Multivalent Antimicrobial Polymer Nanoparticles Target Mycobacteria and Gram-Negative Bacteria by Distinct Mechanisms. *Biomacromolecules, 19*(1), 256-264.

Rizzardo, E., Chen, M., Chong, B., Moad, G., Skidmore, M., & Thang, S. H. (2007). RAFT polymerization: Adding to the picture. *Macromolecular Symposia, 248*, 104-116.

Rockenberger, J., Scher, E. C., & Alivisatos, A. P. (1999). A new nonhydrolytic single-precursor approach to surfactant-capped nanocrystals of transition metal oxides. *Journal of the American Chemical Society, 121*(49), 11595-11596.

Roell, G. W., Zha, J., Carr, R. R., Koffas, M. A., Fong, S. S., & Tang, Y. J. J. (2019). Engineering microbial consortia by division of labor. *Microbial Cell Factories, 18*, 11.

Roka, N., Kokkorogianni, O., & Pitsikalis, M. (2017). Statistical copolymers of N-vinylpyrrolidone and 2-(dimethylamino)ethyl methacrylate via RAFT: Monomer reactivity ratios, thermal properties, and kinetics of thermal decomposition. *Journal of Polymer Science Part a-Polymer Chemistry, 55*(22), 3776-3787.

Roonasi, P., & Holmgren, A. (2009). A Fourier transform infrared (FTIR) and thermogravimetric analysis (TGA) study of oleate adsorbed on magnetite nano-particle surface. *Applied Surface Science, 255*(11), 5891-5895.

Ross, C., Opel, V., Scherlach, K., & Hertweck, C. (2014). Biosynthesis of antifungal and antibacterial polyketides by Burkholderia gladioli in coculture with Rhizopus microsporus. *Mycoses, 57*, 48-55.

Rossez, Y., Holmes, A., Lodberg-Pedersen, H., Birse, L., Marshall, J., Willats, W. G. T.*, et al.* (2014). Escherichia coli Common Pilus (ECP) Targets Arabinosyl Residues in Plant Cell Walls to Mediate Adhesion to Fresh Produce Plants. *Journal of Biological Chemistry, 289*(49), 34349-34365.

Rowe, M. A., Hammer, B. A. G., & Boyes, S. G. (2008). Synthesis of surface-initiated stimuli-responsive diblock copolymer brushes utilizing a combination of ATRP and RAFT polymerization techniques. *Macromolecules, 41*(12), 4147-4157.

Saarela, S., Taira, S., Nurmiaholassila, E. L., Makkonen, A., & Rhen, M. (1995). The *Escherichia coli* G-fimbrial Lectin Protein Participates both in Fimbrial Biogenesis and in Recognition of the Receptor N-acetyl-D-glucosamine. *J Bacteriol, 177*(6), 1477-1484.

Sadhukha, T., Wiedmann, T. S., & Panyam, J. (2013). Inhalable magnetic nanoparticles for targeted hyperthermia in lung cancer therapy. *Biomaterials, 34*(21), 5163-5171.

Sahoo, Y., Pizem, H., Fried, T., Golodnitsky, D., Burstein, L., Sukenik, C. N.*, et al.* (2001). Alkyl phosphonate/phosphate coating on magnetite nanoparticles: A comparison with fatty acids. *Langmuir, 17*(25), 7907-7911.

Saito, M., Takaku, F., Hayashi, M., Tanaka, I., Abe, Y., Nagai, Y.*, et al.* (1983). A role of valency of Concanavalin A and its chemically modified derivatives in lymphocyte-activation - mono-valent monomeric Concanavalin A derivative can stimulate lymphocyte blastoid formation. *Journal of Biological Chemistry, 258*(12), 7499-7505.

Salek, M. M., Carrara, F., Fernandez, V., Guasto, J. S., & Stocker, R. (2019). Bacterial chemotaxis in a microfluidic T-maze reveals strong phenotypic heterogeneity in chemotactic sensitivity. *Nature Communications, 10*, 11.

Sanches-Medeiros, A., Monteiro, L. M. O., & Silva-Rocha, R. (2018). Calibrating Transcriptional Activity Using Constitutive Synthetic Promoters in Mutants for Global Regulators in Escherichia coli. *International Journal of Genomics*, 10.

Sarnovsky, R. J., May, E. W., & Craig, N. L. (1996). The Tn7 transposase is a heteromeric complex in which DNA breakage and joining activities are distributed between different gene products. *Embo Journal, 15*(22), 6348-6361.

Sasmal, D., Guhathakurta, B., Ghosh, A. N., Pal, C. R., & Datta, A. (1992). *N*-Acetyl-D-glucosamine-specific lectin purified from *Vibrio cholerae* 01. *FEMS Microbiol Lett, 98*(1-3), 217-224.

Sattin, S., & Bernardi, A. (2016). Glycoconjugates and Glycomimetics as Microbial Anti-Adhesives. *Trends in Biotechnology, 34*(6), 483-495.

Saucedo, N. M., Gao, Y. N., Pham, T., & Mulchandani, A. (2018). Lectin- and Saccharide-Functionalized Nano-Chemiresistor Arrays for Detection and Identification of Pathogenic Bacteria Infection. *Biosensors-Basel, 8*(3), 11.

Sawamoto, M., & Kamigaito, M. (1997). Living radical polymerization with transition metal complexes. *Kobunshi Ronbunshu, 54*(12), 875-885.

Sayed, F. N., & Polshettiwar, V. (2015). Facile and Sustainable Synthesis of Shaped Iron Oxide Nanoparticles: Effect of Iron Precursor Salts on the Shapes of Iron Oxides. *Scientific Reports, 5*, 14.

Schilli, C., Lanzendorfer, M. G., & Muller, A. H. E. (2002). Benzyl and cumyl dithiocarbamates as chain transfer agent in the RAFT polymerization of N-isopropylacrylamide. In situ FT-NIR and MALDI-TOF MS investigation. *Macromolecules, 35*(18), 6819-6827.

Schnaar, R. L. (2016). Glycobiology simplified: diverse roles of glycan recognition in inflammation. *Journal of Leukocyte Biology, 99*(6), 825-838.

Schwaminger, S. P., Bauer, D., Fraga-Garcia, P., Wagner, F. E., & Berensmeier, S. (2017). Oxidation of magnetite nanoparticles: impact on surface and crystal properties. *Crystengcomm, 19*(2), 246-255.

Schwan, W. R. (2011). Regulation of fim genes in uropathogenic Escherichia coli. *World J Clin Infect Dis, 1*(1), 17-25.

Schwan, W. R., Seifert, H. S., & Duncan, J. L. (1994). Analysis of the fimB promoter region involved in type 1 pilus phase variation in Escherichia coli. *Mol Gen Genet, 242*(5), 623-630.

Selvaprakash, K., & Chen, Y. C. (2018). Functionalized gold nanoparticles as affinity nanoprobes for multiple lectins. *Colloids and Surfaces B-Biointerfaces, 162*, 60-68.

Shah, S. A., Erdmann, S., Mojica, F. J. M., & Garrett, R. A. (2013). Protospacer recognition motifs: Mixed identities and functional diversity. *Rna Biology, 10*(5), 891-899.

Shamout, F., Monaco, A., Yilmaz, G., Becer, C. R., & Hartmann, L. (2020). Synthesis of Brush-Like Glycopolymers with Monodisperse, Sequence-Defined Side Chains and Their Interactions with Plant and Animal Lectins. *Macromolecular Rapid Communications, 41*(1), 6.

Shaner, N. C., Lambert, G. G., Chammas, A., Ni, Y. H., Cranfill, P. J., Baird, M. A*., et al.* (2013). A bright monomeric green fluorescent protein derived from Branchiostoma lanceolatum. *Nature Methods, 10*(5), 407-+.

Sharon, N. (2006). Carbohydrates as future anti-adhesion drugs for infectious diseases. *Biochimica Et Biophysica Acta-General Subjects, 1760*(4), 527-537.

Sharon, N., & Lis, H. (2004). History of lectins: from hemagglutinins to biological recognition molecules. *Glycobiology, 14*(11), 53R-62R.

Shemper, B. S., & Mathias, L. J. (2004). Syntheses and characterization of statistical and block fluorinated copolymers with linear and star-like architectures via ATRP. *European Polymer Journal, 40*(4), 651-665.

Shen, L. F., Laibinis, P. E., & Hatton, T. A. (1999). Bilayer surfactant stabilized magnetic fluids: Synthesis and interactions at interfaces. *Langmuir, 15*(2), 447-453.

Shen, X. F., Wang, Q., Chen, W. L., & Pang, Y. H. (2014). One-step synthesis of water-dispersible cysteine functionalized magnetic Fe3O4 nanoparticles for mercury(II) removal from aqueous solutions. *Applied Surface Science, 317*, 1028-1034.

Shen, Z. H., Huang, M. C., Xiao, C. D., Zhang, Y., Zeng, X. Q., & Wang, P. G. (2007). Nonlabeled quartz crystal microbalance biosensor for bacterial detection using carbohydrate and lectin recognitions. *Analytical Chemistry, 79*(6), 2312-2319.

Sherkhanov, S., Korman, T. P., Clarke, S. G., & Bowie, J. U. (2016). Production of FAME biodiesel in E. coli by direct methylation with an insect enzyme. *Scientific Reports, 6*, 10.

Shields, C. W., Ohiri, K. A., Szott, L. M., & Lopez, G. P. (2017). Translating Microfluidics: Cell Separation Technologies and Their Barriers to Commercialization. *Cytometry Part B-Clinical Cytometry, 92*(2), 115-125.

Shields, C. W., Reyes, C. D., & Lopez, G. P. (2015). Microfluidic cell sorting: a review of the advances in the separation of cells from debulking to rare cell isolation. *Lab on a Chip, 15*(5), 1230-1249.

Shimada, T., Yamazaki, Y., Tanaka, K., & Ishihama, A. (2014). The Whole Set of Constitutive Promoters Recognized by RNA Polymerase RpoD Holoenzyme of Escherichia coli. *Plos One, 9*(3), 21.

Shipp, D. A. (2011). Reversible-Deactivation Radical Polymerizations. *Polymer Reviews, 51*(2), 99-103.

Shong, J., Diaz, M. R. J., & Collins, C. H. (2012). Towards synthetic microbial consortia for bioprocessing. *Current Opinion in Biotechnology, 23*(5), 798-802.

Shultz, M. D., Reveles, J. U., Khanna, S. N., & Carpenter, E. E. (2007). Reactive nature of dopamine as a surface functionalization agent in iron oxide nanoparticles. *Journal of the American Chemical Society, 129*(9), 2482-2487.

Simon, R., Priefer, U., & Puhler, A. (1983). A broad host range mobilization system for *in vivo* genetic-engineering - transposon mutagenesis in gram-negative bacteria. *Bio-Technology, 1*(9), 784-791.

Simula, A., Nurumbetov, G., Anastasaki, A., Wilson, P., & Haddleton, D. M. (2015). Synthesis and reactivity of alpha,omega-homotelechelic polymers by Cu(0)-mediated living radical polymerization. *European Polymer Journal, 62*, 294-303.

Singh, R. (2011). Facts, Growth, and Opportunities in Industrial Biotechnology. *Organic Process Research & Development, 15*(1), 175-179.

Singh, S., Upadhyay, M., Sharma, J., Gupta, S., Vivekanandan, P., & Elangovan, R. (2016). A portable immunomagnetic cell capture system to accelerate culture diagnosis of bacterial infections. *Analyst, 141*(11), 3358-3366.

Skerra, A. (1994). Use of the tetracycline promoter for the tightly regulated production of a murine antibody fragment in *Escherichia coli*. *Gene, 151*(1-2), 131-135.

Slavin, S., Burns, J., Haddleton, D. M., & Becer, C. R. (2011). Synthesis of glycopolymers via click reactions. *European Polymer Journal, 47*(4), 435-446.

Soeriyadi, A. H., Boyer, C., Nystrom, F., Zetterlund, P. B., & Whittaker, M. R. (2011). High-Order Multiblock Copolymers via Iterative Cu(0)-Mediated Radical Polymerizations (SET-LRP): Toward Biological Precision. *Journal of the American Chemical Society, 133*(29), 11128-11131.

Sokurenko, E. V., Chesnokova, V., Doyle, R. J., & Hasty, D. L. (1997). Diversity of the Escherichia coli Type 1 Fimbrial Lectin.

Sommer, R., Wagner, S., Rox, K., Varrot, A., Hauck, D., Wamhoff, E. C.*, et al.* (2018). Glycomimetic, Orally Bioavailable LecB Inhibitors Block Biofilm Formation of Pseudomonas aeruginosa. *Journal of the American Chemical Society, 140*(7), 2537-2545.

Souriau, C., & Hudson, P. J. (2003). Recombinant antibodies for cancer diagnosis and therapy. *Expert Opinion on Biological Therapy, 3*(2), 305-318.

Sperling, O., Fuchs, A., & Lindhorst, T. (2006). Evaluation of the carbohydrate recognition domain of the bacterial adhesin FimH: design, synthesis and binding properties of mannoside ligands. *Organic and Biomolecular Chemistry, 4*, 3913-3922.

Srirangan, K., Liu, X. J., Akawi, L., Bruder, M., Moo-Young, M., & Chou, C. P. (2016). Engineering Escherichia coli for Microbial Production of Butanone. *Applied and Environmental Microbiology, 82*(9), 2574-2584.

Stahlhut, S. G., Tchesnokova, V., Struve, C., Weissman, S. J., Chattopadhyay, S., Yakovenko, O.*, et al.* (2009). Comparative Structure-Function Analysis of Mannose-Specific FimH Adhesins from Klebsiella pneumoniae and Escherichia coli. *J Bacteriol, 191*(21), 6592-6601.

Stellwagen, A. E., & Craig, N. L. (2001). Analysis of gain-of-function mutants of an ATP-dependent regulator of Tn7 transposition. *Journal of Molecular Biology, 305*(3), 633-642.

Stoltenburg, R., Reinemann, C., & Strehlitz, B. (2007). SELEX-A (r)evolutionary method to generate high-affinity nucleic acid ligands. *Biomolecular Engineering, 24*(4), 381-403.

Strachan, E., Mallia, A. K., Cox, J. M., Antharavally, B., Desai, S., Sykaluk, L.*, et al.* (2004). Solid-phase biotinylation of antibodies. *Journal of Molecular Recognition, 17*(3), 268-276.

Stromberg, N., & Karlsson, K. A. (1990). Characterisation of the binding of *Actinomyces Naeslundii* and *Actinomyces Viscosus* to glycosphingolipids, using a solid-phase overlay approach. *Journal of Biological Chemistry, 265*(19), 11251-11258.

Su, T. Y., Liu, F. P., Gu, P. F., Jin, H. Y., Chang, Y. Z., Wang, Q.*, et al.* (2016). A CRISPR-Cas9 Assisted Non-Homologous End-Joining Strategy for One-step Engineering of Bacterial Genome. *Scientific Reports, 6*, 11.

Sun, S. H., & Zeng, H. (2002). Size-controlled synthesis of magnetite nanoparticles. *Journal of the American Chemical Society, 124*(28), 8204-8205.

Takami, S., Sato, T., Mousavand, T., Ohara, S., Umetsu, M., & Adschiri, T. (2007). Hydrothermal synthesis of surface-modified iron oxide nanoparticles. *Materials Letters, 61*(26), 4769-4772.

Tanaka, J., Gleinich, A. S., Zhang, Q., Whitfield, R., Kempe, K., Haddleton, D. M.*, et al.* (2017). Specific and Differential Binding of N-Acetylgalactosamine Glycopolymers to the Human Macrophage Galactose Lectin and Asialoglycoprotein Receptor. *Biomacromolecules, 18*(5), 1624-1633.

Tanaka, T., Nagai, H., Noguchi, M., Kobayashi, A., & Shoda, S. (2009). One-step conversion of unprotected sugars to beta-glycosyl azides using 2-chloroimidazolinium salt in aqueous solution. *Chemical Communications*(23), 3378-3379.

Tang, L. C., Zeng, Y. T., Du, H. Z., Gong, M. M., Peng, J., Zhang, B. X.*, et al.* (2017). CRISPR/Cas9-mediated gene editing in human zygotes using Cas9 protein. *Molecular Genetics and Genomics, 292*(3), 525-533.

Tang, T. H., Bachellerie, J. P., Rozhdestvensky, T., Bortolin, M. L., Huber, H., Drungowski, M.*, et al.* (2002). Identification of 86 candidates for small non-messenger RNAs from the archaeon Archaeoglobus fulgidus. *Proceedings of the National Academy of Sciences of the United States of America, 99*(11), 7536-7541.

Taresco, V., Francolini, I., Padella, F., Bellusci, M., Boni, A., Innocenti, C.*, et al.* (2015). Design and characterization of antimicrobial usnic acid loaded-core/shell magnetic nanoparticles. *Materials Science & Engineering C-Materials for Biological Applications, 52*, 72-81.

Tasdelen, M. A., Kahveci, M. U., & Yagci, Y. (2011). Telechelic polymers by living and controlled/living polymerization methods. *Progress in Polymer Science, 36*(4), 455-567.

Terlizzi, M. E., Gribaudo, G., & Maffei, M. E. (2017). UroPathogenic Escherichia coli (UPEC) Infections: Virulence Factors, Bladder Responses, Antibiotic, and Non-antibiotic Antimicrobial Strategies. *Frontiers in Microbiology, 8*, 23.

Thankavel, K., Madison, B., Ikeda, T., Malaviya, R., Shah, A. H., Arumugam, P. M.*, et al.* (1997). Localization of a domain in the FimH adhesin of Escherichia coli type 1 fimbriae capable of receptor recognition and use of a domain-specific antibody to confer protection against experimental urinary tract infection. *J Clin Invest, 100*(5), 1123-1136.

Thoma, S., & Schobert, M. (2009). An improved Escherichia coli donor strain for diparental mating. *FEMS Microbiol Lett, 294*(2), 127-132.

Thomas, L. A., Dekker, L., Kallumadil, M., Southern, P., Wilson, M., Nair, S. P.*, et al.* (2009). Carboxylic acid-stabilised iron oxide nanoparticles for use in magnetic hyperthermia. *Journal of Materials Chemistry, 19*(36), 6529-6535.

Tsarevsky, N. V., Huang, J., & Matyjaszewski, K. (2009). Synthesis of Hyperbranched Degradable Polymers by Atom Transfer Radical (Co)Polymerization of Inimers with Ester or Disulfide Groups. *Journal of Polymer Science Part a-Polymer Chemistry, 47*(24), 6839-6851.

Tseng, H. C., Harwell, C. L., Martin, C. H., & Prather, K. L. J. (2010). Biosynthesis of chiral 3-hydroxyvalerate from single propionate-unrelated carbon sources in metabolically engineered E. coli. *Microbial Cell Factories, 9*, 12.

Tuerk, C., & Gold, L. (1990). Systematic evolution of ligands by exponential enrichment - RNA ligands to bacteriophage-T4 DNA-polymerase. *Science, 249*(4968), 505-510.

Valenski, M. L., Harris, S. L., Spears, P. A., Horton, J. R., & Orndorff, P. E. (2003). The Product of the fimI gene is necessary for Escherichia coli type 1 pilus biosynthesis. *J Bacteriol, 185*(16), 5007-5011.

Valeur, E., & Bradley, M. (2009). Amide bond formation: beyond the myth of coupling reagents. *Chemical Society Reviews, 38*(2), 606-631.

Varshney, M., Yang, L. J., Su, X. L., & Li, Y. B. (2005). Magnetic nanoparticle-antibody conjugates for the separation of Escherichia coli O157 : H7 in ground beef. *Journal of Food Protection, 68*(9), 1804-1811.

Vayssieres, L., Chaneac, C., Tronc, E., & Jolivet, J. P. (1998). Size tailoring of magnetite particles formed by aqueous precipitation: An example of thermodynamic stability of nanometric oxide particles. *Journal of Colloid and Interface Science, 205*(2), 205-212.

Vazquez-Dorbatt, V., Tolstyka, Z. P., Chang, C. W., & Maynard, H. D. (2009). Synthesis of a Pyridyl Disulfide End-Functionalized Glycopolymer for Conjugation to Biomolecules and Patterning on Gold Surfaces. *Biomacromolecules, 10*(8), 2207-2212.

Venkidasubramonian, G., Kratzer, D., Trouillet, V., Zydziak, N., Franzreb, M., Barner, L*., et al.* (2018). Surface-initiated RAFT polymerization from vapor-based polymer coatings. *Polymer, 150*, 26-34.

Ventola, C. L. (2017). Progress in Nanomedicine: Approved and Investigational Nanodrugs. *P & T : a peer-reviewed journal for formulary management, 42*(12), 742-755.

Vikram, S., Dhakshnamoorthy, M., Vasanthakumari, R., Rajamani, A. R., Rangarajan, M., & Tsuzuki, T. (2015). Tuning the Magnetic Properties of Iron Oxide Nanoparticles by a Room-Temperature Air-Atmosphere (RTAA) Co-Precipitation Method. *Journal of Nanoscience and Nanotechnology, 15*(5), 3870-3878.

von Werne, T. A., Germack, D. S., Hagberg, E. C., Sheares, V. V., Hawker, C. J., & Carter, K. R. (2003). A versatile method for tuning the chemistry and size of nanoscopic features by living free radical polymerization. *Journal of the American Chemical Society, 125*(13), 3831-3838.

Vukojicic, P., Behar, G., Tawara, M. H., Fernandez-Villamarin, M., Pecorari, F., Fernandez-Megia, E*., et al.* (2019). Multivalent Affidendrons with High Affinity and Specificity toward Staphylococcus aureus as Versatile Tools for Modulating Multicellular Behaviors. *Acs Applied Materials & Interfaces, 11*(24), 21391-21398.

Wan, S. R., Huang, J. S., Yan, H. S., & Liu, K. L. (2006). Size-controlled preparation of magnetite nanoparticles in the presence of graft copolymers. *Journal of Materials Chemistry, 16*(3), 298-303.

Wang, B. Z., & Anzai, J. (2015). Recent Progress in Lectin-Based Biosensors. *Materials, 8*(12), 8590-8607.

Wang, D. H., Guo, S. T., Zhang, Q., Wilson, P., & Haddleton, D. M. (2017). Mussel-inspired thermoresponsive polymers with a tunable LCST by Cu(0)-LRP for the construction of smart TiO2 nanocomposites. *Polymer Chemistry, 8*(24), 3679-3688.

Wang, E. X., Ding, M. Z., Ma, Q., Dong, X. T., & Yuan, Y. J. (2016a). Reorganization of a synthetic microbial consortium for one-step vitamin C fermentation. *Microbial Cell Factories, 15*, 11.

Wang, Q., Chittaboina, S., & Barnhill, H. N. (2005). Advances in 1,3-dipolar cycloaddition reaction of azides and alkynes - A prototype of "click" chemistry. *Letters in Organic Chemistry, 2*(4), 293-301.

Wang, R. E., Wu, H., Niu, Y., & Cai, J. (2011). Improving the Stability of Aptamers by Chemical Modification. *Current Medicinal Chemistry, 18*(27), 4126-4138.

Wang, W., Chance, D. L., Mossine, V. V., & Mawhinney, T. P. (2014). RAFT-based tri-component fluorescent glycopolymers: synthesis, characterization and application in lectin-mediated bacterial binding study. *Glycoconjugate Journal, 31*(2), 133-143.

Wang, X. Y., Sun, X. L., Chen, Z. H., Wang, F., Wang, S., & Tang, Y. (2018). Highly efficient access to well-defined linear polymers with substantial vinyl pendants via ATRP of divinyl monomers. *Polymer Chemistry, 9*(32), 4309-4315.

Wang, Y., Wang, H., Wei, L., Li, S., Liu, L., & Wang, X. (2019). Synthetic Promoter Design in Escherichia coli based on Generative Adversarial Network. *bioRxiv*.

Wang, Y., Wu, S.-l., & Hancock, W. S. (2006). Approaches to the study of N-linked glycoproteins in human plasma using lectin affinity chromatography and nano-HPLC coupled to electrospray linear ion trap—Fourier transform mass spectrometry.

Wang, Y. H., Chen, Q., Gan, C. Q., Yan, B., Han, Y. Q., & Lin, J. H. (2016b). A Review on Magnetophoretic Immunoseparation. *Journal of Nanoscience and Nanotechnology, 16*(3), 2152-2163.

Wang, Z. D., Mo, Y. R., Chiou, C. L., & Liu, M. H. (2010). A Simple Preparation of 2,3,4,6-Tetra-O-acyl-Gluco-, Galacto- and Mannopyranoses and Relevant Theoretical Study. *Molecules, 15*(1), 374-384.

Weissig, V., Pettinger, T. K., & Murdock, N. (2014). Nanopharmaceuticals (part I): products on the market. *International Journal of Nanomedicine, 9*, 4357-4373.

Wesener, D. A., Dugan, A., & Kiessling, L. L. (2017). Recognition of microbial glycans by soluble human lectins. *Current Opinion in Structural Biology, 44*, 168-178.

Wessel, A. K., Hmelo, L., Parsek, M. R., & Whiteley, M. (2013). Going local: technologies for exploring bacterial microenvironments. *Nature Reviews Microbiology, 11*(5), 337-348.

Wever, D. A. Z., Raffa, P., Picchioni, F., & Broekhuis, A. A. (2012). Acrylamide Homopolymers and Acrylamide-N-Isopropylacrylamide Block Copolymers by Atomic Transfer Radical Polymerization in Water. *Macromolecules, 45*(10), 4040-4045.

White, N. J. (1997). Assessment of the pharmacodynamic properties of antimalarial drugs in vivo. *Antimicrobial Agents and Chemotherapy, 41*(7), 1413-1422.

Williams, D. C., Vanfrank, R. M., Muth, W. L., & Burnett, J. P. (1982). Cytoplasmic inclusion-bodies in *Escherichia coli* producing biosynthetic human insulin proteins. *Science, 215*(4533), 687-689.

Wilton, R., Ahrendt, A. J., Shinde, S., Sholto-Douglas, D. J., Johnson, J. L., Brennan, M. B*., et al.* (2018). A New Suite of Plasmid Vectors for Fluorescence-Based Imaging of Root Colonizing Pseudomonads. *Frontiers in Plant Science, 8*, 15.

Wolkow, C. A., DeBoy, R. T., & Craig, N. L. (1996). Conjugating plasmids are preferred targets for Tn7. *Genes & Development, 10*(17), 2145-2157.

Wright, K. J., Seed, P. C., & Hultgren, S. J. (2005). Uropathogenic Escherichia coli flagella aid in efficient urinary tract colonization. *Infect Immun, 73*(11), 7657-7668.

Wright, K. J., Seed, P. C., & Hultgren, S. J. (2007). Development of intracellular bacterial communities of uropathogenic Escherichia coli depends on type 1 pili. *Cellular Microbiology, 9*(9), 2230-2241.

Wu, L., Glebe, U., & Boker, A. (2015). Surface-initiated controlled radical polymerizations from silica nanoparticles, gold nanocrystals, and bionanoparticles. *Polymer Chemistry, 6*(29), 5143-5184.

Wu, W., Jiang, C. Z., & Roy, V. A. L. (2016). Designed synthesis and surface engineering strategies of magnetic iron oxide nanoparticles for biomedical applications. *Nanoscale, 8*(47), 19421-19474.

Wu, W., Yang, S. L., Pan, J., Sun, L. L., Zhou, J., Dai, Z. G.*, et al.* (2014). Metal ion-mediated synthesis and shape-dependent magnetic properties of single-crystalline alpha-Fe2O3 nanoparticles. *Crystengcomm, 16*(25), 5566-5572.

Xia, P. P., Song, Y. J., Zou, Y. J., Yang, Y., & Zhu, G. Q. (2015). F4(+) enterotoxigenic Escherichia coli (ETEC) adhesion mediated by the major fimbrial subunit FaeG. *Journal of Basic Microbiology, 55*(9), 1118-1124.

Xie, Y. X., Peng, C., Gao, Y. Y., Liu, X. H., Liu, T. B., & Joy, A. (2017). Mannose-Based Graft Polyesters with Tunable Binding Affinity to Concanavalin A. *Journal of Polymer Science Part a-Polymer Chemistry, 55*(23), 3908-3917.

Xin, F. X., & He, J. Z. (2013). Characterization of a thermostable xylanase from a newly isolated Kluyvera species and its application for biobutanol production. *Bioresource Technology, 135*, 309-315.

Xing, H. L., Dong, L., Wang, Z. P., Zhang, H. Y., Han, C. Y., Liu, B.*, et al.* (2014). A CRISPR/Cas9 toolkit for multiplex genome editing in plants. *Bmc Plant Biology, 14*, 12.

Xiu, Y., Jang, S., Jones, J. A., Zill, N. A., Linhardt, R. J., Yuan, Q. P.*, et al.* (2017). Naringenin-responsive riboswitch-based fluorescent biosensor module for Escherichia coli co-cultures. *Biotechnology and Bioengineering, 114*(10), 2235-2244.

Xu, C. J., Xu, K. M., Gu, H. W., Zheng, R. K., Liu, H., Zhang, X. X.*, et al.* (2004). Dopamine as a robust anchor to immobilize functional molecules on the iron oxide shell of magnetic nanoparticles. *Journal of the American Chemical Society, 126*(32), 9938-9939.

Xu, J. T., He, J. P., Fan, D. Q., Wang, X. J., & Yang, Y. L. (2006). Aminolysis of polymers with thiocarbonylthio termini prepared by RAFT polymerization: The difference between polystyrene and polymethacrylates. *Macromolecules, 39*(25), 8616-8624.

Xu, Y. F., Li, C. C., Zhu, X., Huang, W. E., & Zhang, D. Y. (2014). APPLICATION OF MAGNETIC NANOPARTICLES IN DRINKING WATER PURIFICATION. *Environmental Engineering and Management Journal, 13*(8), 2023-2029.

Xue, C., Velayudham, S., Johnson, S., Saha, R., Smith, A., Brewer, W.*, et al.* (2009). Highly Water-Soluble, Fluorescent, Conjugated Fluorene-Based Glycopolymers with Poly(ethylene glycol)-Tethered Spacers for Sensitive Detection of Escherichia coli. *Chemistry-a European Journal, 15*(10), 2289-2295.

Xue, X., Pasparakis, G., Halliday, N., Winzer, K., Howdle, S. M., Cramphorn, C. J.*, et al.* (2011). Synthetic Polymers for Simultaneous Bacterial Sequestration and Quorum Sense Interference. *Angewandte Chemie-International Edition, 50*(42), 9852-9856.

Yan, X. B., Sivignon, A., Alcouffe, P., Burdin, B., Favre-Bonte, S., Bilyy, R.*, et al.* (2015a). Brilliant glyconanocapsules for trapping of bacteria. *Chemical Communications, 51*(67), 13193-13196.

Yan, X. B., Sivignon, A., Yamakawa, N., Crepet, A., Travelet, C., Borsali, R.*, et al.* (2015b). Glycopolymers as Antiadhesives of E. coil Strains Inducing Inflammatory Bowel Diseases. *Biomacromolecules, 16*(6), 1827-1836.

Yang, Q., Strathmann, M., Rumpf, A., Schaule, G., & Ulbricht, M. (2010). Grafted Glycopolymer-Based Receptor Mimics on Polymer Support for Selective Adhesion of Bacteria. *Acs Applied Materials & Interfaces, 2*(12), 3555-3562.

Yang, Y., Ma, H. X., Zhuang, J., & Wang, X. (2011). Morphology-Controlled Synthesis of Hematite Nanocrystals and Their Facet Effects on Gas-Sensing Properties. *Inorganic Chemistry, 50*(20), 10143-10151.

Ye, F. P., Mi, Q. L., Zhang, N., Li, X. M., Yu, J., Gao, Z. P.*, et al.* (2016). Probing the Key Binding Sequence and Improvement of the Stability of a -Bungarotoxin-binding Aptamer in Snake Venom. *Bulletin of the Korean Chemical Society, 37*(5), 649-654.

Yilmaz, G., & Becer, C. R. (2014). Glycopolymer code based on well-defined glycopolymers or glyconanomaterials and their biomolecular recognition. *Frontiers in Bioengineering and Biotechnology, 2*, 39.

Yilmaz, G., & Becer, C. R. (2015). Glyconanoparticles and their interactions with lectins. *Polymer Chemistry, 6*(31), 5503-5514.

Yilmaz, G., Messager, L., Gleinich, A. S., Mitchell, D. A., Battaglia, G., & Becer, C. R. (2016). Glyconanoparticles with controlled morphologies and their interactions with a dendritic cell lectin. *Polymer Chemistry, 7*(41), 6293-6296.

Zacharias, D. A., Violin, J. D., Newton, A. C., & Tsien, R. Y. (2002). Partitioning of lipid-modified monomeric GFPs into membrane microdomains of live cells. *Science, 296*(5569), 913-916.

Zang, J., Feng, M. J., Zhao, J., & Wang, J. P. (2018). Micellar and bicontinuous microemulsion structures show different solute-solvent interactions: a case study using ultrafast nonlinear infrared spectroscopy. *Physical Chemistry Chemical Physics, 20*(30), 19938-19949.

Zengin, A., Yildirim, E., Tamer, U., & Caykara, T. (2013). Molecularly imprinted superparamagnetic iron oxide nanoparticles for rapid enrichment and separation of cholesterol. *Analyst, 138*(23), 7238-7245.

Zhang, G. L., & Ye, X. S. (2018). Synthetic Glycans and Glycomimetics: A Promising Alternative to Natural Polysaccharides. *Chemistry-a European Journal, 24*(26), 6696-+.

Zhang, H. R., Li, Z. J., Pereira, B., & Stephanopoulos, G. (2015a). Engineering E-coli-E-coli cocultures for production of muconic acid from glycerol. *Microbial Cell Factories, 14*, 10.

Zhang, H. R., Pereira, B., Li, Z. J., & Stephanopoulos, G. (2015b). Engineering Escherichia coli coculture systems for the production of biochemical products. *Proceedings of the National Academy of Sciences of the United States of America, 112*(27), 8266-8271.

Zhang, L. W., & Chen, Y. M. (2006). Allyl functionalized telechelic linear polymer and star polymer via RAFT polymerization. *Polymer, 47*(15), 5259-5266.

Zhang, P. B., Lu, H., Chen, H., Zhang, J. Y., Liu, L. B., Lv, F. T.*, et al.* (2016a). Cationic Conjugated Polymers-Induced Quorum Sensing of Bacteria Cells. *Analytical Chemistry, 88*(6), 2985-2988.

Zhang, Q., Collins, J., Anastasaki, A., Wallis, R., Mitchell, D. A., Becer, C. R.*, et al.* (2013a). Sequence-Controlled Multi-Block Glycopolymers to Inhibit DC-SIGN-gp120 Binding. *Angewandte Chemie-International Edition, 52*(16), 4435-4439.

Zhang, Q., Nurumbetov, G., Simula, A., Zhu, C., Li, M., Wilson, P.*, et al.* (2016b). Synthesis of well-defined catechol polymers for surface functionalization of magnetic nanoparticles. *Polymer Chemistry, 7*, 7002-7010.

Zhang, Q., Wilson, P., Anastasaki, A., McHale, R., & Haddleton, D. M. (2014). Synthesis and Aggregation of Double Hydrophilic Diblock Glycopolymers via Aqueous SET-LRP. *Acs Macro Letters, 3*(5), 491-495.

Zhang, Q., Wilson, P., Li, Z. D., McHale, R., Godfrey, J., Anastasaki, A.*, et al.* (2013b). Aqueous Copper-Mediated Living Polymerization: Exploiting Rapid

Disproportionation of CuBr with Me6TREN. *Journal of the American Chemical Society, 135*(19), 7355-7363.

Zhang, S., Merino, N., Okamoto, A., & Gedalanga, P. (2018). Interkingdom microbial consortia mechanisms to guide biotechnological applications. *Microbial Biotechnology, 11*(5), 833-847.

Zhang, X. W., Giani, O., Monge, S., & Robin, J. J. (2010). RAFT polymerization of N,N-diethylacrylamide: Influence of chain transfer agent and solvent on kinetics and induction period. *Polymer, 51*(14), 2947-2953.

Zhang, Z. J., Wang, C. X., Zhang, L. R., Meng, Q. T., Zhang, Y. M., Sun, F.*, et al.* (2017). Fast detection of Escherichia coli in food using nanoprobe and ATP bioluminescence technology. *Analytical Methods, 9*(36), 5378-5387.

Zhao, D., Wu, X., Guan, H., & Han, E. (2007). Study on supercritical hydrothermal synthesis of CoFe2O4 nanoparticles. *Journal of Supercritical Fluids, 42*(2), 226-233.

Zheng, L. B., Wan, Y., Qi, P., Sun, Y., Zhang, D., & Yu, L. M. (2017). Lectin functionalized ZnO nanoarrays as a 3D nano-biointerface for bacterial detection. *Talanta, 167*, 600-606.

Zheng, Z. C., Ling, J., & Muller, A. H. E. (2014). Revival of the R-Group Approach: A "CTA- shuttled" Grafting from Approach for Well- Defined Cylindrical Polymer Brushes via RAFT Polymerization. *Macromolecular Rapid Communications, 35*(2), 234-241.

Zhou, Y. Y., Li, Z. H., Wang, X. N., & Zhang, H. R. (2019). Establishing microbial co-cultures for 3-hydroxybenzoic acid biosynthesis on glycerol. *Engineering in Life Sciences, 19*(5), 389-395.

Zobrist, C., Sobocinski, J., Lyskawa, J., Fournier, D., Miri, V., Traisnel, M.*, et al.* (2011). Functionalization of Titanium Surfaces with Polymer Brushes Prepared from a Biomimetic RAFT Agent. *Macromolecules, 44*(15), 5883-5892.

7. Appendices

7.1 Design of Inducible *Fim* Mutation Cassette

CAG**CTCGAG**CTAAACAAGGGGAGCTTTGCAAGCTAACTCAGTGAGCTTGGTGAAAATCAGTGT
TTACCCGCCATCAGGCTGAGCATAATTCTCATCATGAAATATGTTTCCTGGTTTGTGGCTTGT
AACTGGTCACTTCTGAAGTCGATCTGGAGAGGCTTGTTGATGTTGGTGTTTTCAGGATGATGT
TTCACTTAGTTTGTTTGCCGTATCGCCCGGCGAATGGCTGTGATTGAGGAAGGTTTAAGTCGT
AGTGACCAAAGCTATATTTACCAACGAATGTAGATGAAAAAATCATCTCCTGCGTTCCCCCAT
ATCTCTAGGATAAAAAGGAATGTAACAATCTCATGGCGTAAGCTGACGAATCAGCAGGAATAA
TCGCTAGGGACCTAAGAATTAGCATGATAATAGCCACTAAGAAATTACTGCGCTCCATGAAAT
AGCCATTTTGTGGCAAATGGAGTTGACTAATAATGTCATATGTGAGACGGCTAGTTGAACGAA
TAtcacactggctcaccttcgggtgggcctttctgcgtttatatactagagagagaatataaa
aagccagattattaatccggctttttattatttTCAATCGTCACCCTTTCTCGGTCCTTCAA
CGTTCCTGACAACGAGCCTCCTTTTCGCCAATCCATCGACAATCACCGCGAGTCCCTGCTCGA
ACGCTGCGTCCGGACCGGCTTCGTCGAAGGCGTCTATCGCGGCCCGCAACAGCGGCGAGAGCG
GAGCCTGTTCAACGGTGCCGCCGCGCTCGCCGGCATCGCTGTCGCCGGCCTGCTCCTCAAGCA
CGGCCCCAACAGTGAAGTAGCTGATTGTCATCAGCGCATTGACGGCGTCCCCGGCCGAAAAAC
CCGCCTCGCAGAGGAAGCGAAGCTGCGCGTCGGCCGTTTCCATCTGCGGTGCGCCCGGTCGCG
TGCCGGCATGGATGCGCGCGCCATCGCGGTAGGCGAGCAGCGCCTGCCTGAAGCTGCGGGCAT
TCCCGATCAGAAATGAGCGCCAGTCGTCGTCGGCTCTCGGCACCGAATGCGTATGATTCTCCG
CCAGCATGGCTTCGGCCAGTGCGTCGAGCAGCGCCCGCTTGTTCCTGAAGTGCCAGTAAAGCG
CCGGCTGCTGAACCCCCAACCGTTCCGCCAGTTTGCGTGTCGTCAGACCGTCTACGCCGACCT
CGTTCAACAGGTCCAGGGCGGCACGGATCACTGTATTCGGCTGCAACTTTGT**CAT**GCTTGACA
CTTTATCACTGATAAACATAATATGTCCA**C**CAACTTATCAGTGATAAAGAATCCGCGCGTTCA
ATCGGACCAGCGGAGGCTGGACACAGGAAACAGCTATGAAAATTAAAACTCTGGCAATCGTTG
TTCTGTCGGCTCTGTCCCTCAGTTCTACAGCGGCTCTGGCCGCTGCCACGACGGTTAATGGTG
GGACCGTTCACTTTAAAGGGGAAGTTGTTAACGCCGCTTGCGCAGTTGATGCAGGCTCTGTTG
ATCAAACCGTTCAGTTAGGACAGGTTCGTACCGCATCGCTGGCACAGGAAGGAGCAACCAGTT
CTGCTGTCGGTTTTAACATTCAGCTGAATGATTGCGATACCAATGTTGCATCTAAAGCCGCTG
TTGCCTTTTTAGGTACGGCGATTGATGCGGGTCATACCAACGTTCTGGCTCTGCAGAGTTCAG
CTGCGGGTAGCGCAACAAACGTTGGTGTGCAGATCCTGGACAGAACGGGTGCTGCGCTGACGC
TGGATGGTGCGACATTTAGTTCAGAAACAACCCTGAATAACGGAACCAATACCATTCCGTTCC
A**ACTAGT**cag

NNN – NagC binding site (complement strand)
NNN – fim upstream homology arm for removal of PfimA, fimB, fimE and BasR regulator binding site
nnn – Bba_B0014. Synthetic directional transcription terminator biopart.
NNN – tetR (in reverse orientation) followed by ptetA (tet0 in yellow) and RBS in blue
NNN – Fim downstream homology arm (homologous to fimA, ATG at start is FimA start codon)
C/TCGAG – XhoI for insertion into pDM4
A/CTAGT – SpeI for insertion into pDM4

Appendix 7.1.1. Design of synthetic cassette for construction of inducible *fim* mutant in *E. coli.* Whole construct 1837bp.

7.2. NMR Spectra

7.2.1. Protected Mannose Monomer (1)

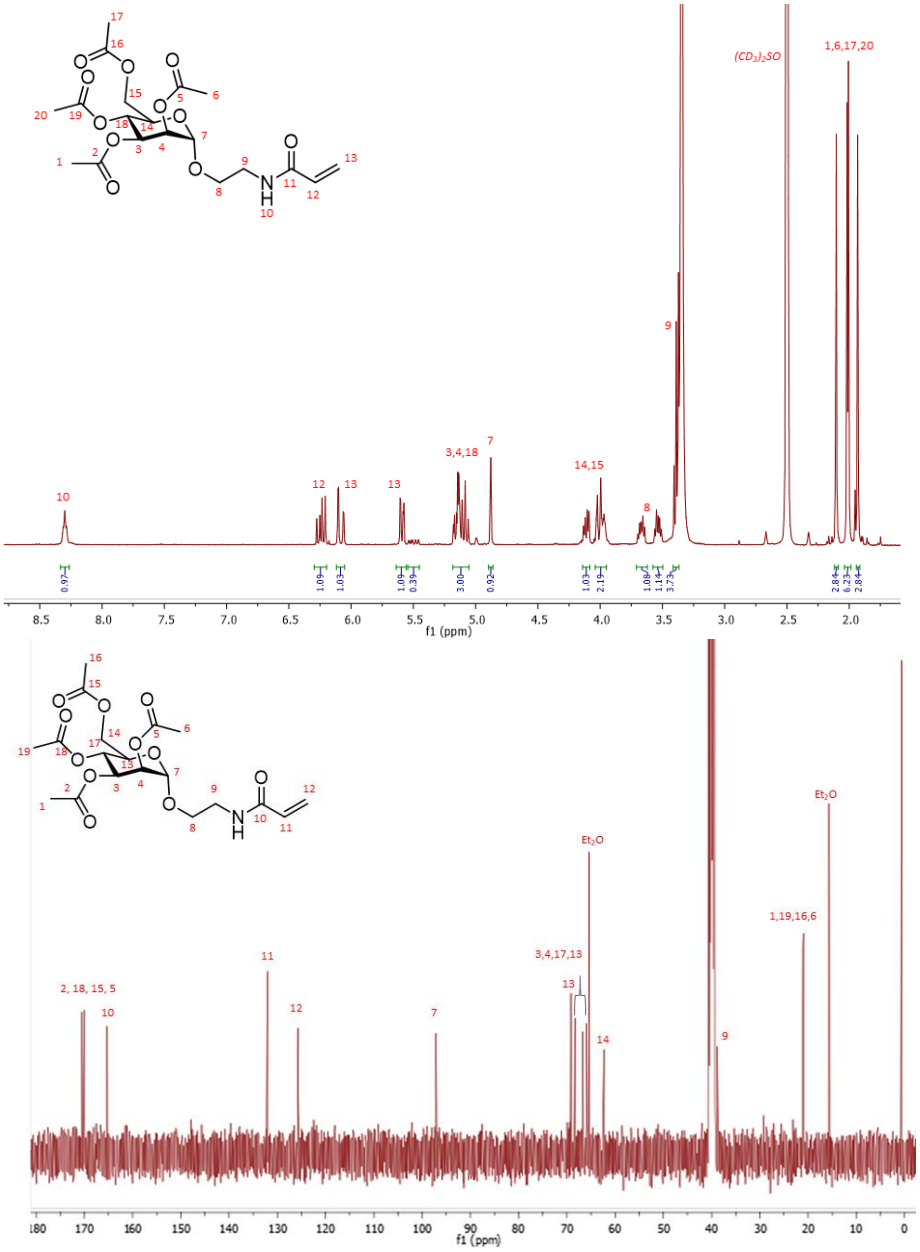

Appendix 7.2.1. ^{1}HNMR and ^{13}CNMR spectra of protected mannose acrylamide monomer **(1)** in d6-DMSO

7.2.2. Deprotected Mannose Monomer (2)

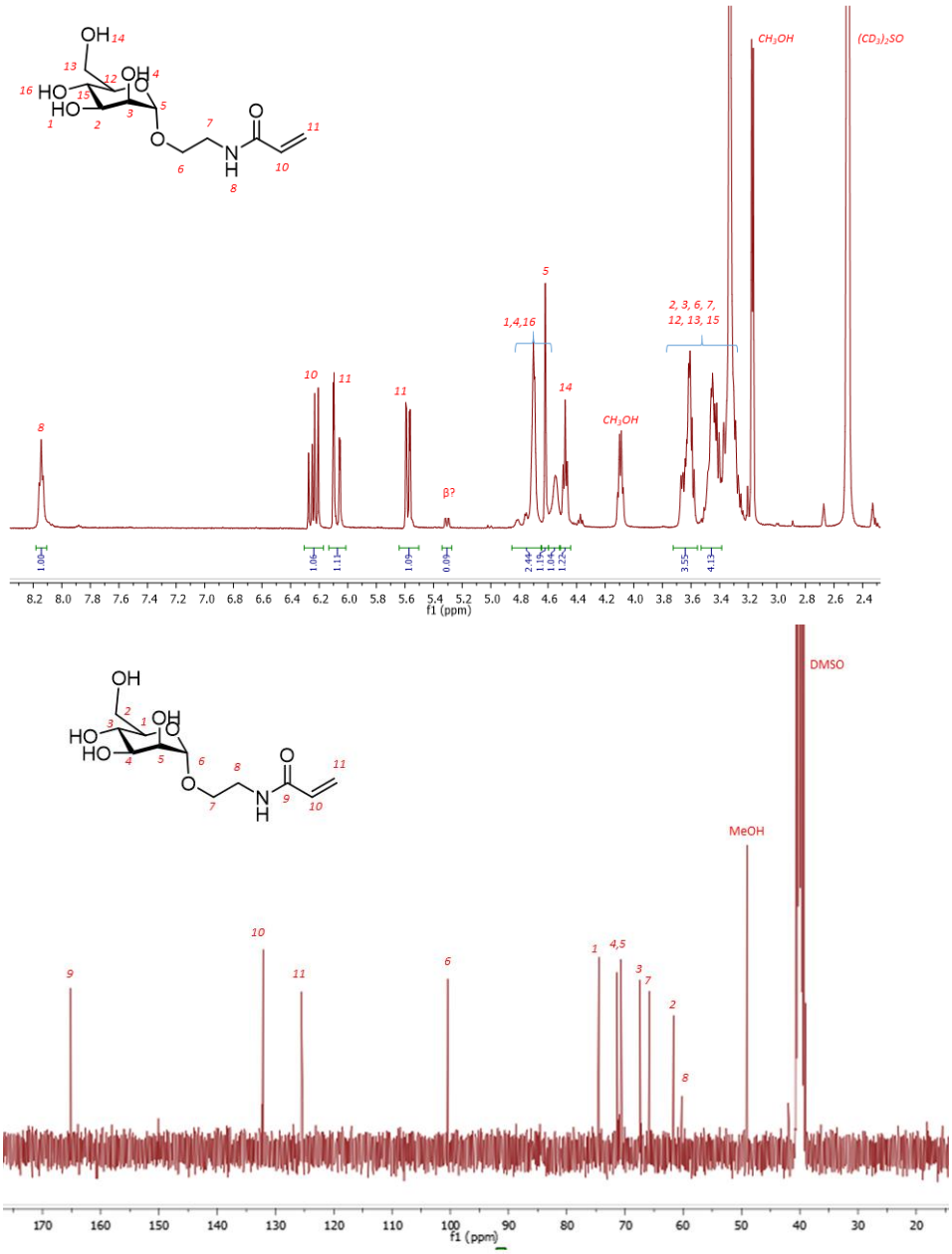

Appendix 7.2.2. ^{1}HNMR and ^{13}CNMR spectra of protected mannose acrylamide monomer **(2)** in d6-DMSO

7.2.3. Protected Galactose Monomer (3)

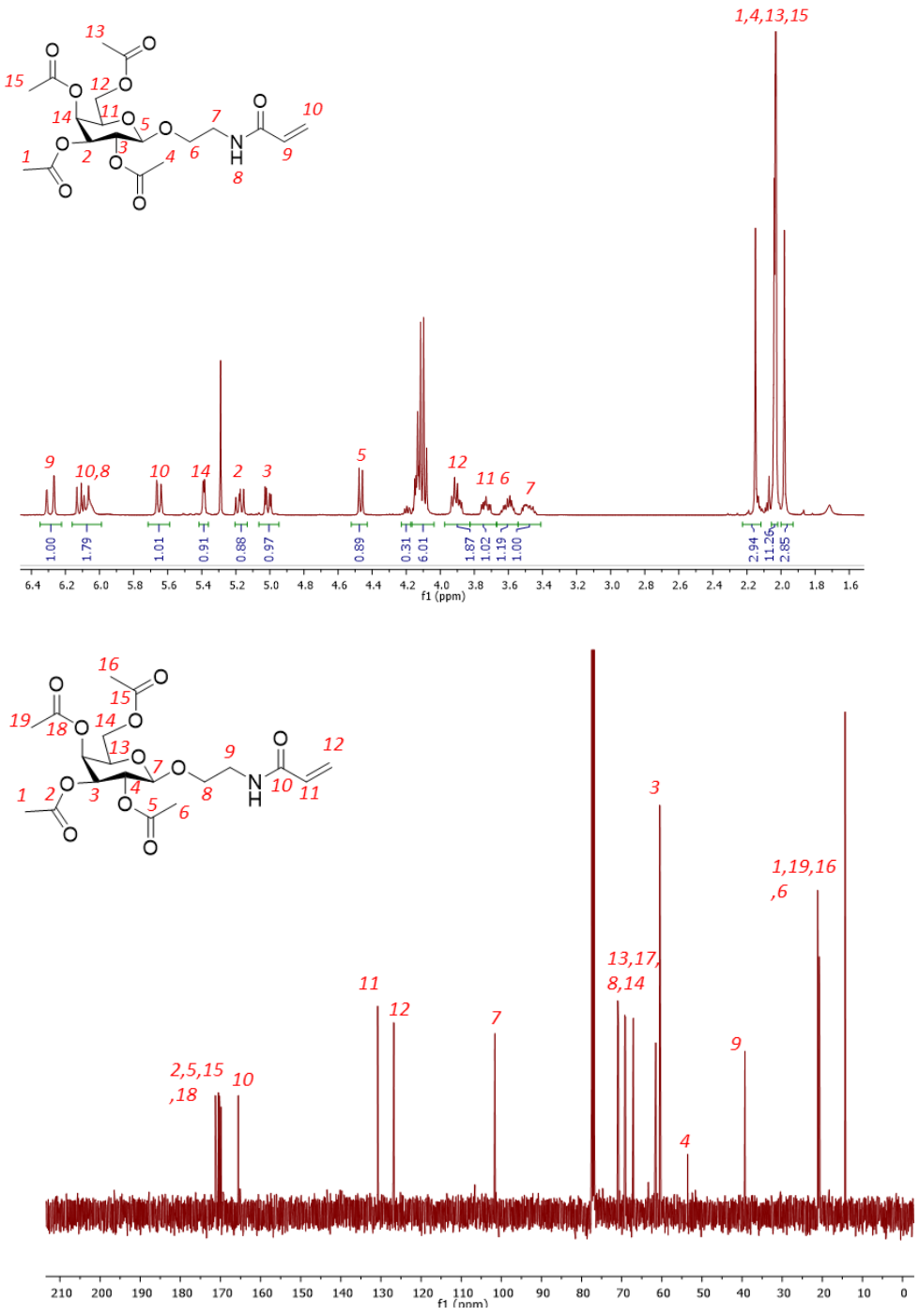

Appendix 7.2.3. ^{1}HNMR and ^{13}CNMR spectra of protected galactose acrylamide monomer **(3)** in $CDCl_3$

7.2.4. Deprotected Galactose Monomer (4)

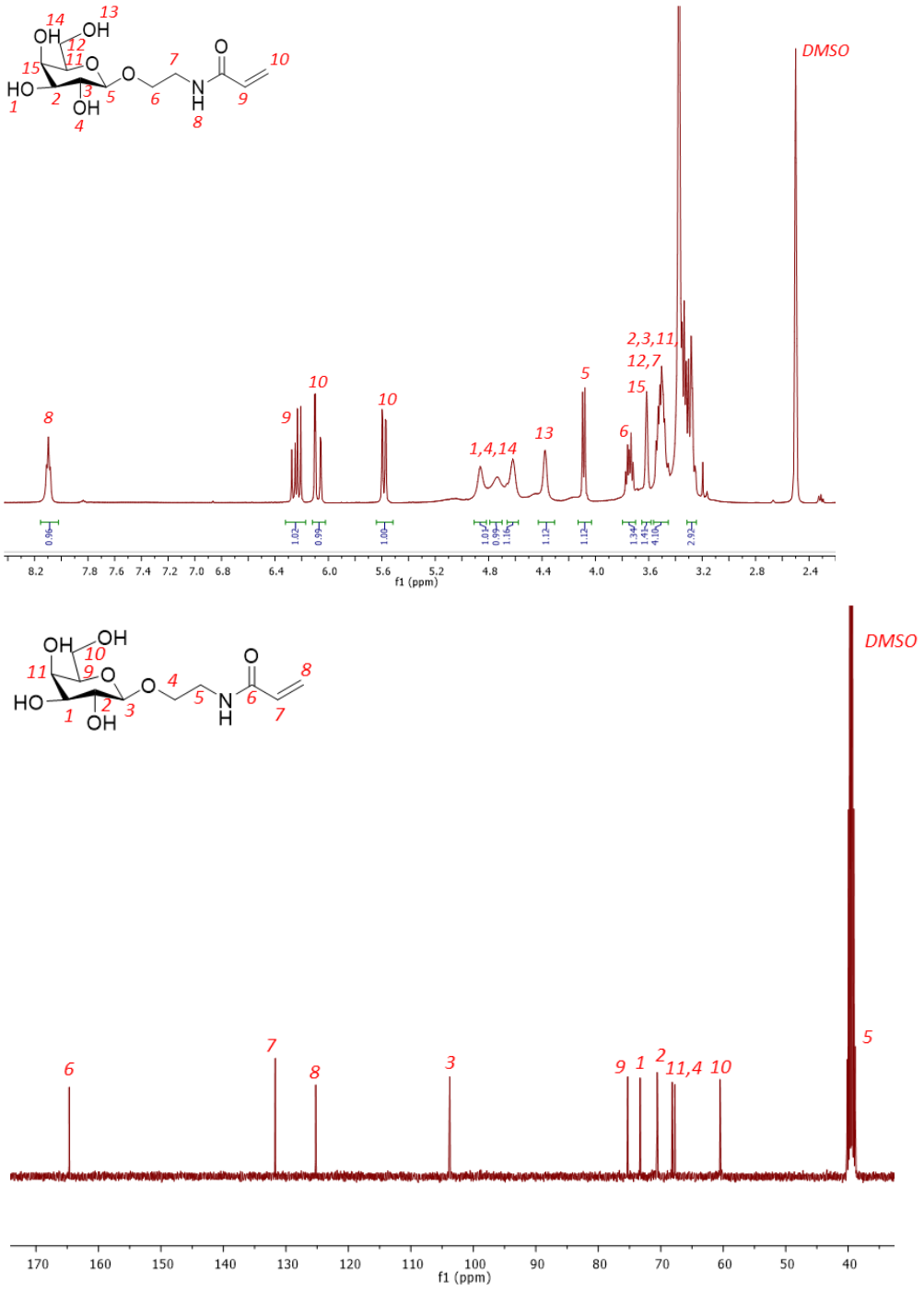

Appendix 7.2.3. ^{1}HNMR and ^{13}CNMR spectra of deprotected galactose acrylamide monomer **(4)** in d6-DMSO

7.2.5. PABTC (5)

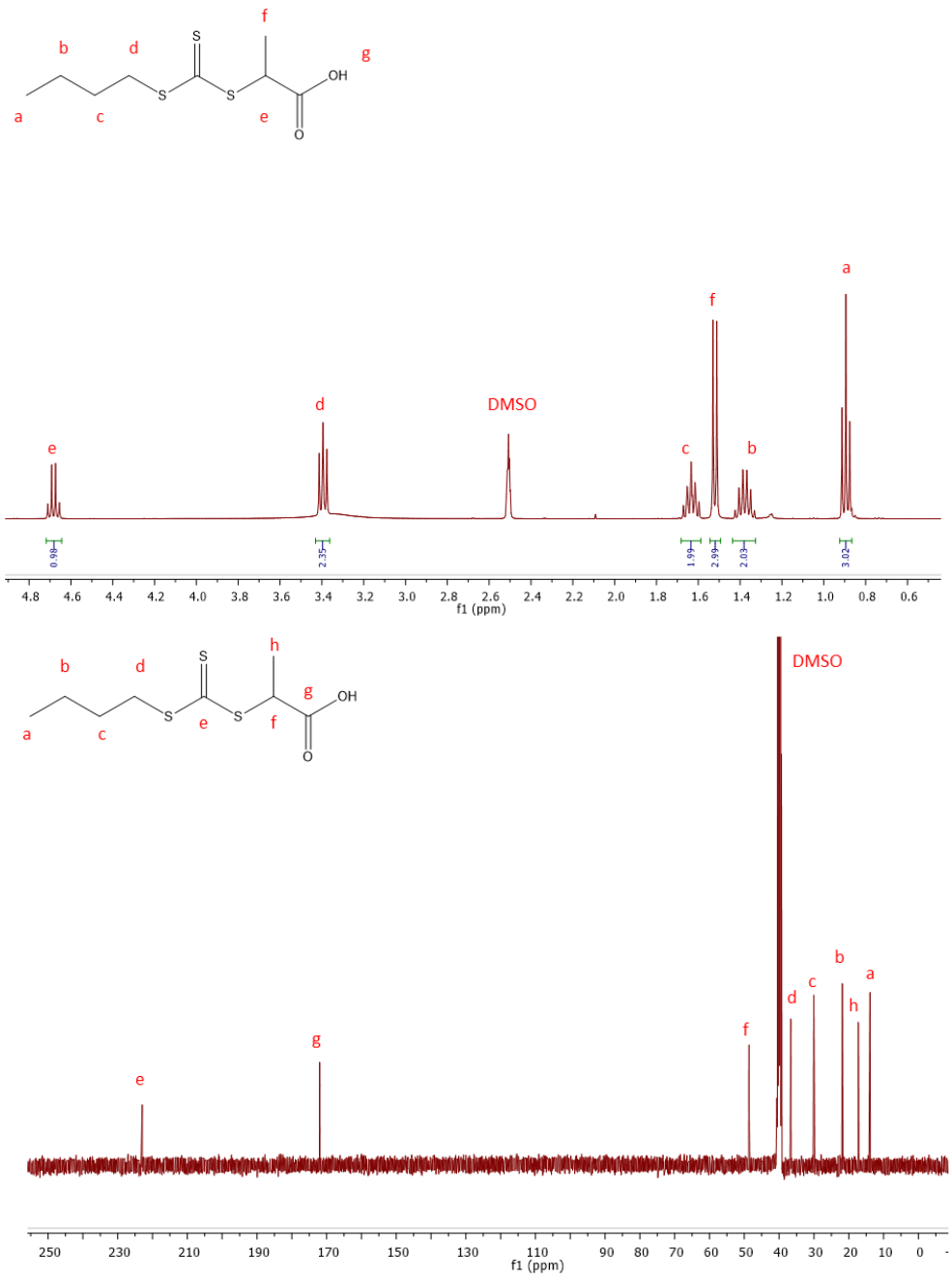

Appendix 7.2.5. ^{1}HNMR and ^{13}CNMR spectra of PABTC **(5)** in d6-DMSO

7.2.6. NHS-PABTC (6)

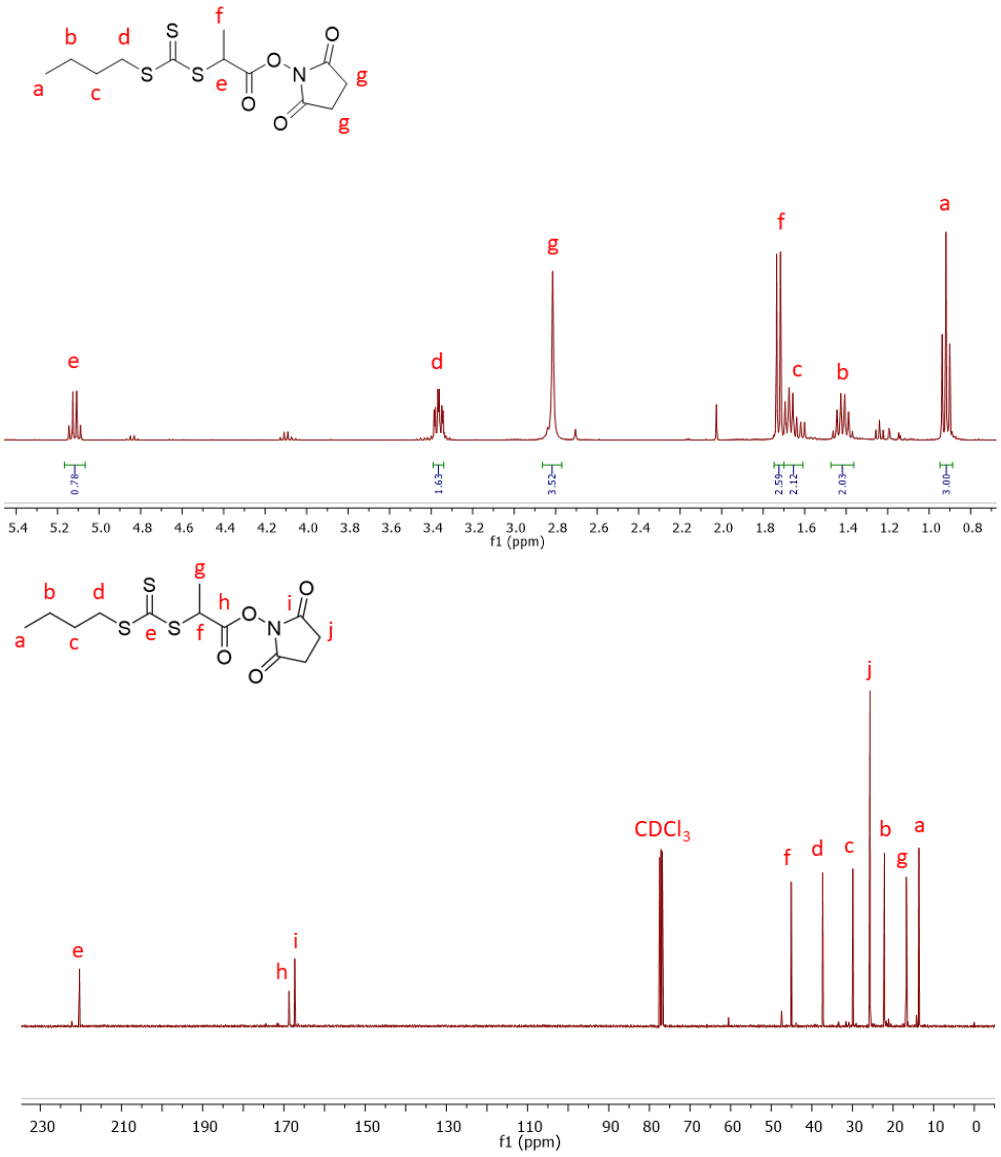

Appendix 7.2.6. ^{1}HNMR and ^{13}CNMR spectra of NHS-PABTC **(6)** in $CDCl_3$

7.2.7. Dopa-PABTC (7)

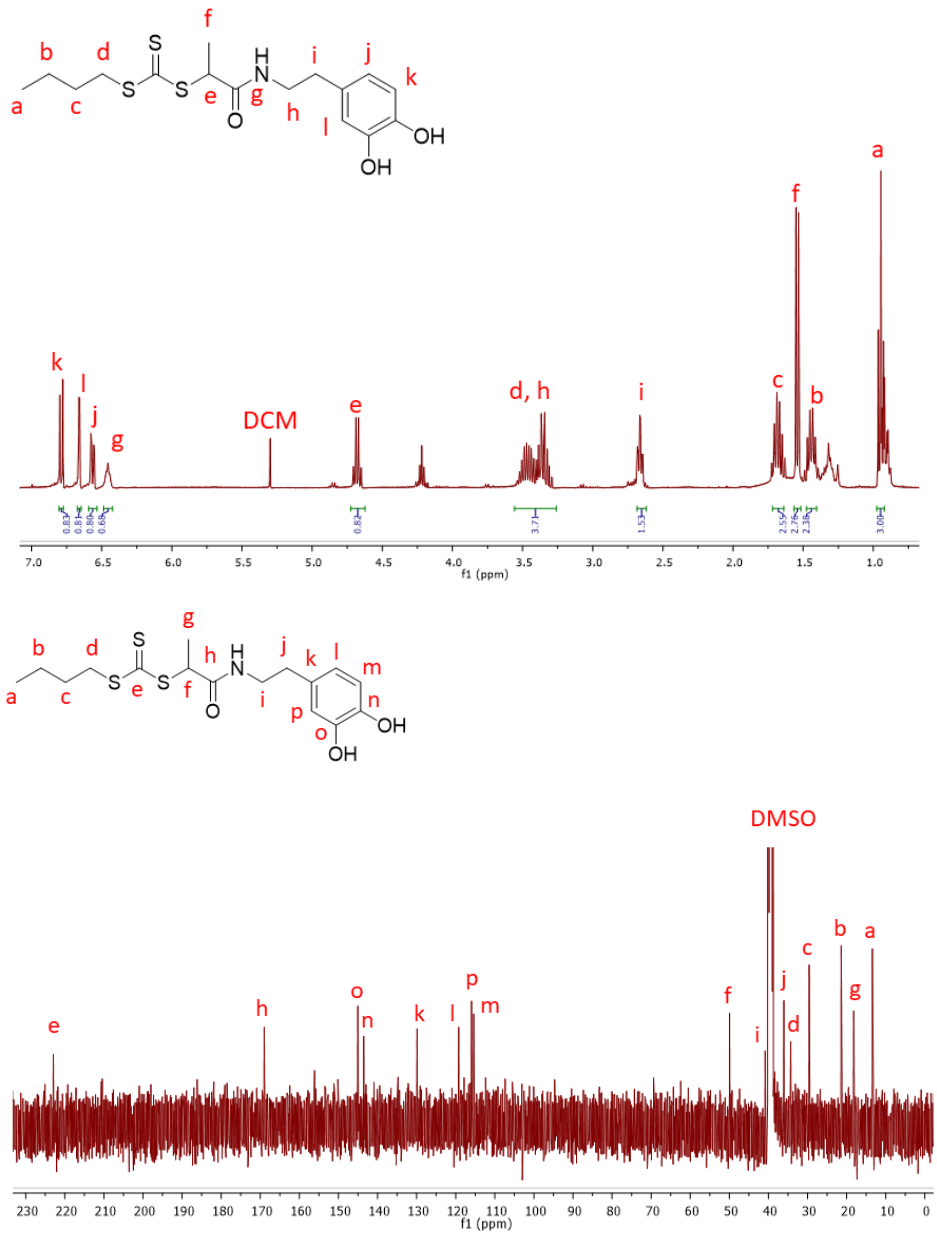

Appendix 7.2.7. ^{1}HNMR and ^{13}CNMR spectra of Dopa-PABTC **(7)** in d6-DMSO

7.2.8. Dopa-(ManAA)$_{50}$ as exemplar glycopolymer

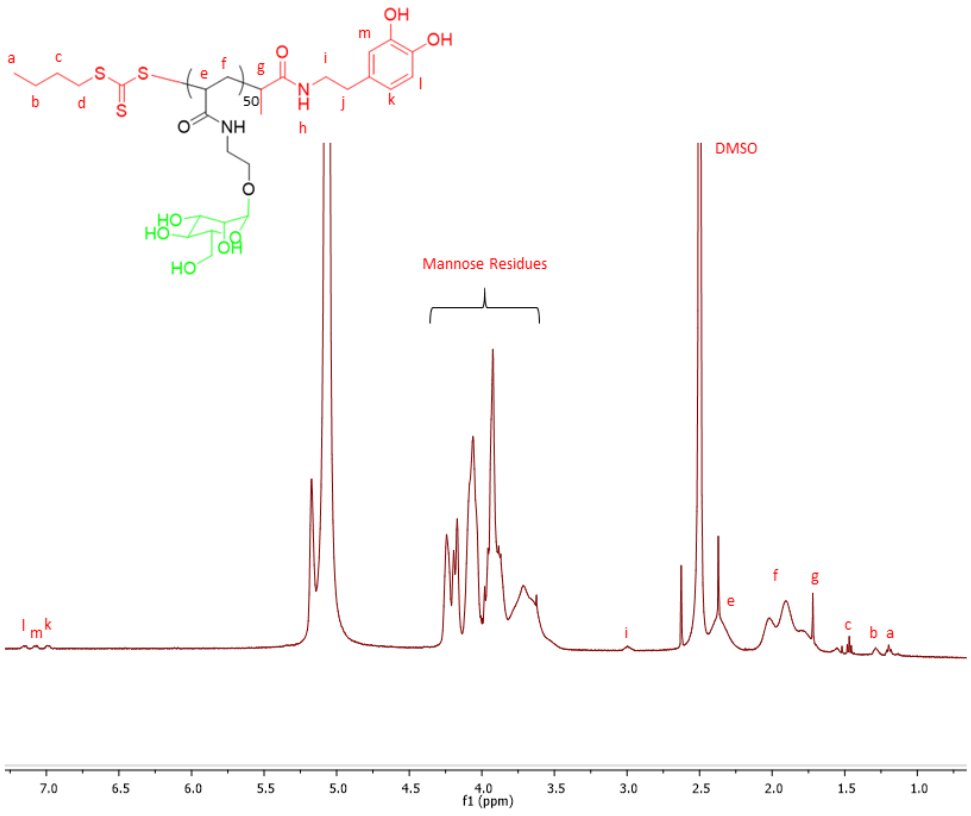

Appendix 7.2.8. ^{1}HNMR spectrum of Dopa-(ManAA)$_{50}$ in d6-DMSO as example spectrum of dopamine terminal glycopolymers.